PhD THESIS DECLARATION

The undersigned

SURNAME *Ali*

FIRST NAME *Sajid*

PhD Registration Number *1612621*

Thesis title: *Stochastic Models for High-Quality Process Monitoring*

PhD in *Statistics*

Cycle *27*

Candidate's tutor *Antonio Pievatolo*

Year of thesis defence *2016*

DECLARES

Under *his* responsibility:

1) that, according to Italian Republic Presidential Decree no. 445, 28th December 2000, mendacious declarations, falsifying records and the use of false records are punishable under the Italian penal code and related special laws. Should any of the above prove true, all benefits included in this declaration and those of the temporary embargo are automatically forfeited from the beginning;

2) that the University has the obligation, according to art. 6, par. 11, Ministerial Decree no. 224, 30th April 1999, to keep a copy of the thesis on deposit at the "Bilioteche Nazionali Centrali" (Italian National Libraries) in Rome and Florence, where consultation will be permitted, unless there is a temporary embargo protecting the rights of external bodies and the industrial/commercial exploitation of the thesis;

3) that the Bocconi Library will file the thesis in its "Archivio istituzionale ad accesso aperto" (institutional registry) which permits online consultation of the complete text (except in cases of a temporary embargo);

4) that, in order to file the thesis at the Bocconi Library, the University requires that the thesis be submitted online by the candidate in unalterable format to Società NORMADEC (acting on behalf of the University), and that NORMADEC will indicate in each footnote the following information:

   - thesis *Stochastic Models for High-Quality Process Monitoring*;
   - by *Ali Sajid*;
   - defended at Università Commerciale "Luigi Bocconi" – Milano in *2016*;
   - the thesis is protected by the regulations governing copyright (Italian law no. 633, 22th April 1941 and subsequent modifications). The exception is the right of Università Commerciale "Luigi Bocconi" to reproduce the same for research and teaching purposes, quoting the source;

5) that the copy of the thesis submitted online to NORMADEC is identical to the copies handed in/sent to the members of the Thesis Board and to any other paper or digital copy deposited at the University offices, and, as a consequence, the University is absolved from any responsibility regarding errors, inaccuracy or omissions in the contents of the thesis;

6) that the contents and organization of the thesis is an original work carried out by the undersigned and does not in any way compromise the rights of third parties (Italian law, no. 633, 22nd April 1941 and subsequent integrations and modifications), including those regarding security of personal details; therefore the University is in any case absolved from any responsibility whatsoever, civil, administrative or penal, and shall be exempt from any requests or claims from third parties;

7) that the PhD thesis is not the result of work included in the regulations governing industrial property, was not produced as part of projects financed by public or private bodies with restrictions on the diffusion of the results, and is not subject to patent or protection registrations, and therefore not subject to an embargo;

Date *21 October 2015*

SURNAME *Ali*
FIRST NAME *Sajid*

Contents

This page is left blank intentionally.

List of Figures

List of Tables

Acknowledgements

The completion of this dissertation is simply because of the grace of Almighty Allah and His beloved prophet Hazart Muhammad (PBUH, infinite Darood-o-Salam upon him and his family) who granted me with the spirit and enthusiasm required for this adventurous task.

Four years ago, I had an incredible fortune to begin my Ph.D in Statistics at Bocconi University, and it is an unforgettable journey for me. During this period, I have been fully trained as a research student, learnt lots of academic knowledge and enjoyed Bocconi research environment.

I express my sincere and deepest gratitude to my research *advisor* Professor **Antonio Pievatolo** (CNR-IMATI Milano). This work could never have been completed without his constant guidance and supports. His thoughtful motivations invaluably enhanced this thesis and taught me to examine a problem from all angles. As an advisor, he allowed me to feel comfortable asking even the most basic. In the end, he was more than an advisor to me; he was not only continually helped me to shape my career but, importantly, is a caring friend. Moreover, I must sincerely thank my *co-advisor*, Professor **Sonia Petrone** (Bocconi University), for her invaluable advice. I am especially grateful for her encouragement in times of difficulties and warmhearted care during the whole period of my study. Despite her busy schedule whenever I knocked her office door, she heard me carefully and therefore, I am grateful for all the time she dedicated to working with me. Her clever ideas are of great inspiration to me. I want to say my advisor and co-advisor: Dear Respected Professors, this little work is the first fruit of that literary and philosophical training, which I have received from you for the last two years. If there is something good in this thesis, that is due to you while deficiencies are due to my ignorance. You have always judged me liberally; I hope you will judge these pages in the same spirit.

Furthermore, I would like to pay my gratitude to the professors of Decision Sciences Department at Bocconi University for their wonderful courses and encouragement, including Professor Pietro Muliere, who encouraged me when I was disappointed about my study, and Professor Sandra Fortini. I am also thankful to Dr. Gualtiero Valsecchi (CADES Bocconi University) who took pain and helped me out when I had a visa prob-

lem. Ms. Angela Baldassarre, Ms. Silvia Acquati, and Ms. Paola Mascia deserve special thanks to their help and support throughout last four years.

I am also very grateful to the external reviewer, Professor Bianca Maria Colosimo (Department of Mechanical Engineering, Politecnico di Milano), for excellent suggestions to improve my thesis.

Besides, I would like to express my gratitude to all who supported me and made this PhD thesis possible. Many thanks to Dr. Muhammad Aslam (Professor at Riphah International University, Pakistan) for his constant support, Dr. Muhammad Riaz (KFUPM), Mr. Kizar Hayat and Mr. Walait Ali Sabir for their encouragement. Special thanks go to my PhD-mates, Fred Ronald Munwankia and Aleksandar Pramov, for their support and great company. I am sincerely thankful to Sumeda Siriwardena for reading and correcting some parts of my work. I would also like to acknowledge the PhD students of other cycles for their friendship.

Last but not the least; I am thankful to my Parents, especially My Mother Mumtaz Begum, who was aware about child care when nobody knew it in our village, Khala Sehnaz and Nishat for their love and support which I cannot express in words, Father Nawazish Ali and Brother Majid Ali. Any project owes its success to two kinds of people, one who executes the project and takes the credit and others who lend their invaluable support and guidance, and remain unknown (unsung heroes). The successful completion of this dissertation, also, was made possible only with the support and guidance of many others. My profound thanks to all those people and friends who helped me timely, and I cannot write their name.

Dedication

To all those people who have served their lives for knowledge:

- Moinuddin Chishti (1141 - 1236) also known as Gharīb Nawāz (Benefactor of the Poor), was an Imam, Islamic scholar and philosopher from South Asia. Chishti introduced and established the Chishti Order of Sufism in the Indian subcontinent,

- Abul Hassan Ali Ibn Usman al-Jullabi al-Hajveri al-Ghaznawior Abul Hassan Ali Hajvari (sometimes spelled Hajvari, Hajweri, Hajveri), also known as Daata Ganj Bakhsh which means the master who bestows treasures) or Daata Sahib, was a Persian Sufi and scholar in the 11th century who spent his life in Pakistan,
  (They came to an unknown country, lived there and changed the minds and hearts of the native people with their teachings. It is a sign of their significant contributions that still people respect them.), and especially

- my aunt, who first time introduced me to the world of knowledge.

Abstract

With the intense competition in the current industrial and business economies, satisfying customer requirements is a crucial factor to industrial success, in which one of the most important elements is the quality of products or services. Due to the modern technological revolution, human beings are becoming more and more machines/systems dependent. Only with high-quality products/systems or services, organizations can take advantage in attracting and satisfying their customers, and consequently, achieve business profit. Therefore, sustaining and improving quality is essential to all kinds of industries and statistical quality control (SQC) techniques play an important role to achieve this goal.

The application of traditional process monitoring techniques has certain problems and cannot be used for the high-quality process monitoring. The time-between-events (TBE) charts have shown to be very effective in monitoring high-quality processes in manufacturing, medical and business industries. However, existing TBE control charts are based on the Poisson and geometric processes. This research aims to introduce advanced TBE charts for complex TBE data using stochastic models. The new charts are introduced based on the renewal process, renewal reward process (with fixed and random threshold), nonhomogeneous and homogeneous Poisson processes. The renewal process in TBE setup is used to generalize the existing TBE charts based on the Poisson process while the renewal reward process for joint monitoring of the time and the magnitude. Similarly, the nonhomogeneous Poisson process with power law intensity is used to generalize the existing work to a situation where failure risk varies over time. A control chart based on the Bayesian predictive control limits is also introduced in this thesis. Since the control limits of the nonhomogeneous and Bayesian predictive charts are sequentially updated, therefore, both charts are suitable for the online adaptive (sequential) monitoring. The proposed control charts are assessed using different commonly used performance measures, including average run length, coefficient of variation of the run length and of the length of inspection distributions. The guidelines for various situations in which a proposed chart would work is given in each respective chapter.

We have shown mathematically and numerically that proposed approaches improve the effectiveness of the TBE charts. Moreover, this thesis shows that the proposed approaches do generalize the existing TBE control charts for complex TBE data. This thesis not only focuses on the development of the stochastic models suitable for advanced process monitoring but also on the practical applications. Therefore, this research may provide a basis for the future research work to improve the effectiveness of the TBE charts.

Chapter 1

Introduction

This thesis is about the control charts' construction based on stochastic processes. The work is motivated by both methodological and applied problems. The aim of this chapter is to introduce the research topics and concepts.

1.1 Introduction

Statistical quality control (SQC) techniques play a paramount role in many manufacturing and service industries. SQC is a branch of industrial statistics (currently not limited to industry but also present in the medical field, business and other application domains) which includes, primarily, the areas of acceptance sampling, statistical process control (SPC), design of experiments (DOE), and capability analysis. Briefly speaking, acceptance sampling methods are used in industry to take decisions about the disposition of "lots" of manufactured items, including, accepting or rejecting individual lots; SPC techniques are employed to monitor production processes over time to detect changes in process performance; DOE are applied to identify significant factors affecting process and product quality, referred to as screening or characterization, and to identify the specific levels of the important factors that lead to optimum (or near optimum) performance; the objective of process capability analysis is to assess whether or not a process is capable of meeting specification limits on key quality characteristics, which include the gauge or measurement systems' capability analysis (cf. Woodall and Montgomery [1999]).

This research is classified under the SPC framework. However, SPC should not be confused with ordinary process control in control theory, which mainly focuses on engineering perspective (e.g. particle, and Kalman filters) while SPC deals from a statistical point of view to improve the quality of a process. SPC is a powerful collection of problem-solving tools useful in achieving process stability and improving capability through the reduction of variability (cf. Montgomery [2009]). The major seven tools of SPC include histogram or stem-and-leaf plot, check sheet, Pareto chart, cause-and-effect diagram, defect concen-

tration diagram, scatter diagram and control chart. It has been increasingly realized that SPC is not simply a collection of quality control tools but a way of thinking, which is essential for a never-ending improvement of quality. SPC builds an environment in which all individuals in an organization seek continuous improvement in quality and productivity (cf. Montgomery [2009]). This environment is best developed when management becomes involved in the process. Arguably, SPC tools can be applied to any process.

Rao [1997] stated: "It is not surprising that the recent book on modern inventions lists statistical quality control as one of the technological inventions of the past century. Indeed, there has rarely been a technological invention like statistical quality control, which is so wide in its application yet so simple in theory, which is so effective in its results so easy to adopt and which yields so high a return yet needs so slow an investment."

1.1.1 What are Control Charts exactly?

Among the SPC tools, the control chart is probably the most technically sophisticated. The fundamentals of SPC and control charting were proposed by Walter Shewhart in the 1920s and 1930s. Until the mid to late 1970s there were many important advances but relatively few individuals conducting research in this area as compared with other areas of applied statistics. Research activity has greatly increased since about 1980 onward. Much of the increase in interest was due to the quality revolution, which was caused by an increasingly competitive international marketplace. Improvement in quality is still required for the survival of many industries.

A typical control chart is shown in Figure-1.1. The control chart is a graphical display of a quality characteristic that has been measured or computed from a sample versus the sample number or time. The chart contains a center line (CL) that represents the average value of the quality characteristic corresponding to the in-control state. (That is, only chance causes are present.) Two other horizontal lines, called the upper control limit (UCL) and the lower control limit (LCL), are also shown on the chart. These control limits are chosen so that if the process is in-control, nearly all of the sample points will fall between them. As long as the points fall within the control limits, the process is assumed to be in control, and no action is necessary. However, a point that plots outside the control limits is interpreted as evidence that the process is out-of-control, and investigation and corrective action are required to find and eliminate the assignable cause or causes responsible for this behavior. According to Montgomery [2009], "It is customary to connect the sample points on the control chart with straight-line segments, so that it is easier to visualize how the sequence of points has evolved over time." Even if all the points plot inside the control limits, if they behave in a systematic or non-random manner, then this could be an indication that the process is out-of-control. To identify such non-random patterns, sensitizing rules/run rules are commonly used (cf. Montgomery [2009],

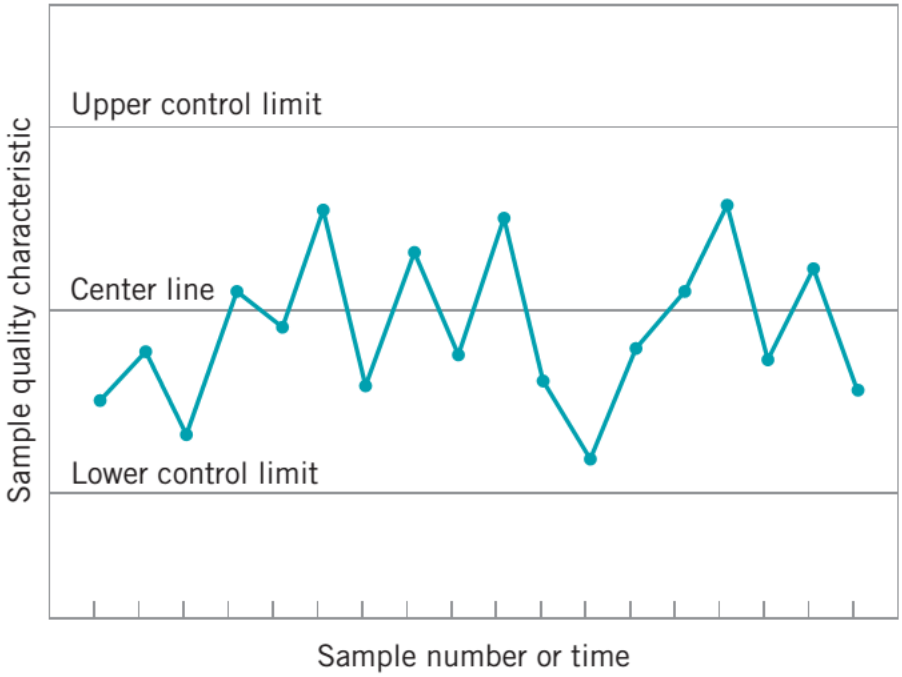

Figure 1.1: A typical Control Chart (Source: Montgomery [2009])

page 197).

It is important to distinguish a pair of concepts, chance causes (or common causes) and assignable (or special) causes, in SPC. In any production process, regardless of how well designed or carefully maintained it is, a certain amount of inherent or natural variability will always exist. This natural variability or background noise is the cumulative effect of many small, essentially unavoidable causes. This natural variability, in the framework of SPC, is often called a "stable system of chance causes." A process that is operating with only chance causes of variation present is said to be in statistical control.

Other kinds of variability, which are generally large when compared to the background noise, usually represent an unacceptable level of process performance, which may occasionally be present in the output of the process. This source of variability that is not part of the chance cause pattern, is usually referred to as "assignable causes." A process that is operating in the presence of assignable causes is said to be out-of-control (cf. Montgomery [2009]). A graphical presentation for illustration of chance and special causes is given in Figure-1.2 (where μ and σ represent the target mean and standard deviation of a process).

One of the main purposes of control charts is to distinguish between the variation due to the chance causes and the variation due to the assignable causes in order to prevent overreaction and under-reaction to the process. The distinction between chance causes and assignable causes is context dependent. The causes generally evolve over time. A chance cause today can be an assignable cause tomorrow. One is needed to react and remove an

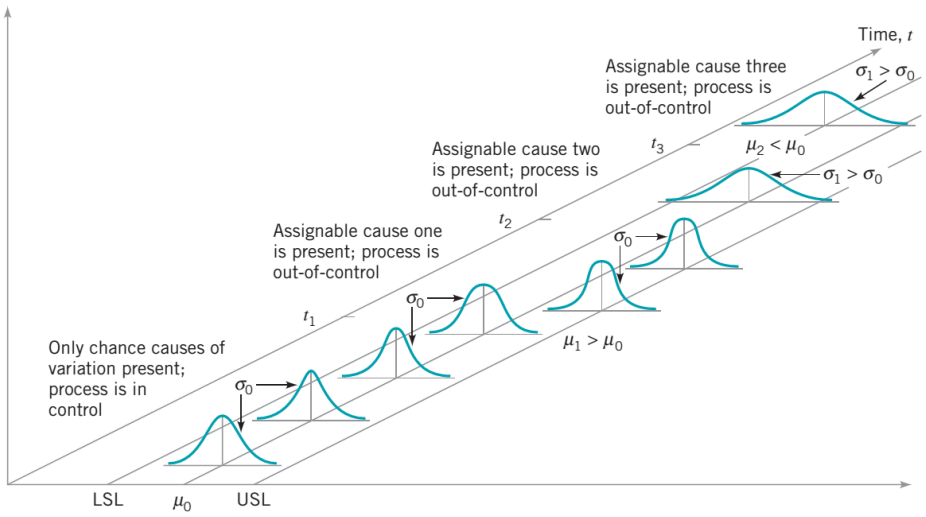

Figure 1.2: Chance and assignable causes of variation (Source: Montgomery [2009])

assignable cause only if it has an economic or safety impact. Hence, these control charts are not just an explanatory data technique but much more. Other purposes of the control chart include assessing effectiveness of changes and communicate the performance of a process to a user/customer.

Standard control chart usage involves phase-I and phase-II applications, with two different and distinct objectives. According to Montgomery [2009], "In phase-I, a set of process data is gathered and analyzed all at once in a retrospective analysis, constructing trial control limits to determine if the process has been in control over the period of time where the data were collected, and to see if reliable control limits can be established to monitor future production." This is typically the first thing that is done when control charts are applied to any process. Control charts in phase-I primarily assist operating personnel in bringing the process into a state of statistical control. Sometimes this type of analysis will require several cycles in which the control chart is employed, assignable causes are detected and corrected, revised control limits are calculated, and the out-of-control action plan is updated and expanded. Eventually the process is stabilized, and a clean set of data that represents in-control process performance is obtained for use in phase II. Phase-II begins after we have a clean set of process data gathered under stable conditions and representative of in-control process performance. In phase II, we use the control chart to monitor the process by comparing the sample statistic for each successive sample, as it is drawn from the process, to the control limits. We refer to Montgomery [2009] (page 198-199) for comprehensive details of phase I & II control charts.

1.1.2 Hypothesis Testing and Control Charts

There is a close connection between control charts and hypothesis testing or confidence intervals. To illustrate this connection, suppose that $X_t \sim N(\mu, \sigma^2)$ where μ is unknown and σ^2 is known. We want to test the hypothesis $H_0 : \mu = \mu_0$ versus $H_1 : \mu \neq \mu_0$. To accomplish this task, take a random sample from the process and compute $z_0 = |\bar{X} - \mu_0|/\sigma/\sqrt{n}$, i.e., based on the central limit theorem; choose a Type-I error probability, i.e., α, and find the critical value $z_{\alpha/2}$ (cf. Figure-1.3b). Reject the hypothesis H_0 if $|z_0| > z_{\alpha/2}$ (or via confidence interval, if $\mu_0 > \bar{X} + z_{\alpha/2}(\sigma/\sqrt{n}) = UCL$ and $\mu_0 < \bar{X} - z_{\alpha/2}(\sigma/\sqrt{n}) = LCL$, where $CL = \mu_0$. A general representation might be written as $UCL(LCL) = \mu \pm L\sigma$, where L is the distance of the control limits from the center line $CL = \mu$, expressed in standard deviation units.). To connect these settings with the control charts, suppose that the vertical axis in Figure-1.1 is the sample average. Now, if the current value falls between the control limits, we conclude that the process mean is in-control; that is, it is equal to some value μ_0. On the other hand, if it exceeds either control limit, we conclude that the process mean is out-of-control; that is, it is equal to some value μ_1. In a sense, then, the control chart is a test of the hypothesis that the process is in a state of statistical control. A point plotting within the control limits is equivalent to failing to reject the hypothesis of statistical control, and a point plotting outside the control limits is equivalent to rejecting the hypothesis of statistical control. Therefore, there is a trade-off between narrow and wide control limits (cf. Figure-1.4) and close connection to Type-I & II errors. A control chart that never finds anything wrong with a process, but the process produces a bad product, (i.e., insensitivity of the control chart) is analogous to Type-II error in statistical hypothesis testing. On the other hand, too many false alarms destroy the operating personnels confidence in the control chart, and they stop using it. This situation is analogous to Type-I error in statistical hypothesis testing (cf. Montgomery [2009], page 189).

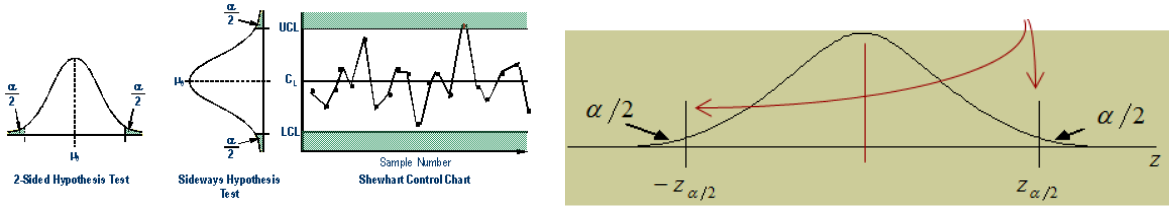

(a) Hypothesis Test versus Control Chart (b) Hypothesis Test for Normal Sample

Figure 1.3: Moving from Hypothesis Testing to Control Charts (Source: Jensen [2010])

Controversies: The fundamentals of the control charts were introduced in 1920-1925 by Walter Andrew Shewhart working at Bell Lab., whereas the theory of statistical hypothesis and confidence was mainly developed in 1925-1945, i.e., Karl Pearson (introduced p-value in 1901), Ronald Fisher (popularized p-value, 1920-1925), Jerzy Neyman

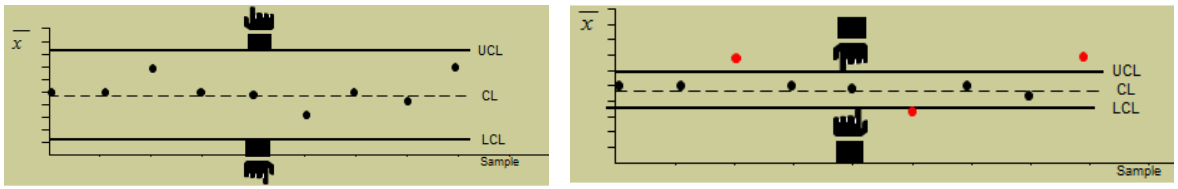

(a) Wide Control Limits (b) Narrow Control Limits

Figure 1.4: Trade-off Between Wide or Narrow Control Limits (Source: Jensen [2010])

(confidence interval), Egon Pearson (Type-I & II error for testing) and Abraham Walds (sequential testing). Due to simultaneous developments, some authors write that control charting and hypothesis testing are equivalent or very related. Juran [1997] (page 79) referred to the control chart as "a perpetual test of significance." Box and Kramer [1992] stated that "process monitoring resembles a system of continuous statistical hypothesis testing." Vining [1998] (page 218) wrote, "The current peer review literature, which represents the standard for evaluating the effectiveness and efficiency of these methodologies, tends to view the control chart as a sequence of hypothesis tests."

On the other side of the issue, Deming [2000] (page 369) stated (without elaboration), "Some books teach that use of a control chart is test of hypothesis: the process is in control, or it is not. Such errors may derail self-study." Further Deming wrote (page 335), "Rules for detection of special causes and for action on them are not tests of a hypothesis that a system is in a stable state." Therefore, Deming strongly advocated the use of control charts, but argued 'emphatically' against the use of hypothesis testing, e.g., (cf. Deming [2000], page 272) "Incidentally, the chi-square and tests of significance, taught in some statistical courses, have no application here or anywhere."

According to Woodall [2000] "Deming argued that practical applications in industry required "analytical" studies because of the dynamic nature of the processes for which there is no well-defined finite population or sampling frame. He held that hypothesis testing was inappropriate in these cases. Hahn [1996] provides a clear summary of the distinction between what Deming referred to as analytical and enumerative studies." Wheeler [1995] (page 17 and Chapter 19) and Hoerl and Palm [1992] also emphasize the difference between control charting and hypothesis testing.

Nelson [1999] noted that the following statements are incorrect:

- Shewhart charts are a graphical way of applying a sequential statistical significance test for an out-of-control condition;
- Control limits are confidence limits on the true process mean;
- Shewhart charts are based on probabilistic models;
- Normality is required for the correct application of a chart;

- The theoretical basis for the Shewhart control chart has some obscurities that are difficult to teach.

Shewhart control charts are used to indicate the presence of causes that produce important deviations from the stable operation of a process. Shewhart [1931] called these causes "assignable," while Deming [2000] called these causes "special" causes. When special causes are no longer indicated, the process is said to be "in statistical control." "In control" does not imply that only random causes remain, nor does it imply that the remaining values are normally distributed.

Tukey [1946] pointed out that the Shewhart control chart is not a method for detecting deviations from randomness. He writes: "This was not Shewharts purpose, and it is easy to construct artificial examples where non-randomness is in control or randomness is out of control. A state of control, in Shewharts basic sense, is reached when it is uneconomic to look for assignable causes, and experience shows that the compactness of the distribution associated with a good control chart implies this sort of control." A control chart tests for the practical significance of an effect, which is different than a statistical significance despite the fact that the word significance can be used for both. Shewhart charts are not based on any particular probabilistic model. He did not base his choice of the 3σ limit on any particular statistical distribution. Montgomery [2009] (page 183) added, "We should not worry too much about assumptions such as the form of the distribution or independence when we are applying control charts to a process to reduce variability and achieve statistical control."

It is sometimes suggested that data can be improved by transforming the data so it behaves as though it came from a normal distribution. This can be appropriate if the non-normal distribution to be transformed is known. However, there could be problems if it has to be estimated from preliminary data. Many skewed distributions can be traced from two normally distributed sources with different parameters (cf. Breyfogle [2003], page 247-248).

Breyfogle [2003] wrote, "If one were to view the control chart as a statistical significance test for each point in succession, the question would then become, what is the significance of the test? This calculation does not make sense for a situation where the test is continued repeatedly until a significant result is obtained, even though there are no special causes present. Similarly, when a control chart is not a statistical significance test, the upper and lower limits do not form a confidence interval. The control chart was developed empirically by Shewhart. Its applicability has withstood the test of time."

However, despite of all discussions by different researchers, Shewhart in Shewhart and Deming [1939] (page 40) seemed to take more of a middle ground in this debate as he wrote, "As a background for the development of the operation of statistical control, the formal mathematical theory of testing a statistical hypothesis is of outstanding impor-

tance, but it would seem that we must continually keep in mind the fundamental difference between the formal theory of testing a statistical hypothesis and the empirical theory of testing of hypotheses employed in the operation of statistical control. In the latter, one must also test the hypothesis that the sample of data was obtained under conditions that may be considered random."

To summarize above different views, we can say there are many similarities between hypothesis testing and control charts, but there are certainly some differences in viewpoint between control charts and hypothesis tests. For example, with stated hypothesis we look for evidence to falsifying the null hypothesis, so that the analysis is similar to that of statistical control. Moreover, an assignable cause can result in many different types of shifts in the process parameters. For example, the mean could shift instantaneously to a new value and remain there (this is sometimes called a sustained shift); or it could shift abruptly; but the assignable cause could be short-lived and the mean could then return to its nominal or in-control value; or the assignable cause could result in a steady drift or trend in the value of the mean. In this case the power of the test remains the same across samples whereas it changes slowly in case of shifts. We think that the main difference is that hypothesis testing is a one-off, whereas control chart is repeated. Therefore, it is close to sequential hypothesis testing approach. One place where the hypothesis testing framework is useful is in analyzing the performance of a control chart (cf. Montgomery [2009], page 183-189).

We also agree with Woodall [2000] that some of the disagreement over the relationship between control charting and hypothesis testing appears to result from a failure to distinguish between Phase-I and Phase-II applications. The theoretical approach to control charting in Phase-II, in which the form of the distribution is assumed to be known along with values of the in-control parameters, does closely resemble repeated hypothesis testing, especially if one considers an assignable cause to result in a sustained shift in the parameter of interest. In some cases there is mathematical equivalence. Therefore, at best the view that control charting is equivalent to hypothesis testing is an oversimplification. At worst the view can prevent the application of control charts in the initial part of Phase-I because of the failure of independence and distributional assumptions to hold. Moreover, we think that the closest thing in nonparametric statistics literature (cf. Tibor [1993], and Mann [1945]) to control chart is the following: H_0 : the process is in-control, versus H_1 : the process is out-of-control, is the testing of trend, i.e., H_0 : the observed process has no trend, versus H_1 : the observed process has some kind of trend. For more detailed discussion of hypothesis testing, the role of statistical theory, and control charts, see Woodall [2000], Montgomery [2009], and Breyfogle [2003].

1.1.3 Classification of Control Charts

To date, a great number of control charts or control charting techniques has been proposed under a variety of assumptions for monitoring a wide range of industrial processes. These control charts can be classified into different categories depending on the criteria used and the views taken. For example, control charts can be classified into variable data control charts and attribute data control charts based on the nature of quality characteristics. They can also be classified into phase-I control charts and phase-II control charts depending on whether the chart is used for retrospective analysis or prospective monitoring. Phase-I deals with the better understanding of the process and its stability, i.e., construction of control limits and estimation of the parameter in the case when unknown, while Phase-II deals with the monitoring process and is heavily dependent on the Phase-I. An efficient control chart is a chart which detects any change quickly. Thus, Phase-I analysis is an integral part of statistical process control. Chakraborti et al. [2008] gave an overview of the literature for this phase, i.e., phase-I. Control chart can also be classified into univariate and multivariate control charts. Furthermore, control charts may also be classified into parametric and non-parametric control charts, short-run and long-run control charts, and so on and so forth.

The variable control charts usually refer to those control charts monitoring quality characteristics that are variables; that is, they can be measured and expressed on a numerical or continuous (i.e., ratio) scale, e.g., time, length, temperature, weight and radiation dose, etc. These control charts include $\bar{X}$ chart, R chart, S chart, S^2 chart, range and moving range charts, quantile chart, and so on. They can be used to monitor process mean or process variation. In many cases, they are used jointly to monitor both. Nonetheless, in real practice, many quality characteristics cannot be conveniently represented numerically. In such cases, we usually classify each item inspected as either conforming or nonconforming to the specifications on that quality characteristic, e.g. pass/fail, yes/no, presence/absence, etc. Quality characteristics of this type are called attributes (cf. Calvin [1983], and Montgomery [2009]), and control charts for monitoring this type of quality characteristics are consequently called attribute control charts.

Before proceeding further the following definitions and notations are necessary: A point process is a stochastic model that describes the occurrence of events in time along the time axis.

Definition 1.1.1 *A point process is a sequence* $t = (t_n)_{n\geq 1}$ *of* $\mathbb{R}_+$*-valued random variables defined on* $(\Omega, \mathcal{F}, \mathbb{P})$ *such that*

1. $P(0 < t_1 \leq t_2 \leq, \cdots) = 1$,
2. $P(t_n \leq t_{n+1} < \infty) = P(t_n < \infty)(n \geq 1)$,
3. $P(\lim_{n\to\infty} t_n = \infty) = 1$ *(nonexplosive)*

Thus, a point process is an almost surely increasing sequence of strictly positive, possibly infinite random variables strictly increasing as long as they are finite and with almost sure limit ∞. The interpretation of T_n is that, if finite, it is the time point at which the n^{th} recording of an event occurs in any random finite time interval.
Another equivalent way to describe a point process is by a counting process, which is:

Definition 1.1.2 *(Counting process) A stochastic process* $\{N(t) = \sum_{i\geq 0} \mathbb{I}(t_i \leq t), t \geq 0, t \in T\}$ *is said to be counting process if* $N(t)$ *represents the total numbers of events that have occurred up to the time* t. *When* N *has as its argument an interval, such as* $N(a, b]$, *the result is the number of events (failure) in that particular interval.*

Thus, one can write the number of failures in the interval $(a, b]$ as $N(a, b] = N(b) - N(a)$. For a repairable system, let $0 < T_1 < T_2 < \cdots$ denote the failure times of the system measured in global time/scale (i.e., the time since the initial start up of the system). The times between failures (i.e., failure times are recorded as time since the previous failure), local time or the gaps, will be denoted by $X_1, X_2, \cdots$. We have $X_i = T_i - T_{i-1}$ or equivalently $T_i = \sum_{j=1}^{i} X_j$.

Theorem 1.1.3 *(Norris [1997]) Let* $(N(t))_{t\geq 0}$ *be an increasing, right-continuous integer valued processes starting from zero. Let* $0 < \lambda < \infty$, *then the following 3 conditions are equivalent:*

1. *(jump chain/holding time definition) The holding times* $X_1, X_2, \cdots$ *of* $(N(t))_{t\geq 0}$ *are independent exponential random variables of parameter* λ *and the jump chain is given by* $T_i = i, \forall i$.

2. *(infinitesimal definition)* $(N(t))_{t\geq 0}$ *has independent increments and as* $h \downarrow 0$ *uniformly in t,*$Pr\{N(t + h) - N(t)\} = 1 - h\lambda + o(h)$.

3. *(transition probability definition)* $(N(t))_{t\geq 0}$ *has stationary independent increments and for each t,* $N(t)$ *has a Poisson distribution of parameter* λt.

If $(N(t))_{t\geq 0}$ *satisfies any of these conditions then it is called a Poisson process of rate* λ.

Let $N(t) \sim F(., \theta), t \in T$ denotes the number of events, e.g. defects, in time interval $(0, t]$. To monitor $N(t)$, the most commonly used attribute control charts include p chart, np chart, c chart and u chart. In these charts, $F(., \theta)$ can be Bernoulli, binomial, geometric, negative binomial and the Poisson distribution. A graphical presentation of charts based upon the type of data set is given in Figure-1.5. On contrary, some control charting techniques may be applied to both types of data. A representative is the CUSUM (cumulative sum), synthetic and the EWMA (exponentially weighted moving average) control charts (cf. Bourke [2001]).

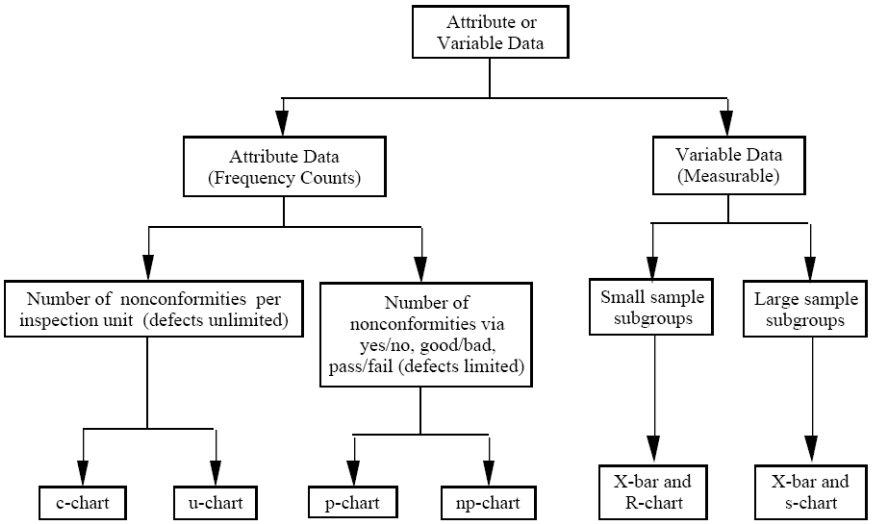

Figure 1.5: Traditional Control Charts based on the types of Data

1.1.4 Problems of High Quality Processes with Existing Methodologies

A physical process is said to be a high-yield/high-quality process if it has a very few $N(t)$, i.e., defect rate is very low, e.g. parts per million (ppm) level or even parts per billion (ppb). In statistics and medical applications, such rare defects are called rare events. The common approach to monitor the fraction of nonconformities of a process, attribute control charts like p, u, np and c, are the well-known charts where the number of a defects $N(t)$ follows binomial, negative binomial or a Poisson processes. However, for high-quality processes where the defect rate is very low (i.e., per million or per billion, especially in the fields of manufacturing of integrated circuits, weapon system, airplane generator, automobile engine and many other automated processes) these charts have certain drawbacks, i.e., high false alarm rate, the negative value of lower control limit, control limits depend on sample size (or sample size is dependent on control limits) and poor approximation to the normal distribution (cf. Chan et al. [2002]). For example, if we construct a control chart where the control limits are based on the Poisson (P), binomial (B), negative binomial (NB) and zero-inflated Poisson (ZIP) processes, the upper control

limit (UCL) and lower control limit (LCL) are given as below:

$$\lambda \pm k\sqrt{\frac{\lambda}{n}} \tag{1.1}$$

$$n\lambda \pm k\sqrt{n\lambda(1-\lambda)} \tag{1.2}$$

$$\frac{r(1-\lambda)}{\lambda} \pm k\sqrt{\frac{r(1-\lambda)}{n\lambda^2}} \tag{1.3}$$

$$(1-\pi)\lambda \pm k\sqrt{\frac{\lambda(1-\pi)[1+\pi\lambda]}{n}} \tag{1.4}$$

where $r, \pi, \lambda > 0$ and k is the width of confidence level, which is usually set 3 for $3-\sigma$ limit (i.e., normal approximation case). Note that when $r = 1$ in the NB case, Equation-1.3 will result into the geometric (G) chart. To avoid the LCL to be zero or negative, the following conditions must be satisfied by each of these processes: $k \leq \sqrt{n\lambda}; k \leq \sqrt{n\lambda/(1-\lambda)}; k \leq \sqrt{nr(1-\lambda)}; k \leq \sqrt{\frac{n\lambda(1-\pi)}{1+\pi\lambda}}$ respectively. Table-1.1 is given for the above discussed processes where λ denotes defect rate, which is part per million (ppm). Thus, to set LCL positive one needs to consider k less than equal to the computed values which are given in Table-1.1. In case of normal distribution, $\pm 3\sigma$ covers 99.73% of the area below the curve, but in case of high-quality processes based on the skewed lifetime distributions, normal approximation does not work. in any probability distribution, "nearly all" values are close to the mean the precise statement being that no more than 1/k2 of the distribution's values can be more than k standard deviations away from the mean (or equivalently, at least 11/k2 of the distribution's values are within k standard deviations of the mean).

Chebychev's inequality guarantees that the probability of a sample from its expected value by more than k standard deviation, is at most $1/k^2$. Hence, to cover 99.73% area, one can construct control limits which will give a larger interval than the one based on the gaussian approximation. Another finer result than Chebychev's inequality is Vysochanskii-Petunin inequality, i.e., if $k > \sqrt{8/3} = 1.63299$ then $P(|X - \mu| \geq k\sigma) \leq 4/(8k^2)$ can be used for the construction of the control chart. However, this result is valid only for uni-modal distribution. Similarly, one can suggest the use of only upper control limit without lower control limit based on the quantiles of the considered distribution. For example, upper 99.73% control limits with $p = 0.01$ as $n = 5, 10, 20, 50$ and 100 are $1, 2, 2, 3$ and 5 for the binomial distribution. Since time is measured in the number of units and due to discreteness, the upper control limit would be meaningless for very small p, e.g. $p = 0.0001$ and $n = 5$, upper control limit is zero. It is observed from Table-1.1, as the numbers of nonconformities increase, the value of the coefficient of width decreases in case of the GM chart while the reverse is true for other processes. Note that the computations given in Table-1.1 are done by assuming the parameters are known. Another way to look at the lower-sided control limit is in term of sample size, i.e.,

Table 1.1: Values of the confidence constant k to get LCL positive for various processes

	p(ppm)					
Process	100	400	800	5000	10000	200000
G	0.999949	0.999799	0.999599	0.997497	0.994987	0.894427
P	0.010000	0.020000	0.028284	0.070712	0.100000	0.447214
Bernoulli	0.010001	0.020004	0.028296	0.070888	0.1000504	0.500000
B (n=100)	0.100005	0.200040	0.282956	0.708881	1.005038	5.000000
B (n=300)	0.173214	0.346479	0.490094	1.227818	1.740777	8.660254
NB (r=3)	0.017321	0.034641	0.048989	0.122474	0.173205	0.774597
NB (r=100)	0.100000	0.200000	0.282843	0.707107	1.000000	4.472136
ZIP ($\pi = 0.2$)	0.008944	0.017888	0.025296	0.063214	0.089353	0.392232
ZIP ($\pi = 0.4$)	0.007746	0.015491	0.021905	0.054718	0.077305	0.333333

$n \geq k^2/\lambda; n \geq k^2(1-\lambda)/\lambda; n \geq \frac{k^2}{r(1-\lambda)}; n \geq \frac{k^2(1+\pi\lambda)}{\lambda(1-\pi)}$. Table-1.2 is given for the sample size calculation for $3-\sigma$ control limits. It is evident from Table-1.2, one needs a very large sample size to inspect the specified nonconformities.

Table 1.2: Sample size (n) requirement with confidence constant $k = 3$ to get LCL positive for various processes

	p(ppm)					
Process	100	400	800	5000	10000	200000
P	90000	22500	11250	1800	900	45
b	89991	22491	11241	1791	891	36
B	89991	22491	11241	1791	891	36
NB (G-r=1)	90000	22500	11250	1800	900	45
NB (r=10)	9000	2250	1125	180	90	5
ZIP ($\pi = 0.2$)	112502	28127	14065	2252	1127	59
ZIP ($\pi = 0.4$)	150006	37506	18756	3006	1506	81

Another drawback with count data is that the boundaries of the cells are arbitrary. If the cells are too narrow, then sampling variability can cause unreliable estimates. If the cells are too wide, then it is possible to miss a trend. Thus, traditional process monitoring techniques for count data are not sufficient for high-quality processes.

Some previous work deals with the transformation of skewed data to be approximately normal (cf. Brouke [1984]). However, it is observed by Santiago and Joel [2013] that the fit in tails of the distribution can be very poor in case of transformation of the data, which affects the ability of a control chart to detect a shift in the process. Moreover, because charts are mostly built under the assumption of equal tail distribution of the monitoring statistics, a transformation that does not provide a symmetric distribution may lead to wrong conclusions when a shift occurs, thus resulting in a biased ARL.

1.2 Scope of the Research

To overcome problems mentioned in Section-1.1.4 (i.e., high false alarm rate, meaningless control limits and dependent on sample size), time-between-events (TBE) charts are very useful. This research is focused on the TBE control charts, especially for high-quality processes. A TBE control chart is defined as a control chart where the sample statistic to plot on the chart is characterized by the time between events of concern. It must be noted that time and event may have different interpretations depending on the particular context. For example, in the manufacturing industry, an event means the occurrence of the nonconforming items while time means time between two nonconforming items; arrival of a customer is an event while time means the time between customer arrival in the service industry, and event means the failure of a system while time means the time between the system failures in the reliability area. An example of process data which could be monitored by a TBE chart (specifically by a cumulative conformance control (CCC) chart) is shown in Figure-1.6, where dots correspond to items as they are produced by the process, T_i is the index of the i-th nonconforming item, the appearance of which is termed "an event", and $X_i = T_i - T_{i-1}$ is the (discrete) time between events, the quantity which is monitored by TBE charts. If the production process is continuous, time

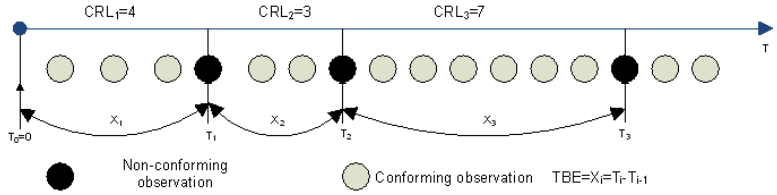

Figure 1.6: Difference between Count and Time-Between-Events Data

is measured by units of produced quantities and an event is the appearance of a defect in the product, so that TBE is the quantity of product between two consecutively observed defects (and a cumulative quantity control (CQC) chart would be used for monitoring). Finally, TBE charts can arise either from continuous monitoring or from samples collected at time intervals. For example, in the monitoring of item conformance, one may inspect all items and time will increase by one at each inspection, or one may sample and inspect n consecutive items using a given sampling interval, in which case the value of time at the moment of inspecting the i-th unit of, let us say, the k-th sample, will be $(k-1)n+i$. In a broader sense, TBE control charts may be categorized into two groups based on data type, i.e., variable and attribute. For the first group, the sample statistic is usually the variable data (e.g. time) observed between consecutive events of concern while for the second group, the sample statistic is usually the attribute or count data.

Control charting techniques based the TBE concept has found applications in many applied areas, especially in high-quality or high-yield processes. However, many practical

issues with TBE control charts need to be addressed sufficiently. This has been the motivation behind this research. The existing work is based on the Poisson process where the distribution of time is assumed exponential. However, the major weakness of the exponential distribution is the constant hazard rate. Examples of the exponential chart could be seen in, exponential chart (see, e.g. Chan et al. [2000], Xie et al. [2002b]), the exponential CUSUM (see, Borror and Keats [2003]) and the exponential EWMA (see, Liu et al. [2007]).

This research will address a few issues, theoretical and practical, concerning the variable data TBE control charts based on more appropriate stochastic processes. The overall objective of this study is to solve the phase-I problems by using some more flexible and comprehensive processes for the TBE data, and thus make the monitoring of high-quality processes where event occurrence rate is low more effectively and efficiently. Specifically, this thesis focuses on several topics regarding TBE charts to fulfill the following targets or objectives of the study.

1. *Development of control charts based on some generalized processes.*
   Most of the previous TBE work is based on the Poisson process where the distribution of TBE is exponential. The exponential distribution has a constant hazard, i.e., memoryless property. However, in reality, the defect risk may increase or decrease, which might lead to process improvement and deterioration. Thus, we need to focus more general stochastic processes to overcome these deficiencies of the TBE charts.

2. *Classical and Bayesian methodologies for parameter estimation.*
   Most of the previous work on control charts has been done by assuming known parameter's value (an engineer has knowledge about the process) but in reality, this assumption is difficult to meet. Classical statistics's techniques are somehow popular in process monitoring but based on very simple processes like normal, Poisson, binomial, negative binomial and the exponential. Using Bayesian methodology, one can include prior information, which will improve analysis. Moreover, sequential updating is very helpful for online process monitoring using Bayesian methodology.

3. *Joint control charts for monitoring frequency and magnitude.*
   There are two types of events, i.e., negative ones and positive ones. A negative event may be a quality problem, a natural disaster or a damaging accident of any type, whilst a positive event may refer to the purchase order of a product, the success of an activity, the profit of business and so on. A statistical process control system can continuously monitor the collected data of an event, which involves the time interval X between two consecutive occurrences and the magnitude M of each occurrence, and accordingly decides whether the situation is under control, out of control or whether any immediate and reinforced action should be taken. Both X

and M are random variables. An increase in the event ratio indicates a move in a loss direction for a negative event which implies a higher than the usual rate in damage, cost, or loss incurred by the occurrences of the events. Hence, an upward shift represents a move in gain positive direction; downward shift results indicate a gain movement toward the negative direction. For example, the loss of market competence of an aged product is indicated not only by the decreased number of purchase orders but also by the decreased amount in each order (cf. Wu et al. [2009b] and Wu et al. [2009a]). Similarly, a fire department must be enhanced not only when the fire outbreaks become very frequent but also when the average damage caused by outbreaks gets very high. Hence, to study such phenomenon, we need to consider some general processes with some advanced techniques of analysis. The existing rate and joint X and M charts to deal such situations are not free from criticism. For example, what to do if each event, especially magnitude is not directly observable? Consider a process where deterioration/ improvement occurs gradually (e.g., atomic power station) and only observable when it crosses a certain threshold. Similarly, it is hard to distinguish and give a quick response, i.e., what has changed, time or magnitude? Moreover, in the rate chart proportional changes of time and magnitude, i.e., ratio M/X, stays constant.

Chapter wise breakup of the thesis is given as: In Chapter 2, we will give a comprehensive overview about the existing literature related to TBE charts. In Chapter 3, a new TBE chart based on the renewal process is proposed, allowing for a general parametric family for the inter-arrival times' distribution. After deriving the control structure for the general class, the Weibull distribution chart is studied in-detail. The effect of parameter estimation is also discussed in Chapter 3. A method to decide whether a shift is in the shape or rate parameter is also proposed. Some real data sets as well as hypothetical studies are included to highlight the effectiveness of the proposal.

Chapters 4 and 5 deal with joint monitoring of time and magnitude based on the renewal reward processes. In Chapter 4, a general mathematical framework for joint monitoring of time and magnitude with a fixed threshold is proposed. The control charts' effectiveness is highlighted numerically. We noticed that to get an explicit form of the first-passage distribution is difficult (and sometime impossible) therefore, we proposed an algorithm to find the control limits for a process monitoring. Similarly, a control chart based on the renewal reward process by assuming a random threshold is proposed in Chapter 5.

Chapters 6 and 7 deal with sequential and adaptive process monitoring. In Chapter 6, we develop a TBE chart based on the nonhomogeneous Poisson process where a power law intensity is particularly assumed. The control structure of the nonhomogeneous TBE chart is designed mathematically and numerically. The effect of parameter estimation

and some real data examples are discussed in this chapter. Contrary to sustained shifts, a new experiment of random and time varying shifts is also conducted in Chapter 6. Since the control limits of the proposed chart are sequentially updated, we proposed a test to stop deterioration or drift of the control limits. By numerical studies, we showed that proposed test improves the detection ability of the nonhomogeneous TBE chart.

In Chapter 7, we proposed a Bayesian predictive chart for the homogenous Poisson process. The problem of sequentially updated control limits and the effect of different shifts are discussed in this chapter. To stop deterioration or drift of the control limits, we proposed a predictive cumulative distribution check (commonly known as a Bayesian p-value). Some suggestions to revise prior are also discussed in Chapter 7. A procedure to revise (select) the false alarm probability after an out-of-control signal (before setting control limits) based on decision theory is also proposed in Chapter 7. Moreover, CUSUM and EWMA charts are also discussed in this chapter.

To test the assumptions of the renewal process, some statistical tests are discussed in Chapter 8. fSome tests for testing exponentiality are also discussed in Chapter 8. Similarly, hazard rate testing, i.e., constant versus increasing or decreasing hazard rate, is also discussed in the same chapter.

Finally, some concluding remarks and future recommendations are given in Chapter 9.

This page is left blank intentionally.

Chapter 2

An Overview of Control Charts for High Quality Processes

Major difficulties in the study of high-quality processes with traditional process monitoring techniques are high false alarm rate and negative lower control limit. The purpose of time between events control charts is to overcome the existing problems in the high-quality process monitoring setup. Time between events charts detect an out-of-control situation without a great loss of sensitivity as compared to the existing charts. High-quality control charts gained much attention over the last decade due to the technological revolution. This chapter is dedicated to providing an overview of recent research, and to presenting it in a unifying framework. To summarize results and draw a precise conclusion from the statistical point of view, cross tabulations are also given in this chapter.

2.1 Introduction

One of the main purposes of control charts is to distinguish between the variation due to chance causes and the variation due to assignable causes in order to prevent overreaction and underreaction to the process. The distinction between chance causes and assignable causes is context dependent. The classification of causes generally evolves over time. A chance cause today can become an assignable cause tomorrow.

For a high-quality processes with a very low defect rate (i.e., per million or per billion, especially in the fields of manufacturing of integrated circuits, weapon system, airplane generator, automobile engine and many other automated processes), there are certain drawbacks in the traditional process monitoring techniques, i.e., high false alarm rates, negative values of lower control limits for strictly positive monitored quantities, undesirable dependencies between sample size and control limits (when admissibility of the latter is enforced) and poor approximation to the normal distribution (cf. Chan et al. [2002]). There are some approximations available in the literature, however these approximations

have certain drawbacks. Recently, Emura and Lin [2015] compared five frequently used rules for n and p required for the normal approximation to the binomial distribution, which is relevant for the monitoring of nonconforming units. They also proposed a new rule for approximation, i.e., $np \geq 10$ and $p \geq 0.1$ or $np > 15$, which works well compared to existing ones. However, the problem is not yet solved for other distributions.

To overcome these problems of traditional process monitoring techniques, an alternative is to use time-between-events (TBE) control charts (cf. Xie et al. [2002a]), which are the focus of this review (for a general introduction to SPC and current research problems, see instead Woodall and Montgomery [2014]).

A self-explanatory flowchart about the implementation of TBE charts is given in Figure-2.1.

To make the review more statistically informative, a cross tabulation method with the aid of graphs is used. Results are summarized in the conclusion section. We reviewed 114 articles related to the continuous and discrete TBE concept. Approximately 63% of the reviewed articles deal with attribute data. As for parameter estimation, only 20.2% of the reviewed articles is concerned with it, using either maximum likelihood, Bayesian or nonparametric methods. As for the underling process distribution model, the geometric distribution is being commonly used for attribute data, appearing in 21% of all articles, while the exponential distribution, for the continuous case, is present in 23% of articles.

The rest of this chapter is organized as follows: Section 2.2 deals with the CCC and continuous TBE charts, while the control charts based on approximations are discussed in Section 2.3. Nonparametric control charts are discussed in Section 2.4, while Section 2.5 is devoted to the EWMA and CUSUM charts for high-quality processes. Economic design studies of high-quality control charts is discussed in Section 2.6 while some information on other related charts, which are very close to high-quality charting methodology, is given in Section 2.7. The use of Bayesian methodology in SPC setup is discussed in Section 2.8 while Section 2.9 deals with control charts applications in health studies. To assess the control charts' performance some measures are discussed in Section 2.10. Some concluding remarks and future suggestions to researchers are given in Section 2.11.

2.2 Time-Between-Events Control Charts

Depending on the type of data, different authors used different names for TBE chart based on nonconformities distribution, e.g., geometric/exponential cumulative quantity control (CQC) chart, cumulative count of conforming (CCC) chart, conforming run length (CRL) chart, etc (see, Albers [2010]).

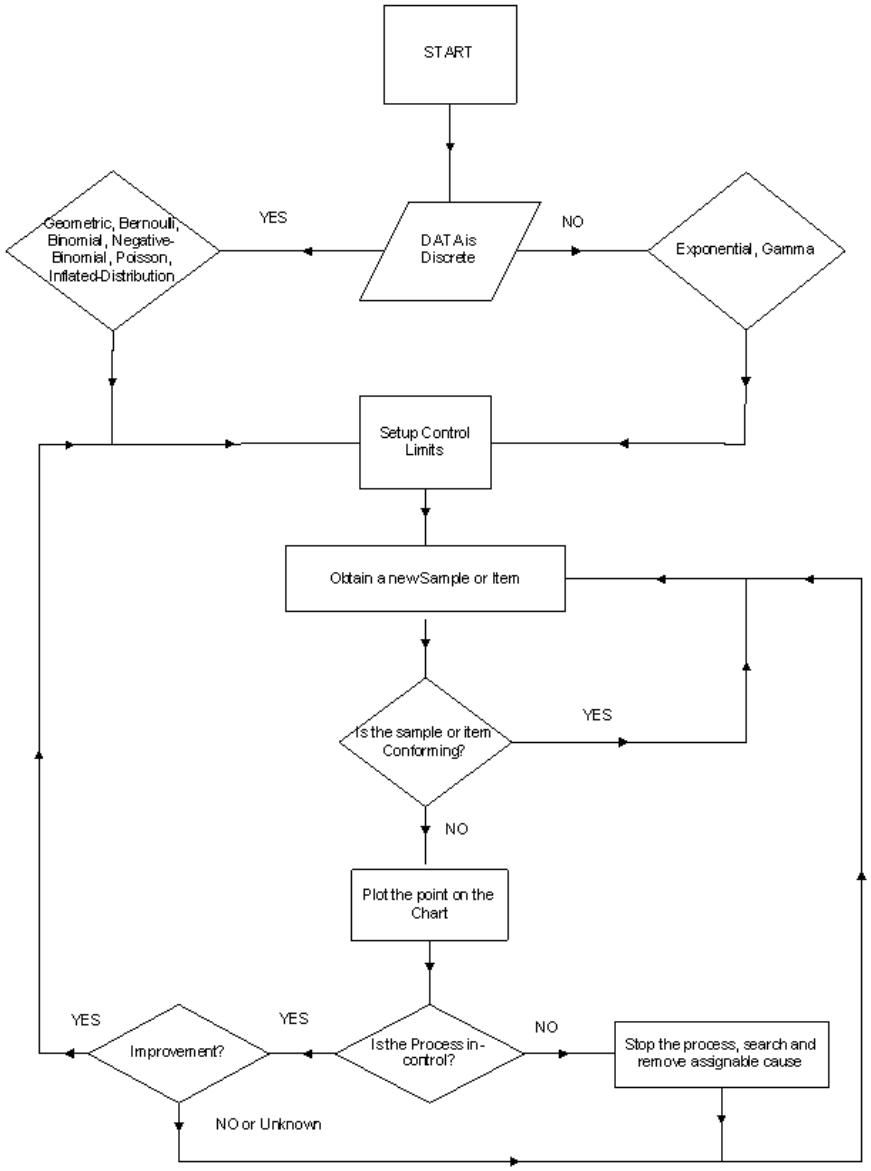

Figure 2.1: A charting procedure of TBE charts

2.2.1 CCC Charts

Origin of the CCC chart

The story begins with Calvin [1983], who proposed the first high quality control chart for geometric counts based on the geometric process. The items are inspected one by one in each sample, and the cumulative number of sampled items is plotted against the index of the sampling interval until when either the sample is exhausted or a nonconforming item appears; at this point the counting is restarted. If the cumulative count falls between the control limits, then the process is considered to be in statistical control. Goh [1987] studied the properties of the geometric chart and named it cumulative conforming control (CCC) chart. He recommended to plot cumulative counts only when a nonconforming

item appears. Thus, the CCC charts differ from Shewhart-type control charts in that in the former each time a sample is inspected one may not obtain a set of data points for the chart statistics as in latter.

Generalization of CCC charts

Chan et al. [2003], inspired by the idea of double sampling procedures in acceptance sampling, proposed a two-stage CCC-chart in order to improve the performance of the one-stage CCC-chart. Analytic expressions for the average number inspected (ANI) of this two-stage CCC-chart are obtained and compared with a previous results provided by Chan et al. [1997b].

Lai et al. [2000] studied the high quality process in the presence of serial dependence and developed a control chart to handle this problem. Later, Adnaik et al. [2013] employed the idea of Lai et al. [2000] and proposed a control chart in which consecutive samples should be distant enough in time, so that for all practical purposes, they can be considered as if they were independent.

Lai [1997] extended the idea of Calvin [1983] and studied some properties of CCC charts where the TBE is the waiting time for the appearance of the first pair of a conforming and a nonconforming unit. Di Bucchianico et al. [2005] used CCC-r (a generalization of the geometric CCC-chart) based on a negative binomial distribution. He et al. [2012] proposed what they call a counted-number between omega-event attribute control chart, abbreviated as CBΩ chart. They defined omega as: an event which denotes that one observation falls into some certain defined interval. The purpose of the chart is to monitor the number of consecutive parts between r successive omega events. The He et al. [2012] proposal is not so much different from the well known CCC-r chart approach. The only difference is the discretization of events that come from continuous normal data, i.e., instead of considering continuous data, they are classifying them as either conforming or nonconforming, and use a CCC-r chart.

Noorossana et al. [2007] showed that the conditional procedure developed by Kuralmani et al. [2002] is misleading because the properties of the conditional procedure were determined based on an assumption of independence, by ignoring the information available in the previous run, which underestimates the true ARL for the CCC chart. They incorporated the values of the previous runs or observations into the decision rule using conditional probability, and modified the design of CCC chart.

Chang and Gan [2007] proposed an improved Shewhart np chart by using run rules for monitoring high quality processes. They observed that runs rules are appropriate for monitoring a distribution which is approximately unimodal and symmetric. Acosta-Mejia [2013] suggested two geometric charts (simple and run sum chart) with runs rules. He concluded that the proposed charts could be compared favorably with the two sided

geometric chart based on probability limits when the fraction is very small.

Traditional cumulative conformance count (CCC) charts are used when the items from a process are inspected one-at-a-time following the production order. In recent years, the CCC chart has been generalized to accommodate some industry practices, where items from a process are inspected sample by sample and not according to the production order. (In case of variable sample size, the performance of the chart should be measured by the average number/length inspected (ANI/ALI) instead of ARL). Lai and Govindaraju [2008] noticed that in the case of attribute high-quality processes, although a longer in-control ARL is ensured by design, the variance of the run length distribution may also be large for such a design. They emphasized to compare coefficients of variation (CVs) instead of comparing the ARL of two different charts directly. They showed that for the fixed false alarm rate, the CV does not drop very much when the proportion of the defective items increases drastically. The same approach is later used by Chen and Cheng [2010] to derive the unbiased design of CCC-r charts based on negative binomial process.

For over-dispersed data, He et al. [2006] introduced a control chart for monitoring the high-quality processes based on the generalized Poisson distribution. The performance of the proposed control chart is evaluated in term of ARL. To validate the use of the generalized Poisson distribution, they recommended to test it against the Poisson distribution by means of formal hypothesis testing. Aebtarm and Bouguila [2010] proposed an optimal bivariate Poisson chart for monitoring two correlated characteristics of defects simultaneously. The authors considered the word 'optimal' in the sense of finding a bivariate Poisson probability set such that the in-control ARL is above a prescribed level. By testing their proposal under different situations and comparing it with some previously proposed charts, such as the NORTA (see Niaki and Abbasi [2007]), they concluded that it is a good candidate for high-quality process monitoring.

Attribute charts seen as TBE charts

Wu et al. [2009d] used attribute inspection for normal process monitoring and suggested an np_x chart. Since the monitoring variable is continuous, in order to employ the idea of attribute inspection and enhance the sensitivity of the proposal, they introduced warning limits along with the traditional control limits. The warning limits help in making the decision whether the inspected units are conforming or not, i.e., if the value of an item lies above or below the warning limit declare it as nonconforming. If the number of nonconforming units in a particular sampling interval is greater than the specified level of nonconformities, the said process is declared as out-of-control. To have a desired in-control run length, Wu et al. [2009d] optimized the warning limits and concluded that the np_x chart outperforms the traditional $\bar{X}$ chart for the same inspection cost. Later, Ho and Quinino [2013], motivated by the simplicity and performance of the np_x control chart

of Wu et al. [2009d], proposed an np_S^2 control chart based on the binomial distribution, to monitor the variability of a process. The comparison study is given with some traditional control charts.

Gadre and Rattihalli [2005] proposed three group-inspection-based multi-attribute control charts to identify process deterioration, where time between non-acceptable groups (that is, samples) is monitored. Their proposed charts are: the Multi-Attribute np (MAnp) chart, the Multi-Attribute Synthetic (MASyn) chart and the Multi-Attribute Group Runs (MAGR) chart. It is shown numerically that MAGR chart performs better than the MA-np and MA-Syn charts for deterioration detection. Later, Gadre and Rattihalli [2008] generalized the work of Gadre and Rattihalli [2005] and proposed a unit and group run chart to identify the increase of nonconformities in multi-attribute process. Haridy et al. [2014] proposed a multi-attribute synthetic np (MSyn-np) chart to monitor a multi-attribute system. To read more about multi-attribute charts, see Topalidou and Psarakis [2009].

Variable sample size charts

Chen and Chen [2012] improved the power of the CCC chart to detect process changes by generalizing it to variable sample size (VSS) for geometric process. To define VSS, let n_1 and n_2 be the minimum and maximum sample sizes, respectively, such that $n_1 \leq n \leq n_2$ while keeping the sampling interval fixed at h. The decision to switch between the maximum and minimum sample size depends on the position of the prior sample point on the control chart. If the prior sample point falls into the safe region, the minimum sample size n_1 will be used for the current sample point and if the prior sample point falls into the warning region, the maximum sample size n_2 will be used for the current sample point. Finally, if the sample point falls into an action region, then the process is considered to be an out-of-control. Their proposed methodology works well as compared to existing ones in the literature. However, their adopted approach for the calculation of the average number of observations to signal (ANOS) is the same as suggested by Kotani et al. [2005] for the EWMA charts based on the negative binomial in high-quality processes, except for the VSS feature. Later, Chen [2013b] employed the idea of Chen and Chen [2012] and proposed a generalized CCC (GCCC) chart based on the variable sampling interval (VSI) which also takes into account the correlation between observations. The comparison of results helps us to conclude that the presence of correlation has significant effect on the control chart detection ability. Also, using the VSI scheme improves the detection speed of chart in detecting changes of the fraction nonconforming than the fixed sampling interval.

Bersimis et al. [2014] proposed a high-quality control chart which suggests to declare the process out-of-control by utilizing information available at different stages, i.e., the

number of conforming units observed between the $(i-1)th$ and the ith nonconforming item and the number of conforming items observed between the $(i-2)th$ and the $(i-1)th$ nonconforming item. To accomplish this task they proposed a compound decision rule. By a numerical study they showed that their proposal works effectively.

Parameter estimation

Zhang et al. [2013] addressed the problem of unknown parameter estimation in a geometric chart for high-quality processes. They used the standard deviation of the run length (SDRL) and the standard deviation of the number of inspected items to signal (SDNIS) to show that much larger phase-I sample sizes are required in practice than stipulated by previous research. They recommended a Bayes estimator for the in-control proportion nonconforming to take advantage of practitioner knowledge and to avoid estimation problems when no nonconforming items are observed in phase-I sample. Recently, Chiu and Tsai [2013] investigated the impact of estimated nonconforming fraction in a one-sided CCC chart based on a geometric process. The run length distribution is derived as well as the conditional probability of a false alarm rate (CFAR). With the help of a simulation study, they showed that CFAR decreases for large estimated values of the parameter associated with nonconforming.

Zhang et al. [2014b] investigated the performance of the CCC chart with VSI in presence of estimation effect. The optimized design parameters of the CCC chart with variable sampling intervals are obtained by using Bayesian methodology. The average time to signal (ATS) and its standard deviation (SDTS) are calculated for both in-control and out-of-control situations.

Biasedness of ARL

Chen [2009] motivated by the non-maximal and biased properties of the CCC-r chart (non-maximal in the sense that the chart might not quickly detect the upward shift of p from its nominal value p_0, while biasedness means an inflation in ARL), developed a procedure to overcome these problems. The basic idea of Chen [2009]'s approach is to find a control interval $I = [L, U]$ in an admissible set S such that the slope of ARL_0 is approximately equal to zero. Later, Chen [2013a] extended his previous work reported in Chen [2009] to obtain control limits with near-maximal and near-unbiased ARL, also taking estimation effect into account. Chen [2013a] concluded that simulated ANI's using the MUVE (minimum unbiased variance estimator) are smaller than the MLE (maximum likelihood estimator) when $p > p_0$ while the simulated ANI's using the MUVE are larger than the MLE when $p < p_0$. Hence, the MVUE is better than the MLE for detecting the process deterioration while the MLE is better than the MVUE for detecting the process improvement.

Control charts with inspection error

In the usual implementation of CCC chart, it is assumed that the inspection is free of error. However, this assumption is not true in general and may have a significant impact on the interpretation of the control charts and their limits. To deal with this problem, Ranjan et al. [2003] extended the work of CCC chart in presence of inspection error. They concluded that the probability of classifying a conforming item as nonconforming has a greater impact on the average run length (ARL) than the probability of classifying a nonconforming item as conforming.

Regression charts

An exception alternative to CCC or CQC charts is monitoring a high quality process with the help of regression methodology. Steiner and MacKay [2004] introduced this technique based on the explanatory variables which cause the defects, and used the logit regression. Although their approach is new, it is difficult to completely specify all the explanatory variables, especially for a person who is not an engineer.

Change Point

Amiri and Khosravi [2012] proposed a maximum likelihood estimator for the change point of the nonconforming fraction in the high-quality process with a linear-trend based on the geometric process. The proposed estimator is compared with the estimator based on a single step change of the process nonconforming fraction. The results supports that the linear-trend based estimator performs better, especially when a linear trend disturbance is present in the process.

2.2.2 Continuous TBE Charts

Introducing continuous time through CQC charts

An important generalization in the idea of Calvin is the introduction of the cumulative quantity control (CQC) chart which was introduced by Chan et al. [2000] based on the homogeneous Poisson process. *They noticed that the CQC chart can be used no matter whether the process defect rate is low or not, and when the process defect rate is low or moderate the chart does not have the shortcomings as the* c *and* u *charts.* CQC chart doesn't need a rational subgroup (a group of units produced under the same set of conditions, i.e., phase-I data set) of samples which is necessary in usual charts, hence the new chart is appropriate for monitoring manufacturing processes. Later, it was observed by Chan et al. [2002] that sometimes in the CQC chart the interpretation of control limits becomes cumbersome and to resolve technical inconvenience related to plotting, Chan

et al. [2002] proposed a cumulative probability control (CPC) chart for exponential and geometric processes. In the new proposed chart, the cumulative probability of the TBE is plotted against the sample number and since the vertical axis is always between zero and one, its interpretation is easy as compared to CCC and CQC.

Generalizations

A generalization of the CQC chart was proposed by Zhang et al. [2007a] to handle the situation where one has to wait until the specified number, i.e. *rth*, of event occurrences. Since in case of the Poisson process the distribution of time is exponential, waiting up to the *rth* event leads to an Erlang distribution (gamma distribution with an integer shape parameter). They also discussed the role of fixed and random shifts for control chart development.

Fang et al. [2013] proposed three synthetic-type control charts to monitor the mean TBE of a Poisson process. A synthetic control chart is particularly based on a T-chart which is used for monitoring two different types of statistics, i.e., the location and variation or some other summaries. In process monitoring, synthetic type charts are developed by combining the regular Shewhart or memory type charts with conforming run length (CRL) chart. The first proposed chart of Fang et al. [2013] is a combination of an ordinary Erlang chart with a CRL-chart, the second is an exponential and a group CRL-chart, while the third is an Erlang and a group CRL-chart. Their proposal outperforms in detection of small to moderate shifts. Recently, Fang et al. [2015] extended the work of Fang et al. [2013] and proposed a generalized group run TBE chart named $GGR_g - T_r$ (where r denotes the time until the r-th event occurrence and g denotes the index of the CRL group), to monitor the mean TBE of a homogenous Poisson process. With the help of a numerical study, they showed that the choices of $r = 1$ or $r = 2$ are good for the detection of a large size shifts, while $r = 3$ or $r = 4$ are appropriate for small to moderate shifts. They also noticed that increasing r for fixed g does not improves the performance of a control chart. However, increasing g (but not above 5) for the same r improves detection speed.

Santiago and Joel [2013] used supplementary runs rules to identify whether the process is out-of-control or not for the TBE chart (called t-chart) based on the exponential distribution. It is observed by Santiago and Joel [2013] that the fit in tails of the distribution can be very poor in case of transformation of the data, which affects the ability of a control chart to detect a shift in the process. Moreover, because charts are mostly built under the assumption of equal tail distribution of the monitoring statistics, a transformation that does not provide a symmetric distribution may affect the ARL in the wrong direction when a shift occurs, thus resulting in a biased ARL.

Xie et al. [2011] considered a bivariate TBE and proposed a control chart. They used a Gumbel's bivariate exponential distribution to monitor the mean vector of TBE. However, Xie et al. [2011] did not give sufficient justification about the related counting process which has a bivariate distribution of time.

Aslam et al. [2014] introduced an exponential TBE control chart based on the concept of repetitive sampling by employing two control limits, i.e., warning limits and action limits. With the help of a numerical study they showed that repetitive sampling improves the control chart performance. Later, Aslam et al. [2015] introduced a t-control chart for exponentially distributed quality characteristics using multiple dependent state sampling. The proposed control chart has double control limits as the repetitive sampling chart has, with two control coefficients. They used a $k\sigma$ approach to define control limits and showed that their proposal works effectively under different conditions.

Comparisons among TBE charts

A comparison study between the Shewhart exponential, the gamma, and the exponential CUSUM charts, is also given in Zhang et al. [2007a]. They concluded that the gamma chart is more sensitive than the exponential chart. However, the performance of a gamma chart is comparable with the optimally designed exponential CUSUM chart only with waiting up to the 4th event, i.e., $r = 4$.

Due to limitations in resources and working conditions, sampling inspection has to be adopted for many SPC applications, especially when testing is destructive and/or expensive. For this purpose, Qu et al. [2014] used sequential analysis and curtailment techniques for the TBE control charts.

Dogu [2014] used a comparative approach to investigate the performance of the change point methodology with the TBE control charts, i.e., CQC-r, EWMA and CUSUM charts. The change point parameter for the gamma process was estimated using the maximum likelihood method. Dogu [2014] recommended the use of CQC-r chart in the cases where the prediction of the shift is difficult, the exact change detection is necessary and the assignable cause identification is also difficult. However, if the magnitude of shift is small, the exact change detection is not the primary focus, the design parameters are easy to define and collecting more information about the change is costly, then EWMA and CUSUM charts are recommended.

Parameter estimation

Kumar and Chakraborti [2015] considered the robustness problem of the in-control alarm probability using phase-I data, i.e., how large phase-I observations should be considered from an exponential distribution to estimate the unknown mean and have a desired in-control performance. They proposed a two-sided control chart for monitoring the median

based on the quartiles, i.e., the lower control limit is based on the distance between the median and a multiple of the spacing between the median and first quartile, while for upper sided chart it is the distance between the median and a multiple of the spacing between the median and third quartile. With the help of numerical comparison with some existing charts, Kumar and Chakraborti [2015] showed that the new proposal is more in-control robust. Kumar and Chakraborti [2014a] presented improved results for t_r chart by considering the impact of parameter estimation on the performance of the phase-II t_r chart. They observed that the practitioner-to-practitioner variability (i.e., the uncertainty in the phase-I parameter estimation) may determine control chart performances which are far from nominal values. As a remedy, they proposed a rule for the phase-I sample size such that the ARL (conditional on the estimated parameters) is within a given distance from the nominal ARL with a certain high probability. They considered MLE and UMVE estimates and noticed that using UMVUE, significantly less phase-I samples are required to get desired control chart performances.

Biasedness of ARL

When the process is in-control the ARL must be equal to a pre-defined fixed value, say $ARL_{in-control} = ARL_0$, and when the process is out-of-control the ARL must be smaller than this fixed nominal value whenever possible, i.e., $ARL_{out-of-control} \leq ARL_{in-control}$, a property known as unbiasedness. Zhang et al. [2006] noticed that the exponential chart designed with the conventional approach has the disadvantage that an ARL value may increase when the process deviates from the nominal value. Thus, Zhang et al. [2006] proposed an ARL unbiased design approach for phase I and II. They adopted a sequential sampling scheme which provides a self-starting feature and can improve significantly the ARL performance. Later, Chen and Cheng [2011] extended the work of Zhang et al. [2006] and studied the effect of unbiasedness with unequal tails. Cheng and Chen [2011] incorporated the runs rules into the CQC chart design to study its ARL unbiasedness. Recently, Yang et al. [2015b] also adopted the same procedure as presented in Zhang et al. [2006], to study the unbiasedness of the exponential chart based on the average time to signal performance measure. They studied the phase-I and phase-II performance of the two-sided control chart by using an unbiased estimator of the parameter and gave a comparison study to highlight the advantages/improvements of the new proposal.

2.2.3 Joint control charts for monitoring frequency and magnitude

In the usual TBE charts implementation, the user continuously monitors the collected data of an event, which involves the time interval X between two consecutive occurrences.

However, there are many situations where a magnitude M is attached to each TBE occurrence. The ordinary TBE charts are incapable to handle such a situation. An example of such systems is the monitoring of a fire department which must be enhanced not only when the fire outbreaks become very frequent but also when the average damage, caused by outbreaks, gets very high. To monitor such events, one needs to consider marked Poisson processes instead of ordinary Poisson processes. Wu et al. [2009b] proposed control charts which jointly monitor TBE and the associated magnitude, without clearly mentioning the marked Poisson assumption. Later, Wu et al. [2009a] proposed a single control chart to monitor TBE and magnitude data by considering the ratio M/X. Wu et al. [2009a] compared the control chart performance with Wu et al. [2009b] and showed that joint monitoring (the so called rate chart) is more efficient than the separate control charts. Liu et al. [2009] extended the work of Wu et al. [2009b] by considering the associated magnitude as discrete. Liu et al. [2010] also proposed a joint control chart by considering a truncated Poisson distribution for magnitude. The use of the exponential distribution is common in all the above cited papers on time and magnitude charts.

2.3 TBE charts with approximations

It is noted by several authors that the high-quality chart based on the geometric distribution is quite slow to pick up relatively mild deteriorations of the process for the small parameter value, which is unacceptable, especially in health care. To overcome this problem, a negative binomial process chart was proposed (cf. Ohta et al. [2001b], Wu et al. [2001] and Zhang et al. [2007a]). However, the problem of the optimal choice of r (r is denoting the numbers of nonconformities in a given sample of size n) with estimation effect in a negative binomial case, was unanswered in existing literature. Albers [2010] motivated by this problem, noticed that a quite large sample size is required for the optimal choice of r in the presence of estimation effect (optimality is determined by the achievement of a desired run length). The same issue was addressed by Albers and Kallenberg [2004a] without estimation effect. Albers [2010] obtained the approximated optimal value of r and numerically showed that his proposal works very well. Later, the author extended results in Albers [2011a] to the case of the binomial process. Joekes and Barbosa [2011] also introduced a high quality control chart based on the Cornish-Fisher expansion corrected to order $n^{-1.5}$.

In industry, most systems are regularly maintained to prevent future sudden failures. The usual reliability techniques are not helpful for the detection of early warnings of system failures, and thus an alternative is to study such systems with control charts. To study the properties of regularly maintained systems based on an approximation of the Weibull distribution by an exponential distribution, Khoo and Xie [2009] used a TBE

control chart approach. Earlier, Xie et al. [2002b] also presented a control chart for reliability monitoring.

2.4 Nonparametric Control Charts

The standard control charts are very sensitive to estimation effects and deviations from the normality assumption. To choose the most appropriate monitoring statistics, the first step is the choice of the underlying distribution. In reality, this choice is often one of many possible alternatives that fit the data equally well (or equally bad). An alternative option is represented by nonparametric control charts.

2.4.1 High-quality processes

Albers [2011b] proposed a nonparametric version of the negative binomial chart for the high-quality process monitoring. To minimize the effect of estimation on the proposed MAX chart performance measure, Albers [2011b] suggested a correction factor. Later, Albers [2012a] made a comparison study between the MAX and CUMAX for the high-quality process monitoring. He concluded that both charts show very little difference in performance and the choice of MAX or CUMAX remains with the practitioner or the user.

For bivariate process monitoring, the only contribution to nonparametric control charts for high-quality processes is that of Albers [2012b], who studied these charts for the simultaneous monitoring of two quality characteristics.

2.5 EWMA and CUSUM

Control charts with Shewhart structure are commonly used for the detection of shifts which are larger in size (i.e. $\geq 1.5\sigma$), and they have the memoryless property (do not take into account previous data and just deal with current information). To detect small size shifts ($\leq 1.5\sigma$) and to get benefit from memory of existing data, the exponentially weighted moving average (EWMA) and cumulative sum (CUSUM) control charts are preferred.

2.5.1 EWMA and CUSUM Charts using the nonconforming idea

Gan [1993] proposed a CUSUM chart for the binomial distribution and an optimal design strategy, which allows an easy way to determine the parameters of a CUSUM chart. The optimal choice of n, the relationship between the CUSUM chart and the sequential

probability ratio test are also investigated in Gan [1993]. Wu et al. [2008] proposed a CUSUM for the detection of an upward shift, while Brouke [1984] proposed a CUSUM control chart based on non-transformed geometric counts, which is effective for the $p_0 \geq 0.002$. Assuming the feasibility of 100% continuous inspection, Reynolds Jr and Stoumbos [1999] proposed a CUSUM control chart which is quite effective for $p_0 > 0.01$. Chang and Gan [2001] studied the CUSUM chart based on the geometric, binomial and Bernoulli distributions. They found that the use of CUSUM is effective when p_0 is as small as *0.0001*, which is close to the actual fraction nonconforming level seen in many high quality processes. Later, Yeh et al. [2008] proposed an EWMA control chart based on geometric, binomial and Bernoulli counts by extending the idea of Shu et al. [2007]. Yeh et al. [2008] concluded that an EWMA based on geometric counts is better for the detection of small gradual changes than the CUSUM.

Since the variance of the Bernoulli/binomial is also a function of the p_0 parameter, it significantly affects the performance of the control chart especially in phase-I. To alleviate this problem, Spliid [2010] proposed an EWMA chart based on Bernoulli counts with a variance stabilizing transformation. The distribution of the transformation is derived and some comparisons are also made to the double square root transformation of the normal distribution. Spliid concluded that the proposed EWMA works better than the CUSUM. Duran and Albin [2009] proposed a two-sided CUSUM Arcsine method which is efficient for the detection of both large and small shifts.

Reynolds [2013] gave a solution to the equations used in defining the Markov chain for the Bernoulli CUSUM chart (for more detail about attribute control charts, we refer the interested readers to a recent review provided by Woodall [1997]).

Count data are often analyzed under the assumption that they follow a Poisson distribution. This distribution is very useful, but it is not appropriate when data are overdispersed. Chen [2012] introduced an EWMA chart based on the Poisson geometric distribution for the compound Poisson process. Mavroudis and Nicolas [2013] discussed the efficiency and verified the performance behavior of the one-sided EWMA control chart for high-quality processes. Their designed chart is an efficient tool for detection of both upward and downward shifts for the non-transformed geometric process. Later, Mavroudis and Nikolaos [2011] extended their work on the two sided EWMA to one-sided EWMA charts.

2.5.2 CUSUM and EWMA for continuous TBE

Control charts for time monitoring

Borror and Keats [2003] studied the robustness of the TBE CUSUM. They reported an ARL-based study for the Weibull (fixed scale parameter) and the Lognormal (for fixed σ) distributions. They showed that the TBE CUSUM is more robust for different sets of

parameter values in different cases. They also noticed that there is a significant relationship between the skewness of the time-between-failure distribution and the robustness of the TBE CUSUM. However, recently Shafae et al. [2015] showed that the robustness with respect to the shape parameter of the Weibull distribution is not as good as claimed in the literature about CUSUM. Due to the significant impact of the shape parameter on the control chart performance, they concluded that the value should be chosen/estimated carefully.

Both EWMA and CUSUM are used for detection of a small size shift; however, it is not clear which one outperforms for TBE monitoring. For this purpose, Liu et al. [2006b] compared the TBE charts and concluded that for the processes with small improvements, exponential EWMA charts are slightly better than the exponential CUSUM charts. Furthermore, the EWMA and the CUSUM are better than the usual upper-sided CQC and CQC-r charts. On the contrary, for the lower side, an exponential TBE chart is better than CUSUM and EWMA. Liu et al. [2004], in a work on a general architecture for online process monitoring, found that a simple chart (CQC-r) is more robust for small size shift than EWMA and CUSUM in the two-sided case.

Ozsan et al. [2010], motivated by the estimation of parameter and its effect on the control chart detection ability, studied properties of the TBE EWMA chart based on the exponential distribution. Zhang et al. [2014a] also addressed the problem of estimation in CUSUM chart based on the exponential TBE.

Frequency and time monitoring

Qu et al. [2011] proposed a combined Shewhart-T and a TCUSUM chart to monitor the time interval T between the occurrences of an event. They showed that this integration of T and TCUSUM improves the overall performance over the individual charts. Wu et al. [2010a] proposed a CUSUM chart, called the TC-CUSUM, for monitoring a negative or hazardous event. Their proposal uses the information from both sources, i.e., TBE and the size of each occurrence. They used the Poisson distribution for the magnitude of events while the exponential distribution is used for TBE. Recently, Qu et al. [2013] proposed a generalized CUSUM (GCUSUM) for simultaneously monitoring the time interval and magnitude of an event for which they assumed a normal distribution. In a comparison study, they showed that the new proposal is more efficient in the detection of shifts as compared to existing ones.

2.6 Economic Design of Control Charts

The economic design approach to control charts advocates the determination of the control chart design parameters based on a cost-minimization model that takes into account all

costs accepted by the choice of these parameters. Although this approach is useful, work in this area is very slow as pointed by Woodall and Montgomery [2014]. This is happening due to complex optimization procedures and poor statistical properties of the economic models, which are, in general, incapable to detect process improvements as noted by Woodall and Montgomery [1999].

2.6.1 Economic design of CCC charts

The comparative study of Ou et al. [2012] not only compares the detection speed of the charts, but also investigates their robustness in performance. They also studied the probability distribution of the mean shift explicitly, because it is an influential factor in an experiment on the chart performance as the values of the shift distribution parameters are changed following a factorial design. Yilmaz and Burnak [2013] developed a specific cost model and with the help of a numerical study they showed that it works well as compared to existing ones.

It is well known that, as r gets larger, the CCC-r chart becomes more sensitive to small upward shifts. However, too many observations are required to obtain a plotting point on the chart, and the related cost is fairly high. Thus, to trade off this problem, Ohta et al. [2001a] determined the optimal value of r for the CCC-r chart using an economic model. They obtained expected profits per cycle using the proposed optimal design and compared it with existing methods. They also studied the performance of the proposed model in the case of cost parameter misspecification. Later, Zhang et al. [2008] also proposed an economic model to monitor the cumulative number of samples inspected until a nonconforming sample is encountered. Zhang et al. [2008] model is useful especially when one is interested in inspection of samples or lots without preserving the original production order.

2.6.2 Economic design of continuous TBE charts

Zhang et al. [2011a] developed an economic model for the exponential chart for monitoring TBE data. The design of the proposed model takes into account the random characteristic of the process shifts and therefore better reflects the actual process conditions. The random process shift is modelled by a Rayleigh distribution.

The fabrication of a product usually goes through several process stages in series and integration of all these stages constitutes a multistage manufacturing system. Using valuable information available at each stage of the process, one can enhance the detection ability of control charts. Zhang et al. [2011b], inspired by this concept, presented an economic design of the control chart which also takes into account multistage information as it becomes available at each stage of the process.

2.7 Some other Control Charts for Count Data

From now on, we will examine contributions from the literature that are not about TBE control charts, with some exceptions. They have been included in this review because one of the following reasons: they are recent, introduce generalizations, and are based on non-mainstream approaches.

2.7.1 Control charts based on transformations

A traditional approach in the development of control charts is based on the transformation of data from a skewed to an approximately normal distribution, and then use the normal theory for the control chart development. Liu et al. [2006a] proposed a CUSUM scheme for monitoring the TBE by transforming the exponential distributed data to approximately normal distribution shape. Later, Liu et al. [2007] proposed an EWMA chart to monitor the exponentially distributed TBE data by using the double square root (SQRT) transformation.

To monitor the multi-attribute high quality processes, the presence of correlation between different attributes is an important problem which affects the control chart detection ability if multivariate normality is incorrectly assumed. Recently, Niaki and Abbasi [2007] proposed two new methods that are based on the transformation technique to deal with non-normality. The first method is the root transformation X^r, i.e., find r such that the data set skewness becomes almost negligible. The second method is transforming the data using the inverse of the NORmal-To-Anything (NORTA) transformation/algorithm. With the help of a numerical study they showed that NORTA transformation remarkably improves the monitoring of a process which has some dependence structure.

2.7.2 Other charts

Chen et al. [2008] proposed a control chart to monitor attribute data based on a generalized zero-inflated Poisson (GZIP) distribution. Katemee and Mayureesawan [2012] developed a control chart based on the zero-inflated Poisson (ZIP) distribution which is a special case of the Chen et al. [2008] proposed chart. Katemee and Mayureesawan [2012] studied the control chart performance in detail and concluded the proposal is more effective for over or under dispersed data than the ordinary c-chart. We refer the interested readers to Saghir and Lin [2015] for the control charts based on the dispersed count data.

Wang [2009] compared different existing approximations for p charts. He also proposed a new approximation which can substantially improve the performance of the existing control chart, especially when the nonconformities rate is very low. Sant'Anna and Caten [2012] proposed a beta chart based on the beta probability distribution. The comparative

study showed that the Beta approximation to the Binomial distribution is more appropriate than the normal approximation. They also highlighted that the proposed chart is more sensitive in the detection of both in-control and out-of-control situations.

Xie and Goh [1997] introduced probability control limits for the geometric distribution which is not different from the CCC chart idea.

2.8 Bayesian Control Charts

The standard (frequentist) methods for SPC depend on long run stability to establish a pattern against which further samples may be compared, hence very short production runs would severely affect the performance of these methods. The use of the Bayesian methods has an advantage due to the inclusion of prior knowledge about the process gained through experience. Also, the sequential use of Bayes theorem is helpful in online process monitoring.

2.8.1 Bayesian Charts for non-high-quality processes

Short Run Production Controlling

Woodward and Naylor [1993] used Bayesian methods for short run production based on the normal process. They compared the performance of a Bayesian significance test with a Bayesian two-stage test and concluded that the Bayesian significance test performs slightly better. They minimized the cost of inspection in the two-stage test using a quadratic loss function.

Sturm et al. [1990] proposed a process control procedure based on the sufficient statistics for short run processes where high volume/intensive data is available. To effectively control the mean of the normal distribution, they introduced weighted empirical Bayes estimators for the mean and the variance. For the detection of an abrupt change, a two-sample z type test based on the posterior distribution, is also developed. Later, Sturm et al. [1991] used a similar approach for real time controlling.

Wu et al. [2015] proposed a conjugate Bayesian approach in low volume and multi-batch process monitoring. The control limits are calculated using Bayes estimates of the mean and the variance. They also compare the Bayesian and the traditional approach.

Shewhart Charts

Shewhart control limits for individual observations are usually based upon the average of moving range, and their performance is quite good if the underlying distribution is normal and the sample size is greater than 250. However, if the underlying distribution is not normal, then the recommended chart is nonparametric, which requires at least 1000

observations. Vermaat and Does [2006] proposed an alternative individual control chart based on a semi-Bayesian method, which works well under non-normality for moderate sample size within the range 250 to 1000.

Control chart pattern (CCP) recognition techniques are widely used to identify the potential process problem. Naeini et al. [2012] used artificial neural network (ANN) techniques with the help of Bayesian methodology in finding the suitable architecture of an ANN-based CCP recognizer. Eto and Pallotta [2007] proposed a Shewhart type control chart for the Weibull percentile. The parameters are estimated by using what they called the Practical Bayes Estimator method, i.e., specify the prior distribution on the parameters of interest by leaving nuisance parameters "unspecified."

Menzefricke introduced various control charts using the Bayesian methodology in a series of articles (cf. Menzefricke [2002, 2007, 2010a,b, 2013a,b]). Menzefricke [2002] approach for the normal distribution consists of two stages, (i) construction of the control chart by using a predictive distribution to derive the rejection region; (ii) evaluation of the control chart by use of a sampling theory approach to examine the performance of the proposed chart. Although his approach works very well for the normal distribution, for other families like the Weibull, etc., it is extremely difficult to find the sufficient statistics for all parameters. Riaz [2011] adopted the approach mentioned in Menzefricke [2002] and compared of the Bayesian $\bar{X}$ chart with the classical $\bar{X}$ chart.

Tan and Shi [2012] noticed that multivariate quality characteristics are usually monitored by a few summary statistics, i.e., either mean or variance. However, if a control chart detects a shift in one of the summary statistics, the quality engineer needs to find which quality characteristics have shifted and in which direction. To facilitate the identification of the root causes, Tan and Shi [2012] proposed a Bayesian approach. They introduced an indicator variable for each mean, that indicates whether the mean has shifted upward, shifted downward, or remained unchanged.

Perakis and Xekalaki [2015] used a Bayesian approach for assessing the proportion of conforming of normally distributed data. The posterior probabilities are used to decide whether the proportion of conformance exceeds the given threshold or not. By a numerical study, they showed that new technique is quite effective in the process capability analysis.

Memory Type / Sequential charts

Tsiamyrtzis and Hawkins [2005] proposed a control chart using the Bayesian methodology for short production runs. Since their assumed model is a linear state space model, their approach is a generalized version of the Kalman filter methodology for the normal process. Later, Apley [2012] extended the work of Tsiamyrtzis and Hawkins [2005], by developing a Markov (random walk) Bayesian model for monitoring and graphically exploring the process mean.

The u chart is very common for monitoring defective items based on the Poisson process. However, the proper use of this chart requires a phase-I data to setup control limits. In many practical situations, to obtain a sufficient phase-I data is difficult especially due to limited resources. Bayarri and García-Donato [2005], motivated by this fact, introduced a sequential monitoring scheme based on the predictive distribution. They used objective, empirical and proper (sequential) Bayes methods for this purpose. They also compared their results with the traditional frequentist implementation. They noticed that empirical Bayes methods are somewhat easy to implement and useful to deal with extra-Poisson variability; however, they still need the phase-I data. The sequential full Bayesian approach, on the other hand, avoids this drawback of traditional u-charts which makes it a powerful tool of process monitoring especially for online process monitoring. Although Bayarri and García-Donato [2005] approach is interesting, they did not show any performance evaluation of the proposed chart. Since the pure Bayesian credible interval is wider than the classical or empirical Bayes ones, this approach is better suited for the detection of large size of shifts.

Eva [2012] studied the properties of the moving range m-chart based on credible intervals and posterior odds. Change point methodology is also considered (with geometric prior) for normally distributed data. Eva [2012] concluded that Bayesian methodology helps in detection of shifts.

Marcellus [2007] presented a Bayesian methodology to jointly monitor the mean and standard deviation of a normal random variable. He compared the proposed chart performance with the Shewhart and cumulative sum chart, and concluded that it works well for the small size shifts.

Economic Design using the Bayesian Approach

In process monitoring, the process may go out-of-control due to the occurrence of any of several independent assignable causes, while in existing literature, only a single cause is considered for an assignable cause. It is also assumed widely that the time until each specific cause occurs has an identical exponential distribution. This assumption of identical distribution may be hard to meet in practice. Silver and Bischak [2004] proposed a control chart where the distribution of an assignable cause is assumed to be exponential with unknown parameter, not necessarily the same of other causes. They considered the Bayesian approach to deal with random causes of failure. Later, Bischak and Silver [2004] generalized their work with data augmentation through MCMC approach.

Nenes and Tagaras [2007] studied the economic design of $\bar{X}$ chart using the Bayesian methodology for a short run production. The numerical study of Nenes and Tagaras [2007] indicates that there are potential savings by using the Bayesian scheme.

Wang [2012] extended the ideas presented in Makis [2009] and Yin and Makis [2011]; and proposed a simulation-based multivariate Bayesian (economic) control chart. The proposed control chart is very useful for monitoring real-time condition-based maintenance of complex systems. Wang [2012] used the concept of delay time discussed by Wang and Jia [2007] to compute the posterior probability function of the underlying state given observed monitoring information history. Since, the model involves many parameters, Wang [2012] used Markov Chain simulations to obtain the optimal parameters of the chart. This author also noticed that the computation using MCMC could be time consuming if the number of simulated renewal cycles are substantially large.

2.8.2 Bayesian Charts for high-quality processes

Bayesian Tolerance Intervals control charts

Tolerance intervals can be used for the monitoring of a process. As opposite to confidence intervals, which tell us about an unknown population parameter, a tolerance interval provides information on the entire population with the specified probability. To be more precise, a tolerance interval is expected to capture a certain proportion or more of the population with a given confidence level. Hamada [2002] motivated by this idea, used Bayesian tolerance intervals for determining the control limits of Poisson distribution. He compared results with the frequentist tolerance interval and concluded that the Bayesian methodology helps to improve the process monitoring. Later, Demirhan and Hamurkaroglu [2014] constructed a $\bar{X}$ control chart using the Bayesian tolerance interval for the exponential distribution. To obtain an initial guess of the hyperparameters, they used an empirical Bayesian approach. The performance of the Bayesian tolerance interval chart was also compared with the EWMA and CUSUM.

Regular Bayesian Charts

Toubia-Stucky et al. [2012] used the sequential Bayesian approach for detection of a small process deterioration in the case of CCC chart. Their approach is self-starting, and thus suitable for short runs production monitoring.

Lee et al. [2013] introduced a Bernoulli CUSUM chart by using the Bayesian methodology. They notice that the usage of prior (previous run) information not only helps to improve process monitoring but also useful when no nonconforming items are observed in the process.

Raubenheimer and van der Merwe [2014] designed a Bayesian c chart using uniform and Jeffreys' priors. They compared the performance of the Bayesian chart with the classical chart, and concluded that the Bayesian chart performance is better than the classical.

2.9 Control Charts in Medical Studies

In health care monitoring, the occurrence of some types of failures, i.e., a malfunctioning instrument or delayed help to a patient, the discovery of some kind of physiological defect (a potentially fatal disease or a congenital defect), are rare phenomena. One needs to pay special attention to study these rare events and the idea of TBE is particularly suited for medical studies. To see some reviews about the use of control charts in health care monitoring, we refer to Sonesson and Bock [2003], Thor et al. [2007] (for a meta analysis about control charts usage in health care monitoring), Shaha [1995], Benneyan [1998a,b], Woodall [2006] and Mohammed et al. [2008] (for x, u, c, p, mr charts). A comprehensive overview about the use of the p chart in the surveillance is given by Szarka and Woodall [2011]. Some other recent contributions to this area are: correlated multi-attributes charts proposed by Niaki and Abbasi [2007]; an EWMA chart for Poisson counts with time-varying sample size based on probability control limits by Shen et al. [2013]; sample size varying smoothing parameter of EWMA chart by Shu et al. [2014]; time varying Bernoulli CUSUM by Tian et al. [2015], and charts based on a truncated zero-inflated binomial distribution studied by Fatahi et al. [2010]. An application in animal sciences of control charts could be seen in De Vries and Reneau [2010] where an advantage of control charts is pointed out over the randomized experiments. De Vries and Reneau [2010] noticed that with the help of control charts, an immediate intervention decision is possible, because in the case of an experiment one has to wait till the end of the experiment to evaluate a treatment effect.

Albers [2011c], motivated by the heterogeneity among the patients in medical studies, noticed that the assumption of every unit having the same probability p of being defective is rarely met, hence a richer parametric family is needed to overcome this problem. Although the geometric chart is most commonly used in such situations, a known drawback of this chart is that it requires a rather long time to react to a moderate increase of the failure probability p. Only large deteriorations quickly produce a signal of an out-of-control process. In health monitoring, this is not a usually accepted criterion. An alternative control chart is based on the negative binomial distribution, which is more useful in such situations, besides allowing for overdispersion. Earlier, Hoffman [2003] had introduced a control chart based on the negative binomial distribution instead that on the Poisson distribution. Albers [2012a] extended Albers [2011c] to nonparametric control charts by proposing MAX and MIN charts and studied their properties.

Spliid [2007] introduced an EWMA chart by assuming a geometric distribution for the failure counts and showed that the proposed EWMA helps in online surveillance of medical procedures.

Alemi and Neuhauser [2004] used the TBE control charts based on the exponential distribution for monitoring the asthma attacks. Dogu [2012] compared the performance of

the CQC-r charts with EWMA and CUSUM charts, and suggested the use of the CQC-r chart for monitoring medical errors. Recently, Schuh et al. [2014] analyzed the frequency of accidents by using the CUSUM chart. They compared the performance of a Poisson CUSUM with an exponential CUSUM and showed that shorter periods of aggregation for the TBE monitoring leads to a more timely indication of an increased accident frequency. They also highlighted some issues related to data aggregation and its effect on the control charts performance.

From an applied point of view, the problem of zero inflation/rare events, is not only common in the industrial or medical processes, but it is also present in agricultural sciences, i.e., counting the number of insects per leaf in pest counting studies, etc. Therefore, Sim and Lim [2008] proposed zero inflated models to study the pest counting problem with zero inflated binomial and Poisson models. They used uniform and Jeffreys' priors to design the charts, and noticed that control charts based on intervals resulting from assuming Jeffreys' prior are more efficient than the classical methodology.

2.10 Different Performance Evaluation Criteria of control charts

In this section, we recall some widely accepted criteria to evaluate control charts performance, which are suitable for high-quality process monitoring as well. The first performance measure is average run length (ARL) defined as: the average number of data points that must be plotted before a point indicates an out-of-control situation (or the expectation of the stopping time defined as $ARL = \min_i\{i : X_i \notin [LCL_i, UCL_i]\}$). Ideally, one wants larger in-control ARL (denoted by ARL_0) and shorter/smaller out-of-control ARL (denoted by ARL_1). Another criterion used as an alternative of the ARL is average time to signal (ATS) or average length of inspection (ALI) defined as the average time taken by a chart to produce an out-of-control signal. Mathematically, it is $ATS = ARL \times E(X)$. Depending on the type of data being monitored, some other names for ATS are: ANI-average number of items inspected, AQI-average quantity of products inspected. To compare the performance of two charts, the in-control ARL should be large enough while an out-of-control ARL should be small (the same rule is valid/true for ATS and ALI). A chart with smaller out-of-control ARL at specific shift is considered to be more effective than the other. Some other supplementary indicators are being used by many practitioners and researchers, are the standard deviation of the run length distribution (SDRL) (standard deviation of the length of inspection, SDLI) and quartiles of the run length (and length of inspection) distribution.

The ARL is the most commonly used criterion to evaluate the performance of control charts, but it is not free from criticism, i.e., change point problem with mixture pre-

change models, detection schemes with finite detection delays can have an infinite ARLs, the underlying geometric distribution, dispersion in ARL curve etc. (see Mei [2008], and Tartakovsky [2008]). It is also difficult to predict the values of process shifts in most applications, especially in the case of online process monitoring. Therefore, it is important to have a control chart which has a good performance over the entire/whole range of process shifts rather than at a specific shift point. Thus, for this purpose, ratio of ARL (RARL), extra quadratic loss (EQL) and the performance comparison index (PCI) measures are used. Let $f(\delta)$ be a distribution of shifts selected on the basis of the process behavior, then RARL can be written as

$$RARL = \int_{\delta_{min}}^{\delta_{max}} \frac{ARL(\delta)}{ARL_S(\delta)} f(\delta) d\delta \tag{2.1}$$

Note that a chart producing the smallest ARL is usually selected as the specific or benchmark in case of RARL. This measure is quite useful not only when the impact of a range of shifts is the main focus but also when one wants to compare control charts having a scale difference in the ARL (this measure has minimum impact/effect of the scale differences).

Another criterion is EQL which directly evaluates the expected loss due to poor quality. EQL can be calculated as

$$EQL = \int_{\delta_{min}}^{\delta_{max}} \delta^2 ARL(\delta) f(\delta) d\delta \tag{2.2}$$

This EQL has two advantages over the RARL. First, the loss function behind the derivation of EQL, is a more comprehensive measure of the charting performance than ARL because it considers all the contributors to the quality cost including the time to signal and the magnitude of δ shift. Second, the evaluation of EQL does not require a pre-specified benchmark chart. Thus, minimization of EQL will reduce the loss in quality incurred in the out-of-control situations.

A Performance Comparison Index (PCI), is also used as the measure of the relative overall performance of the charts. This is the ratio between the EQL values of two control charts and serves as a measure of the relative effectiveness of two charts like RARL (see details in Wu et al. [2009c], Wu et al. [2010b], Ou et al. [2011], and references cited therein).

Since, all the performance criteria are a function of ARL, so if the ARL has some poor characteristics then other criteria too have poor properties. Thus, it is indeed a necessity of modern quality to have a new criterion, which should not be a function of ARL.

2.11 Conclusion

We have reviewed 114 articles (cf. Table-2.1, Figure-2.2) related to the TBE or high-quality concept and 63% of the reviewed articles deal with discrete or attribute data while 31% deal with continuous data and the remaining (6%) with both. Thus, the trend of research is highly influenced by the discrete distributions. Of our reviewed articles, only 23 deal with the parameter estimation problem while in the remaining ones (i.e. 91 articles) the parameter is assumed known (cf. Table- 2.2, Figure-2.3). The maximum likelihood method is used 4 times in the continuous case while 6 times in the discrete case. The use of Bayesian methods is not very popular in the continuous case as compared to the discrete case (cf. Table- 2.3). Geometric and negative Binomial models are commonly used in discrete cases while the exponential model is used for continuous data (cf. Table-2.4). The category "others" in Table-2.4, includes charts based on nonparametric, multivariate, Lognormal, inflated and normal models. It is observed that CUSUM, EWMA and synthetic or joint charts are used for both types of data.

Table 2.1: Article Reviewed by Data Type

Data Type	Count	%
Discrete	72	63.16
Continuous	35	30.70
Both	7	6.14
Total	114	100

Table 2.2: Parameter Estimation for TBE Setup

Method	Count	%
No	91	79.82
MLE	10	8.77
Bayesian	7	6.14
MLE& Bayesian	3	2.63
Nonparametric	3	2.63
Total	114	100

It is evident from the cited literature, that earlier control charts are either based on approximations or simple processes. Therefore, this thesis make a number of contributions to the field of high-quality process monitoring. First, we generalize the existing TBE control charts by assuming renewal process (cf. Chapter 3) for events $N(t)$. Second, we

Table 2.3: Parameter Estimation with respect to Data Type

Method	Continuous	Discrete	Both	Total
No	28	56	7	91
MLE	4	6		10
Bayesian	1	6		7
MLE& Bayesian	1	2		3
Nonparametric	1	2		3
Total	35	72	7	114

Table 2.4: The use of different Processes for the designing of TBE Charts

Process	Count	%	Total
Bernoulli	6	5.26	
Binomial	4	3.51	
Exponential	26	22.81	
Geometric	24	21.05	
Negative Binomial	16	14.04	
Poisson	6	5.26	
Others	32	28.07	
Total	114	100	114
	Data		
Chart	Continuous	Discrete	Total
Shewhart	27	54	81
CUSUM	8	10	18
EWMA	3	9	12
Nonparametric	.	3	3
Total	38	76	114

extend TBE control charts to handle both the time and the associated magnitude using the renewal reward processes (cf. Chapters 4 and 5). We consider fixed (cf. Chapter 4) and random (cf. Chapter 5) threshold scenarios for time and magnitude monitoring. Third, we introduce a TBE chart for online process monitoring (cf. Chapter 6) based on nonhomogeneous Poisson process with power law intensity. Finally, we develop an adaptive TBE chart for sequential process monitoring using the Bayesian predictive approach.

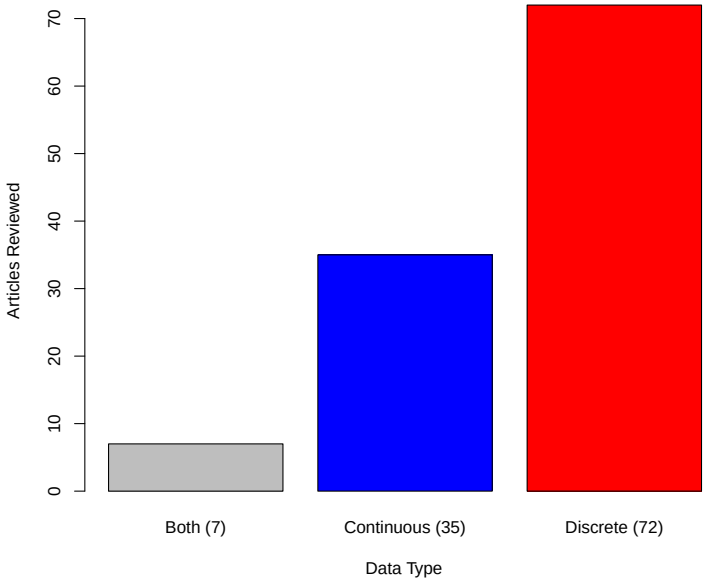

Figure 2.2: Article Reviewed by Data Type

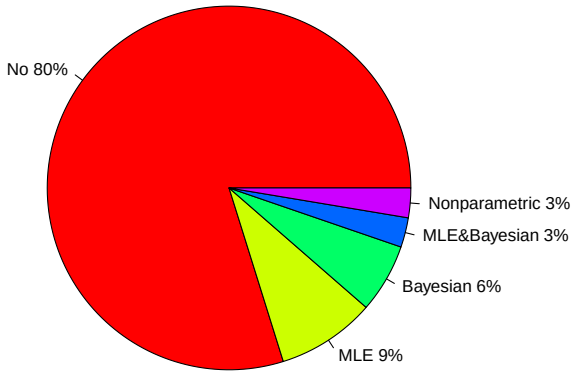

Figure 2.3: Parameter Estimation for TBE Setup

This page is left blank intentionally.

Chapter 3

High Quality Process Monitoring using a Class of inter-arrival Time Distributions of the Renewal Process

For high-quality processes where defect rate is very low, e.g. part per million (ppm), TBE control charts have several advantages over the ordinary control charts. Existing TBE control charts are based on the Poisson process, thus the distribution for TBE is assumed to be exponential. However, the exponential distribution is not suitable in many applications, where the failure rate is not constant. In this chapter, we develop a new TBE control chart based on the renewal process where any continuous lifetime distribution for TBE can be assumed. Particularly, we allow for a parametric class of absolutely continuous distributions for TBE, which includes some well known and commonly used lifetime distributions, i.e., exponential, Rayleigh, Weibull, Burr type XII, Pareto and Gompertz distributions. The control structure of the proposed chart is designed mathematically and numerically (for numerical calculations, we used the Weibull distribution due to its relevance in reliability). The performance of the proposed control charts is evaluated in terms of some standard useful measures, including average run length (ARL), standard deviation of run length, coefficient of variation of the run length, expected quality loss (EQL) and relative ARL (RARL). The effect of parameter estimation, using both maximum likelihood and Bayesian methods, is also discussed. The study also presents an illustrative example and four case studies to highlight the practical aspects of the proposal.

3.1 Motivation

The available TBE control charts can be categorized into two groups: attribute TBE and variable TBE. Most of the attribute TBE charts are based on the geometric distribution (cf. Section-2.11), such as the cumulative count control (CCC) chart, or on the negative

binomial distribution (e.g. the CCC-r chart). One special variable TBE chart is the cumulative quantity control (CQC) chart. As the occurrence of the events follows a Poisson process, the time between two events follow an exponential distribution, so CQC can also be called exponential chart, sometimes denoted as t-chart. From the substantial review presented in Chapter-2, it is apparent that the existing available CQC charts are based on the exponential distribution, i.e., Poisson process, (cf. Section-2.2.2 and 2.11). Therefore, the main aim of this chapter is to introduce a generalized version of the existing CQC charts.

In this chapter, we consider the development of a control chart based on the renewal process where the distribution of TBE is assumed to belong to a class of absolutely continuous distributions. This class includes exponential, Rayleigh, Weibull (there is a debate about the distribution name in the literature, e.g., Stoyan [2013]), Burr type XII, Pareto and Gompertz distributions. A renewal process can be regarded as a generalization of the ordinary Poisson process, where the distribution of time is replaced by any other lifetime distribution in place of the exponential distribution. Thus, the present chapter is a generalization of the existing TBE charts. We also include a study of the control chart performance in the presence in presence of parameter estimation error.The Poisson process defined by Theorem-1.1.3 is also called the homogenous Poisson process (HPP). The major weakness of this process is the constant rate assumption. However, HPP(λ) can be generalized to a renewal process by letting any other lifetime distribution instead of exponential distribution.

Definition 3.1.1 *A counting process* $\{N(t), t \geq 0, t \in T\}$ *with independent and identically distributed (iid) inter-arrival times* $X_1, X_2, \cdots$ *having a common distribution* F *is called a renewal process.*

The use of a renewal process is motivated by TBE with a non-constant hazard rate. Consider, for example, an industrial process in which a sensor signals that a filter must be substituted. The hazard of getting a substitution signal increase with time because impurities trapped within the filter accumulate. After changing the filter a renewal takes place, represented by a new filter with the same hazard function. An increased renewal frequency with respect to the nominal, would indicate an upstream problem in the process because filters are changed too often. The renewal theory has many applications, especially in the field of repairable systems, component testing, the time intervals of successive earthquakes in a particular region and so on.

The rest of the chapter is organized as follows: in Section 3.2, the class of distributions is defined. The design of the TBE chart for high-quality processes is discussed in Section 3.3. In Section 3.4, some performance criteria for the evaluation of control chart performance are presented. These performance criteria are: average run length, expected quadratic loss and relative average run length. The Bayesian and the classical methods

for the estimation of unknown parameters are discussed in Section 3.5. In Section 3.6, an illustrative example to explain how the proposed methodology in real situations can be used is discussed with four case studies. Finally, we conclude the chapter in Section 3.7.

3.2 A Class of Absolutely Continuous Distributions

The purpose of this section is to introduce a general class for $N(t)$, renewal process, to generalize existing TBE charts. Consider the following parametric family of distribution functions:

$$F_{\lambda,\beta}(x) = 1 - \exp\{-\lambda^{\beta} M(x)\}; \quad x, \beta, \lambda > 0 \tag{3.1}$$

where λ, β are the rate and shape parameters, and $M(x)$ is an increasing and positive function in x, which may be dependent on the shape parameter, β. This general model includes several lifetime distributions such as exponential, Rayleigh, Weibull, Burr type XII (compound Weibull), Pareto, linear failure rate and Gompertz, among others. Ahmadi et al. [2015] defined a similar class of distributions, but with a different parametrization. Table-3.1 displays the functions $M(x)$ and the corresponding distribution functions $F_{\lambda,\beta}(x)$ for some lifetime distributions.

Table 3.1: Some well-known lifetime distributions belongs to the general family in Equation-3.1

Distribution	$M(x)$	Condition	$F_{\lambda,\beta}(x)$
exponential	x	$\beta = 1$	$1 - \exp(-\lambda x)$
Rayleigh	x^2	$\beta = 2$	$1 - \exp(-(\lambda x)^2)$
Weibull	x^{β}	$\beta > 0$	$1 - \exp\big(-(\lambda x)^{\beta}\big)$
Burr type XII	$\ln(1 + x^{\beta})$	$\beta > 0$	$1 - \big(1 + x^{\beta}\big)^{-\lambda^{\beta}}$
Pareto	$\ln\big(1 + x/\beta\big)$	$\beta > 0$	$1 - \big(1 + x/\beta\big)^{-\lambda^{\beta}}$
Gompertz	$\{\exp(\beta x) - 1\}/\beta$	$\beta > 0$	$1 - \exp\big(-\lambda^{\beta}\{\exp(\beta x) - 1\}/\beta\big)$
Linear Failure Rate	$x + x^2/2$	$\beta = 1$	$1 - \exp\big(-\lambda(x + x^2/2)\big)$

The Rayleigh, Gompertz and linear failure rate distributions have increasing failure rates while the Pareto one is decreasing. The Burr XII is a uni-modal distribution and has a non-monotone failure rate (for $\beta > 1$, the failure rate has one critical point at $(\beta - 1)^{1/\beta}$), which makes its interpretation technical especially in reliability. This distribution is a good candidate to study a system or disease whose mortality reaches a peak after some finite time period and then gradually decreases. Moreover, the limiting distribution of the Burr XII as $x \to \infty$, is a Weibull distribution. The Weibull distribution allows increasing, decreasing and constant failure rates, depending upon the shape parameter β. This property not only gives an advantage over the exponential which only allows a constant failure rate, but also over other distributions which have increasing, decreasing or

non-monotone failure rates. Thus, among the distributions given in Table-3.1, the Weibull distribution is very popular lifetime distributions, and other distributions mentioned in Table-3.1 are somehow special cases of the Weibull distribution. Since its introduction, the Weibull distribution, has been used in many applied fields to model lifetimes of many types of manufactured items, such as vacuum tubes, ball bearings and electrical insulation. It is also used in biomedical applications, for example, as the distribution of time to the occurrence (diagnosis) of tumors in human population or in laboratory animals. Furthermore, it is a suitable model for extreme value data, such as the strength of certain materials. Recently, empirical studies have shown that Weibull distribution is superior to the classical stable distributions, including the normal distribution, for fitting empirical economic data; see, for example, Murthy et al. [2004], and Yannaros [1994]. Although we shall provide TBE control charts construction based on the distributions mentioned in Table-3.1, our main focus will be on the Weibull distribution for numerical study.

In this work we focus on TBE charts and not interested in CCC charts. If someone is interested in developing a control chart based on counts $N(t)$, the exact distribution of the counting process could be found from the direct relationship between the arrival time and the number of events. Let T_n be a time from the measurement origin at which the n-th event occurs and let $N(t)$ denote the number of events that have occurred up until the time t. Thus, $T_n \leq t \Longleftrightarrow N(t) \geq n$. To derive a Weibull count model, the challenge is associated with the solution of the convolution integral implied by this relationship. As noted by McShane et al. [2008], this type of integral is easily solved for the exponential as well as the gamma distributions. However, by Taylor's series approximation obtained by expanding the exponential factor "$\exp(-(\lambda x)^{\beta})$" for both the cdf and the pdf of the Weibull, we have $F(x) = \sum_{j=1}^{\infty} \frac{(-1)^{j+1}(\lambda x)^{\beta j}}{\Gamma(j+1)}$ and $f(x) = \sum_{j=1}^{\infty} \frac{(-1)^{j+1}\beta j \lambda^{\beta j} x^{\beta j-1}}{\Gamma(j+1)}$, respectively. Thus, using the relationship between inter-arrival time and number of events, McShane et al. [2008] developed a Weibull count model as

$$\begin{aligned} C_n(t) &= Pr(N(t) = n) = Pr(N(t) \geq n) - Pr(N(t) \geq n+1) \\ &= Pr(T_n \leq t) - Pr(T_{n+1} \leq t) = \sum_{j=n}^{\infty} \frac{(-1)^{j+n}(\lambda t)^{\beta j}\phi_j^n}{\Gamma(\beta j+1)}, \qquad n = 0, 1, 2, \cdots . \end{aligned} \tag{3.2}$$

Here, $\phi_j^0 = \Gamma(\beta j+1)/\Gamma(j+1), j = 0, 1, 2, \cdots$ and $\phi_j^{n+1} = \sum_{m=n}^{j-1} \phi_m^n \Gamma(\beta j - \beta m + 1)/\Gamma(j - m + 1)$, for $n = 0, 1, \cdots$ and $j = n+1, n+2, \cdots$.

3.3 Control Charts based on Generalized class of inter-arrival Times

Let X be the time between the appearance of two nonconformities (inter-arrival time), with distribution given in Equation-3.1. After choosing $M(x)$, a two-sided generalized quantity control chart (GQCC) can be constructed by equating Equation-3.1 to $\alpha/2$, $1-\alpha/2$ and $1/2$ which results in the lower control limit (LCL), upper control limit (UCL) and central limit (CL), respectively (cf. Chan et al. [2000]), where α is the pre-specified probability of false alarm. Mathematically, we can write it as: i.e., $F_{\lambda,\beta}(LCL) = 1-\exp\{-\lambda^{\beta}M(LCL)\} = \alpha/2$, $F_{\lambda,\beta}(UCL) = 1-\exp\{-\lambda^{\beta}M(UCL)\} = 1-\alpha/2$, and $F_{\lambda,\beta}(CL) = 1-\exp\{-\lambda^{\beta}M(CL)\} = 0.5$. Table-3.2 displays the simplified forms of LCL and UCL for the distributions mentioned in Table- 3.1.

Table 3.2: Lower and Upper control limits for the distributions given in Table-3.1

Distribution	LCL	UCL
exponential	$\lambda^{-1}[-\ln(1-\alpha/2)]$	$\lambda^{-1}[-\ln(\alpha/2)]$
Rayleigh	$\lambda^{-1}\sqrt{[-\ln(1-\alpha/2)]}$	$\lambda^{-1}\sqrt{[-\ln(\alpha/2)]}$
Weibull	$\lambda^{-1}\big[-\ln(1-\alpha/2)\big]^{1/\beta}$	$\lambda^{-1}\big[-\ln(\alpha/2)\big]^{1/\beta}$
Burr type XII	$\big[(1-\alpha/2)^{-1/\lambda^{\beta}}-1\big]^{1/\beta}$	$\big[(\alpha/2)^{-1/\lambda^{\beta}}-1\big]^{1/\beta}$
Pareto	$\beta\big[(1-\alpha/2)^{-1/\lambda^{\beta}}-1\big]$	$\beta\big[(\alpha/2)^{-1/\lambda^{\beta}}-1\big]$
Gompertz	$\beta^{-1}\ln\big[1+\beta\{-\ln(1-\alpha/2)\}/\lambda^{\beta}\big]$	$\beta^{-1}\ln\big[1+\beta\{-\ln(\alpha/2)\}/\lambda^{\beta}\big]$
Linear Failure Rate	$\sqrt{1+2\{-\ln(1-\alpha/2)\}/\lambda}-1$	$\sqrt{1+2\{-\ln(\alpha/2)\}/\lambda}-1$

The control chart is obtained by plotting the observed value of TBE X_i against the failure/sample number. If the point is plotted below the LCL $X_i < LCL$ then it is a signal that the process may have deteriorated while if a point is plotted above the UCL $X_i > UCL$, it is a sign of that process may have improved.

In some areas of application, one-directional changes are the ones of the greatest concern. For example, in the manufacturing industry, engineers want to prevent an increase in the nonconformities, but decreases in the nonconforming fraction is in-consequential. In health care applications, detecting the increase of medication administration errors is very important since it might lead to morbidity and mortality of patients. However, the decrease of medication administration errors is taken for granted. Thus, a one-sided control chart would be more suitable than traditional two-sided charts in these circumstances. A one sided Weibull quantity control chart (WQCC) can be obtained by equating the Equation-3.1 (i.e., with $M(x) = x^{\beta}$) equal to α, so that LCL is $LCL_{one-sided} = \lambda^{-1}\Big[-\ln(1-\alpha)\Big]^{\frac{1}{\beta}}$ without UCL.

Remark 3.3.1 *The cumulative probability control chart is a control chart in which the observed cumulative probability is plotted against the failure number. Since the cumulative*

probability is plotted and due to this reason the vertical axis of plot always lies between zero and one which makes its interpretation easier. To construct a cumulative probability chart, the lower and upper control limits for the two-sided control charts are $\alpha/2$ *and* $1-\alpha/2$ *respectively. Similarly, a one-sided control chart can be constructed by taking* $LCL = \alpha$ *and* $UCL = 1-\alpha$.

3.4 Performance Evaluation

In this section, we will examine various control chart performance measures commonly used by practitioners. These are: average run length (ARL), expected quality loss (EQL) and relative average run length (RARL). The first measure (i.e. ARL) is used to evaluate the performance of a chart at any specified shift, while EQL and RARL are used for performance evaluation on an assumed shift range. The description of these measures for the proposed chart is given in the following subsections.

3.4.1 Average Run Length (ARL)

The average run length (ARL) is a measure of the expected number of consecutive samples taken until the sample statistic fall outside the control limits. Mathematically, the ARL is expectation of stopping time $L = \min\{i : X_i \notin [LCL_i, UCL_i]\}$ and L in most cases is a discrete random variable, taking on integer values. As a consequence, L as a function of the parameter will be piecewise constant with jumps (cf. Fu and Hu [1999], page 398).

Suppose that a TBE chart is constructed such that the probabilities of false alarm for the one-sided charts are α_U and α_L to get the UCL and LCL, respectively, while $\alpha = \alpha_U + \alpha_L$ is the false alarm probability for the two-sided chart. To compute ARL, we have the following proposition:

Proposition 3.4.1 *The expressions of the ARLs to receive a signal for the un-natural variations below the LCL, above the UCL and either below the LCL or above the UCL are given in Table-3.3, where* $\beta^* = \frac{\beta_1}{\beta_0}$ *and* $\lambda^* = \frac{\lambda_1}{\lambda_0}$ *denote the magnitude of the shifts in the shape and the rate parameters of the process.*

Proof : *The expressions of the ARLs are obtained as* $ARL_L = \frac{1}{F(LCL)}$, $ARL_U = \frac{1}{1-F(UCL)}$ *and* $ARL_{L\cup U} = \frac{1}{F(LCL)+1-F(UCL)}$, *where* $F(.)$ *is taken from Table-3.1.*

The usage of λ^* and β^* simplifies the notations and it is clear that $0 < \beta^*, \lambda^* < 1$ indicates process improvement, while $\beta^*, \lambda^* > 1$ indicates process deterioration.

Table-3.3 contains the explicit expressions of the ARL for the distributions mentioned in Table-3.1. It is interesting to note that the expressions of ARL for the exponential linear failure rate distributions are the same, because $LCL_{linear failure} + (LCL^2_{linear failure})/2 =$

$LCL_{exponential}$. Moreover, the behavior of the TBE control charts could not match expectations. For example, consider that the probability of an alarm for process deterioration in the Weibull case is $Pr(X \leq LCL) = 1 - \exp\{-(\lambda_0 LCL)^{\beta_1}\}$, with $\lambda = \lambda_0$ and $\beta = \beta_1$, where LCL is obtained from Table 3.2. Then, if $\lambda_0 LCL < 1$, the alarm probability decreases as β_1 increases, so that it is smaller than its under-control nominal value for $\beta_1 > \beta_0$. For example, with $\alpha = 0.0027$, $\lambda_0 = 0.0005$, $\beta_0 = 1.5$, $\beta_1 = 1.8$ one obtains an alarm probability of $0.0004 < 0.0027$. Hence, one should be very careful about the control chart design, due to the significant effect of the shape parameter. The control chart' detection ability in such a situation would be undermined, which results into the biased performance (first mentioned in Mann [1945]) of the chart. Thus, one should be very careful about the control chart design due to the significant effect of the shape parameter. We refer to Yang et al. [2015a,c] for some recent developments about biasedness of exponential and gamma charts.

Since the design of a control chart is often based on ARL, a large in-control ARL is ensured by design, but the variance of the run length distribution can be large. This basically poses difficulties on the shop floor because of widely varying frequencies of false alarms and, in general, control chart signals. As a consequence, the chart signal might be ignored or acted upon selectively. Thus, in such scenario, sometimes the coefficient of variation (CV) is examined when control chart performances are considered and we also do so in our study.

As we mentioned above, from here our discussion will be restricted to the WQCC chart due to the vast application of the Weibull distribution. The implementation of the Weibull charts requires the knowledge of the both parameters whereas, in reality, one might have the knowledge about either the shape or the rate parameter. To tackle such a situation, we suggest to find the shifted/adjusted value of the non-available parameter by using the mean. To explain it further, let us suppose that β_0 and λ_0 are the in-control shape and rate parameters which result into $m_0 = \lambda_0^{-1}\Gamma(\beta_0^{-1} + 1)$. Furthermore, suppose that we know β_1 and interested in finding the λ_1. To accomplish this task, we denote $m_b(\beta_1, \lambda_0) = \lambda_0^{-1}\Gamma(\beta_1^{-1} + 1)$ and equate it to $\lambda_1^{-1}\Gamma(\beta_0^{-1} + 1)$ which would result into $\lambda_1 = \frac{\lambda_1\Gamma(\beta_0^{-1}+1)}{m_b(\beta_1,\lambda_0)} = \frac{\lambda_0\Gamma(\beta_0^{-1}+1)}{\Gamma(\beta_1^{-1}+1)}$. For example, if the in-control rate and shape parameters are $\lambda_0 = 0.0005$, $\beta_0 = 1.5$ while we know $\beta_1 = 1.3$ the out-of-control shape parameter, then the $\lambda_1 = 0.000489$ should be used to design the Weibull chart. Similarly, by knowing the λ_1 one can find β_1 by solving $\Gamma(\beta_1^{-1} + 1) = \Gamma(\beta_0^{-1} + 1)\lambda_0/\lambda_1$.

Table 3.3: ARL expressions for the distributions listed in Table-3.1.

Distribution	ARL_L	ARL_U	$ARL_{L\cup U}$
exponential	$[1-(1-\alpha_L)^{\lambda^*}]^{-1}$	$[\alpha_U^{\lambda^*}]^{-1}$	$[1-(1-\alpha/2)^{\lambda^*}+(\alpha/2)^{\lambda^*}]^{-1}$
Rayleigh	$[1-(1-\alpha_L)^{\lambda^{*2}}]^{-1}$	$[\alpha_U^{\lambda^{*2}}]^{-1}$	$[1-(1-\alpha/2)^{\lambda^{*2}}+(\alpha/2)^{\lambda^{*2}}]^{-1}$
Weibull	$\Big[1-\exp\big(-\lambda^{*\beta_0\beta^*}\{-\ln(1-\alpha_L)\}^{\beta^*}\big)\Big]^{-1}$	$\exp\big(\lambda^{*\beta_0\beta^*}\{-\ln(\alpha_U)\}^{\beta^*}\big)$	$\Big[1-\exp\big(-\lambda^{*\beta_0\beta^*}\{-\ln(1-\alpha/2)\}^{\beta^*}\big)+\exp\big(-\lambda^{*\beta_0\beta^*}\{-\ln(\alpha/2)\}^{\beta^*}\big)\Big]^{-1}$
Burr Type XII	$\Big[1-\{1+((1-\alpha_L)^{-1/\lambda_0^{\beta_0}}-1)^{\beta^*}\}^{-\lambda_1{}^{\beta_1}}\Big]^{-1}$	$\Big[\{1+((\alpha_U)^{-1/\lambda_0^{\beta_0}}-1)^{\beta^*}\}^{-\lambda_1^{\beta_1}}\Big]^{-1}$	$\Big[1-\{1+((1-\alpha/2)^{-1/\lambda_0^{\beta_0}}-1)^{\beta^*}\}^{-\lambda_1{}^{\beta_1}}+\{1+((\alpha/2)^{-1/\lambda_0^{\beta_0}}-1)^{\beta^*}\}^{-\lambda_1{}^{\beta_1}}\Big]^{-1}$
Pareto	$\Big[1-\{1+\beta^{*-1}((1-\alpha_L)^{-1/\lambda_0^{\beta_0}}-1)\}^{-\lambda_1^{\beta_1}}\Big]^{-1}$	$\Big[\{1+\beta^{*-1}((\alpha_U)^{-1/\lambda_0^{\beta_0}}-1)\}^{-\lambda_1^{\beta_1}}\Big]^{-1}$	$\Big[1-\{1+\beta^{*-1}((1-\alpha/2)^{-1/\lambda_0^{\beta_0}}-1)\}^{-\lambda_1^{\beta_1}}+\{1+\beta^{*-1}((\alpha/2)^{-1/\lambda_0^{\beta_0}}-1)\}^{-\lambda_1^{\beta_1}}\Big]^{-1}$
Gompertz	$\Big[1-\exp-(\lambda_1{}^{\beta_1}/\beta_1)\{(1-\beta_0\ln(1-\alpha_L)/\lambda_0^{\beta_0})\}^{\beta^*}\Big]^{-1}$	$\Big[\exp-(\lambda_1{}^{\beta_1}/\beta_1)\{(1-\beta_0\ln(\alpha_U)/\lambda_0^{\beta_0})\}^{\beta^*}\Big]^{-1}$	$\Big[1-\exp-(\lambda_1{}^{\beta_1}/\beta_1)\{(1-\beta_0\ln(1-\alpha/2)/\lambda_0^{\beta_0})\}^{\beta^*}+\exp-(\lambda_1{}^{\beta_1}/\beta_1)\{(1-\beta_0\ln(\alpha/2)/\lambda_0^{\beta_0})\}^{\beta^*}\Big]^{-1}$
Linear Failure Rate	$[1-(1-\alpha_L)^{\lambda^*}]^{-1}$	$[\alpha_U^{\lambda^*}]^{-1}$	$[1-(1-\alpha/2)^{\lambda^*}+(\alpha/2)^{\lambda^*}]^{-1}$

Table 3.4: ARL study of the PI-IHR case using $\alpha=0.0027, \lambda_0=0.0005, \beta_0=1.5$ and $\lambda_1\in\{0.0003, 0.0001, 0.00005\}$, $\beta_1\in\{1, 1.2, 1.4, 1.5, 2\}$ for the upper and two-sided Weibull charts.

β	λ	Two-Sided				Upper-Sided			
		0.0005	0.0003	0.0001	0.00005	0.0005	0.0003	0.0001	0.00005
1	ARL	23.9761	7.79972	2.0124	1.41962	26.3241	7.11561	1.9234	1.38687
	CV	0.978924	0.933697	0.709282	0.543679	0.980822	0.927073	0.692884	0.528158
	CVLI	1.0000	1.0000	1.0000	1.0000	1.0000	1.0000	1.0000	1.0000
1.2	ARL	63.1362	11.272	1.92542	1.33024	63.1237	9.44529	1.82368	1.29893
	CV	0.992049	0.954612	0.693277	0.498252	0.992047	0.945583	0.672055	0.479722
	CVLI	0.997625	0.986621	0.918913	0.880217	0.997624	0.984013	0.914177	0.877127
1.4	ARL	198.18	16.9804	1.84354	1.26091	191.254	13.0609	1.73663	1.23263
	CV	0.997474	0.970108	0.676436	0.454888	0.997382	0.960955	0.651286	0.434426
	CVLI	0.998798	0.985879	0.861221	0.788892	0.998754	0.981601	0.85194	0.783381
1.5	ARL	370.37	21.2746	1.80541	1.23232	370.37	15.6241	1.69725	1.20567
	CV	0.998649	0.976215	0.667914	0.434193	0.998649	0.967469	0.640946	0.413018
	CVLI	0.999272	0.987251	0.837527	0.750075	0.999272	0.9826	0.826091	0.743602
2	ARL	6516.86	86.4081	1.64208	1.13201	44182	47.0206	1.53395	1.11289
	CV	0.999923	0.994197	0.625312	0.341485	0.999989	0.989309	0.589988	0.318495
	CVLI	0.999944	0.995786	0.746601	0.598322	0.999992	0.992242	0.725407	0.589034

Table 3.5: ARL study of the TD-IHR case using $\alpha = 0.0027, \lambda_0 = 0.0005, \beta_0 = 1.5$ and $\lambda_1 \in \{0.005,\ 0.01, 0.1\}$, $\beta_1 \in \{1, 1.2, 1.4, 1.5, 2\}$ for the lower and two-sided Weibull charts.

β	λ	Two-Sided				Lower-Sided			
		0.0005	0.005	0.01	0.1	0.0005	0.005	0.01	0.1
	ARL	23.9761	8.69323	4.61187	1.09506	52.0284	5.66884	3.1086	1.02105
1	CV	0.978924	0.940727	0.884968	0.294629	0.990343	0.907522	0.823597	0.143598
	CVLI	1.0000	1.0000	1.0000	1.0000	1.0000	1.0000	1.0000	1.0000
	ARL	63.1362	12.9661	5.93864	1.05686	113.855	7.66384	3.6399	1.00619
1.2	CV	0.992049	0.960664	0.911927	0.231959	0.995599	0.932479	0.851626	0.0784368
	CVLI	0.997625	0.98838	0.974449	0.846478	0.998683	0.980259	0.957962	0.838003
	ARL	198.18	19.475	7.70011	1.03132	249.871	10.436	4.284	1.00126
1.4	CV	0.997474	0.973988	0.932808	0.17427	0.997997	0.950883	0.875542	0.0354862
	CVLI	0.998798	0.987699	0.968586	0.733675	0.999047	0.976919	0.942786	0.724166
	ARL	370.37	23.912	8.78621	1.0224	370.37	12.2034	4.65541	1.00048
1.5	CV	0.998649	0.978867	0.941374	0.14801	0.998649	0.958152	0.886113	0.0218503
	CVLI	0.999272	0.988665	0.968841	0.687609	0.999272	0.977667	0.94033	0.679158
	ARL	6516.86	67.4636	17.2456	1.00255	2655.51	27.0532	7.15007	1.000010
2	CV	0.999923	0.992561	0.970574	0.0504509	0.999812	0.981344	0.927438	0.000535165
	CVLI	0.999944	0.994599	0.978702	0.52449	0.999863	0.986477	0.947817	0.522723

Table 3.6: ARL study of the TI-DHR case using $\alpha = 0.0027, \lambda_0 = 0.0005, \beta_0 = 0.5$ and $\lambda_1 \in \{0.0003,\ 0.0001, 0.00005\}$, $\beta_1 \in \{0.3, 0.45, 0.5, 0.55, 0.8\}$ for the upper and two-sided Weibull charts.

β	λ	Two-Sided				Upper-Sided			
		0.0005	0.0003	0.0001	0.00005	0.0005	0.0003	0.0001	0.00005
	ARL	2.14293	2.11003	2.03261	1.98093	4.16563	3.8799	3.36945	3.1062
0.1	CV	0.730308	0.725308	0.712757	0.703695	0.871746	0.861546	0.83858	0.823446
	CVLI	293.626	295.907	301.489	305.397	210.602	218.218	234.165	243.885
	ARL	15.7135	11.6483	6.29416	4.53652	18.2658	12.0888	6.00446	4.28862
0.3	CV	0.967657	0.956112	0.917127	0.882931	0.972241	0.957747	0.912939	0.875685
	CVLI	1.67254	1.85058	2.34247	2.68807	1.59569	1.82656	2.38824	2.75419
	ARL	146.618	66.5816	13.9264	6.92151	141.37	51.1389	11.0219	5.79396
0.45	CV	0.996584	0.992462	0.963428	0.924945	0.996457	0.990174	0.953557	0.909619
	CVLI	1.01956	1.0426	1.18995	1.35535	1.02028	1.05512	1.23515	1.41416
	ARL	370.37	142.202	18.9822	8.05326	370.37	97.6466	14.0841	6.49044
0.50	CV	0.998649	0.996478	0.973303	0.935856	0.998649	0.994866	0.963845	0.919743
	CVLI	1.00539	1.01397	1.10033	1.22339	1.00539	1.02028	1.13314	1.27133
	ARL	962.073	339.947	26.7218	9.46367	1170.24	207.368	18.4535	7.32416
0.55	CV	0.99948	0.998528	0.98111	0.945692	0.999573	0.997586	0.972528	0.929228
	CVLI	1.00149	1.0042	1.05218	1.1412	1.00122	1.00688	1.07473	1.17926
	ARL	38992.5	54818.4	286.875	25.8247	28971500	90944.6	114.578	15.228
0.8	CV	0.999987	0.999991	0.998256	0.980448	1	0.999995	0.995627	0.966608
	CVLI	1.00001	1.00001	1.00103	1.01134	1.0000	1.0000	1.00257	1.01915

Table 3.7: ARL study of the PD-DHR case using $\alpha = 0.0027, \lambda_0 = 0.0005, \beta_0 = 0.5$ and $\lambda_1 \in \{0.005,\ 0.01, 0.1\}$, $\beta_1 \in \{0.3, 0.45, 0.5, 0.55, 0.8\}$ for the lower and two-sided Weibull charts.

β	λ	Two-Sided				Lower-Sided			
		0.0005	0.005	0.01	0.1	0.0005	0.005	0.01	0.1
	ARL	2.14293	2.24911	2.26264	2.23078	3.78845	3.12392	2.95264	2.4641
0.1	CV	0.730308	0.745238	0.74702	0.742783	0.857927	0.824554	0.813216	0.770825
	CVLI	293.626	286.612	285.754	287.787	220.837	243.193	250.147	273.824
	ARL	15.7135	25.5046	21.7161	11.2554	35.2424	17.916	14.6482	7.5997
0.3	CV	0.967657	0.9802	0.976704	0.954544	0.98571	0.971691	0.965263	0.931888
	CVLI	1.67254	1.45168	1.51676	1.87331	1.34216	1.60512	1.71117	2.17171
	ARL	146.618	136.152	99.8061	35.7372	205.26	73.1526	53.6855	19.3748
0.45	CV	0.996584	0.996321	0.994978	0.98591	0.997561	0.993141	0.990643	0.973851
	CVLI	1.01956	1.02105	1.02861	1.07801	1.01401	1.03884	1.05257	1.13974
	ARL	370.37	234.585	166.023	52.8445	370.37	117.464	83.2065	26.657
0.50	CV	0.998649	0.997866	0.996984	0.990493	0.998649	0.995734	0.993973	0.981064
	CVLI	1.00539	1.00849	1.01197	1.03716	1.00539	1.01688	1.02375	1.07241
	ARL	962.073	404.434	276.395	78.2588	668.62	188.802	129.114	36.7506
0.55	CV	0.99948	0.998763	0.998189	0.99359	0.999252	0.997348	0.99612	0.986301
	CVLI	1.00149	1.00353	1.00516	1.01812	1.00214	1.00755	1.01102	1.0382

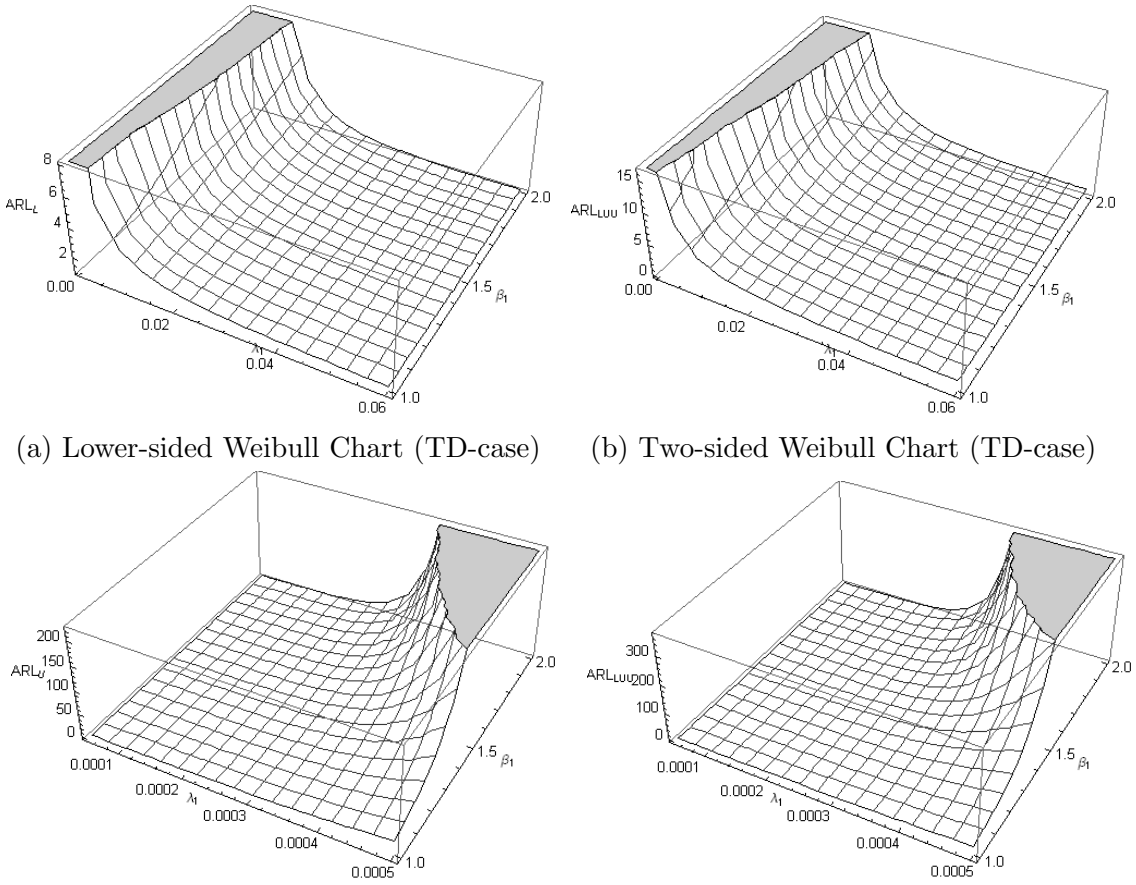

(a) Lower-sided Weibull Chart (TD-case)

(b) Two-sided Weibull Chart (TD-case)

(c) Upper-sided Weibull Chart (PD-case)

(d) Two-sided Weibull Chart (PD-case)

Figure 3.1: Process Deterioration Detection using $\lambda_0 = 0.0005, \beta = 1.5$

3.4.2 Average Length of Inspection (ALI)

Suppose $S_N = \sum_{i=1}^{N} X_i$ denotes the total length of inspection or elapsed time until the first out-of-control signal is issued. Therefore, by using Wald's equation, we have $ALI = E\{E(S_N|N)\} = E(N)E(X) = ARL \times E(X)$ and $Var(S_N) = Var\{E(S_N|N)\} + E\{Var(S_N$
$|N)\} = E(N \times Var(X)) + Var(N \times E(X)) = E(N)Var(X) + Var(N)E^2(X)$ (cf. Chan et al. [1997a], and Lai and Govindaraju [2008]). For our proposed chart, ALI for the lower-sided, upper-sided and two-sided control charts is defined as: $ALI_L = \lambda^{-1}\Gamma(\beta^{-1} + 1) \times ARL_L$, $ALI_U = \lambda^{-1}\Gamma(\beta^{-1}+1) \times ARL_U$ and $ALI_{L\cup U} = \lambda^{-1}\Gamma(\beta^{-1}+1) \times ARL_{L\cup U}$ where $E(X) = \lambda^{-1}\Gamma(\beta^{-1} + 1)$ is the mean of the Weibull distribution, whereas the variance is given by $Var(X) = \lambda^{-2}\left[\Gamma(2\beta^{-1} + 1) - \Gamma^2(\beta^{-1} + 1)\right]$.

Similarly, the variance of the ALI can be written as $Var(S_N) = \frac{1}{p}Var(X) + \frac{1-p}{p^2}E^2(X) = ARL \cdot Var(X) + [ARL \cdot E(X)]^2 - ARL \cdot [E(X)]^2]$ and finally the coefficient of variation is defined as $CVLI = CV(S_N) = \frac{\sqrt{Var(S_N)}}{E(S_N)}$.

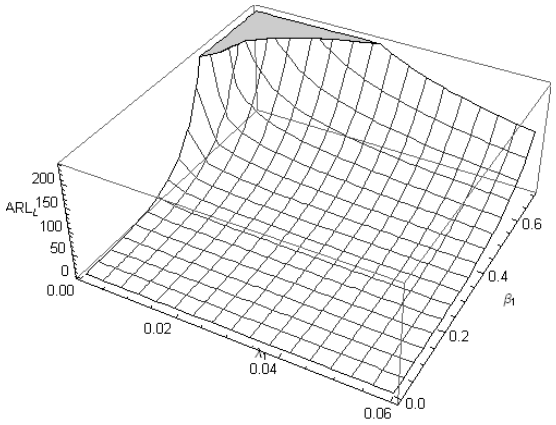

(a) Lower-sided Weibull Chart (PI-case)

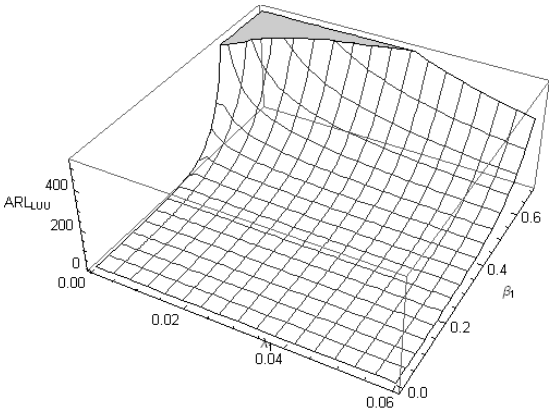

(b) Two-sided Weibull Chart (PI-case)

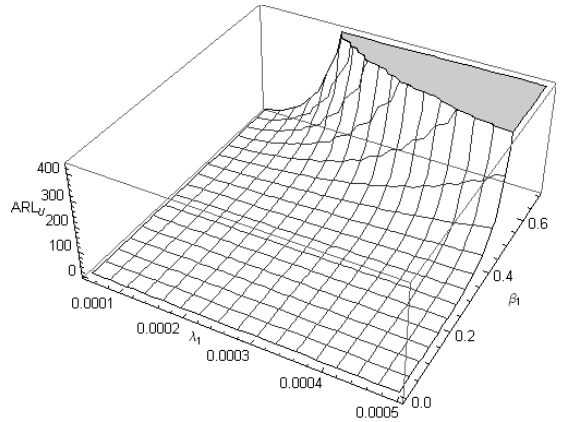

(c) Upper-sided Weibull Chart (TI-case)

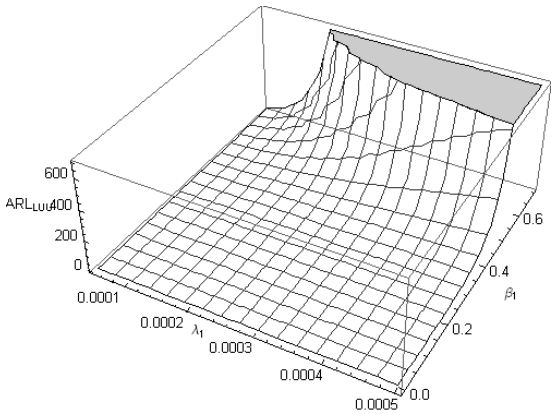

(d) Two-sided Weibull Chart (TI-case)

Figure 3.2: Process Improvement Detection using $\lambda_0 = 0.0005, \beta = 0.5$

3.4.3 Discussion of ARL Study

Definition 3.4.3.1 *For the Weibull distribution, if $\beta > 1$, i.e., increasing hazard rate (IHR), and λ is decreasing then the system is partial improvement (PI). We label this situation as the PI-IHR.*

Definition 3.4.3.2 *For the Weibull distribution, if $\beta > 1$, i.e., increasing hazard rate (IHR), and λ is increasing then the system is totally deteriorating (TD). We label this situation as the TD-IHR.*

Definition 3.4.3.3 *For the Weibull distribution, if $\beta < 1$, i.e., decreasing hazard rate (DHR), and λ is decreasing then the system is totally improving (TI). We label this situation as the TI-DHR.*

Definition 3.4.3.4 *For the Weibull distribution, if $\beta < 1$, i.e., decreasing hazard rate (DHR), and λ is increasing then the system is partially deteriorating (PD). We label this situation as the PD-DHR.*

We considered shifts for the following cases:

A Increasing Hazard Rate (IHR), i.e., $\beta > 1$)

1. λ decreases from $\lambda_0 = 0.0005$ to $\lambda_1 \in \{0.0003, 0.0001, 0.00005\}$ for $\beta_0 = 1.5$ to $\beta_1 \in \{1, 1.2, 1.5, 2\}$ [i.e. Partial Improvement (PI)].
2. λ increases from $\lambda_0 = 0.0005$ to $\lambda_1 \in \{0.005, 0.01, 0.1\}$ for $\beta_0 = 1.5$ to $\beta_1 \in \{1, 1.2, 1.5, 2\}$ [i.e. Total Deterioration (TD)].

B Decreasing Hazard Rate (DHR), i.e., $\beta < 1$)

1. λ decreases from $\lambda_0 = 0.0005$ to $\lambda_1 \in \{0.0003, 0.0001, 0.00005\}$ for $\beta_0 = 0.5$ to $\beta_1 \in \{0.1, 0.3, 0.45, 0.55\}$ [i.e. Total Improvement (TI)].
2. λ increases from $\lambda_0 = 0.0005$ to $\lambda_1 \in \{0.005, 0.01, 0.1\}$ for $\beta_0 = 0.5$ to $\beta_1 \in \{0.1, 0.3, 0.45, 0.55\}$ [i.e. Partial Deterioration (PD)].

We noticed from the ARL tables that when the $\lambda_1 = \lambda_0$ and $\beta_1 = \beta_0$, the ARL value is equal to the nominal value, i.e., 370. Note that here we are reporting ARL discussion for $\alpha = 0.0027$. However, the graphical presentation for some other choices of α is given in Figure-A.1 of Appendix A, i.e., Section-3.7. We examine the control chart's detection performance, varying one parameter as the other one is held fixed.

Case A-1 (PI-IHR) a decrease in λ: When the system improves, the effect should be reflected by decrease in λ, i.e., the system fails occasionally. However, in case of two or more parameters families, the behavior (i.e., related to improvement or deterioration) is also dependent on the other parameters, e.g. the shape, location or both parameters. Since the Weibull distribution is a two parameters distribution, we fixed the shape parameter $\beta_0 = 1.5$ (for in-control process) while $\beta_1 \in \{1, 1.2, 1.5, 2\}$ to represent an out-of-control situation. The rate parameter shifts from $\lambda_0 = 0.0005$ to $\lambda_1 \in \{0.0003, 0.0001, 0.00005\}$. This situation can be labeled as a partial improvement (PI) because $\beta > 1$ and the rate parameter of the distribution is gradually decreasing, which will result into a decrease rate of events' occurrences. When the system partially improve, the practitioner is more generally concerned in the process improvement detection for its sustainability/maintainability, and for this purpose, the upper-sided control chart is commonly used/employed. In Table-3.4, we computed the ARL values for two-sided and upper-sided charts. The coefficient of variation (CV) value is also reported without parentheses below the ARL (standard deviation of the run length can be recovered by using the CV and the ARL values).

Some remarks are very clear from Table-3.4. The shift in the shape parameter has a significant effect, and it is not robust as claimed in some previous studies, e.g. Borror and Keats [2003]. As the size of a shift gets larger, the ARL values also increases, which is a clear sign of its significant impact on the control chart performance. For $\beta < 1.5$, the ARL

values are smaller than the case of $\beta > 1.5$. For fixed β, the shift in the rate parameter, i.e. λ, is detected very quickly; however, the detection of a shift with two-sided chart is quicker than the upper-sided chart. We also studied the average length of inspection (ALI) properties and noticed that this measure is not scale free. Therefore, we are only reporting the CV values, here. For small to moderate shifts, the CV values of the ARL are smaller than ALI. The CV value also gradually decreases as the size of the shift in the rate parameter increases. Some selected graphical presentations of this are given in Figure-3.1.

Case A-2 (TD-IHR) an increase in λ: This is an important case because it detects process deterioration. When λ increases (with $\beta > 1$) from its nominal value, we expect a process/system would fail more frequently. This situation can be named as a total deterioration (TD). In our study, we fixed the shape parameter $\beta_0 = 1.5$ (for in-control process) while $\beta_1 \in \{1, 1.2, 1.5, 2\}$ to represent out-of-control situation. The rate parameter shifts from $\lambda_0 = 0.0005$ to $\lambda_1 \in \{0.005, 0.01, 0.1\}$. We used the lower-sided chart and further it was compared to the two-sided chart. To detect process deterioration, the ARL values of the lower and the two sided charts have been tabulated in Table-3.5.

The ARL values for $\beta < 1.5$ in the first two columns are smaller as compared to the case when we have $\beta > 1.5$. This conclusion is the same as noted in the case of process improvement. Thus, again the effect of the shape parameter is very significant on the control chart performance. As a shift in the rate parameter occurs, the lower-sided chart outperforms than the two-sided chart. The CV values gradually decrease, as the size of a shift in λ increases, which means that the out-of-control situations will be detected very quickly with the Weibull chart. The graphical presentation of ARL is given in Figure-3.1.

Case B-1 (TI-DHR) a decrease in λ: It is a sign of system improvement if the shape parameter β of the Weibull distribution is less than one. Moreover, if the rate λ parameter also becomes small, i.e., $\lambda_1 < \lambda_0$, then such a situation can be labeled as a total improvement (TI) (as the rate of occurrences for the renewal process is defined as $E(X)^{-1}$ and for the Weibull distribution it depends on both, i.e., the rate and the shape parameters). Thus, here one needs to use an upper-sided control chart for the improvement detection. For study purposes, we fixed the shape parameter $\beta_0 = 0.5$ (for in-control process) while $\beta_1 \in \{0.1, 0.3, 0.45, 0.55\}$ to represent out-of-control situation. The rate parameter shifts from $\lambda_0 = 0.0005$ to $\lambda_1 \in \{0.0003, 0.0001, 0.00005\}$. In Table-3.6, we computed the ARL values for the two-sided and the upper-sided charts. The coefficient of variation (CV) value is also reported without parentheses below the ARL (standard deviation of the run length distribution can be recovered by using the CV and ARL values).

From Table-3.6 (and Figure-3.2), it is clear that large-size shifts either in the shape or rate parameter can be detected quickly. The two-sided chart is good to detect large-size shifts in the shape parameter β. However, for small to moderate shifts, the upper-sided

chart is efficient in the detection of shifts than the two-sided chart. For $\beta > 0.5$ and $\lambda = 0.0005$, the ARL value is larger than the nominal standard, which is a sign that the shape parameter significantly affects the control chart performance.

For fixed β, the CV values decrease with the occurrence of a shift in the rate parameter, which means that the proposal is good to detect large size shifts. This conclusion is also true for the case when the rate parameter is fixed and a shift occurs in the shape parameter β. The proposal would take larger time/data points to detect shifts in the case of $\beta > 0.5$ than $\beta < 0.5$.

Case B-2 (PD-DHR) an increase in λ: In this case, we consider a situation where β is less than one and event's occurrence rate increases. Thus, a system will have some deterioration, and we label this case as a partial deterioration (PD). For this purpose, we fixed the shape parameter $\beta_0 = 0.5$ (for in-control process) while $\beta_1 \in \{0.1, 0.3, 0.45, 0.55\}$ to represent out-of-control situation. The rate parameter shifts from $\lambda_0 = 0.0005$ to $\lambda_1 \in \{0.005, 0.01, 0.1\}$. The ARL study is conducted to study the chart performance, and results are given in Table-3.7 (Figure-3.2).

For fixed λ, to detect a large shift in the shape parameter, the two-sided chart is efficient while the lower-sided chart is appropriate for the detection of small to moderate shifts. We also notice that the CV values are less than one for large size shifts and are close to one for small to moderate shifts. Therefore, the proposal chart is good to detect large shifts. When the process is in-control, i.e., $\lambda_1 = \lambda_0$ and $\beta_1 = \beta_0$, the ARL value is equal to the nominal value, i.e., 370. But if $\beta_1 > \beta_0$ and $\lambda_1 = \lambda_0$, the ARL values are greater than 370. Thus, we suggest to consider either unbiased design of ARL or different sensitizing rules to improve the control chart performance.

3.4.4 EQL and RARL for the Weibull chart

To assess the overall performance of the control charts, the expected quadratic loss (EQL) and relative average run length (RARL) are commonly used measures. EQL (Ou et al. [2012]) evaluate the expected loss due to poor quality. It can be described as the weighted average of the ARL over a range of shifts, i.e., $\theta_{min} < \theta < \theta_{max}$ with the weight θ^2, where θ is general notation, which may denote a shift in the shape or rate parameter.

$$EQL(.) = \frac{1}{\theta_{max} - \theta_{min}} \int_{\theta_{min}}^{\theta_{max}} \theta^2 ARL(\theta)\, d\theta \tag{3.3}$$

In Equation-3.3, we considered the uniform distribution of the shifts; however, this distribution can be any other distribution. A general equation of EQL can be written as given below:

$$EQL(.) = \int_{\theta_{min}}^{\theta_{max}} \theta^2 ARL(\theta) f(\theta)\, d\theta \tag{3.4}$$

where $f(\theta)$ is a distribution of the shifts. For the joint monitoring of shifts in rate and shape parameters of the Weibull distribution, one can write the EQL equation as follows:

$$EQL = \int_{\lambda^*_{min}}^{\lambda^*_{max}} \int_{\beta^*_{min}}^{\beta^*_{max}} \lambda^{*2}\beta^{*2} ARL(\beta^*, \lambda^*) f(\lambda^*) f(\beta^*)\, d\lambda^* d\beta^* \tag{3.5}$$

A chart with minimum EQL is considered to be a standard chart. Similarly, the RARL is defined as the integration of the ratio of ARL of the specific and existing charts over a range of shifts.

$$RARL(.) = \frac{1}{\theta_{max} - \theta_{min}} \int_{\theta_{min}}^{\theta_{max}} \frac{ARL(\theta)}{ARL_{specific}(\theta)}\, d\theta \tag{3.6}$$

For the specific chart $RARL = 1$ while for other charts' $RARL > 1$ which implies that the performance of the specific chart is mediocre as compared to existing chart. The general equation for any distribution of the shift is given below (Equation-3.7):

$$RARL(.) = \int_{\theta_{min}}^{\theta_{max}} \frac{ARL(\theta)}{ARL_{specific}(\theta)} f(\theta)\, d\theta \tag{3.7}$$

$$RARL(.) = \int_{\lambda^*_{min}}^{\lambda^*_{max}} \int_{\beta^*_{min}}^{\beta^*_{max}} \frac{ARL(\lambda^*, \beta^*)}{ARL_{specific}(\lambda^*, \beta^*)} f(\lambda^*) f(\beta^*)\, d\lambda^* d\beta^* \tag{3.8}$$

These types of performance measures have been considered many authors in literature, e.g. see Ou et al. [2012], Shamsuzzaman and Wu [2012] and Chan et al. [2000], and references cited therein.

Table 3.8: EQL and RARL estimation at different false alarm probability

	EQL			RARL		
ARL_0	Lower-Sided	Upper-Sided	Two-Sided	Lower-Sided	Upper-Sided	Two-Sided
20,000	0.494749	16.93226	1.05824	17.3723	98.1932	22.18
2000	0.219303	16.51073	0.229966	5.05194	75.2284	7.79427
740.74	0.21592	16.28782	0.217552	2.70819	65.3263	4.17344
370.37	0.215468	16.11149	0.215912	1.84688	58.4179	2.70819
200	0.215352	15.93651	0.215491	1.42448	52.2782	1.91887

The EQL and RARL with $\lambda_0 = 0.0005$ and $\beta_0 = 1.5$ have been numerically computed using the statistical software R, R Core Team [2013], considering a uniform distribution for both shifts over the range of $[0.00005 < \lambda < 0.5]$ and $[0.5 < \beta < 2.5]$. The choice of uniform distribution has been done purely illustrative purposes, and one can consider some more realistic distributions for shifts. We compared the exponential chart to the Weibull chart. Both the EQL and RARL have a decreasing trend with the increase of the false alarm probability (Table-3.8), and the Weibull chart is superior to the counterpart according to the RARL index.

3.5 Effect of Parameters Estimation on ARL

In the traditional quality control setup, the parameters are assumed to be known, i.e., an engineer has knowledge about the system including the parameters. However, outside this engineering box, most researchers and practitioners, have little knowledge about the system so that the assumption of known parameters is difficult to fulfil. When the parameters are unknown or unspecified, these should be estimated from reference data or Phase-I data. A comprehensive overview of the effect of parameter estimation is given by Psarakis et al. [2014]. Here, to see the effect of estimation on ARL, we examine two estimation methods, namely the maximum likelihood and the Bayesian method. Here we are reporting only results while the derivations can be seen in Appendix B (cf. Section-3.7).

Case I- Maximum Likelihood estimation: The maximum likelihood method is the most commonly used method, and it has very nice properties, e.g. invariance property, asymptotic efficiency, etc. To estimate parameters with the maximum likelihood method, some necessary derivations are given in the Appendix B (cf. Section-3.7). When the parameters are estimated using the ML method, we have Table-3.9, while Table-3.12 is devoted to the ARL with estimation effect.

Table 3.9: MLE Estimation with $\beta_0 = 1.5$ and $\lambda_0 = 0.0005$

Sample Size	$\hat{\beta}$	Shift in β	$\hat{\lambda}$	Shift in λ
$n = 30$	1.63	1.086667	0.00042	0.840000
	(0.232667)		(0.000050)	
$n = 60$	1.519768	1.013179	0.000487	0.974000
	(0.152778)		(0.000044)	
$n = 100$	1.545705	1.030470	0.000504	1.008000
	(0.120719)		(0.000034)	
$n = 150$	1.5410593	1.027373	0.000494	0.988000
	(0.098105)		(0.000028)	
$n = 300$	1.50314	1.002093	0.000507	1.014
	(0.050815)		(0.000008)	

Case II: Bayesian estimation: Bayesian methodology is the most comprehensive way of combining current state of knowledge with the prior information available about phenomena, which are summarized by posterior distribution with the help of Bayes theorem. However, for parameter estimation in Bayesian, the choice of an appropriate loss function plays an important role, and it is very reliant on the phenomena under study. Many researchers believe that loss function is part of the problem or phenomena, but most of the time it is extremely difficult to find appropriate loss function, hence analysts prefer to use well known square error loss function. Serel [2009] highlighted various important aspects of loss functions. Here, for general purpose, we are comparing eight different loss

functions named as squared error loss function (SELF), weighted squared error loss function (WSELF), modified squared error loss function (MSELF), squared logarithmic loss function (SLLF), entropy loss function (ELF), K- loss function (KLF), precautionary loss function (PLF) and the Degroot loss function (DLF). Table-3.10 shows the estimators of θ under various loss functions (LF) while the numerical procedure to evaluate them in given in Appendix B (cf. Section-3.7).

Table 3.10: Best decision functions d for estimating θ under various loss functions

LF	Mathematical Form	Form of d^*	Posterior Risk
SELF	$(\theta - d)^2$	$E(\theta\|\mathbf{x})$	$Var(\theta\|\mathbf{x})$
WSELF	$\frac{(\theta-d)^2}{\theta}$	$(E(\theta^{-1}\|\mathbf{x}))^{-1}$	$E(\theta\|\mathbf{x}) - E^{-1}(\theta^{-1}\|\mathbf{x})$
MSELF	$\left(1 - \frac{d}{\theta}\right)^2$	$\frac{E(\theta^{-1}\|\mathbf{x})}{E(\theta^{-2}\|\mathbf{x})}$	$1 - \frac{E^2(\theta^{-1}\|\mathbf{x})}{E(\theta^{-2}\|\mathbf{x})}$
SLLF	$(\log\theta - \log d)^2$	$\exp(E(\log\theta\|\mathbf{x}))$	$Var(\log\theta\|\mathbf{x})$
ELF	$\frac{d}{\theta} - \log\frac{d}{\theta} - 1$	$(E(\theta^{-1}\|\mathbf{x}))^{-1}$	$E(\log\theta\|\mathbf{x}) + \log(E(\theta^{-1}\|\mathbf{x}))$
KLF	$\left(\sqrt{\frac{d}{\theta}} - \sqrt{\frac{\theta}{d}}\right)^2$	$\sqrt{\frac{E(\theta\|\mathbf{x})}{E(\theta^{-1}\|\mathbf{x})}}$	$2[\sqrt{E(\theta\|\mathbf{x})E(\theta^{-1}\|\mathbf{x})} - 1]$
DLF	$\frac{(\theta-d)^2}{d^2}$	$\frac{E(\theta^2\|\mathbf{x})}{E(\theta\|\mathbf{x})}$	$\frac{Var(\theta\|\mathbf{x})}{E(\theta^2\|\mathbf{x})}$
PLF	$\frac{(\theta-d)^2}{d}$	$\sqrt{E(\theta^2\|\mathbf{x})}$	$2[\sqrt{E(\theta^2\|\mathbf{x})} - E(\theta\|\mathbf{x})]$

The samples of sizes 30, 60, 100, 150, 300, 500, 700, 1000, 1500 and 2000 are considered from a Weibull distribution with parameters $\lambda = 0.0005$ and $\beta = 1.5$, using the different loss functions for the Bayesian estimation. To get an idea of the effect of the different loss functions, in Table-3.11 we have reported the Bayesian estimates, their posterior risk and the "shift", that is, the ratio between the estimated value of the parameter and the true value. We may observe that DLF and PLF are unsuitable for analysis because they have a high value of posterior risk as compared to the other loss functions. The hyperparameters value's for the rate parameter λ are such that the mean of prior distribution is greater or equal to three times its variance, while for the shape parameter, hyperparameters are considered such that the prior distribution has variance less than 0.1, i.e., very informative prior. The following steps have been followed for the computation of ARL:

1. Select a sample size (say n).

2. Choose a very large m to repeat the process of calculation (we used $m = 100000$).

3. Generate a sample of selected size n, find the MLE and the Bayes estimates (i.e., at each iteration of m, MLE is obtained by satisfying the stopping criteria, i.e., 0.00000001 while Bayes estimates using the information given in Appendix-B, Section-3.7), and compute the ARL using the estimated parameters.

The effect of estimation on the control chart performance is multidimensional because it is not only a result of the accuracy and precision of parameter estimates, but also of

Table 3.11: Bayes estimates with respective posterior risk under different loss functions

Sample Size	$n=30$				$n=60$				$n=100$				$n=150$			
LF	β	Shift	λ	Shift	β	Shift	λ	Shift	β	Shift	λ	Shift	β	Shift	λ	Shift
SELF	1.531303	1.020869	0.000508	1.016000	1.605174	1.070116	0.000523	1.046000	1.529093	1.019395	0.000534	1.068000	1.509314	1.006209	0.000517	1.034000
	(0.052960)		(0.020633)		(0.064625)		(0.020834)		(0.022366)		(0.021491)		(0.021615)		(0.021225)	
WSELF	1.495602	0.997068	0.000419	0.838000	1.582318	1.054879	0.000430	0.860000	1.516002	1.010668	0.000459	0.918000	1.499861	0.999907	0.000449	0.898000
	(0.035701)		(0.00089)		(0.022857)		(0.000093)		(0.013091)		(0.000074)		(0.009453)		(0.000068)	
MSELF	1.459923	0.973282	0.000410	0.820000	1.559483	1.039655	0.000425	0.850000	1.503023	1.002015	0.000457	0.914000	1.490303	0.993535	0.000447	0.894000
	(0.023856)		(0.020117)		(0.014431)		(0.014431)		(0.008561)		(0.006445)		(0.006373)		(0.004369)	
SLLF	1.513494	1.008996	0.000423	0.846000	1.593757	1.062505	0.000432	0.864000	1.522534	1.015023	0.000461	0.922000	1.504607	1.003071	0.000450	0.900000
	(0.023593)		(0.021872)		(0.014342)		(0.012309)		(0.008599)		(0.006588)		(0.006283)		(0.004446)	
ELF	1.495602	0.997068	0.000419	0.838000	1.582318	1.054879	0.000430	0.860000	1.516002	1.010668	0.000459	0.918000	1.499861	0.999907	0.000449	0.898000
	(0.816950)		(0.010656)		(0.924985)		(0.006077)		(0.836453)		(0.003273)		(0.813905)		(0.002213)	
KLF	1.513347	1.008898	0.000461	0.922000	1.593705	1.062470	0.000474	0.948000	1.522533	1.015022	0.000495	0.990000	1.50458	1.003053	0.000482	0.964000
	(0.047741)		(0.423362)		(0.028890)		(0.432027)		(0.017270)		(0.323537)		(0.012605)		(0.304122)	
DLF	1.565888	1.043925	40.65165	81303.3	1.645435	1.096957	39.83485	79669.7	1.54372	1.029147	40.24954	80499.08	1.523635	1.015757	41.0309	82061.8
	(0.022087)		(0.999988)		(0.024468)		(0.999987)		(0.009475)		(0.999987)		(0.009399)		(0.999987)	
PLF	1.548499	1.032333	0.143643	287.286	1.62518	1.083453	0.144342	288.684	1.536389	1.024259	0.146598	293.196	1.516458	1.010972	0.145689	291.378
	(0.034392)		(0.286271)		(0.040011)		(0.287637)		(0.014592)		(0.292129)		(0.014287)		(0.290345)	

Table 3.12: ARL comparison based on the MLE and Bayes method using $\alpha = 0.0027$ for the lower, upper and two-sided Weibull charts.

Method		MLE			Bayes		
Sample Size		Two-Sided	Upper-Sided	Lower-Sided	Two-Sided	Upper-Sided	Lower-Sided
30	ARL	1778.4870 (1779.87)	1743.0491 (1743.0491)	987.4395 (986.9394)	2249.1078 (2248.6073)	3674.4069 (3673.9068)	1234.1535 (1233.6529)
	CV	0.9972	1.0	0.9995	0.9979	0.9993	0.9979
60	ARL	709.3625 (708.8623)	1400.1993 (1400.1943)	553.1646 (552.6644)	1933.3382 (1932.8381)	3372.2518 (3371.7518)	1136.3468 (1135.8467)
	CV	0.9993	0.9999	0.9991	0.9997	0.9999	0.9996
100	ARL	534.7478 (534.2476)	965.4525 (964.9523)	463.4751 (462.9748)	971.1008 (970.6007)	1206.0304 (1205.5303)	691.1763 (690.6761)
	CV	0.9991	0.9995	0.99989	0.9995	0.9996	0.9993
150	ARL	469.7063 (469.2059)	614.2744 (613.7742)	427.5369 (427.0367)	476.3881 (475.8878)	543.2111 (542.7108)	413.0249 (412.5246)
	CV	0.9989	0.9992	0.9988	0.9989	0.99908	0.9988
300	ARL	416.6861 (416.1858)	460.8013 (460.3010)	397.6209 (397.1206)	408.0156 (407.0127)	447.1089 (446.3073)	385.1683 (384.0327)
	CV	0.9988	0.9989	0.9987	0.9975	0.9982	0.9971
500	ARL	396.5640 (396.0637)	418.5591 (418.0588)	385.9183 (385.4180)	388.0156 (387.0127)	398.1090 (397.0729)	375.1683 (374.0367)
	CV	0.99874	0.9988	0.9987	0.9974	0.9974	0.9969
700	ARL	390.0456 (389.5453)	404.7264 (404.7264)	382.1929 (381.6926)	378.1043 (377.1253)	390.1256 (389.1675)	373.0459 (372.4051)
	CV	0.9987	0.9988	0.9987	0.9974	0.9975	0.9983
1000	ARL	383.5246 (383.0243)	393.4354 (392.9351)	378.1595 (377.6592)	376.4287 (375.4081)	385.6921 (384.0621)	372.5679 (372.0121)
	CV	0.9987	0.9987	0.9987	0.9973	0.9958	0.9985
1500	ARL	379.0529 (378.5526)	385.4103 (384.9099)	375.4691 (374.9688)	374.0565 (373.5061)	379.1487 (378.4173)	371.9874 (370.0987)
	CV	0.9987	0.9987	0.9987	0.9985	0.9981	0.9949
2000	ARL	376.8916 (376.3913)	381.6237 (381.1234)	374.1894 (373.6890)	372.4629 (371.0427)	378.1090 (373.2092)	371.0863 (370.0326)
	CV	0.9987	0.9987	0.9987	0.9962	0.9978	0.9972

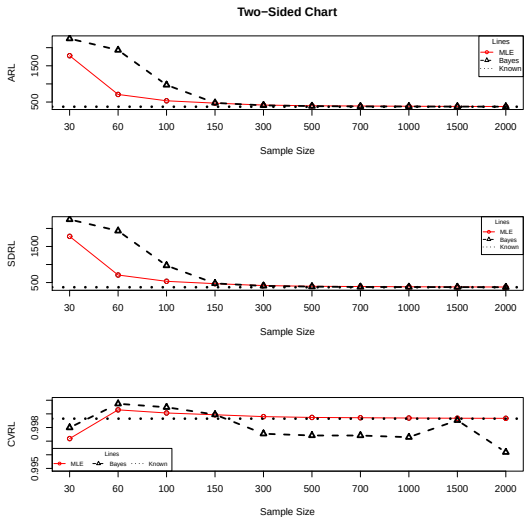

(a) Estimation effect on Two-Sided chart for MLE versus Bayes

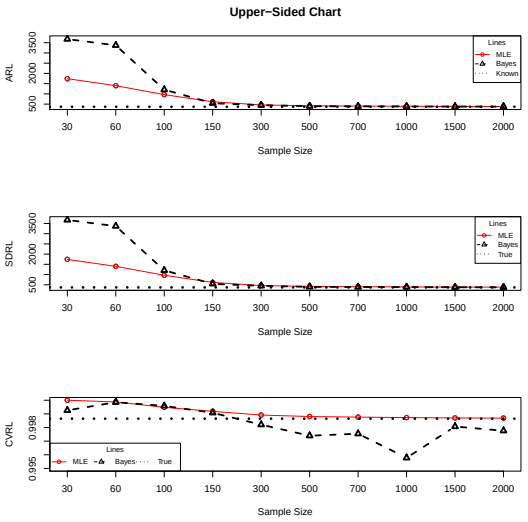

(b) Estimation effect on Upper-Sided chart for MLE versus Bayes

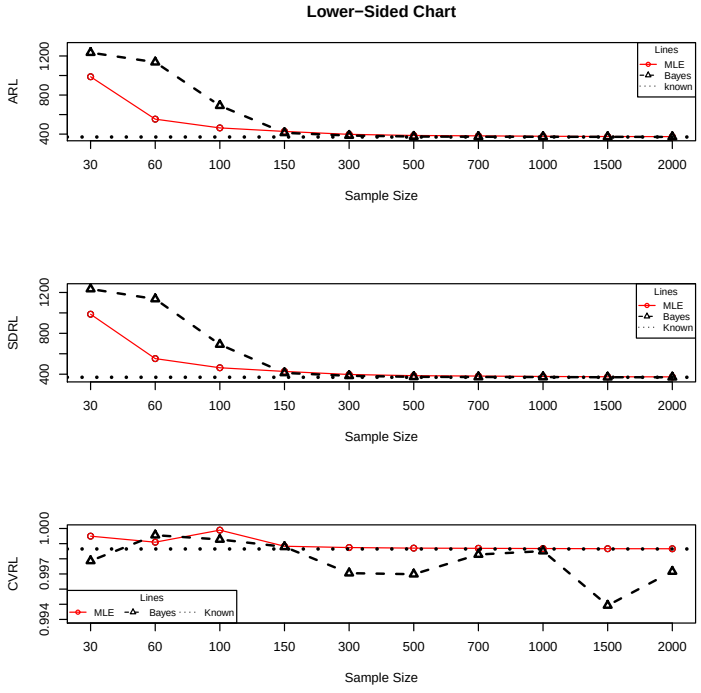

(c) Estimation effect on Lower-Sided chart for MLE versus Bayes

Figure 3.3: Sample size requirement to minimize the effect of estimation on the Weibull chart

the choice of the design parameter and of the size of a shift to be detected. In Table-3.12, or Figure-3.3, we have reported the estimated ARL obtained as an average over the m samples, along its sample standard deviation and CV. The estimated ARL should be close to its (true) nominal value of 370.37. The ARL estimated from the Bayesian method is larger than that obtained from the MLE for the smaller sample sizes. As the sample size increases, the Bayesian methodology starts to do better than the MLE on the CV. Thus, for small sample sizes the Bayesian estimates should be used with care (because of a possibly adverse effect of a bad choice of hyperparameters). Table-3.12 or Figure-3.3 may also suggest the phase-I sample size required to attain the nominal ARL, which is between 1000 and 1500 for the MLE and between 700 and 1000 for the Bayesian estimator.

To see the estimation effect, we compared the relative estimation error or $\%deviation$. The relative estimation error is defined as the difference between the true parameter and its estimated value divided by the true value, i.e., %deviation$= 100 \times$ (Known $-$ Estimated)/Known. Thus, we have obtained the results (for the two-sided chart at the sample of size $n = 700$) %deviation$= 100 \times$ (MLE $-$ Known)/Known $= 5.04$, and %deviation$= 100 \times$ (Bayes $-$ Known)/Known $= 2.05$. Thus, the %deviation for the Bayes estimates is less as compared to the MLE. This also signify the usefulness of the Bayesian methodology.

3.6 Applications

We present an illustrative example about the proposed chart by using the terminologies as suggested by Chan et al. [2000] in this section.

A radar speed is an electronic device that is used to measure the speed of moving objects. It is used in law-enforcement to measure the speed of moving vehicles and is often used in professional spectator sport, for such things as the measurement of the speed of pitched baseballs, runners and tennis serves. A radar speed gun is a Doppler radar unit that may be hand-held, vehicle-mounted or static. A radar speed gun should be efficient in the detection of true over-speeding as compared to false alarm. False alarms can occur; however, due to the large number of devices, such as automatic door openers (such as the ones at supermarkets) and adaptive automotive cruise control, that operates in the same part of the electromagnetic spectrum as radar guns.

Since, the speed of each moving object is considered independent of others, thus, radar speed gun is a good example of the renewal process. A study of the detection ability of over-speeding, i.e., to differentiate between true and false alarm over speeding, has been designed by considering the Weibull distribution for time-between-events. For this purpose, we generated fifteen observations from the in-control process with $\beta = 1.5$ and $\lambda = 0.0005$ while the next 8 observations by using $\beta = 1.8$ and $\lambda = 0.05$, and the

last 7 observations from $\beta = 1.2$ and $\lambda = 0.0001$. The resulting data set is given in Table-3.13, where X denotes time in second between the detection of faults (i.e., over-speed events) using the speed gun. The value of the false alarm probability has been assigned as $\alpha = 0.0027$ to design a two-sided control chart. For these specifications, we have: Lower limit-$\ln(LCL) = 3.196252$, Central limit-$\ln(CL) = 7.356561$ and Upper limit-$\ln(UCL) = 8.859721$. The natural logarithm of the data (cf. Table-3.13) and of the control limits is taken for a better presentation of the chart. The lower control limit for a single limit Weibull chart is $\ln(LCL) = 3.658801$. For comparison purposes, the exponential chart has also been constructed, with $\ln(LCL) = 0.891371$, $\ln(CL) = 7.131833$ and $\ln(UCL) = 9.386574$. Note that the control limits for the exponential chart have been derived assuming an exponential distribution with the same expectation of the Weibull. For example, by assuming $\lambda = 0.0005$ and $\beta = 1.5$, the mean of the Weibull distribution is 1805.491. Thus, we obtain the rate parameter $\lambda = 0.000554$ of the exponential distribution by solving $\frac{1}{\lambda} = 1805.491$. The graphical presentation of the chart is given in Figure-3.4. A cumulative probability control (CPC) chart has also been designed using the Weibull distribution and results are given in the last column of Table-3.13.

For the above specifications and computed control limits, Table-3.13 contains a hypothetical data set for monitoring and implementation of Weibull chart. In Table 3.13, 'i.c', 'im.', and 'o.c' stand for 'in-control', 'improved', and 'out-of-control', respectively, as defined by Chan et al. [2000]. It is clear from Table-3.13 and Figure-3.4 that using our proposal an out-of-control signal is detected efficiently as compared to the exponential chart. Using the CPC chart the conclusion is almost similar except for sample numbers 21 and 24 where Weibull chart has marked them in-control observations while with CPC chart, sample number 21 is out-of-control (deteriorated) and 24 is improved. Note that this discrepancy is probably due to rounding up on the probability scale. The CPC and the TBE charts must give the same result, because the one is obtained as a monotone transformation of the other. In Figure-3.4 we plotted black $'*'$s to represent in-control observations, red circles $\bullet$ for process deterioration and blue filled triangles $\triangle$ for the process improvement. The vertical line at the sample number 15 indicates the change from in-control to out-of-control. It is clear from Figure-3.4 that the Weibull charts detects over-speeding more efficiently than the exponential chart.

In the rest of this section we have re-examined four existing case studies on real data with our proposed methodology. In the first three ones there is no phase-I sample, therefore we use in-sample estimates of the Weibull parameters to set up the control chart and monitor the data retrospectively, just to highlight differences in detection ability with respect to the previously used charts. Then it will be the task of the quality engineer to inspect out-of-control signals and decide which ones are to be retained for the estimation sample.

Table 3.13: Inspection of the over-speeding Process

Sample #	X	log of X	Indication	Cumulative Probability
1	1340.45480	7.200764 >LCL	i.c.	0.422298
2	4945.24666	8.506182 >LCL	i.c.	0.979516
3	810.16855	6.697242 >LCL	i.c.	0.227266
4	3101.73864	8.039718 >LCL	i.c.	0.855049
5	341.21877	5.832524 >LCL	i.c.	0.068044
6	1320.22008	7.185554 >LCL	i.c.	0.415104
7	2855.82146	7.957115 >LCL	i.c.	0.818461
8	877.76561	6.777380 >LCL	i.c.	0.252299
9	3129.40554	8.048598 >LCL	i.c.	0.858755
10	2112.02827	7.655404 >LCL	i.c.	0.662161
11	1444.51715	7.275530 >LCL	i.c.	0.458719
12	3786.18889	8.239115 >LCL	i.c.	0.926075
13	792.63814	6.675367 >LCL	i.c.	0.220808
14	2406.01341	7.785726 >LCL	i.c.	0.732725
15	683.47965	6.527197 >LCL	i.c.	0.181086
16	16.12755	2.780529 <LCL	o.c.	0.000724
17	20.43008	3.017008 <LCL	o.c.	0.001032
18	15.65355	2.750698 <LCL	o.c.	0.000692
19	19.39071	2.964794 <LCL	o.c.	0.000954
20	15.53536	2.743118 <LCL	o.c.	0.000684
21	32.41899	3.478744 >LCL	i.c.	0.002062*
22	20.92817	3.041096 <LCL	o.c.	0.001069
23	20.15432	3.003419 <LCL	o.c.	0.001011
24	6813.59698	8.826675 <UCL	i.c.	0.998142**
25	1913.52687	7.556703 <UCL	i.c.	0.607748
26	7171.13431	8.877819 >UCL	im.	0.998875
27	8100.56679	8.999689 >UCL	im.	0.999712
28	1383.17086	7.232134 <UCL	i.c.	0.437370
29	8186.35518	9.010224 >UCL	im.	0.999747
30	10853.47681	9.292241 >UCL	im.	0.999997

In the fourth case-study, a phase-I sample has been assumed instead.

3.6.1 Case Study-1

Using the data set given by Chan et al. [2000], we established a chart based on the Weibull distribution. With the help of Kolmogorov-Smirnov test, we found distance $D = 0.08081$ and p-value $= 0.8875$ based on simulation because the parameters of the Weibull distribution have been estimated from the data. Hence, TBE data are Weibull distributed. The estimated parameter values from the data set are $\hat{\lambda} = 0.000541$ and $\hat{\beta} = 2.386482$ while standard errors are 0.000034 and 0.274314, respectively. For the exponential distribution, we have $\hat{\lambda} = 0.000611$ with standard error 0.000088. Thus, for the Weibull distribution, we have $LCL = 116.000132$, $CL = 1585.273981$ and $UCL = 4077.786333$ respectively at $\alpha = 0.0027$ and $LCL = 719.910558$, $CL = 1585.273981$ and $UCL = 2621.686928$ respectively at $\alpha = 0.2$. For the exponential chart, we have, $LCL = 2.210985$, $CL = 1134.447104$ and $UCL = 10814.48558$ respectively at $\alpha = 0.0027$ while $LCL = 172.439469$, $CL = 1134.447104$ and $UCL = 3768.551707$ respectively at

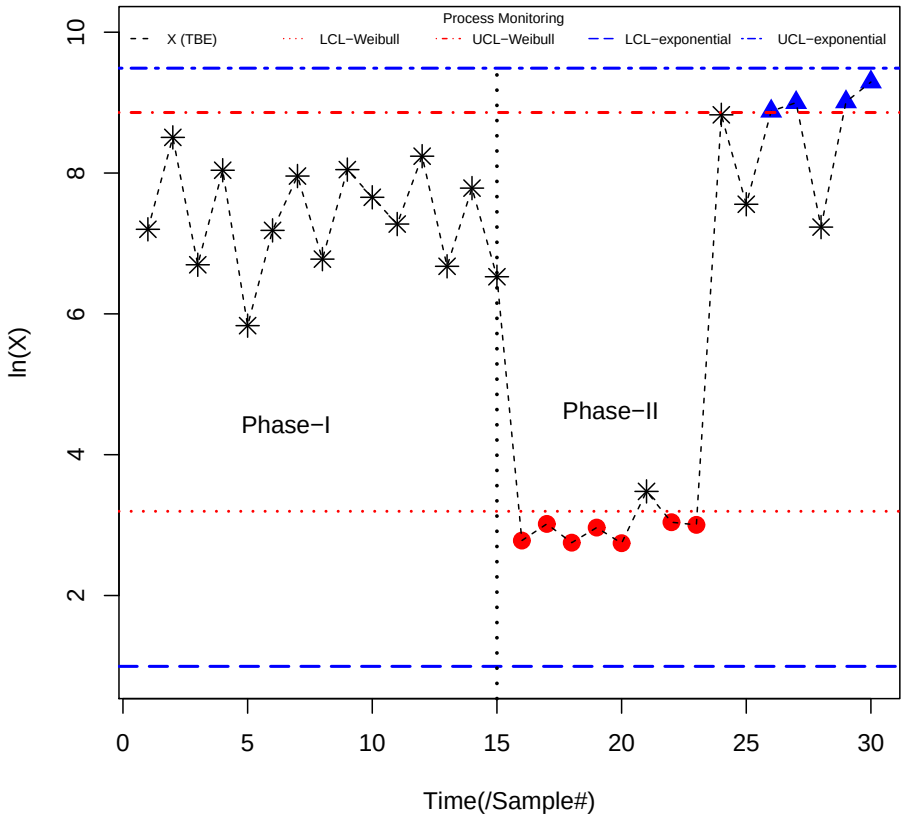

Figure 3.4: Weibull Quantity Control Chart for Radar Speed Gun

$\alpha = 0.2$. Chan et al. [2000] concluded that there is no indication that the process is an out-of-control even for $\alpha = 0.2$. But in our case, with $\alpha = 0.2$, six values, i.e., 262.53, 445.65, 500.5, 525.4,600.1 and 644.99 are out-of-control (cf. Figure-C.1 given in Appendix C, i.e., Section-3.7) while for $\alpha = 0.0027$ the performance of both charts, i.e., the Weibull and the exponential charts, is the same. Hence, our proposed methodology proves more sensitive to out-of-control situations.

3.6.2 Case Study-2

Chen [2014] provided the number of hours between failures for the last 20 failures of an important valve. The time between failures data are right skewed and therefore not normally distributed. Using the Kolmogorov-Smirnov test and computing the p-value from simulation, we found $D = 0.1108$ and $p - value = 0.9431$. To apply the proposed control scheme to monitor the failure data, we have $\hat{\lambda} = 0.001408$ with standard error 0.000315 based on the exponential distribution while $\hat{\lambda} = 0.001548$ and $\hat{\beta}_0 = 0.827572$ with standard errors 0.000439, 0.147769, respectively, based on the Weibull distribution. Further,

suppose that $\alpha = 0.0027$ and for this we have $LCL = 0.220298$ for the Weibull chart while $LCL = 0.959215$ for the exponential chart. Thus, both charts, neither the exponential nor the Weibull chart signalled an alarm, which leads us to the same conclusion as Chen [2014] that the failure mechanism of this valve is in-control.

3.6.3 Case Study-3

Santiago and Joel [2013] considered a data set of a large hospital system concerned with a very high rate of hospital-acquired urinary tract infections (UTIs). Specifically, the hospital would like to track the frequency of patients being discharged who had acquired a UTI, and to quickly identify an increase in infection rate or, conversely, monitor whether material changes result in fewer infections or not. They considered data set of days in between discharge of males patients in nosocomial urinary tract infections. The parameter of the exponential distribution is estimated 4.755961 with 0.647204 standard error. Using the Weibull, we have $\hat{\lambda} = 4.677767$ and $\hat{\beta} = 1.040100$ with standard errors 0.646299 and 0.108493 respectively. For the exponential chart, we have $LCL = 0.000284$ and $UCL = 1.387734$ while for the Weibull chart, we have $LCL = 0.000373$ and $UCL = 1.313386$, respectively. Hence, it is evident from these limits that the data do not show any signs of process degradation or improvement. However, the established chart can be used to detect such changes as quickly as possible in future.

3.6.4 Case Study-4

This data set is taken from Jarrett [1979] and has recently been used by Yang et al. [2015a,c] to develop unbiased design of the exponential and gamma charts. The data set is about the time intervals in days between explosions in coal mines from 15 march 1851 to 22 March 1962. There are total 190 observations and Yang et al. [2015a] considered first 30 observations as a phase-I to estimate the rate parameter of the exponential chart. Therefore, for comparison purpose, we are also considering first 30 observations to estimate the parameters of the Weibull distribution with false alarm probability $\alpha = 0.002703$. The estimated parameters of the Weibull distribution with standard deviation (given in parentheses) using first 30 observations are: $\hat{\lambda} = 0.009439(0.000005)$ and $\hat{\beta} = 0.821536(0.012857)$, for the exponential distribution we have $\hat{\lambda} = 0.008408(0.001535)$.

For comparison, the simple exponential and the corresponding ARL-unbiased exponential (cf. Yang et al. [2015a]) charts are also given in Figure- 3.5a. The control limits, i.e., LCL and UCL, of the two-sided charts are given as: $(0.1608485, 785.7446)$ for the exponential, $(0.23, 884.5)$ for the ARL-unbiased exponential and finally $(0.03411682, 1054.806)$ for the Weibull chart. These control limits are used to monitor the later data, i.e., from number 31 to 190 plotted in Figure-3.5a. In Figure-3.5a we have labelled the first 30 ob-

servations as phase-I data while the rest as phase-II, a vertical line is used to differentiate these two phases. There is a signal of process deterioration at the 80th sample number by all charts. Ten sample points, 14, 134, 137, 151, 153, 156, 182, 187, 188, 189, fall outside the upper control limit of a simple exponential chart while seven sample points, 134, 153, 156, 182, 187, 188 and 189, do the same with the ARL-unbiased exponential chart. With our proposed Weibull chart, it is observed that six sample points, 134, 153, 156, 182 187 and 188, are above the upper-control limit. Therefore, the Weibull chart gives less alarm than the exponential and ARL-unbiased exponential charts. After the first out-of-control signal at the 80th sample point, there is no alarm during a long period, i.e., from 81 to 133. The first TBE observation above the Weibull UCL is on the 134th point and then we start to observe more signal which all fall above the UCL. Therefore, it means that the safety of coal-mining began to improve between $1900 - 1920$.

To diagnose the cause of an alarm and to decide which parameter has been shifted, we suggest the use of the coefficient of variation of the Weibull distribution, which should be calculated at every signal point, using all TBEs in the monitoring sample up to that point. The rationale for doing this is that the CV of the Weibull distribution depends on the shape parameter β only (i.e., $E(X) = \lambda^{-1}\Gamma(\beta^{-1}+1)$, $Var(X) = \lambda^{-2}\{\Gamma(2\beta^{-1}+1) - \Gamma^2(\beta^{-1}+1)\}$ and $CV = \frac{\sqrt{\Gamma(2\beta^{-1}+1)-\Gamma^2(\beta^{-1}+1)}}{\Gamma(\beta^{-1}+1)}$), so if it does not change after a signal, it is likely that a shift as occurred in the rate parameter λ, whereas if the CV changes, then the shift will be attributed to β. To get a first impression of this use of the CV, we have produced Figure-3.5b, where we labeled the CV curve segments with the parameter which is more likely to have shifted. We noticed that the shape parameter is shifting and our previous conclusion 'that the safety of coal-mining began to improve between $1900-1920$' is supported by Figure-3.5b. Note that to estimate parameters of the Weibull distribution, we excluded the 80th point because its value is zero and computation of the ML estimates in case of the Weibull distribution are impossible with this value.

3.7 Some Final Remarks

The fundamental assumption of a Poisson process is that inter-arrival times are exponential distributed, which limits application to phenomena with constant hazard rate. Thus, one needs to consider some more flexible processes than Poisson process. In this chapter, we have proposed a new control chart for high-quality process monitoring based on the renewal process, allowing for a general parametric family for the inter-arrival times' distribution. This class includes not only the well-known Weibull distribution, but also the exponential, the Rayleigh, the Pareto, the Burr type XII, the Gompertz and the linear failure rate distributions. The expressions of LCL, UCL and ARL have been provided for all distributions while a numerical study has been carried out on the Weibull distribution,

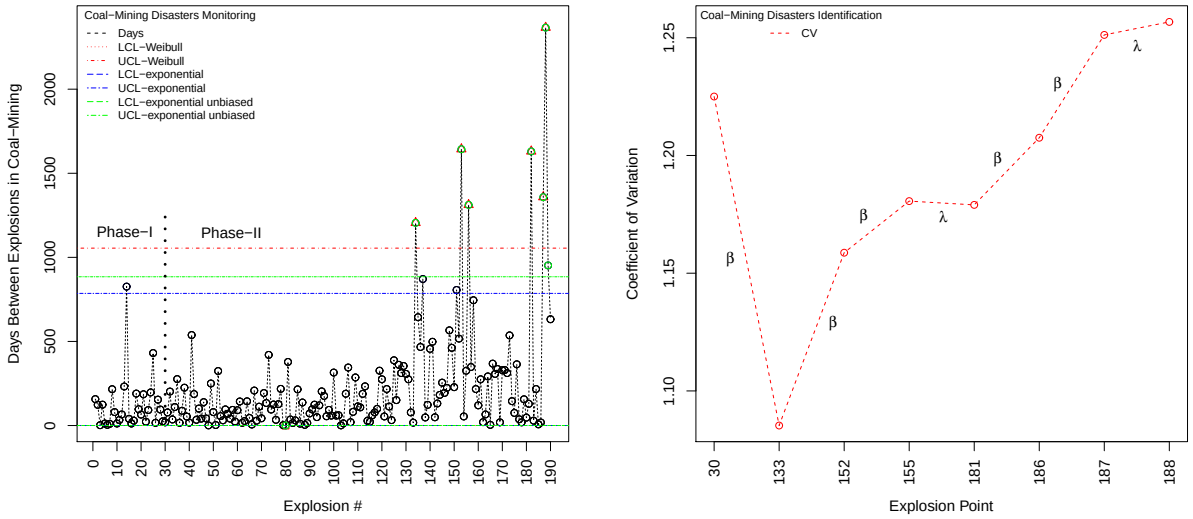

(a) Coal-mining explosion monitoring using the Weibull Chart

(b) Identification of Shifts in the coal-mining explosion using the Weibull chart

Figure 3.5: Coal-mining Explosion Monitoring and Identification of Shifts

due to its application in different fields.

Different properties of WQCC have been investigated in-detail, including ARL, CVLI, EQL and RARL. The effect of parameter estimation on the in-control run length has been discussed in detail considering both the MLE and Bayesian estimation methods. A similar work should be done to assess the effect of estimation on the out-of-control run length distribution. To identify the shift, i.e., which parameter has been shifted after getting an alarm/signal, we proposed the use of a coefficient of variation as it has been illustrated in case study 4.

Since the new proposed control chart is the generalization of the existing exponential cumulative quantity control chart, we believe that it will be more useful to monitor complex reliability data.

In the next chapter, we extend TBE control charts to handle both the time and associated magnitude using the renewal reward process with a fixed threshold (cf. Chapter-4).

Appendix

In this appendix, some additional plots and necessary derivations to estimates of the unknown parameters of the Weibull distribution are given.

Appendix A: Additional ARL Plots

The graphical presentation of the ARL for $\alpha = 0.0001, \beta_0 = 1.5$ and $\lambda_0 = 0.0005$ is given in Figure-A.1 (cf. Section-3.4.3)

Appendix B: Estimation of the Weibull Parameters

In this appendix, some derivation details about the maximum likelihood and the Bayesian method (cf. Section-3.5) are given to estimate unknown parameters of the Weibull distribution.

Case I: Method of Maximum Likelihood (ML): The following are the likelihood and log-likelihood equations for the Weibull distribution.

$$L(\lambda, \beta, \mathbf{x}) = \beta^n \prod_{i=1}^{n} x_i^{\beta-1} \lambda^{n\beta} \exp\left(-\sum_{i=1}^{n} (x_i\lambda)^\beta\right) \tag{B.1}$$

$$\ln L(\lambda, \beta, \mathbf{x}) = l(\lambda, \beta, \mathbf{x}) = n \ln \beta + (\beta - 1) \sum_{i=1}^{n} \ln x_i + n\beta \ln \lambda - \lambda^\beta \sum_{i=1}^{n} x_i^\beta \tag{B.2}$$

To obtain maximum likelihood estimators, the partial derivative with respect to λ is

$$\frac{\partial l(.)}{\partial \lambda} = \frac{n\beta}{\lambda} - \beta\lambda^{\beta-1} \sum_{i=1}^{n} x_i^\beta = 0 \Longrightarrow \hat{\lambda} = \left[\frac{n}{\sum_{i=1}^{n} x_i^{\hat{\beta}}}\right]^{1/\hat{\beta}}$$

The profile log-likelihood, i.e., after replacing the value of $\hat{\lambda}$ is given by

$$l_p(\hat{\lambda}, \beta, \mathbf{x}) = n \ln \beta + (\beta - 1) \sum_{i=1}^{n} \ln x_i + n(\ln n - 1) - n \ln(\sum_{i=1}^{n} x_i^\beta) \tag{B.3}$$

$$\frac{\partial l_p(.)}{\partial \beta} = \frac{n}{\beta} + \sum_{i=1}^{n} \ln x_i - \frac{n \sum_{i=1}^{n} x_i^\beta \ln(x_i)}{\sum_{i=1}^{n} x_i^\beta} = 0$$

$$\Longrightarrow \frac{1}{\beta} = \frac{1}{n} \sum_{i=1}^{n} \ln \frac{1}{x_i} + \frac{\sum_{i=1}^{n} x_i^\beta \ln(x_i)}{\sum_{i=1}^{n} x_i^\beta} = h(\beta)$$

We propose a simple iterative scheme to solve for β. Start with an initial guess of $\beta^{(0)}$,

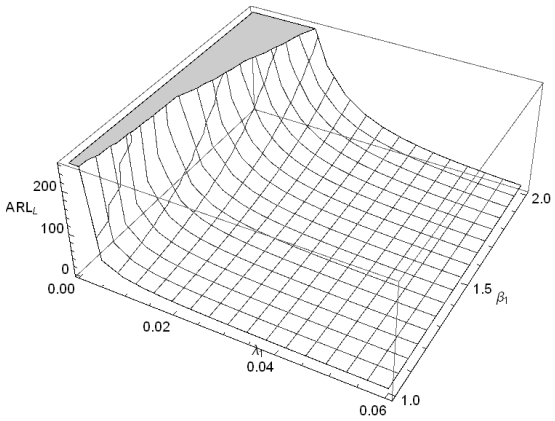

(a) Lower-sided ARL for $\beta_0 = 1.5$ (TD-case)

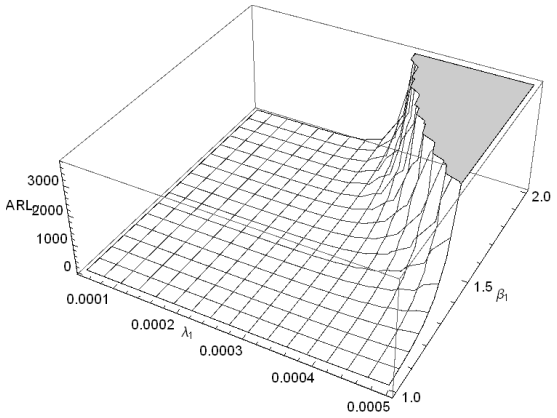

(b) Upper-sided ARL for $\beta_0 = 1.5$ (PD-case)

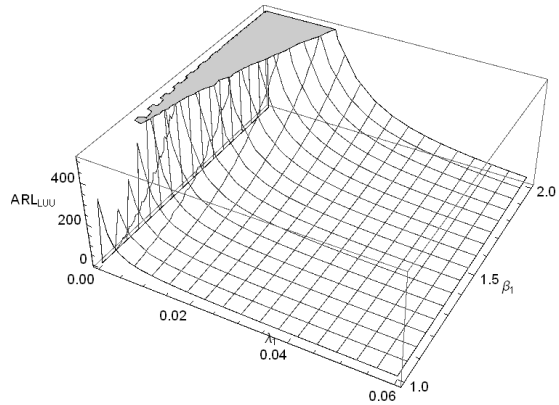

(c) Two-sided ARL for $\beta_0 = 1.5$

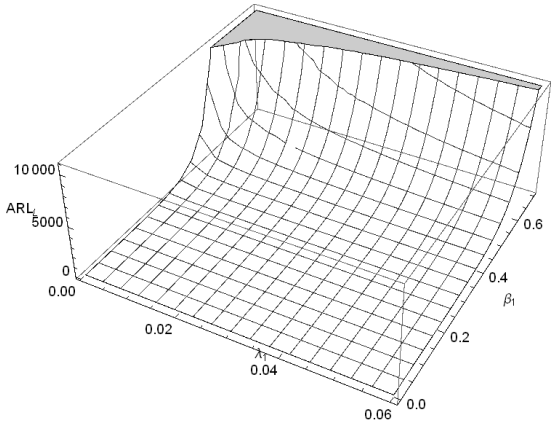

(d) Lower-sided ARL for $\beta_0 = 0.5$ (PI-case)

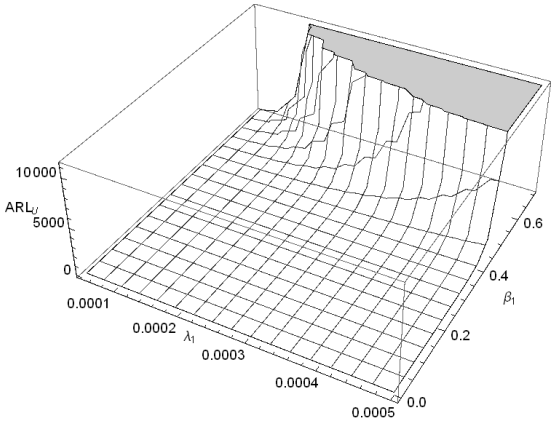

(e) Upper-sided ARL for $\beta_0 = 0.5$ (TI-case)

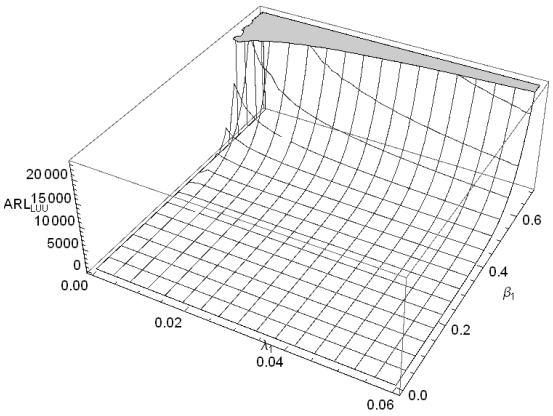

(f) Two-sided ARL for $\beta_0 = 0.5$

Figure A.1: Plots of ARL for $\alpha = 0.0001$ and $\lambda_0 = 0.0005$

obtain $\beta^{(1)} = h(\beta^{(0)})^{-1}$ and proceeding in this way, obtain $\beta^{(n+1)} = h(\beta^{(n)})^{-1}$. Stop the iterative procedure, when $|\beta^{(n+1)} - \beta^{(n)}| < \epsilon$, some pre-assigned tolerance limit.

Case 2: Bayesian Method: For the Bayesian estimation of the Weibull distribution, let re-parameterized the density function by assuming $\phi = \lambda^\beta$ and we have $f(x, \beta, \lambda) = \beta x^{\beta-1}\phi \exp(-\phi x^\beta)\mathbb{I}_{(0,\infty)}$. Following the approach suggested by Joarder et al. [2011], it is assumed that ϕ has a gamma prior $Gamma(c, d); c, d > 0$ while for β no specific form of prior $p(\beta)$ is assumed. However, it is only assumed that the support of β prior is $(0, \infty)$, is independent of ϕ and log-concave density. We have the joint posterior distribution is given as $p(\beta, \phi|\mathbf{x}) \propto \beta^n \exp(\beta(\sum_{i=1}^n \ln x_i))\phi^{(n+c)-1} \exp(-\phi(d + \sum_{i=1}^n x_i^\beta)) \cdot p(\beta)$. Thus, $p(\beta|\mathbf{x}) \propto \frac{\beta^n \exp(\beta(\sum_{i=1}^n \ln x_i))}{(d+\sum_{i=1}^n x_i^\beta)^{n+c}} \times p(\beta)$ and $p(\phi|\beta, \mathbf{x}) = \text{Gamma}(n + c, d + \sum_{i=1}^n x_i^\beta)$. We need the following results for further development.

Theorem B.1 *The conditional density function of β given data is log-concave.*

Proof : *Ignoring the additive constant, the posterior of β given data can be written as* $\ln p(\beta|\mathbf{x}) \propto n \ln \beta + \beta \sum_{i=1}^n x_i + \ln p(\beta) - (n + c) \ln(d + \sum_{i=1}^n x_i^\beta)$ *and* $\partial \ln p(\beta|\mathbf{x})/\partial\beta = \frac{n}{\beta} + \sum_{i=1}^n \ln(x_i) - \frac{(n+c)\sum_{i=1}^n x_i \ln x_i}{d+\sum_{i=1}^n x_i^\beta} + \frac{\partial \ln(p(\beta))}{\partial\beta}$.
Thus, it is log-concave.

Note that we used gamma distribution as a prior for the shape parameter, i.e., $p(\beta)$. A simulation based consistent estimate of $E[g(\beta, \lambda)] = \theta$ can be obtained using following steps:

1. Generate β from $p(\beta|\mathbf{x})$ using the method suggested by Devroye [1984].
2. Generate ϕ from $p(\phi|\beta, \mathbf{x})$.
3. Repeat Step 1 and Step 2 and obtain (β_i, ϕ_i) for $i = 1, 2, \cdots, M$.
4. Obtain λ_i from step 3, i.e., $(\beta_i, \lambda_i = \phi_i^{1/\beta_i})$.
5. An approximate Bayes estimate of θ under the squared error loss function can be obtained by
$$\hat{\theta} = \hat{g}_B(\beta, \lambda) = \frac{1}{M} \sum_{i=1}^{M} \theta_i$$

Similarly, the Bayes estimates for other loss functions can be computed with the help of the above algorithm.

Appendix C: CQC and CPC charts for Case Study-1

The CQC and CPC charts of the Case Study-1 (cf. Section-3.6) at $\alpha = 0.0027$ and $\alpha = 0.2$ false alarm probabilities:

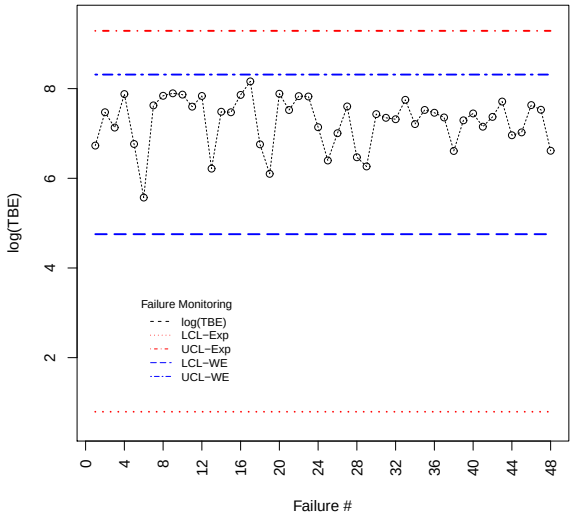

(a) Cumulative Quantity Plot at $\alpha = 0.0027$

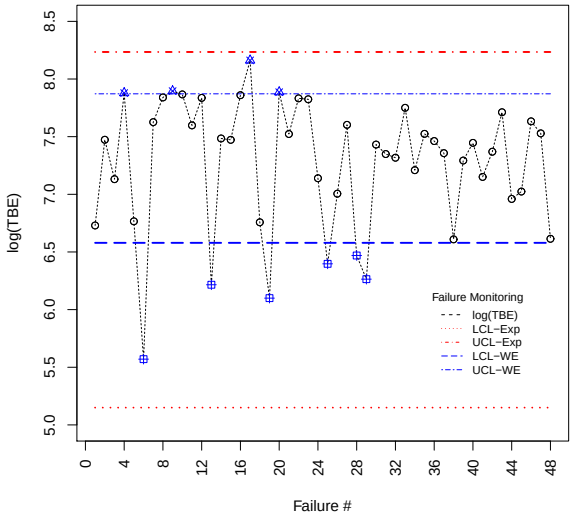

(b) Cumulative Quantity Plot at $\alpha = 0.2$

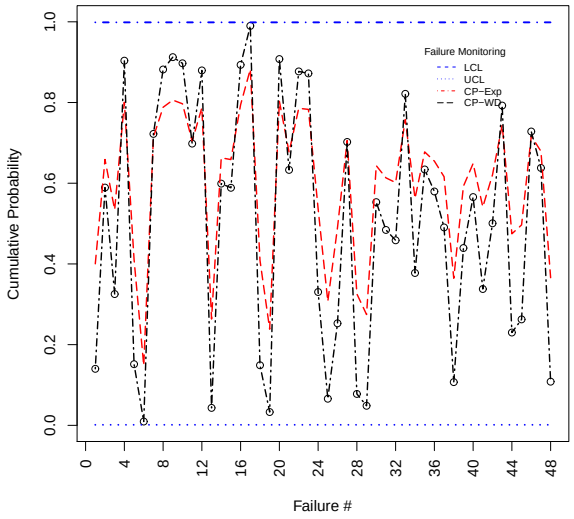

(c) Cumulative Probability Plot at $\alpha = 0.0027$

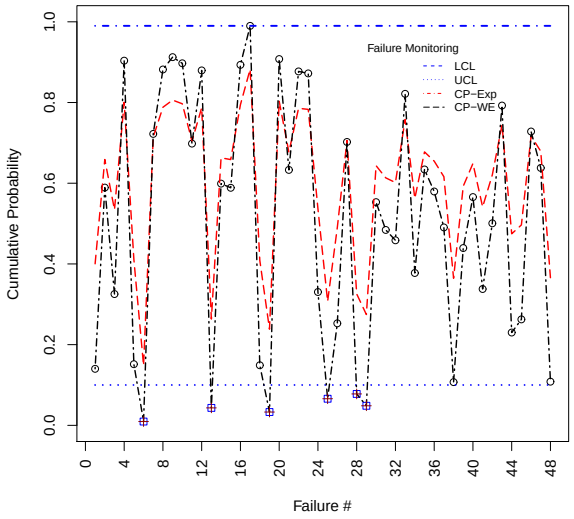

(d) Cumulative Probability Plot at $\alpha = 0.2$

Figure C.1: Control Charts for the Case Study-1 at various False Alarm Probabilities

Chapter 4

Monitoring the Time and Magnitude based on the Renewal Reward Process with a Fixed Threshold

In Chapter 3, we proposed a high-quality chart to monitor TBE based on the renewal process. In this chapter, we extend Chapter 3 and propose a new control chart for the joint monitoring of time and magnitude based on the renewal reward process. Existing charts to monitor such scenarios are based on the assumptions of the marked Poisson process which are not suitable to handle complex monitoring, i.e., proportional changes in time and magnitude which especially occur in reliability (damage) engineering. Particularly, we are considering two cases for reward/magnitude; (i) magnitude is cumulative over time and, (ii) magnitude is non-cumulative or independent over time. Therefore, our proposal is not only a generalization of the existing charts, but also suitable for complex monitoring. Some comparison studies are also conducted in this chapter to show the flexibility of our proposal.

4.1 Motivation

Traditional TBE charts considered the time interval X between the occurrences of an event by completely ignoring the magnitude M (or frequency F) attached to the particular time point (cf. Chapter 2-3). However, there are many real applications where the time as well as the magnitude is very important and ignoring one of them leads to misleading conclusions. The M or F may be the amount of loss or the number of items incurred by the occurrence of a particular event, and in turn determines the severity of the event. For example, a task team to control the infectious disease like bird flu (malaria prevention and elimination) must be enhanced not only when the outbreaks of this infection become very frequent, but also when the number of poultry (people) infected in each outbreaks get

very high. Similarly, the loss of market competitiveness of an aged product is indicated not only by the decreased number of purchase order, but also by the decreased number of items in each order. The fire department must be well equipped not only after a specific time period or when the outbreaks become very frequent, but also when the average damaged caused by each outbreak gets very high. Similarly, the traffic police must be enhanced in terms of capacity when the number of deaths increases in traffic accidents. In the textile industry, a printing machine should be replaced not only when it frequently stops working, but also when it prints large pieces of defected cloth.

Usually, there are two types of events in the above reported cases: negative ones and positive ones. A negative event may be the failure of a system, a traffic accident, an outbreak of infection or rejection of a product lot; whilst a positive event may refer to the success of a program, the arrival of a customer or control of an infection in the population, etc. Consider the random times where we are interested in the magnitude/damage caused by the occurrence of each event, e.g., people affected by the earthquake (alternatively magnitude of the earthquake), area (of land) affected by the earthquake or flood, etc. In each of such situations, both the magnitude/damage and the TBE are random variables, and will be denoted by M and X, respectively. Note that this procedure of collecting data is different from the traditional sampling approach where a constant sampling interval is used to develop traditional control charts. One can consider this method as similar to the event sampling, i.e., records every occurrence of certain pre-determined events.

The existing time and magnitude control charts (cf. Section-2.2.3 and 2.5.2) are based on the marked Poisson process (though the authors did not mention it explicitly) that worked well in somehow simple problems. For example, the rate chart does not react timely if there are proportional changes in time and magnitude. This happens because the ratio of M/X stays constant. Moreover, there are certain situations where magnitude is not directly observable. Therefore, to deal such complex situations, the existing time and magnitude charts have poor performance. It is to be noted that the basic assumption of a marked Poisson process is that inter-arrival times are exponentially distributed, which limits application to phenomena with constant hazard rate. Hence, one needs to consider some more flexible processes than a Poisson process.

In this chapter, we propose a control chart to monitor the TBE, X, and magnitude, M, based on the renewal reward process where *any* lifetime distribution for the time and magnitude can be considered. Therefore, our proposal is not only a generalization of the existing charts, but also suitable for complex monitoring, i.e., when damage is not directly observable. We quote here some motivational examples from such complex fields:

Example 1: Boxing In a boxing fight, a knockout may be caused either by a series of small to moderate punches or just by a really big punch. Each player has its own critical threshold after which he wins or loses. The real challenge is how to differ-

entiate either match is fixed or genuine one. Similarly the decision and monitoring of the effect of physical or mental training on the player's performance, is of a great interest.

Example 2: Fatigue, tenacity (Gut and Hüsler [2010]) A material, for example, a rope or a wire, can break either because of the cumulative effect of "normal" loads after a certain time period or because of a sudden big load, e.g., coat hanger. The potential threat to such material is to determine critical time and how to sort out faulty material with respect to material capacity.

Example 3: Environmental damage (Gut and Hüsler [2010]) There are environmental protocols, which must be followed and ensured by each factory before releasing wastage. A factory may leak poisonous waste products into a river; however, after some time the vegetation and the fish in the river are dead due to cumulative effect of poison. Alternatively, they might be killed because of some catastrophe in the factory that, instantaneously, pours a huge amount of waste into the river.

Example 4: Doping test The use of banned performance-enhancing drugs in sports is commonly referred to as doping particularly by the organizations that regulate sporting competitions. The use of drugs to enhance performance is considered unethical by most international sports organizations, including the International Olympic Committee, although ethicists have argued that it is not different from the use of new materials in the construction of suits and sporting equipment, which can also aid performance and give competitors an unfair advantage. To test whether a player has used banned drug or not, blood and urine samples of the player are taken. However, some certain elements which are banned might be present in some other medications. Therefore, results from the blood and urine tests would be positive if the player is using any medicine, which includes that particular elements of the banned drugs. Thus, there could be two types of effects from banned drugs on a player's health, i.e., cumulative and independent. Since every element in the human blood has a certain threshold and if any un-natural treatment is taken to enhance the performance would simply increase the ratio of particular cells. To test whether it is a natural presence of the particular element or an un-natural is a big question which modern sport industry is facing.

Note that a failure of a system or unit is generally categorized into two failure modes: catastrophic failure, in which the system or unit fails by some sudden shock or damage, and degradation failure, in which the system fails by physical deterioration suffered from some reward or damage. In this study we shall assume that both the X and M are independent; however, these could be dependent in some application. The rest of the study is organized as follows: Section 4.2 deals with some definitions about the renewal,

renewal reward and damage processes. Discussion about the compound Poisson process, which is a special case of the renewal reward process, is given in Section 4.3. The control chart construction and a numerical study of performance measures, are given in Section 4.4. Control charts based on the nonhomogeneous Poisson process (NHPP) are discussed in Section 4.5. The implementation of the proposals in the real-life situations, is given in the Section 4.6. Finally, we conclude the chapter in Section 4.7.

4.2 Cumulative and Independent Processes

In this section, we shall introduce some necessary definitions and derivations that are required for the development of time and magnitude charts. We denote $N(t)$ as a renewal process while X_i TBE and M_i as a reward associated with X_i for $i \geq 1$. A fundamental characterization of the Poisson process is given in Theorem-1.1.3. However, it is interesting to note that the points of a Poisson process might be labeled with some extra information. Such kind of a process is known as marked Poisson process in literature. The formal definition is given below:

Definition 4.2.1 *Suppose that $X_1, X_2, \cdots$, are the waiting times of the Poisson process, and $M_1, M_2, \cdots$ are independent random variables denoting the outcome of an associated random variable, the mark, having a common distribution function G. The sequence of pairs $(X_1, M_1), (X_2, M_2), \cdots$ is called a marked Poisson process.*

Definition 4.2.2 *A counting process $\{N(t), t \geq 0, t \in T\}$ with independent and identically distributed (iid) inter-arrival times $X_1, X_2, \cdots$ with a common distribution* F *is called a renewal process.*

Definition 4.2.3 *Let M_i denote the reward (such as damage, wear, fatigue, cost or risk) that is attached with each inter-arrival times X_i, i.e., there is a associated renewal counting process $N(t) = \sup\{n \geq 0, S_n \leq t\}$ where $S_n = \sum_{i=1}^{n} X_i$ with $S_0 = 0$, for $i \geq 1$. If the sequence of pairs (X_i, M_i) for $i = 1, 2, \cdots$ is independent and identically distributed (might be dependent), then the stochastic process $Y(t) = \sum_{i=1}^{N(t)} M_i$ is called a renewal reward process.*

Therefore, the renewal reward process is a generalization of the marked Poisson process. There are various names of the renewal reward process in the literature, e.g., cumulative process, jump process or doubly stochastic process (cf. Nakagawa [2005]).

To construct a control chart based on the renewal reward process, we need to work out: (i) the distribution of the total increment at time t, that is $Pr\{Y(t) \leq m\}$, (ii) the total expected increment at time t, i.e., $E(Y(t))$, (iii) $Pr\{Z \leq t\}$ where $Z = \min_t\{Y(t) > K\}$, i.e., the first-passage distribution to a critical point; and finally, (iv) the mean time to

a critical point $E\{Z\}$. All these four points are very important, but for the (complex) time and magnitude monitoring point (iii) is the most important. Therefore, in the below sections, we shall discuss these points in-detail.

4.2.1 Cumulative Damage Process

Definition 4.2.1.1 *A unit/system is subject to shocks and suffers some damage (M). Suppose that each damage is additive and the system or unit fails when the total damage has exceeded a failure threshold K (sometimes also known as a critical threshold), where $0 < K < \infty$, for the first time (cf. Figure-4.1). A process with such a behavior is known as a cumulative damage process.*

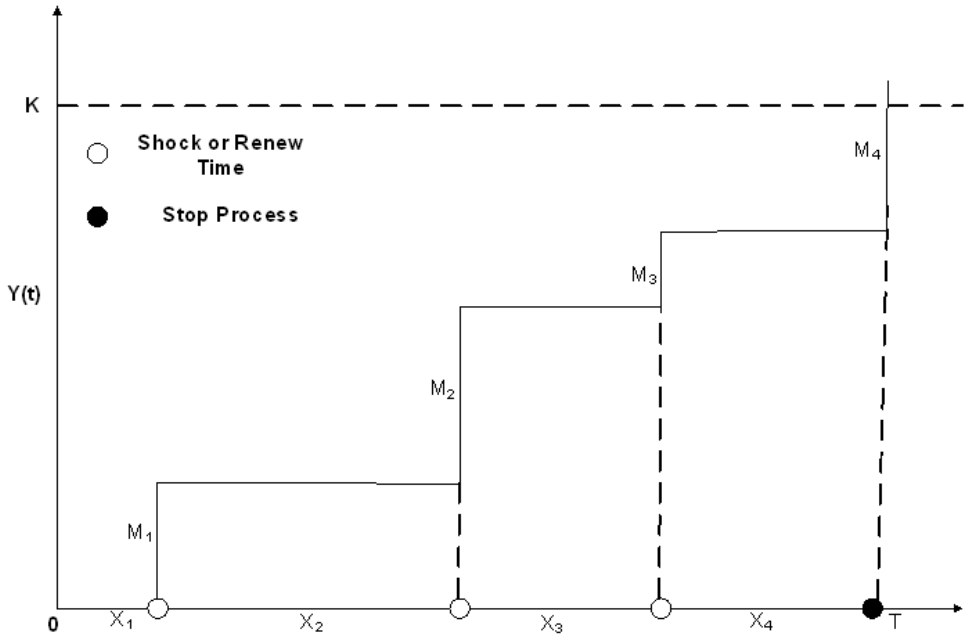

Figure 4.1: Process for a standard cumulative damage model

Let $F(x) = Pr\{X_i \leq x\}$ and $G(m) = Pr\{M_i \leq m\}$ be the cumulative distribution functions of X_i and M_i respectively, with finite means. In addition, suppose K be a fixed threshold of the increment and define $Z = \min_t\{Y(t) > K\}$. We are interested in the first-passage distribution to a critical point K, i.e., $Pr(Z \leq t)$. Then from elementary renewal theorem, the number of events $N(t)$ in $[0, t]$ has the density, i.e., the probability of an increment at the $(n+1)$th event in $[0, t]$ is,

$$Pr\{N(t) = n\} = F^{(n)}(t) - F^{(n+1)}(t), \qquad n = 0, 1, 2, \cdots \tag{4.1}$$

where $\phi^{(n)}$ denotes the n-fold Stieltjes convolution of any function ϕ with itself, and $\phi^{(0)} = 1$ for $t \geq 0$. Therefore,

$$Pr\left\{\sum_{k=0}^{N(t)} M_k \leq m, N(t) = n\right\} = Pr\left\{\sum_{k=0}^{N(t)} M_k \leq m | N(t) = n\right\} Pr\{N(t) = n\}$$
$$= G^{(n)}(m)[F^{(n)}(t) - F^{(n+1)}(t)]$$

The distribution of the total increment at time t is given by

$$Pr\{Y(t) \leq m\} = \sum_{n=0}^{\infty} Pr\left\{\sum_{k=0}^{N(t)} M_k \leq m, N(t) = n\right\} \tag{4.2}$$
$$= \sum_{n=0}^{\infty} [F^{(n)}(t) - F^{(n+1)}(t)] G^{(n)}(m)$$

and the survival probability is $Pr\{Y(t) > m\} = \sum_{n=0}^{\infty}[G^{(n)}(m) - G^{(n+1)}(m)]F^{(n+1)}(t)$. The total expected increment at time t is

$$E\{Y(t)\} = \int_0^{\infty} m dPr\{Y(t) \leq m\} = E(M)E\{N(t)\} \tag{4.3}$$

where $E\{N(t)\} = \sum_{n=1}^{\infty} F^{(n)}(t)$ is a renewal function with distribution $F(t)$ and represents the expected number of events occurred in $[0, t]$. Moreover, it has a Laplace Stieltjes (LS) transformation which is given by $\frac{F^*(s)}{1-F^*(s)}$. The total expected value can be naturally explained as the product of the average amount of increment suffered from each damage and the expected number of events in time $[0, t]$. From Theorem 3.1 in Nakagawa [2007] (page 55), if $\mu_{i(F)}, \mu_{i(G)} < \infty$ $(i = 1, 2, 3)$ and $\sigma_F^2 = \mu_2 - \mu^2$, then as $t \to \infty$

$$E\{N(t)\} = \frac{t}{\mu} + \frac{\sigma_F^2}{2\mu^2} - \frac{1}{2} + \mathcal{O}(1)$$
$$Var\{N(t)\} = \frac{\sigma_F^2 t}{\mu^3} + \frac{5\sigma_F^4}{4\mu^4} + \frac{2\sigma_F^2}{\mu^2} + \frac{3}{4} - \frac{2\mu_3}{3\mu^3} + \mathcal{O}(1)$$

where $\mathcal{O}(h)/h \to 0$ as $h \to 0$. Thus,

$$E\{Y(t)\} = E\left\{E\left\{\sum_{k=1}^{N(t)} M_k | N(t) = n\right\}\right\} = E(M)E\{N(t)\} \approx E(M)\left(\frac{t}{\mu} + \frac{\sigma_F^2 - \mu^2}{2\mu^2}\right) \tag{4.4}$$

and

$$Var\{Y(t)\} = E\{Y^2(t)\} - (E\{Y(t)\})^2 = E\left\{E\left\{\sum_{k=1}^{N(t)} M_k \sum_{j=1}^{N(t)} M_j | N(t) = n\right\}\right\} - \tag{4.5}$$

$$(E\{Y(t)\})^2 = Var\{N(t)\}(E\{M\})^2 + E\{N(t)\}Var\{M\}$$

$$\approx (E\{M\})^2\left\{\frac{t}{\mu}\left(\frac{\sigma_F^2}{\mu^2} + \frac{\sigma_G^2}{E\{M\}}\right) + \frac{5\sigma_F^4}{4\mu^4} + \frac{2\sigma_F^2}{\mu^2} + \frac{3}{4} - \frac{2\mu_3}{3\mu^3}\right\}$$

$$+ \frac{\sigma_G^2}{2}\left(\frac{\sigma_F^2}{\mu^2} - 1\right)$$

Using Theorem 1.2 (page 8) in Nakagawa [2007], we have $\lim_{t\to\infty} \frac{E\{Y(t)\}}{t} = \frac{E\{M\}}{\mu}$, $\lim_{t\to\infty} \frac{Var\{Y(t)\}}{t} = \frac{(E\{M\})^2}{\mu}\left(\frac{\sigma_F^2}{\mu^2} + \frac{\sigma_G^2}{E\{M\}}\right)$. Similarly, by applying Theorem 1.4, in Nakagawa [2007] (page 9), we have the following asymptotic distribution of $Y(t)$

$$\lim_{t\to\infty} Pr\left\{\frac{Y(t) - E\{M\}t/\mu}{\sqrt{((E\{M\})^2 t/\mu)(\sigma_F^2/\mu + \sigma_G^2/(E\{M\})^2)}} \le x\right\} = \frac{1}{\sqrt{2\pi}}\int_{-\infty}^{x} \exp(-w^2/2)dw \tag{4.6}$$

Now, assume that the process ends when the total increment crosses a threshold level K, a so-called critical point. In such a scenario, the probability that the total increment exceeds a threshold level K at the $(n+1)$th event is $G^{(n)}(K) - G^{(n+1)}(K)$ for $n = 0, 1, 2, \cdots$; then define $Z = \min_t\{Y(t) > K\}$. Since the event of $\{Z \le t\}$ and $\{Y(t) > K\}$ are equivalent, the first-passage distribution to the critical point is

$$\phi(t) = Pr\{Z \le t\} = \sum_{n=0}^{\infty}[G^{(n)}(K) - G^{(n+1)}(K)]F^{(n+1)}(t) \tag{4.7}$$

and its Laplace-Stieltjes (LS) transform is

$$\phi^*(s) = \int_0^{\infty} \exp(-st)dPr\{Z \le t\} = \sum_{n=0}^{\infty}[G^{(n)}(K) - G^{(n+1)}(K)][F^*(s)]^{n+1} \tag{4.8}$$

where ϕ^* denotes the LS transform of any function ϕ i.e., $\phi^*(s) = \int_0^{\infty} \exp(-st)d\phi(t)$. Finally, the mean time to a critical point is

$$E(Z) = \int_0^{\infty} tdPr\{Z \le t\} = \frac{\partial\phi^*(s)}{\partial s}|_{s=0} = \mu[1 + M_G(K)] \tag{4.9}$$

where $M_G(K) = \sum_{n=1}^{\infty} G^{(n)}(K)$ represents the expected number of events before a critical point. Further, it can be simplified using elementary renewal function as $E(Z) \approx \mu\left(\frac{K}{E\{M\}} + \frac{\sigma_G^2 + (E\{M\})^2}{2(E\{M\})^2}\right)$. If the distribution of jumps (reward or shock) has an increasing

failure rate property, then $\frac{\mu K}{E\{M\}} < E(Z) \leq \mu\big(\frac{K}{E\{M\}} + 1\big)$.

If events occur in the nonhomogeneous Poisson process with an intensity function $\lambda(t)$ and a mean value function $\Lambda(t) = \int_0^t \lambda(u)du$, i.e., the density function can be written as $Pr\{N(t) = n\} = \frac{[\Lambda(t)]^n}{n!} \exp(-\Lambda(t))$ for $n = 0, 1, 2, \cdots$; then we have

$$Pr\{Y(t) \leq m\} = \sum_{n=0}^{\infty} G^{(n)}(m) \frac{[\Lambda(t)]^n}{n!} \exp(-\Lambda(t)) \tag{4.10}$$

where $E\{Y(t)\} = \Lambda(t)E\{M\}$ and $E\{Z\} = \sum_{n=0}^{\infty} G^{(n)}(K) \int_0^{\infty} \frac{[\Lambda(t)]^n}{n!} \exp(-\Lambda(t))$. Moreover, if each event is assumed to occur at a constant time T^*, i.e., $F(t)$ is a degenerate distribution placing unit mass at time T^*, then $Pr\{Z \leq t\} = 1 - G^{[t/T^*]}(K)$ and the mean time to a critical point K will be $E\{Z\} = \int_0^{\infty} G^{[t/T^*]}(K)dt$, where $[t/T^*]$ denotes the greatest integer less than or equal to t/T^*. However, if $G(m) = 0$ for $m < 1$ and 1 for $m \geq 1$, and $K = n$, then $Pr\{Z \leq t\} = F^{(n+1)}(t)$ and $E(Z) = (n+1)\mu$.

4.2.2 Independent Damage Process

Definition 4.2.2.1 *Consider a process where the total increment is not additive, i.e., increments are independent. The process will end when one amount of reward exceeds the threshold level K. This type of process is called independent damage model (cf. Figure-4.2).*

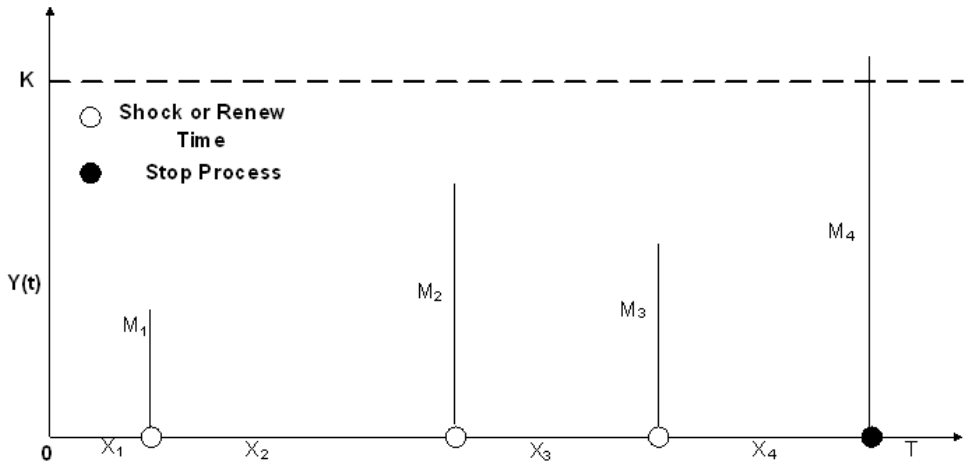

Figure 4.2: Process for a independent damage model

The industrial examples of such models are the fracture of brittle materials and semiconductor parts that have failed by some over-current or fault voltage. To compute the first-passage distribution to a critical point, let F and G be the cumulative distribution functions of time X and magnitude M, respectively, with finite means. In addition, suppose K be the threshold level of the increment and define $Z = \min_t\{Y(t) > K\}$. We are

interested in $Pr(Z \leq t)$ which is the first-passage distribution to a critical point. The first-passage distribution of the critical point is (cf. Nakagawa [2007])

$$Pr\{Z \leq t\} = \sum_{n=0}^{\infty} [G^n(K) - G^{n+1}(K)] F^{(n+1)}(t) \tag{4.11}$$

and its Laplace-Stieltjes (LS) transform is (see derivation details in Appendix-4.7)

$$\phi(s) = \int_0^{\infty} \exp(-st) dPr\{Z \leq t\} = \frac{[1 - G(K)]F^*(s)}{1 - G(K)F^*(s)} \tag{4.12}$$

Note that Equation-4.11 does not have the convolution (.) for the magnitude distribution as compared to Equation-4.7, which is implied by the definition of the independent process, i.e., the process will end when one amount of reward exceeds the threshold level K. The mean time to the critical point K is $E(Z) = \frac{\partial \phi(s)}{\partial s}|_{s=0} = \frac{\mu_X}{1 - G_M(K)}$. If shock occurs in a nonhomogeneous Poisson process with a mean value function $\Lambda(t)$, then

$$Pr\{Z \leq t\} = \sum_{n=0}^{\infty} \{1 - G^n(K)\} \frac{[\Lambda(t)]^n}{n!} \exp(-\Lambda(t)) = 1 - \exp\big[-\{1 - G(K)\}\Lambda(t)\big] \tag{4.13}$$

and $E\{Z\} = \int_0^{\infty} \exp\big[-\{1 - G(K)\}\Lambda(t)\big] dt$. Similarly, if the events occur at a constant time T^*, i.e., $F(t)$ is the degenerate distribution placing unit mass at time T^*, then $Pr\{Z \leq t\} = 1 - [G(K)]^{[t/T^*]}$ and mean time to the critical point would be $E\{Z\} = \int_0^{\infty} [[G(K)]^{[t/T^*]}] dt$, where $[t/T^*]$ denotes the greatest integer less than or equal to t/T^*.

4.3 Compound Poisson Process

A generalization of the Poisson process to a situation where multiple arrivals are allowed, is called the compound Poisson process. The example of this process is batch arrivals, e.g., passengers exiting/entering a train at railway station, or the arrival of multiple claims to an insurance company.

Definition 4.3.1 *Suppose $N(t)$ be a Poisson process where shocks occur with the rate λ and consider a sequence M_i of IID random variables independent of $N(t)$. Then, the counting process $Y(t) = \sum_{i=1}^{N(t)} M_i$ for $N(t) = 0, 1, 2, \cdots$ and $Y(t) = 0$ when $N(t) = 0$, is called a compound Poisson process.*

We are interested in finding the distribution of total increment by considering the cumulative and independent damage scenarios for the compound Poisson process. This task is easy to accomplish as we have defined a flexible framework in Section-4.2. Therefore, the

distribution of the total increment for the **cumulative damage** scenario is:

$$Pr\{Y(t) \leq m\} = \sum_{n=0}^{\infty} G^{(n)}(m) \frac{(\lambda t)^n}{n!} \exp(-\lambda t) \tag{4.14}$$

If we let $G^*(s)$ be the Laplace transformation of $G(m)$, then Equation-4.14 can be written as

$$\int_0^{\infty} \exp(-sm) dPr\{Y(t) \leq m\} = \sum_{n=0}^{\infty} [G^*(s)]^n \frac{(\lambda t)^n}{n!} \exp(-\lambda t) = \exp\{-\lambda t[1 - G^*(s)]\} \tag{4.15}$$

Since, $E\{N(t)\} = Var\{N(t)\} = \lambda t$, we have (cf. Equation-4.3) $E\{Y(t)\} = \lambda t E(M)$ and $Var\{Y(t)\} = \lambda t E(M^2)$, respectively. The distribution of first passage time to a critical point K is

$$\phi(t) = Pr\{Z \leq t\} = Pr\{Y(t) > K\} = \sum_{n=0}^{\infty} [G^{(n)}(K) - G^{(n+1)}(K)] \sum_{j=n+1}^{\infty} \frac{(\lambda t)^j}{j!} \exp(-\lambda t) \tag{4.16}$$

and it has the LS transformation as given below

$$\phi^*(s) = \int_0^{\infty} \exp(-st) d\phi(t) = \sum_{n=0}^{\infty} [G^{(n)}(K) - G^{(n+1)}(K)] \left(\frac{\lambda}{\lambda + s}\right)^{n+1} \tag{4.17}$$

We have $E(Z) = \frac{\partial \phi^*(s)}{\partial s}|_{s=0} = \frac{1+G_M(K)}{\lambda}$ and $Var(Z) = \frac{\partial^2 \phi^*(s)}{\partial s^2}|_{s=0} - \{E(Z)\}^2 = \frac{2}{\lambda} \sum_{n=0}^{\infty} (n+1) G^{(n)}(K) - \{E(Z)\}^2$.

Example#1: Suppose that the time and the damage both have the exponential distribution with mean $1/\lambda$ and $1/\theta$, respectively, i.e., $F(x) = 1 - \exp(-\lambda x)$ and $G(m) = 1 - \exp(-\theta m)$. Then, to derive a first passage distribution for the cumulative process we have to solve $\int_0^{\infty} \exp(-sm) dPr\{Y \leq m\} = \exp(-\lambda t[s/(s+\theta)])$, and its inversion can be written as (cf. Barlow and Proschan [1965], and Graf [2004]) (for an alternative representation, see Appendix A (cf. Section-4.7)

$$Pr\{Y(t) \leq t\} = \exp(-\lambda t)\big[1 + \sqrt{\lambda \theta t} \int_0^x \exp(-\theta w) w^{-0.5} I_1(2\sqrt{\lambda \theta t w}) dw\big] \tag{4.18}$$

where I_i is the Bessel function of order i for the imaginary argument defined as $I_i(x) = \sum_{k=0}^{\infty} \frac{(x/2)^{2k+1}}{k!(k+i)!}$. Thus, we have

$$Pr\{Z \leq t\} = 1 - \exp(-\lambda t)\big[1 + \sqrt{\lambda \theta t} \int_0^K \exp(-\theta w) w^{-0.5} I_1(2\sqrt{\lambda \theta t w}) dw\big] \tag{4.19}$$

and $E\{Y(t)\} = \frac{\lambda t}{\theta}, E\{Z\} = \frac{\theta K+1}{\lambda}, Var\{Y(t)\} = \frac{2\lambda t}{\theta^2}$ and $Var\{Z\} = \frac{2\theta K+1}{\lambda^2}$, respectively. It is to be noted that $E\{Y(t)\}$ is increasing linearly with time t and therefore, we have $\frac{E\{Y(t)\}}{K+\theta^{-1}} = \frac{t}{E(Z)}$.

Example#2: The first passage distribution of the **independent damage** scenario for the exponentially distributed time and magnitude is:

$$Pr\{Z \leq t\} = 1 - \exp(-\lambda t \exp(-\theta K)) \tag{4.20}$$

which is again exponential distribution with parameter $\lambda \exp(-\theta K)$. Therefore, we have $E(Z) = \frac{\exp(\theta K)}{\lambda}$ and $Var(Z) = \frac{\exp(2\theta K)}{\lambda^2}$.

In Equation-4.20, we have considered the exponential distribution for the magnitude. One can also consider a gamma distribution for the magnitude. However, the real task is to solve the Laplace integral $\int_0^\infty \exp(-sx) dPr\{Y \leq x\} = \exp(-\lambda t[1 - (\theta/(s+\theta))^\beta]) = \exp(-\lambda t)\exp(\lambda t(\theta/(s+\theta))^\beta)$. One can write $\exp(\lambda t(\theta/(s+\theta))^\beta)$ as $\sum_{n=0}^\infty \frac{(\lambda t)^n}{n!}\left(\frac{\theta}{s+\theta}\right)^{n\beta}$. Now its LS inversion is $\sum_{n=0}^\infty \frac{(\lambda t)^n}{n!}\left(-n\beta\lambda \times_1 F_1[1+n\beta, 2, -t\lambda]\right)$, where ${}_1F_1$ denotes the Kummer Confluent Hypergeometric function. By comparing this expression with Equation-4.20, one can notice that the first passage distribution has become very complicated after replacing the exponential distribution with a gamma.

Example#3: Suppose that the time of the events' occurrence follows the nonhomogeneous Poisson process with intensity $\Lambda(t)$ (cf. Zacks [2004]), specifically power law intensity. Moreover, let the magnitude (or reward) has the exponential distribution with the rate θ. With these time and magnitude specifications, the first passage distribution to the critical point K of the **cumulative damage** is (cf. Equation-4.10):

$$Pr\{Z \leq t\} = 1 - \sum_{n=0}^{\infty} \frac{(\lambda t)^{n\beta} \exp\left(-(\lambda t)^\beta\right)\Gamma(n, K\theta)}{\Gamma(n+1)\Gamma(n)} \tag{4.21}$$

with the mean $E(Z) = \sum_{n=0}^\infty \frac{\theta^n \Gamma(n+1/\beta) K^{n-1} \exp(-\theta K)}{\lambda\beta\Gamma(n+1)\Gamma(n)} = \frac{\exp(-K\theta)\theta\Gamma(1+1/\beta)_1F_1(1+1/\beta,2,K\theta)}{\beta\lambda}$ and $E(Z^2) = 2\sum_{n=0}^\infty \frac{\theta^n\Gamma(n+2/\beta)K^{n-1}\exp(-\theta K)}{\lambda^2\beta\Gamma(n+1)\Gamma(n)} = 2\frac{\exp(-K\theta)\theta\Gamma(1+2/\beta)_1F_1(1+2/\beta,2,K\theta)}{\beta\lambda^2}$, i.e., $\int_0^\infty \frac{[\Lambda(t)]^n}{\Gamma(n+1)}\exp(-\Lambda(t))dt = \frac{\Gamma(n+1/\beta)}{\lambda\beta\Gamma(n+1)}$.

Example#4: Again, suppose that the magnitude of the events follows the exponential distribution while nonhomogeneous Poisson process for the time. Note that here we consider nonhomogeneous Poisson process with the power law intensity. The first passage distribution in the case of independent damage is given below (cf. Equation-4.13):

$$Pr\{Z \leq t\} = 1 - \exp\left(-\exp(-K\theta)(\lambda t)^\beta\right) \tag{4.22}$$

with $E(Z) = \frac{\Gamma(1+1/\beta)}{\left(\exp(-K\theta)\lambda^\beta\right)^{1/\beta}}$ and $E(Z^2) = \frac{\Gamma(1+2/\beta)}{\left(\exp(-K\theta)\lambda^\beta\right)^{2/\beta}}$.

4.4 Control Chart Construction

To construct control charts using the first passage distribution, we need to modify the definition of TBE presented in Section-1.2. In the current context, we shall consider the following definition:

Definition 4.4.1 *For the cumulative processes, we define TBE as the time of the first passage distribution to cross a critical point (cf. Figure-4.1 or 4.2), i.e.,* $X_i = T_i - T_{i-1} = Z_i$ *for* $i > 0$ *and* $T_0 = 0$*, where* Z_i *is i-th time point at which the damage crossed the critical threshold.*

Let α denotes the probability of the false alarm. To construct a two-sided control chart based on Equations-[4.19-4.22] equate them to $\alpha/2$ and $1-\alpha/2$, i.e., find the specified percentiles of the first passage distribution, to get the lower control limit (LCL) and the upper control limit (UCL), respectively. Statistically speaking, we need to find $LCL = F^{-1}(\alpha/2)$ and $UCL = F^{-1}(1-\alpha/2)$, where $F^{-1}(p) = \inf\{t \in \mathbf{R}_+ : p \leq F(Z)\}$ and $0 < p < 1$, for the two-sided control chart. Note that inf represents infimum function and can be replaced with minimum function if $F(.)$ is continuous. A one-sided control chart could be designed by finding the α percentile of the first passage distributions to get the LCL for the detection of process deterioration. Similarly, the upper-sided control chart could also be designed by finding the $1-\alpha$ percentile to get UCL for the detection of process improvement. We describe the monitoring procedure as follows: If a TBE falls below the LCL, then it means that a process might have been statistically deteriorated, therefore declare it an out-of-control. However, if a point falls above the UCL, then the process could be thought statistically improved at the specified false alarm probability. The process is thought to be statistically in-control if the time point falls between the LCL and the UCL.

To assess the performance of the control chart, we shall use the average run length (ARL) and the average length of inspection (ALI). The ARL is the number of points that, on average will be plotted on the control chart before an out-of-control signal is appeared, i.e., for in-control situation $ARL = 1/\alpha$ while for out-of-control situation, it is $ARL = 1/(1-\zeta)$ where ζ denotes the type-II error. The ALI is defined as the average time (or length) of inspection which one has to wait before to get an out-of-control signal and can be written as $ALI = ARL \times E(X)$ (cf. 2.10).

It is worth mentioning that to get an explicit expression of the first passage distribution, for the construction of a control chart, is extremely difficult in general cases, e.g. consider the Weibull distribution for the time and the magnitude. Therefore, we propose Algorithm-4.1 to compute the control limits in general cases. This algorithm is applicable to any suitable choice of time and magnitude distributions.

Similarly, we have Algorithm-4.2 for the ARL computation.

Algorithm 4.1 Control Limits Computation for the First Passage Distribution' to a fixed Critical Threshold

Select $p = 1$ or $p = 2$ for the Process▷ where $p = 1$ - Cumulative, $p = 2$ - Independent
Choose parameters values to generate X and M from F_X and G_M
Fix K
for $i = 1$ to S **do** ▷ where S is large, e.g., 10^6
    do
        Sample X_j and M_j, $j \geq 1$
        if $p == 1$ **then**
            $SM_j = \sum_{l=1}^{j} M_l$
        else
            $SM_j = M_j$
        end if
    while $SM_j < K$
    $Z_i = \sum_{l=1}^{j} X_l$
end for
Compute the Specified Quantiles of Z_i to find the LCL and UCL, respectively.

Algorithm 4.2 ARL Computation for the Two-Sided Chart based on the Renewal Reward Process with a fixed Critical Threshold

Select $p = 1$ or $p = 2$ for the Process▷ where $p = 1$ - Cumulative, $p = 2$ - Independent
Choose shifted parameters values to generate X and M from F_X and G_M
Fix K
for $h = 1$ to S **do** ▷ where S is large, e.g., 10^6
    for $i = 1$ to S **do**
        do
            Sample X_j and M_j, $j \geq 1$
            if $p == 1$ **then**
                $SM_j = \sum_{l=1}^{j} M_l$
            else
                $SM_j = M_j$
            end if
        while $SM_j < K$
        $Z_i = \sum_{l=1}^{j} X_l$
        if $Z_i < LCL || Z_i > UCL$ **then**
            $RL_h = i$, break
        end if
    end for
end for
Compute Mean of RL_h.

As we have noticed in Section-3.4 that the design of a control chart is often based on ARL, a large in-control ARL is ensured by design, but the variance of the run length distribution can be large. Thus, in such scenario, the coefficient of variation (CV) provides good insights instead of ARL. An advantage of CV is that different control charts with close ARL can be compared. Moreover, it is a scale-free measure. We have noticed in Chapter-3.3, that ALI is not a scale-free measure; therefore, we shall report only the CV values of the ALI.

In addition to these performance measures of the control charts, the quartiles of the run length distribution are also studied in-detail. We give a discussion for the detection of process deterioration and improvement using the one and the two sided control charts, in the following subsections.

It is quite possible that one might have knowledge about a shift in either the time or the magnitude distribution. Therefore, to find the resulting shift in other distribution's parameter, one can use the mean of the first passage distribution. To demonstrate it for the cumulative process, let us suppose that θ_0 and λ_0 are the in-control rate parameters which result into $m_0 = (\theta_0 K+1)/\lambda_0$. Furthermore, suppose that we know θ_1 and interested in finding λ_1. To accomplish this task, we denote $m_t(\theta_1, \lambda_0) = (\theta_1 K + 1)/\lambda_0$ and equate it to $(\theta_0 K + 1)/\lambda_1$ which would result into $\lambda_1 = \frac{\theta_0 K+1}{m_t(\theta_1,\lambda_0)} = \frac{\lambda_0(\theta_0 K+1)}{\theta_1 K+1}$. Hence, by using the knowledge of θ_1 one can find λ_1. For example, if the in-control rate parameters of the time and magnitude are $\lambda_0 = 0.0005$ and $\theta_0 = 0.001$, respectively. We know the out-of-control value of $\theta_1 = 0.003$ and interested in finding the corresponding λ_1 for $K = 300$. For these specifications, we have $\lambda_1 = 0.000342$. Similarly, λ_1 can be found by utilizing the λ_1 from $\theta_1 = \frac{\lambda_0 m_l(\theta_0,\lambda_1)-1}{K)} = \frac{\lambda_0(\theta_0 K+1)-\lambda_1}{\lambda_1 K}$.

To find the shifted/adjusted parameter value in the independent process we have $\theta_1 = \frac{\ln(\lambda_0)+\theta-0K-\ln(\lambda_1)}{K}$, i.e., by using the λ_1, and $\lambda_1 = \lambda_0 \exp\{K(\theta_0 - \theta_1)\}$ for θ_1. Similarly, for the independent process with NHPP for the time, we have: $\theta_1 = \frac{\beta_1}{K}\left[\ln\left\{\frac{\lambda_0\Gamma(1+\beta_0^{-1})}{\lambda_1\Gamma(1+\beta_1^{-1})}\right\} - \frac{K\theta_0}{\beta_0}\right]$, $\lambda_1 = \lambda_0 \exp\big(K\big[\frac{\theta_0}{\beta_1} - \frac{\theta_1}{\beta_0}\big]\big)\frac{\Gamma(1+\beta_1^{-1})}{\Gamma(1+\beta_0^{-1})}$ and solve $\Gamma(1+\beta_1^{-1})\exp(K\theta_0/\beta_1) = \frac{\lambda_1\Gamma(1+\beta_0^{-1})\exp(K\theta_1/\beta_0)}{\lambda_0}$ to get β_1.

4.4.1 Cumulative probability control chart

The cumulative probability control chart is a control chart in which the observed cumulative probability is plotted against the sample number (time) (cf. Chan et al. [2002]). Since the cumulative probability is plotted, the vertical axis of the plot always lies between zero and one, which makes its interpretation easier. To construct a cumulative probability chart, the lower and the upper control limits for the two-sided chart are $\alpha/2$ and $1 - \alpha/2$, respectively. Similarly, a one-sided control chart can be constructed by considering $LCL = \alpha$ and $UCL = 1 - \alpha$. If an unequal probability of the false alarm is

selected, then α might be replaced by α_L and α_U subject to $\alpha_L + \alpha_U = \alpha$. The decision rules regarding the process improvement or deterioration, are similar as in the CQC chart.

4.4.2 Discussion of ARL Study (Cumulative Process)

The performance of the charts is evaluated detecting a wide range of shifts. This is done because in practice, the actual shift size is unknown. We considered the shifts for the following two cases:

A λ decreases from $\lambda_0 = 0.0005$ to $\lambda_1 \in \{0.0003, 0.0001, 0.00005\}$ while θ increases from $\theta_0 = 0.001$ to $\theta_1 \in \{0.005, 0.002, 0.01\}$.

B λ increases from $\lambda_0 = 0.0005$ to $\lambda_1 \in \{0.005, 0.01, 0.1\}$ and θ decreases form $\theta_0 = 0.001$ to $\theta_1 \in \{0.00001, 0.0005, 0.0001\}$.

Note that when the process is in-control, i.e., no shift in the process parameters, the ARL values of the one and the two sided charts are equal to the specified in-control ARL value, i.e., 370.

Case A: an increase in θ (or decrease in λ): The system improves if the damage decreases, which will result an increase of the time, i.e., the system fails occasionally. In other words, θ will increase and result into a decreased rate of the first-passage distribution. In our study, we fixed the magnitude rate parameter $\theta_0 = 0.001$ (for in-control process) while $\theta_1 \in \{0.005, 0.002, 0.01\}$ to represent out-of-control situation. The rate parameter of the time distribution shifted from $\lambda_0 = 0.0005$ to $\lambda_1 \in \{0.0003, 0.0001, 0.00005\}$. Since the system improves, an engineer is generally more concerned in the process improvement detection and for this purpose, the Upper-sided control chart is employed. We have computed the ARL, CVs of the run-length distribution and the length of inspection, for the two-sided and the upper-sided charts in Table-4.1. The standard deviation of the ARL can easily be recovered using the ARL and the CV values.

Table-4.1 shows some interesting results. By examining the ARL values, it is evident that the one-sided chart detects the shifts efficiently than the two-sided control chart. The said effectiveness of the one-sided charts can be assessed by the coefficient of variation values. The ARL values show a decreasing pattern as the shift in the rate parameter of the magnitude distribution occurs. We also have observed that the designed charts, i.e., upper and two-sided charts, obey the unbiased property of the ARL. However, this unbiasedness is not guaranteed if the magnitude/damage starts increasing, suddenly. In this case, ARL would be biased and the two-sided chart outperforms for $\lambda_0 = \lambda_1$ $(\forall\theta)$ than the upper-sided chart. The CV of the run length distribution is smaller and less stable than the CV of the length of inspection. Therefore, one could observe a mixed behavior of the CVLI as compared to the CV of the run length. Moreover, it is indication that the length of inspection distribution is more inflated than the run length distribution. The

quartiles of the run-length distribution are also computed (not reported here for the sake of space), and we noticed that as the large-size shift in the rate parameter of the time distribution occurs, the run length distribution becomes highly skewed and mean of the run length gets greater than Q_3. However, for small to moderate shifts, either in rate parameter of the magnitude or time distribution, the ARL is less than Q_3, but greater than Q_2. Thus, runs rules to study the ARL performance may not be effective in such highly skewed distribution.

Case B: a decrease in θ (or an increase in λ): This is the most important case since it detects the process deterioration. In this case, the rate of the magnitude/damage θ will increase and results into more frequent system failures. In our study, we fixed the rate parameter of the magnitude distribution $\theta_0 = 0.001$ (for in-control process) while $\theta_1 \in \{0.00001, 0.0005, 0.0001\}$ to represent out-of-control situation. The rate parameter of the TBE distribution shifted from $\lambda_0 = 0.0005$ to $\lambda_1 \in \{0.005, 0.01, 0.1\}$. When a system deteriorates, a practitioner or an engineer should use the lower-sided control chart contrary to the upper-sided chart, which is used for the process improvement. Thus, for comparison purposes, we report the ARL values for the lower and two sided control charts with their CV in Table-4.2.

From Table-4.2 we have noticed that the lower-sided chart is efficient in the detection of process deterioration than the two-sided chart. As the shift in the rate parameter of the time distribution occurs, the ARL values get smaller, and this pattern can be verified from the CV values. A shift of large size (either in the magnitude or time distribution) could be detected quickly as compared to the small shift. When the time distribution is in-control, i.e., $\lambda_0 = \lambda_1$, but have a shift in the magnitude, i.e., $\theta_1 < \theta_0$, then for the two-sided chart, we observe a reverse behavior of the ARL as compared to the process improvement case. Here, the ARL is clearly biased, which was not the case in process improvement. However, the lower-sided chart is free from such shortcomings, and we advocate its superiority over the two-sided chart. Again, in this case, the CV values of the run length have been observed smaller than the length of inspection, and both CVs support the superiority of the one-sided chart over the two-sided chart. We have also computed the quartiles, and observed that ARL value was smaller than the Q_3. Therefore, the run length distribution is not highly skewed as we observed in the case of process improvement.

Table 4.1: ARL based on $\alpha = 0.0027, \lambda_0 = 0.0005, \theta_0 = 0.001$ and $\lambda_1 \in \{0.0003, 0.0001, 0.00005\}$, $\theta_1 \in \{0.00001, 0.0001, 0.01\}$ for upper and two-sided cumulative process charts.

θ	λ	Upper-Sided				Two-Sided			
		0.0005	0.0003	0.0001	0.00005	0.0005	0.0003	0.0001	0.00005
0.001	ARL	370.37	32.0474	3.05326	1.73591	370.37	46.1792	3.46456	1.84701
	CV	0.998649	0.984274	0.820049	0.651102	0.998649	0.989113	0.843424	0.67719
	CVLI	0.999928	0.999169	0.991241	0.984541	0.999928	0.999423	0.992285	0.985478
0.002	ARL	160.761	17.9681	2.40352	1.52591	231.902	25.2764	2.66728	1.60262
	CV	0.996885	0.971775	0.764162	0.587072	0.997842	0.980019	0.790624	0.613205
	CVLI	0.999563	0.996079	0.970305	0.952807	0.999697	0.997214	0.973282	0.955119
0.005	ARL	35.3429	6.41082	1.58941	1.22365	57.4729	8.37106	1.69522	1.25651
	CV	0.985751	0.918702	0.608964	0.42752	0.991262	0.938371	0.640394	0.451823
	CVLI	0.994894	0.971517	0.879489	0.840118	0.996863	0.978261	0.88749	0.844684
0.01	ARL	8.95931	2.69559	1.19192	1.06527	13.0939	3.2243	1.22946	1.07618
	CV	0.942541	0.79311	0.401274	0.247524	0.961056	0.830575	0.432009	0.266064
	CVLI	0.968099	0.889565	0.726687	0.686996	0.978285	0.908594	0.736533	0.690883

Table 4.2: ARL based on $\alpha = 0.0027, \lambda_0 = 0.0005, \theta_0 = 0.001$ and $\lambda_1 \in \{0.005, 0.01, 0.1\}$, $\theta_1 \in \{0.00001, 0.0001, 0.0005\}$ for lower and two-sided cumulative process charts.

β	λ	Lower-Sided				Two-Sided			
		0.0005	0.005	0.01	0.1	0.0005	0.005	0.01	0.1
0.00001	ARL	275.351	27.9881	14.2486	1.93436	474.139	55.5067	28.0056	3.28049
	CV	0.998182	0.981973	0.96427	0.695006	0.998945	0.990951	0.981984	0.833767
	CVLI	1.0000	1.0000	1.0000	0.999998	1.0000	1.0000	1.0000	0.999999
0.0001	ARL	282.872	28.74	14.6243	1.97018	470.16	57.0118	28.758	3.35473
	CV	0.998231	0.982449	0.965205	0.701735	0.998936	0.991191	0.98246	0.837803
	CVLI	0.999999	0.999985	0.999971	0.999785	0.999999	0.999993	0.999985	0.999874
0.0005	ARL	318.868	32.3338	16.4177	2.13813	436.744	64.2106	32.3542	3.70586
	CV	0.998431	0.984415	0.969067	0.72959	0.998855	0.992183	0.984425	0.854492
	CVLI	0.999973	0.999737	0.999482	0.996014	0.999981	0.999868	0.999737	0.997702
0.001	ARL	370.37	37.4646	18.9721	2.36971	370.37	74.5005	37.4882	4.19766
	CV	0.998649	0.986564	0.973289	0.760268	0.998649	0.993266	0.986572	0.872795
	CVLI	0.999928	0.999289	0.998596	0.9887	0.999928	0.999643	0.999289	0.993636

4.4.3 Discussion of ARL Study (Independent Process)

We are considering shifts for the following two cases:

A λ decreases from $\lambda_0 = 0.0005$ to $\lambda_1 \in \{0.0003, 0.0001, 0.00005\}$ while θ increases form $\theta_0 = 0.001$ to $\theta_1 \in \{0.005, 0.002, 0.01\}$.

B λ increases from $\lambda_0 = 0.0005$ to $\lambda_1 \in \{0.005, 0.01, 0.1\}$ and θ decreases form $\theta_0 = 0.001$ to $\theta_1 \in \{0.00001, 0.0005, 0.0001\}$.

We examine the system performance by varying one parameter as the other one is holding fixed. It is to be noted that when the process is in-control, i.e., no shift in the process parameters, the ARL is equal to the specified in-control ARL value, i.e., 370.

Case A: an increase in θ (or decrease in λ): In this case, we fixed the rate parameter of the magnitude distribution $\theta_0 = 0.001$ (for in-control process) while $\theta_1 \in \{0.002, 0.005, 0.01\}$ to represent out-of-control situation. Similarly, the rate parameter of the time distribution shifts from $\lambda_0 = 0.0005$ to $\lambda_1 \in \{0.0003, 0.0001, 0.00005\}$. Again for the detection of process improvement, the Upper-sided control chart is being used in this study, and it would further be compared with the two-sided chart. In Table-4.3, we have computed the ARL values of the two-sided and upper-sided charts. The coefficient of variation (CV) value is also reported below the ARL and standard deviation of the run-length can easily be recovered. As noted previously, the ALI is not a scale-free measure, therefore, we decided to report only the CV values of the ALI.

In the process improvement case, as the shift occurs in the rate parameter of magnitude distribution, then time distribution also shifts, i.e., the rate parameter of the first passage time distribution becomes small, and therefore, the mean and the variance get large with the size of the shift. Note that a small parameter value means the case where the parameter has smaller value than its nominal, i.e., the mean with $\lambda = 0.0005$ is smaller than the $\lambda = 0.0001$. The said remark is also true for the variance.

From Table-4.3, it is clear that one-sided chart is more efficient in the detection of shifts than the two-sided control chart. The CV of the run-length and the length of inspection also supports the superiority of the upper-sided control chart. The large-size shifts either in the rate parameter of time distribution or magnitude distribution can be detected quickly contrary to the small shift. It is noticed that ARL values gradually decrease with the shift in the rate parameter of magnitude distribution. However, we observed that if the rate parameter of the time distribution was fixed at the nominal value, i.e., $\lambda = 0.0005$, and the rate parameter of a magnitude distribution decreased, then the ARL values would be greater than the nominal value. Although this behavior violates the unbiased property of the ARL, it is expected as the time to cross the critical threshold is strongly dependent on the magnitude distribution. The CV of the length of inspection distribution is almost noninformative, and it is difficult to decide which chart

outperforms. However, the CV of the run of length distribution supports the superiority of the upper-sided chart. It is observed from the quartiles' (not reported here for the sake of space) that a very large shift either in a damage or time will result into a highly skewed distribution of the run-length, i.e., ARL will be greater than Q_3. However, for small to moderate shifts, the ARL is less than Q_3 but greater than the median, i.e., Q_2.

Case B: a decrease in θ (or an increase in λ): This is a crucial case since it detects the process deterioration. In this case, θ would decrease and result into an increase rate parameter of the first-passage distribution. Hence, the system failure will be more frequent. In our study, we fixed the rate parameter of the damage/magnitude distribution $\theta_0 = 0.001$ (for in-control process) while $\theta_1 \in \{0.00001, 0.0005, 0.0001\}$ to represent out-of-control situation. The rate parameter of the time distribution shifts from $\lambda_0 = 0.0005$ to $\lambda_1 \in \{0.005, 0.01, 0.1\}$. When the process deteriorates, the practitioner needs to use the lower-sided control chart. Thus, in our numerical study, we are presenting the ARL values for the lower-sided chart. Moreover, a comparison of the two-sided control chart with the lower-sided is also given in Table-4.4.

By examining Table-4.4 we noticed that the lower-sided chart is efficient in the detection of process deterioration than the two-sided chart. We observe that the ARL of the two-sided chart is biased as compared to the lower-sided chart, especially when a shift is only in the rate parameter of the magnitude distribution. However, if we fix the damage distribution and introduce a shift in the rate parameter of the time distribution, then the ARL values get small, i.e., control charts' detection ability improves. A shift of large size either in time or damage will be detected quickly as compared to the small shift. The CV of the run length distribution advocates the effectiveness of the lower-sided chart whereas the CV of the length of inspection distribution is not too informative. We also computed the quartiles of the run-length distribution (not reported here) and found that the ARL values lie between the median and Q_3, which means that the run-length distribution is not highly skewed as we have observed in the case of process improvement.

Table 4.3: ARL based on $\alpha = 0.0027, \lambda_0 = 0.0005, \theta_0 = 0.001$ and $\lambda_1 \in \{0.0003, 0.0001\ , 0.00005\}$, $\theta_1 \in \{0.005, 0.002, 0.01\}$ for upper and two-sided Independent process charts.

θ	λ	Upper-Sided				Two-Sided			
		0.0005	0.0003	0.0001	0.00005	0.0005	0.0003	0.0001	0.00005
0.001	ARL	370.37	34.7682	3.26383	1.80661	370.37	50.5407	3.74536	1.93577
	CV	0.998649	0.985514	0.832833	0.668189	0.998649	0.990058	0.856156	0.695276
	CVLI	1.0000	1.0000	1.0000	1.0000	1.0000	1.0000	1.0000	1.0000
0.002	ARL	79.9636	13.8591	2.40203	1.54985	117.873	18.6488	2.66041	1.63125
	CV	0.993727	0.963247	0.763993	0.59563	0.995749	0.972819	0.790012	0.62207
	CVLI	1.0000	1.0000	1.0000	1.0000	1.0000	1.0000	1.0000	1.0000
0.005	ARL	5.93825	2.91202	1.42801	1.19499	7.29518	3.29797	1.48872	1.22014
	CV	0.911921	0.810306	0.547472	0.40395	0.928937	0.834735	0.572959	0.424764
	CVLI	1.0000	1.0000	1.0000	1.0000	1.0000	1.0000	1.0000	1.0000
0.01	ARL	1.48808	1.26933	1.08274	1.04055	1.55882	1.30522	1.09286	1.0454
	CV	0.572707	0.460636	0.276441	0.197406	0.59874	0.483576	0.29149	0.20839
	CVLI	1.0000	1.0000	1.0000	1.0000	1.0000	1.0000	1.0000	1.0000

Table 4.4: ARL based on $\alpha = 0.0027, \lambda_0 = 0.0005, \theta_0 = 0.001$ and $\lambda_1 \in \{0.005, 0.01, 0.1\}$, $\theta_1 \in \{0.00001, 0.0005, 0.0001\}$ for lower and two-sided Independent process charts.

θ	λ	Lower-Sided				Two-Sided			
		0.0005	0.005	0.01	0.1	0.0005	0.005	0.01	0.1
0.00001	ARL	275.33	27.986	14.2476	1.93426	511.818	55.5047	28.0046	3.28039
	CV	0.998182	0.981971	0.964268	0.694987	0.999023	0.990951	0.981983	0.833762
	CVLI	1.0000	1.0000	1.0000	1.0000	1.0000	1.0000	1.0000	1.0000
0.0001	ARL	282.852	28.7381	14.6235	1.9703	514.881	57.0099	28.7572	3.35486
	CV	0.998231	0.982447	0.965203	0.701757	0.999028	0.991191	0.982459	0.837809
	CVLI	1.0000	1.0000	1.0000	1.0000	1.0000	1.0000	1.0000	1.0000
0.0005	ARL	318.85	32.3376	16.4227	2.14376	492.206	64.2144	32.3592	3.71177
	CV	0.998431	0.984417	0.969076	0.730432	0.998984	0.992183	0.984427	0.854744
	CVLI	1.0000	1.0000	1.0000	1.0000	1.0000	1.0000	1.0000	1.0000
0.001	ARL	370.37	37.4893	18.998	2.39419	370.37	74.5252	37.5143	4.22369
	CV	0.998649	0.986573	0.973326	0.763101	0.998649	0.993268	0.986582	0.873636
	CVLI	1.0000	1.0000	1.0000	1.0000	1.0000	1.0000	1.0000	1.0000

4.5 Independent Compound Process with NHPP

We considered shifts for the following cases:

A Increasing Hazard Rate (IHR), i.e., $\beta > 1$ (Process Deterioration)

1. λ shifts from $\lambda_0 = 0.0005$ to $\lambda_1 \in \{0.0003, 0.0001, 0.00005\}$, β from $\beta_0 = 1.5$ to $\beta_1 \in \{1, 1.2, 1.5, 2\}$ [i.e., Partial Improvement (PI)], and θ from $\theta_0 = 0.001$ to $\theta_1 \in \{0.005, 0.01\}$.
2. λ shifts from $\lambda_0 = 0.0005$ to $\lambda_1 \in \{0.005, 0.01, 0.1\}$, β form $\beta_0 = 1.5$ to $\beta_1 \in \{1, 1.2, 1.5, 2\}$ [i.e., Total Deterioration (TD)], and θ from $\theta_0 = 0.001$ to $\theta_1 \in \{0.0001, 0.0005\}$.

B Decreasing Hazard Rate (DHR), i.e., $\beta < 1$ (Process Improvement)

1. λ shifts from $\lambda_0 = 0.0005$ to $\lambda_1 \in \{0.0003, 0.0001, 0.00005\}$, β from $\beta_0 = 0.5$ to $\beta_1 \in \{0.2, 0.45, 0.5, 0.55, 0.7\}$ [i.e., Total Improvement (TI)], and θ from $\theta_0 = 0.001$ to $\theta_1 \in \{0.005, 0.01\}$.
2. λ shifts from $\lambda_0 = 0.0005$ to $\lambda_1 \in \{0.005, 0.01, 0.1\}$, β form $\beta_0 = 0.5$ to $\beta_1 \in \{0.2, 0.45, 0.5, 0.55, 0.7\}$ [i.e., Partial Deterioration (PD)], and θ from $\theta_0 = 0.001$ to $\theta_1 \in \{0.0001, 0.0005\}$.

It is observed that when there is neither a shift in the NHPP parameters nor in the magnitude distribution, the ARL values of the one and the two sided charts are equal to the nominal value, i.e., 370.

Case A-1: an increase in θ (or decrease in λ): When the rate parameter of the magnitude/damage distribution increases, the chances to cross the fixed threshold become less, which results into an increase of the TBE. Here, we consider the NHPP with power law intensity for time, which depends on the rate and the shape parameters, respectively. Therefore, if the shape parameter β is greater than one, the overall performance of the system would deteriorate. However, one could observe some improvements in the system performance if the rate parameter of the NHPP decreases. In a practical sense, this could happen due to replacement of some components in the deteriorating system. Thus, this case can be labeled as a partial improvement (PI). When the system temporarily improves, the effect should be reflected by temporarily increase in the TBE, i.e., failure of the system might be less frequent for a short period of time. In our study, we fixed the magnitude rate parameter $\theta_0 = 0.001$ (for in-control process) while $\theta_1 \in \{0.005, 0.01\}$ to represent an out-of-control situation. The in-control shape parameter of the NHPP is $\beta_0 = 1.5$ while the $\beta_1 \in \{1.0, 1.2, 2.0\}$ to represent an out-of-control situation. The rate parameter of NHPP shifts from $\lambda_0 = 0.0005$ to $\lambda_1 \in \{0.0003, 0.0001, 0.00005\}$. When a system partially improves, an engineer is generally more concerned in the process improvement detection

to maintain its sustainability. Therefore, the upper-sided control chart is a good candidate for this purpose. In Table-4.5, we have computed the ARL values of two and upper-sided charts. The coefficient of variation (CV) values of the run length and of the length of inspection distributions have also been reported below the ARL.

From Table-4.5, clearly, the one-sided chart is efficient in the detection of a shift than the two-sided chart. The said superiority is also evident to the CVs of the run length and the length of inspection distributions. For fixed β, the values of the ARL decrease gradually with the occurrence of a shift in θ, i.e., magnitude's rate parameter, and a large shift either in θ or λ could be detected quickly than the moderate to small shifts. However, the value of the ARL is significantly dependent on the shape parameter β. When the rate parameters of the magnitude and of the time distributions are in-control, both charts follow the unbiased property of the ARL. However, it is violated if the shape parameter becomes greater than its nominal value, i.e., $\beta > 1.5$. This violation is serious in the case of lower-sided chart. We also computed the quartiles of the run length distribution (not reported here for the sake of space) and observed that the ARL is between Q_2 and Q_3 for small to moderate shifts while greater than Q_3 for large shifts. This behavior implies that the run-length distribution is highly skewed for large shifts, and therefore, an extreme care is needed to design ARL unbiased design chart.

Case A-2: a decrease in θ (or an increase in λ): This is the most important case because in this case, a process engineer is concerned to detect the process deterioration. Since we have assumed the shape parameter of the NHPP greater than one, the overall process would deteriorate. However, in the case of the NHPP, deterioration also depends on the magnitude's rate parameter. For a fixed threshold, when the rate of the magnitude/damage increases it shorten TBE and therefore, a system fails frequently. Thus, such kind of situation can be labeled as a total deterioration (TD). In our study, we fixed the rate parameter of the magnitude/damage distribution $\theta_0 = 0.001$ (for in-control process) while $\theta_1 \in \{0.0001, 0.0005\}$ to represent an out-of-control situation. The rate parameter of the NHPP shifts from $\lambda_0 = 0.0005$ to $\lambda_1 \in \{0.005, 0.01, 0.1\}$. Moreover, the in-control shape parameter of the NHPP is assumed $\beta_0 = 1.5$ while $\beta_1 \in \{1.0, 1.2, 2.0\}$ for out-of-control situation. When the system deteriorates, the practitioner should use the lower-sided control chart in contrast to the upper-sided chart. Thus, in our numerical study, we present ARL study of the lower-sided chart and further compare it with the two-sided control chart. The values of the CV of the run length and the length of inspection distributions have also been reported in Table-4.6.

In this case, when $\lambda = 0.0005$ and a large shift occurs in magnitude's rate parameter; the ARL of the two-sided chart is smaller than the lower-sided chart. This behavior is not specific to any particular value of the shape parameter but observed for all assumed choices of the shape parameter, β, in this study. However, we noticed that when a shift occurs in the rate parameter of the TBE distribution, i.e., λ, the lower-sided chart is

efficient in the detection of process deterioration than the two-sided chart. It has also been observed that when $\beta_1 > \beta_0$, the ARL values are greater than the corresponding nominal value, i.e., 370, which is a sign that the shape parameter of the NHPP has a significant effect on the control chart's efficiency. Therefore, one must be very careful in the choice of the shape parameter to study control chart' performance, as it leads to a biased design of the ARL. The CV values also support the effectiveness of the lower-sided chart except the case which we have discussed already. For the fixed β, when a shift occurs in θ, i.e., the magnitude distribution parameter, the values of the ARL decrease with the increase of a shift. From the quartiles' study, it is observed that for the small to moderate shifts, the ARL values are smaller than Q_3 but greater than the median, i.e., Q_2. Moreover, the run length distribution is highly skewed in the presence of large shifts.

Case B-1: an increase in θ (or decrease in λ): In this case, we assume the value of the shape parameter β less than one while the rate parameter λ decreases from its nominal value. Therefore, the overall performance of a system would improve, and this case could be labeled as a total improvement (TI). In the case of TI, the system would take a long time (as the damage/magnitude becomes small) to react and produce an out-of-control signal. For illustration purpose, in our study we fixed the magnitude/damage rate parameter $\theta_0 = 0.001$ (for in-control process) while $\theta_1 \in \{0.005, 0.01\}$ to represent an out-of-control situation. The in-control shape parameter of the NHPP is assumed $\beta_0 = 0.5$ while $\beta_1 \in \{0.2, 0.45, 0.55, 0.7\}$ to represent an out-of-control situation. The rate parameter of the NHPP shifted from $\lambda_0 = 0.0005$ to $\lambda_1 \in \{0.0003, 0.0001, 0.00005\}$. We again consider the upper-sided chart and the two-sided chart to detect the process improvement. In Table-4.7, we have tabulated the ARL values for two-sided and upper-sided charts.

From Table-4.7, one can observe that when a large shift occurs in the shape parameter of the NHPP against a small shift in the magnitude parameter, the two-sided chart becomes more efficient in the detection of a shift than the one-sided chart, and this conclusion is also supported by the CV. However, there is no objection on the superiority of the upper-sided chart when the shift in β is small to moderate. It has also been observed that for the small value of β, i.e., 0.2, the CV of the length of inspection is greater than the process deterioration case. We observed that ARL equal to the nominal value when there was no shift in either the time distribution or magnitude distribution' parameters. However, when $\beta_1 > \beta_0$ and $\theta_1 = \theta_0, \lambda_1 = \lambda_0$, we observed a biased behavior of the ARL. This is again an obvious sign that there is a great impact of the shape parameter on the control charts' detection ability. For fixed β, when the process has an up-sided shift ($\theta > 0.001$) in θ, the ARL values decrease gradually and vice versa. We also computed the quartiles of the run-length distribution, and it is observed that for small to moderate shifts in β, θ and λ, the distribution of the run length is less skewed as compared to the case of large shifts in the process.

Case B-2: a decrease in θ (or an increase in λ): This is another important case because $\beta < 1$, i.e., the overall performance of the system is improving but due to some sudden changes that can occur in the workforce, material or in the environment, the rate parameters of the magnitude distribution might (suddenly) increase. Consequently, the rate parameter of the first-passage distribution to a critical threshold would be increased. Thus, the process deteriorates, and one could label this case as a partial deteriorate (PD). To detect the process deterioration, we used the lower-sided chart which further has been compared with the two-sided chart. In our study, we fixed the rate parameter of the magnitude distribution $\theta_0 = 0.001$ (for in-control process) while $\theta_1 \in \{0.0001, 0.0005\}$ to represent an out-of-control situation. The rate parameter of the NHPP shifts from $\lambda_0 = 0.0005$ to $\lambda_1 \in \{0.005, 0.01, 0.1\}$. Similarly, a nominal value of the shape parameter of the NHPP is $\beta_0 = 0.5$ while $\beta_1 \in \{0.2, 0.45, 0.55, 0.7\}$ to represent an out-of-control situation. The values of the ARL with the CVs of the run-length and the length of inspection have been reported in Table-4.8.

In this case, when $\beta_1 = 0.2$ and $\lambda = 0.0005$, the superiority of the lower-sided chart is undermined by the two-sided chart. This happens because of β, which is less than one and a sign of the process improvement, therefore, two-sided chart with the upper control limit performs better than the counterpart one-sided chart. The superiority of the lower-sided chart has no question mark for a large shift either in λ or θ. For fixed β and θ, the large shifts in the rate parameter would be detected quickly than the small shifts. The CV of the length of inspection is very large as compared to the process deterioration, especially when $\beta_1 = 0.2$, and it leads to a similar conclusion as we did notice in the TI case. Moreover, the CV gradually increases with the shift in the rate parameter of the TBE. Therefore, we can conclude that the effect of the shape parameter on the control chart's detection ability is significant. Although both charts for $\theta = 0.001, \beta = 0.5$ and $\lambda = 0.0005$ have desired in-control performance, i.e., 370, we noticed that the ARL violates the unbiased property when $\beta > 0.5$. Since there is a significant impact of the shape parameter on the control chart' performance, one must be very careful to interpret an out-of-control alarm raised by the chart. Moreover, we suggest to consider the unbiased design of the control charts in such situations.

Table 4.5: ARL study of the PI-IHR case using $\alpha = 0.0027$ $\lambda_0 = 0.0005, \beta_0 = 1.5$, $\theta_0 = 0.001$ and $\lambda_1 \in \{0.0003, , 0.0001, 0.00005\}$, $\beta_1 \in \{1, 1.2, 2\}, \theta_1 \in \{0.005, 0.01\}$ for upper and two sided Independent NHPP charts.

β	θ	λ	Upper Sided				Two Sided			
			0.0005	0.0003	0.0001	0.00005	0.0005	0.0003	0.0001	0.00005
1.0	0.005	ARL	2.43832	1.70708	1.19514	1.09322	2.58833	1.77225	1.21061	1.10032
			0.768038	0.643588	0.404076	0.292018	0.783358	0.66011	0.417098	0.301946
		CVLI	1.0000	1.0000	1.0000	1.0000	1.0000	1.0000	1.0000	1.0000
	0.001	ARL	19.2836	5.90355	1.80733	1.34437	19.1108	6.47495	1.88337	1.37314
			0.973726	0.911378	0.668355	0.50612	0.973485	0.919543	0.521288	0.521286
		CVLI	1.0000	1.0000	1.0000	1.0000	1.0000	1.0000	1.0000	1.0000
	0.01	ARL	1.22003	1.12674	1.04058	1.02009	1.23764	1.13652	1.04359	1.02157
			0.424677	0.335384	0.197472	0.140326	0.438192	0.346584	0.204384	0.145296
		CVLI	1.0000	1.0000	1.0000	1.0000	1.0000	1.0000	1.0000	1.0000
1.2	0.005	ARL	3.24065	1.8907	1.18582	1.07701	3.5952	2.00259	1.2044	1.08433
			0.831517	0.686365	0.395856	0.267397	0.849618	0.707563	0.411963	0.278881
		CVLI	0.952655	0.917357	0.864496	0.849604	0.957428	0.866747	0.850709	0.882145
	0.001	ARL	49.5858	8.28749	1.76097	1.27929	53.1879	9.82679	1.85344	1.30832
			0.989865	0.937729	0.657367	0.467245	0.990555	0.947754	0.678574	0.485452
		CVLI	0.996974	0.981759	0.910972	0.875107	0.99718	0.984638	0.915619	0.878071
	0.01	ARL	1.29998	1.15272	1.03876	1.01669	1.33142	1.16777	1.04238	1.01823
			0.480373	0.363985	0.193171	0.128129	0.49892	0.379034	0.201635	0.133809
		CVLI	0.877234	0.860289	0.843555	0.839836	0.88033	0.862234	0.844148	0.840101
1.5	0.005	ARL	5.93825	2.28857	1.17273	1.05795	7.29518	2.52055	1.19478	1.06494
			0.911921	0.750364	0.383782	0.234043	0.928937	0.776699	0.403767	0.246947
		CVLI	0.953537	0.874346	0.735111	0.700373	0.962349	0.886655	0.740858	0.702758
	0.001	ARL	370.37	15.6241	1.69725	1.20567	370.37	21.2746	1.80541	1.23232
			0.998649	0.967469	0.640946	0.413018	0.998649	0.976215	0.667914	0.434193
		CVLI	0.999272	0.9826	0.826091	0.743602	0.999272	0.987251	0.837527	0.750075
	0.01	ARL	1.48808	1.2029	1.03619	1.01265	1.55882	1.22916	1.04051	1.01414
			0.572707	0.410702	0.18689	0.111763	0.59874	0.431785	0.197313	0.118075
		CVLI	0.798616	0.74291	0.692694	0.683909	0.808842	0.749326	0.69425	0.68448
2	0.005	ARL	35.1777	3.60294	1.15306	1.03625	61.8233	4.41837	1.1795	1.04214
			0.985684	0.84997	0.364335	0.187023	0.991879	0.879586	0.390108	0.201079
		CVLI	0.989616	0.893469	0.608038	0.546498	0.994105	0.914064	0.619549	0.550113
	0.001	ARL	136079	70.496	1.60454	1.12548	6018.7	137.686	1.73	1.14686
			0.999996	0.992882	0.613816	0.333902	0.999917	0.996362	0.649588	0.357851
		CVLI	0.999997	0.994832	0.739636	0.595203	0.99994	0.997357	0.761516	0.605232
	0.01	ARL	2.21319	1.33109	1.03229	1.00798	2.51158	1.3931	1.03752	1.00925
			0.740381	0.498733	0.176855	0.088954	0.775786	0.531203	0.190176	0.095744
		CVLI	0.819526	0.673803	0.544032	0.528195	0.842992	0.691603	0.547288	0.529057

Table 4.6: ARL study of the TD-IHR case using $\alpha = 0.0027$ $\lambda_0 = 0.0005, \beta_0 = 1.5, \theta_0 = 0.001$ and $\lambda_1 \in \{0.005, 0.01, 0.1\}$, $\beta_1 \in \{1, 1.2, 2\}, \theta_1 \in \{0.0001, 0.0005\}$ for lower and two sided Independent NHPP charts.

β	θ	λ	Lower Sided				Two Sided			
			0.0005	0.005	0.01	0.1	0.0005	0.005	0.01	0.1
1.0	0.0001	ARL	43.9732	4.86628	2.71177	1.01015	33.5856	7.41582	3.97598	1.05841
			0.988564	0.89135	0.794504	0.100222	0.985	0.930136	0.865153	0.234925
		CVLI	1.0000	1.0000	1.0000	1.0000	1.0000	1.0000	1.0000	1.0000
	0.0005	ARL	49.5155	5.41837	2.9846	1.01719	26.7066	8.29466	4.41337	1.08293
			0.989851	0.903019	0.815443	0.129997	0.981099	0.937785	0.879441	0.276735
		CVLI	1.0000	1.0000	1.0000	1.0000	1.0000	1.0000	1.0000	1.0000
	0.001		57.4473	6.20921	3.3765	1.03075	19.1108	9.55288	5.04025	1.12301
		ARL	0.991258	0.915942	0.838949	0.172725	0.973485	0.946213	0.89532	0.330964
		CVLI	1.0000	1.0000	1.0000	1.0000	1.0000	1.0000	1.0000	1.0000
1.2	0.0001	ARL	92.3844	6.31182	3.05643	1.00188	100.288	10.6077	4.91497	1.02794
			0.994573	0.91737	0.820256	0.043271	0.995002	0.951698	0.892491	0.164863
		CVLI	0.998377	0.975979	0.949726	0.837237	0.998505	0.985777	0.969043	0.841753
	0.0005	ARL	104.099	7.04936	3.37446	1.00382	79.5717	11.8944	5.47331	1.0426
			0.995185	0.92636	0.838842	0.0617181	0.993696	0.957041	0.904044	0.202139
		CVLI	0.99856	0.97852	0.954577	0.837584	0.998116	0.987326	0.972246	0.844184
	0.001	ARL	120.865	8.10543	3.83085	1.00834	53.1879	13.7362	6.2731	1.06813
			0.995855	0.936283	0.859629	0.09097	0.990555	0.962912	0.916837	0.252562
		CVLI	0.99876	0.981345	0.960101	0.838382	0.99718	0.989035	0.975829	0.848243
1.5	0.0001	ARL	282.852	9.43806	3.68314	1.00004	514.881	18.3742	6.83102	1.00675
			0.998231	0.94554	0.853518	0.006679	0.999028	0.972407	0.92391	0.081867
		CVLI	0.999047	0.971026	0.923936	0.678986	0.999476	0.985223	0.959737	0.681624
	0.0005		318.85	10.5754	4.08265	1.00014	492.206	20.652	7.63504	1.01194
		ARL	0.998431	0.951547	0.868942	0.0117686	0.998984	0.975489	0.932215	0.108646
		CVLI	0.999154	0.974183	0.931653	0.679024	0.999452	0.986864	0.964056	0.683638
	0.001		370.37	12.2034	4.65541	1.00048	370.37	23.912	8.78621	1.0224
		ARL	0.998649	0.958152	0.886113	0.021850	0.998649	0.978867	0.941374	0.14801
		CVLI	0.999272	0.977667	0.94033	0.679158	0.999272	0.988665	0.968841	0.687609
2	0.0001	ARL	1834.4	18.8436	5.10292	1.0	4625.48	46.755	12.0705	1.00018
			0.999727	0.973104	0.896679	0.000018	0.999892	0.989248	0.957681	0.013246
		CVLI	0.999802	0.980526	0.926056	0.522723	0.999921	0.992198	0.969428	0.522845
	0.0005	ARL	2068.22	21.1812	5.68541	1	5212.22	52.6519	13.544	1.00047
			0.999758	0.976109	0.907806	0.000063	0.999904	0.990458	0.962375	0.0215999
		CVLI	0.999824	0.982695	0.933901	0.522723	0.99993	0.993074	0.9728	0.523047
	0.001	ARL	2402.85	24.527	6.51974	1.0	6018.7	61.0914	15.653	1.00136
			0.999792	0.979402	0.920119	0.000242	0.999917	0.991782	0.96753	0.036851
		CVLI	0.999849	0.985073	0.942618	0.522723	0.99994	0.994034	0.976509	0.523666

Table 4.7: ARL study of the TI-DHR case using $\alpha = 0.0027$ $\lambda_0 = 0.0005, \beta_0 = 1.5, \theta_0 = 0.001$ and $\lambda_1 \in \{0.0003, 0.0001, 0.00005\}$, $\beta_1 \in \{0.2, 0.45, 0.55, 0.7\}$, $\theta_1 \in \{0.005, 0.01\}$ for upper and two sided Independent NHPP charts.

β	θ	λ	Upper Sided				Two Sided			
			0.0005	0.0003	0.0001	0.00005	0.0005	0.0003	0.0001	0.00005
0.2	0.001	ARL	5.47706	4.64323	3.42992	2.9241	4.41028	3.95036	3.14587	2.75816
			0.904113	0.885795	0.841694	0.811181	0.87935	0.86421	0.825908	0.798398
		CVLI	6.82971	7.40553	8.59581	9.30034	7.59511	8.01781	8.97046	9.57289
	0.005	ARL	1.66896	1.58797	1.44952	1.38151	1.65791	1.58051	1.44663	1.38016
			0.633107	0.608494	0.556882	0.525504	0.629946	0.606048	0.55564	0.524831
		CVLI	12.2798	12.587	13.1708	13.4893	12.3204	12.6165	13.1839	13.4959
	0.01	ARL	1.12107	1.1087	1.08636	1.07477	1.12186	1.10945	1.08702	1.07537
			0.328631	0.313118	0.281949	0.263765	0.329576	0.314088	0.282938	0.264747
		CVLI	14.9666	15.0496	15.2028	15.2842	14.9614	15.0445	15.1982	15.28
0.45	0.001	ARL	122.125	45.525	10.2672	5.50081	133.657	59.7646	12.9001	6.53913
			0.995897	0.988956	0.950054	0.904549	0.996252	0.991599	0.960459	0.920366
		CVLI	1.02344	1.06172	1.25069	1.43287	1.02144	1.04734	1.20377	1.37328
	0.005	ARL	4.25142	3.15831	2.01671	1.67114	4.92965	3.5555	2.16893	1.76277
			0.874519	0.826665	0.71003	0.633723	0.89283	0.847789	0.734128	0.657807
		CVLI	1.53708	1.68352	1.96788	2.11342	1.47484	1.62152	1.91597	2.07035
	0.01	ARL	1.38116	1.29254	1.16943	1.1214	1.42839	1.32756	1.18867	1.13488
			0.525331	0.47574	0.380637	0.329026	0.547643	0.496727	0.398403	0.344746
		CVLI	2.27911	2.34135	2.44003	2.48313	2.24848	2.31597	2.42354	2.47074
0.5	0.001	ARL	370.37	97.6466	14.0841	6.49044	370.37	142.202	18.9822	8.05326
			0.998649	0.994866	0.963845	0.919743	0.998649	0.996478	0.973303	0.935856
		CVLI	1.00539	1.02028	1.13314	1.27133	1.00539	1.01397	1.10033	1.22339
	0.005	ARL	5.93825	3.97441	2.21815	1.75652	7.29518	4.66515	2.43414	1.87594
			0.911921	0.865096	0.741062	0.656271	0.928937	0.886366	0.767579	0.683326
		CVLI	1.29368	1.41649	1.67431	1.81031	1.24431	1.36287	1.62582	1.76982
	0.01	ARL	1.48808	1.36055	1.19454	1.13394	1.55882	1.4104	1.21963	1.15073
			0.572707	0.514787	0.403557	0.343682	0.59874	0.539429	0.424355	0.361918
		CVLI	1.92042	1.98494	2.08532	2.1278	1.8884	1.95859	2.06874	2.11567
0.55	0.001	ARL	1451.17	243.948	20.1668	7.78204	1013.3	391.732	29.5092	10.1327
			0.999655	0.997948	0.974892	0.933541	0.999506	0.998723	0.98291	0.949373
		CVLI	1.00099	1.00585	1.06859	1.16948	1.00141	1.00365	1.04736	1.13242
	0.005	ARL	8.95966	5.23649	2.47143	1.85521	11.875	6.48334	2.77834	2.00971
			0.942544	0.899462	0.771607	0.678952	0.956969	0.919651	0.800045	0.708814
		CVLI	1.14863	1.24355	1.46893	1.59446	1.11398	1.20055	1.42473	1.55683
	0.01	ARL	1.63112	1.4469	1.22371	1.14785	1.73778	1.5178	1.25613	1.16854
			0.622031	0.55576	0.427567	0.358899	0.651579	0.584083	0.451558	0.379777
		CVLI	1.65957	1.72555	1.82708	1.86888	1.62681	1.69857	1.81048	1.85704
0.7	0.001	ARL	787730	13296.5	81.5081	15.0135	9215.3	10978.9	169.576	23.6435
			0.999999	0.999962	0.993847	0.966123	0.999946	0.999954	0.997047	0.978624
		CVLI	1.0000	1.00004	1.00696	1.03723	1.00006	1.00005	1.00335	1.0238

0.005	ARL	59.6973	17.4601	3.76394	2.26126	118.124	28.1982	4.70145	2.59306
		0.991589	0.970941	0.856925	0.746838	0.995758	0.982108	0.887299	0.783809
	CVLI	1.00949	1.03209	1.14128	1.2262	1.00481	1.01999	1.11454	1.19964
0.01	ARL	2.4904	1.89294	1.34414	1.19968	2.90246	2.10691	1.41253	1.2369
		0.773601	0.686821	0.505992	0.407977	0.809608	0.724825	0.540418	0.437639
	CVLI	1.20716	1.26552	1.3591	1.39612	1.17996	1.24115	1.34392	1.38586

Table 4.8: ARL study of the PD-DHR case using $\alpha = 0.0027$ $\lambda_0 = 0.0005, \beta_0 = 1.5, \theta_0 = 0.001$ and $\lambda_1 \in \{0.005, 0.01, 0.1\}$, $\beta_1 \in \{0.2, 0.45, 0.55, 0.7\}, \theta_1 \in \{0.0001, 0.0005\}$ for lower and two sided Independent NHPP charts.

β	θ	λ	Lower Sided				Two Sided			
			0.0005	0.005	0.01	0.1	0.0005	0.005	0.01	0.1
0.2	0.0001	ARL	10.239	6.65307	5.86033	3.89698	5.8026	7.08964	6.82208	4.94005
			0.949913	0.921788	0.910693	0.862201	0.90976	0.926795	0.923806	0.893069
		CVLI	5.04147	6.21101	6.60755	8.07169	6.63959	6.02185	6.13561	7.18379
	0.0005	ARL	11.4787	7.4343	6.54001	4.32416	5.16783	7.06442	7.07082	5.45709
			0.955448	0.930316	0.920378	0.876779	0.898051	0.926523	0.926592	0.903743
		CVLI	4.77279	5.88455	6.26309	7.66908	7.02682	6.0323	6.02964	6.84193
	0.001	ARL	13.2531	8.55289	7.51333	4.93645	4.41028	6.68151	7.04857	6.11518
			0.961533	0.939724	0.931076	0.892987	0.87935	0.922135	0.926352	0.914589
		CVLI	4.45685	5.49817	5.85442	7.18635	7.59511	6.19812	6.03889	6.47162
0.45	0.0001	ARL	161.57	57.6511	42.338	15.3496	233.988	107.211	78.6173	28.2197
			0.996901	0.991289	0.98812	0.966877	0.997861	0.995325	0.99362	0.982122
		CVLI	1.01777	1.04904	1.06622	1.17363	1.0123	1.02666	1.03619	1.09785
	0.0005	ARL	182.106	64.9374	47.6717	17.2415	198.424	120.815	88.5768	31.7532
			0.997251	0.99227	0.989456	0.970567	0.997477	0.995853	0.994339	0.984128
		CVLI	1.01578	1.04365	1.05902	1.15585	1.01449	1.02369	1.03218	1.0874
	0.001	ARL	211.496	75.3651	55.3052	19.9494	133.657	140.281	102.83	36.8102
			0.997633	0.993343	0.990918	0.974614	0.996252	0.996429	0.995126	0.986323
		CVLI	1.0136	1.03772	1.05107	1.13595	1.02144	1.02044	1.02778	1.07581
0.5	0.0001	ARL	282.852	89.7882	63.637	20.4694	514.881	179.196	126.857	40.4596
			0.998231	0.994416	0.992112	0.975267	0.999028	0.997206	0.996051	0.987565
		CVLI	1.00705	1.02203	1.03095	1.09335	1.00388	1.0111	1.01564	1.04827
	0.0005	ARL	318.85	101.172	71.6864	23.0145	492.206	201.979	142.967	45.5538
			0.998431	0.995046	0.993001	0.978033	0.998984	0.997521	0.996497	0.988963
		CVLI	1.00625	1.01958	1.02752	1.08342	1.00406	1.00985	1.01389	1.04298
	0.001	ARL	370.37	117.464	83.2065	26.657	370.37	234.585	166.023	52.8445
			0.998649	0.995734	0.993973	0.981064	0.998649	0.997866	0.996984	0.990493
		CVLI	1.00539	1.01688	1.02375	1.07241	1.00539	1.00849	1.01197	1.03716
0.55	0.0001	ARL	495.455	139.998	95.7804	27.3565	1039.12	299.742	204.888	58.1058
			0.99899	0.996422	0.994766	0.981553	0.999519	0.998331	0.997557	0.991358
		CVLI	1.00288	1.01017	1.01483	1.051	1.00138	1.00476	1.00696	1.02433
	0.0005	ARL	558.561	157.783	107.928	30.7799	1103.94	337.894	230.947	65.45
			0.999104	0.996826	0.995357	0.983621	0.999547	0.998519	0.997833	0.992331

		CVLI	1.00256	1.00903	1.01317	1.04545	1.0013	1.00423	1.00618	1.02162
		ARL	648.874	183.237	125.313	35.6794	1013.3	392.496	268.241	75.9608
	0.001		0.999229	0.997268	0.996002	0.985887	0.999506	0.998725	0.998134	0.993396
		CVLI	1.0022	1.00778	1.01135	1.03932	1.00141	1.00364	1.00532	1.01866
		ARL	2666.71	532.479	327.971	65.8404	7043.28	1405.73	865.52	173.095
	0.0001		0.999812	0.999061	0.998474	0.992377	0.999929	0.999644	0.999422	0.997107
		CVLI	1.00021	1.00107	1.00173	1.00861	1.00008	1.0004	1.00066	1.00328
		ARL	3006.64	600.304	369.723	74.1708	7940.64	1584.89	975.808	195.1
0.7	0.0005		0.999834	0.999167	0.998647	0.993236	0.999937	0.999684	0.999487	0.997434
		CVLI	1.00019	1.00095	1.00154	1.00765	1.00007	1.00036	1.00058	1.00291
		ARL	3493.14	697.373	429.476	86.0929	9215.3	1841.3	1133.65	226.593
	0.001		0.999857	0.999283	0.998835	0.994175	0.999946	0.999728	0.999559	0.997791
		CVLI	1.00016	1.00082	1.00132	1.00659	1.00006	1.00031	1.0005	1.00251

4.6 Real life examples

In this section, we are intended to discuss some illustrative real-life examples for the implementation of the proposed control charts. Note that we use $\alpha = 0.0027$ to develop these control charts.

4.6.1 Boxing player's Performance Monitoring-Cumulative Process

Let's suppose that we want to study the performance of a boxing player (cf. Eample 1 given in Section-4.1) in a training session. In such games, the mind of a player plays an important role. It could be difficult to win a match when player's mental condition is disturbed. Therefore, suppose that we hire the services of two psychologists, and want to decide whose (psychologists) couching could be effective to improve the player performance. In a boxing fight, a knockout may be caused either by a series of small to moderate punches or just by a really big punch. Thus, we are interested to know/ differentiate whether the player has been lost the game genuinely or due to some psychological issues, i.e., couching is not effective. For this purpose, we have collected a data set of 40 observations, which is about the game lost by a player after 300 seconds, i.e., critical threshold is equal to 300 second. The first 20 observations have been collected before introducing the intervention of a therapist. Note that we shall examine the effectiveness of a therapy by two different therapists to decide which one was good for the player couching. The first 20 in-control observations as given in Table-4.9 were generated using $\lambda = 0.0005, \theta = 0.001$, and the next 10 (i.e., collected after the therapy of the first psychologist) from $\lambda = 0.0001, \theta = 0.001$. Similarly, the last 10 (i.e., collected after the therapy of second psychologist) from $\lambda = 0.01, \theta = 0.001$. The bold values in Table-4.9 denote the occurrence of a shift while the values with a $\star$ represent the detection of the shift by the control chart. Using the first 20 observations, the control limits are $LCL = \ln(3.64695) = 1.293891$ and $UCL = \ln(16321.1) = 9.700214$. In Figure-4.3a, the natural logarithm of the data and of the control limits is taken for a better presentation of the chart. It is clear from Figure-4.3a that our proposed chart detects the player's performance, i.e., improvement and deterioration, in terms of the treatment, very efficiently. Moreover, this conclusion is in accordance with the simulation study (cf. Section-4.4). It is observed from Figure-4.3a that the therapy of the first psychologist is effective as compared to the second therapist. The cumulative probability control chart also leads to the same conclusion (cf. Figure-4.3b).

Table 4.9: Simulated failure time data of the Cumulative Process

Failure #	Inter-failure time (X)	ln(X)	Cumulative Probability	Failure #	Inter-failure time (X)	ln(X)	Cumulative Probability
1	924.377	6.8291	0.4742	21	18283.98	**9.8138***	0.2641
2	2601.66	7.8639	0.4444	22	4082.99	8.3146	0.9779
3	2895.77	7.9710	0.9785	23	695.201	6.5442	0.9971
4	268.329	5.5922	0.5521	24	819.318	6.7085	0.9996*
5	1672.99	7.4224	0.3936	25	7070.88	8.8637	0.2991
6	2024.72	7.6132	0.7941	26	2716.55	7.9071	0.1408
7	1002.97	6.9107	0.3192	27	6546.95	8.7868	0.7931
8	999.332	6.9071	0.2779	28	1478.42	7.2987	0.9565
9	650.125	6.4772	0.1244	29	2421.04	7.7919	0.9999
10	526.436	6.2661	0.5235	30	10508.8	9.2599	0.9999
11	4926.25	8.5023	0.3253	31	29.3991	**3.3809**	0.0029
12	1372.49	7.2244	0.5779	32	118.681	4.7764	0.0049
13	892.819	6.7945	0.7437	33	54.1987	3.9927	0.0232
14	854.872	6.7509	0.2375	34	22.09	3.0951	0.0075
15	496.659	6.2079	0.1135	35	1.3452	0.2965*	0.0359
16	10943.1	9.3005	0.9481	36	101.146	4.6166	0.0195
17	1759.06	7.4725	0.9903	37	39.7277	3.6821	0.0006
18	2409.34	7.7871	0.9944	38	34.1069	3.5295	0.0226
19	1972.39	7.5870	0.3097	39	26.2636	3.2682	0.0024
20	29.2355	3.3754	0.8301	40	220.035	5.3938	0.0115

4.6.2 Water Quality Monitoring-Independent Process

There are the environmental protocols which must be followed and ensured by each factory before releasing wastage. A factory may leak poisonous waste products into a river; however, after some time the vegetation and the fish in the river are dead due to a cumulative or an accidental effect of poison pouring. To differentiate between an accidental and intentional wastage/checmical/poison poring into river, which caused to die the under-water habitant, we propose an independent process to monitor water quality. Conductivity of the water can be used to check water quality.

Conductivity is a measure of the capability of a solution such as water in a stream to pass an electric current. This is an indicator of the concentration of dissolved electrolyte ions in the water. It doesn't identify the specific ions in the water. However, significant increases in conductivity may be an indicator that polluting discharges have entered the water. Every creek will have a baseline conductivity depending on the local geology and soils. Higher conductivity will result from the presence of various ions, including nitrate, phosphate, and sodium. The basic unit of measurement for conductivity is micromhos per centimeter (mhos/cm) or microsiemens per centimeter (S/cm). Either can be used; they are the same. It is a measure of the inverse of the amount of resistance an electric charge meets in traveling through the water. Distilled water has a conductivity ranging from 0.5 to 3 S/cm, while most streams range between 50 to 1500 S/cm. Freshwater streams ideally should have a conductivity between 150 to 500 S/cm to support diverse aquatic life.

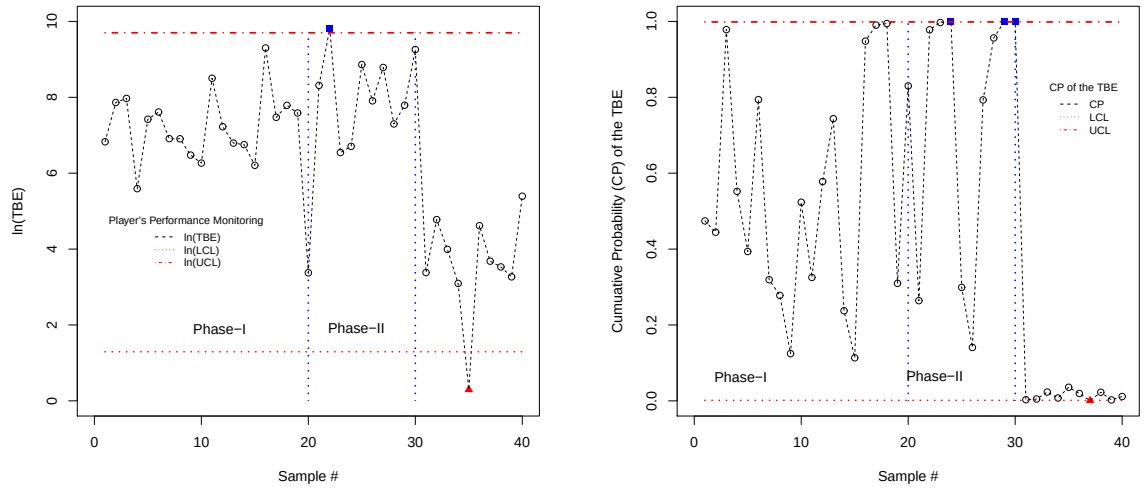

(a) Cumulative Quantity Control Chart (b) Cumulative Probability Control Chart

Figure 4.3: Control Chart for the Cumulative Process Monitoring

Let suppose that conductivity should be at-least 300 S/cm for a particular river/stream which is near to a factory. The 40 observations have been generated in Table-4.10 to check the stream water quality where data are about the hours between crossing the threshold of the conductivity. First 20 in-control observations (cf. Table-4.10) are generated using $K = 300, \lambda = 0.0005, \theta = 0.001$, the next 10 (i.e., process deterioration) from $\lambda = 0.1, \theta = 0.0001$ and the last 10 (i.e., process improvement) from $\lambda = 0.0001, \theta = 0.001$. The bold values in Table-4.10 denote the occurrence of a shift while values with a $\star$ represent the detection of the shift by the proposed control chart. Using the first 20 observations, the control limits are $LCL = \ln(3.64708) = 1.293927$ and $UCL = \ln(17838.8) = 9.789131$. Note that here the process improvement means the water quality is improving, i.e., conductivity level is decreasing, while the process deterioration means that conductivity level is increasing, i.e., water quality is becoming poor. In Figure-4.4a, the natural logarithm of the data and of the control limits is taken for a better presentation of the chart. From Figure-4.4a, clearly, the process is in-control for the first 20 observations. A shift of the process deterioration was occurred at the sample number 21, and it was immediately detected by the chart. Similarly, another shift was occurred at the sample number 31 which was detected at the sample number 36. A cumulative probability control chart has also been constructed (cf. Figure-4.4b), and it leads to a similar conclusion as we have in Figure-4.4a.

Table 4.10: Simulated failure time data of the Independent Process

Failure #	Inter-failure time (X)	ln(X)	CP	Failure #	Inter-failure time (X)	ln(X)	CP
1	28.1469	3.3374	0.0104	21	1.6689	**0.5122***	**0.0006***
2	5375.9799	8.5897	0.8635	22	38.7736	3.6577	0.0143
3	4899.0753	8.4968	0.8371	23	30.4048	3.4146	0.0112
4	326.0282	5.7869	0.1138	24	6.0719	1.8037	0.0023
5	3792.8213	8.2409	0.7546	25	7.2365	1.9791	0.0027
6	468.8966	6.1504	0.1594	26	1.6809	0.5193*	0.0006*
7	7043.6737	8.8599	0.9264	27	9.3069	2.2308	0.0034
8	8111.0884	9.0009	0.9504	28	14.0128	2.6399	0.0052
9	1824.1795	7.5089	0.4912	29	8.7200	2.1656	0.0032
10	524.2249	6.2619	0.1765	30	4.8538	1.5798	0.0018
11	5259.7901	8.5679	0.8575	31	2710.1264	**7.9048**	**0.6335**
12	1500.3225	7.3134	0.4264	32	4673.8559	8.4497	0.8229
13	2280.1749	7.7320	0.5703	33	834.6655	6.7270	0.2659
14	1772.6952	7.4803	0.4814	34	91.5559	4.5169	0.0334
15	2828.1483	7.9474	0.6492	35	13853.8589	9.5363	0.9941
16	2570.5627	7.8519	0.6141	36	33313.4361	10.4137*	0.9999*
17	498.3389	6.2113	0.1686	37	1697.9908	7.4372	0.4669
18	3595.0558	8.1873	0.7359	38	418.0323	6.0356	0.1435
19	2743.4973	7.9169	0.6380	39	33.6614	3.5164	0.0124
20	1489.9068	7.3065	0.4241	40	2546.4320	7.8425	0.6106

4.6.3 Wire rope strength Monitoring-Cumulative Process with NHPP

Wire ropes of a properly designed and maintained crane will deteriorate throughout their entire service life by two principal deterioration mechanisms, which are: external and internal fatigue, caused by bending over sheaves or winding on drums, and crushing caused by spooling on multilayered drums (cf. Weischedel [2003]). An experiment is designed to see the compatibility of wire rope with two different sheaves/winding on drums. Suppose that a wire rope of diameter 1 in., (or 26 mm) have 300 kN (Kilonewton) breaking strength. A data set of the damage of a wire rope is collected and given in Table-4.11. Note that there are two methods for the inspection of wire ropes, i.e., visual and electromagnetic inspection, and electromagnetic inspection was used in our experiment. The first 20 in-control observations are generated using $K = 300, \beta = 1.5, \lambda = 0.0005, \theta = 0.001$, the next 10 (i.e., a new model of the sheave was introduced for testing the wire compatibility) from $\lambda = 0.0001, \theta = 0.005, \beta = 1.2$ and the last 10 (i.e. a second model of the sheave was introduced for testing wire compatibility) from $\lambda = 0.01, \theta = 0.0005, \beta = 1.6$. The bold values given in Table-4.11 denote the occurrence of the shift, i.e., a new model of the sheave was introduced, while values with $\star$ represent the detection of the shift, i.e., compatibility of the sheave with wire rope, by the control chart. Using the first 20 observations we have the control limits $LCL = \ln(2.781067) = 1.022835$ and $UCL = \ln(7810.433) = 8.963216$. From Table-4.11 or Figure-4.5, clearly, the first model of the sheave is more compatible with the wire rope than the second one.

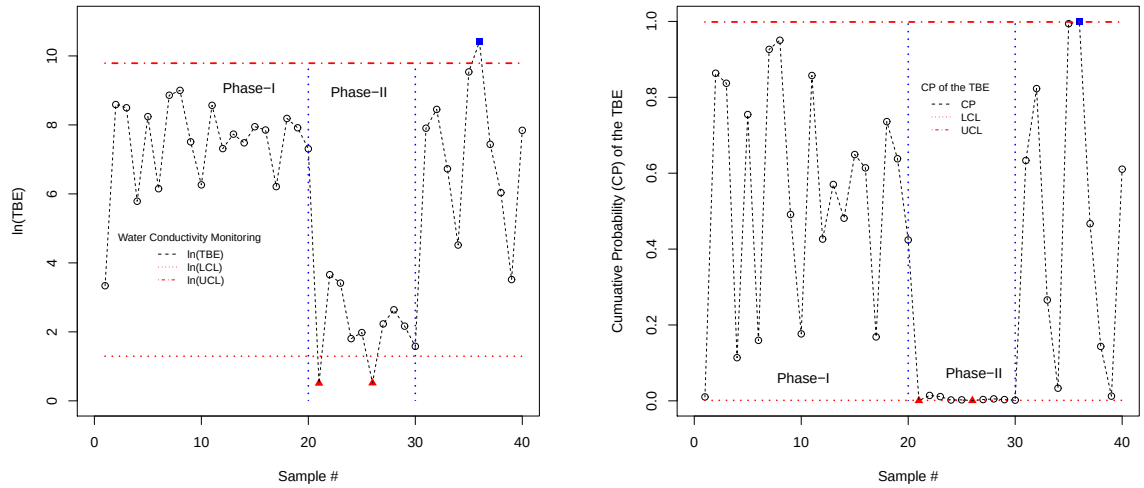

(a) Cumulative Quantity Control Chart (b) Cumulative Probability Control Chart

Figure 4.4: Control Chart for the Independent Process

4.6.4 Blood/Urine Monitoring-Independent Process with NHPP

We have quoted the example of banned performance-enhancing drugs in Section-4.1 (cf. Example 4). Sport regulatory authorities are very conscious of conducting a banned performance -enhancing drug test, which ends up them in a court for intentionally defaming the player. Modern sport industry is facing a hard challenge to differentiate/ decide whether the presence of a particular element is natural or un-natural. Therefore, to assist the decision committee, we are proposing the use of the control chart based on the NHPP. Most of the international sports organizations support the view that sample should be taken at random or surprised interval of the time to check the ratio of blood/urine elements. If the player has used banned medicine, then we should expect that the ratio of particular elements in blood or urine would be greater than a normal threshold and consequently, it shortened TBE and vice versa. Moreover, the presence of the particular element might increase or decrease over time; therefore, the use of NHPP for the time is justified.

Suppose that the time follows the NHPP and the magnitude exponential distribution. The first 20 in-control observations are generated using $K = 300, \beta = 1.5, \lambda = 0.0005, \theta = 0.001$, the next 10 (i.e., the player has not used any un-natural medication to enhance performance and crossing a threshold might be due to couching effect or something else) from $\lambda = 0.0001, \theta = 0.0001, \beta = 1.5$ and the last 10 (i.e., the player has used something related to banned elements) from $\lambda = 0.01, \theta = 0.001, \beta = 1.2$. The bold values in

Table 4.11: Simulated failure time data of the Cumulative NHPP Process

Failure #	Inter-failure time (X)	$\ln(X)$	Failure #	Inter-failure time (X)	$\ln(X)$
1	2768.6589	7.9261	21	30661.352	**10.3308***
2	509.6796	6.2338	22	4800.129	8.4764
3	65.0466	4.1751	23	39422.263	10.5821*
4	1996.4771	7.5991	24	2814.991	7.9427
5	2460.8649	7.8083	25	45614.794	10.7279*
6	362.6931	5.8936	26	3294.383	8.0999
7	4691.9587	8.4536	27	29880.27	10.3049*
8	1618.9652	7.3895	28	18598.064	9.8308*
9	1047.5022	6.9542	29	13269.856	9.4933*
10	251.1014	5.5259	30	3807.075	8.2446
11	1594.2674	7.3742	31	24.4297	**3.1958**
12	1609.6292	7.3838	32	1.9718	0.6789*
13	326.3924	5.7881	33	33.5553	3.5132
14	1921.9849	7.5611	34	1.1259	0.1186*
15	1100.0725	7.0031	35	186.1773	5.2267
16	1392.7834	7.2391	36	29.3798	3.3803
17	274.8661	5.6163	37	28.1168	3.3364
18	438.0057	6.0822	38	81.9651	4.4063
19	1390.1253	7.2372	39	69.5601	4.2422
20	4681.3031	8.4513	40	108.9579	4.6909

Table-4.12 denote the occurrence of a shift while values with $\star$ represent the detection of a shift by the control chart. Using the first 20 observations, the control limits are $LCL = \ln(29.852) = 3.396252$ and $UCL = \ln(8601.75) = 9.059721$. In Figure-4.6a, the natural logarithm of the data and of the control limits is taken for a better presentation of the chart. From Figure-4.6a it is clear that for the first 20 observations, the process is under control. A process improvement shift occurs at the sample number 21, and it is detected by the chart at the sample number 24. Another process deterioration shift occurs at the sample number 31 which is detected efficiently at the sample point 37. Note that the process improvement means that the player's blood/urine is normal or the specific element of the prohibited drug has been decreased. Similarly, the process deterioration indicates that the particular element of the banned drug is found in the blood/urine above the allowed or normal level, i.e., its usage has been increased. Note that in the process improvement case, the chances of the TBE to cross a threshold will be increased and vice versa for the process deterioration. A cumulative probability control chart has also been constructed (cf. Figure-4.6b), and it leads to a similar conclusion as we have in Figure-4.6a.

4.7 Conclusion

In the existing literature to jointly monitor the time and the magnitude, the marked Poisson process is commonly used. However, control charts based on the marked Poisson

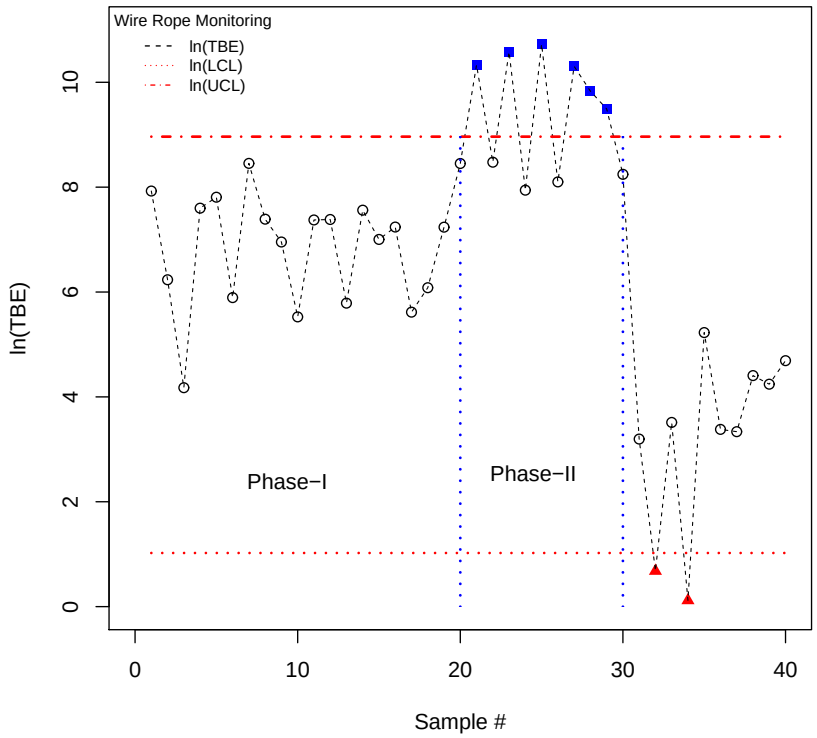

Figure 4.5: Control Chart for the NHPP Cumulative Process

process are not suitable for the situations where we have proportional changes either in the time or magnitude and if the damage is not directly observable. Moreover, due to a restrictive assumption of the Poisson process, i.e., constant failure rate, the existing charts are unsuitable for complex process monitoring, especially in reliability engineering. In this chapter, we proposed four different control charts based on the renewal reward process. Algorithms to compute the control limits and the ARL have also been proposed in this study, and therefore, one could consider any lifetime distribution for the time and the magnitude to develop/construct a control chart. Our work is not only a generalization of the existing work, but also open a new era in the development and monitoring of time and magnitude charts, especially in the reliability. Furthermore, the proposed methodology is different from the existing work in the sense that we do not consider a ratio of the time and magnitude. Instead, we develop the first passage distribution using the renewal reward processes to design a control chart.

The performance of the new chart has been examined in detail, i.e., from the rational and design assessment point of view. The effectiveness of the proposed charts lies in their sensitivity to detect simultaneous shifts, i.e., time and magnitude. The ARL, CVs of the run-length and the length of inspection distributions have been studied in detail to assess

Table 4.12: Simulated failure time data of the NHPP Independent Process

Failure #	Inter-failure time (X)	$\ln(X)$	Cumulative Probability	Failure #	Inter-failure time (X)	$\ln(X)$	Cumulative Probability
1	1819.5871	7.5064	0.4742	21	1110.7636	**7.0128**	**0.2641**
2	1714.0535	7.4466	0.4444	22	5959.7661	8.6928	0.9779
3	5988.3976	8.6976	0.9785	23	7935.5397	8.9791	0.9971
4	2110.8378	7.6548	0.5521	24	9721.0584	9.1821*	0.9996*
5	1539.3253	7.3391	0.3936	25	1225.4800	7.1111	0.2991
6	3313.9600	8.1059	0.7941	26	694.9024	6.5438	0.1408
7	1291.5744	7.1636	0.3192	27	3307.8218	8.1041	0.7931
8	1156.4074	7.0531	0.2779	28	5233.0565	8.5628	0.9565
9	636.0273	6.4552	0.1244	29	13679.2098	9.5236*	0.9999*
10	2000.7505	7.6013	0.5235	30	12267.1852	9.4147*	0.9999*
11	1311.5818	7.1789	0.3253	31	50.5818	**3.9236**	**0.0029**
12	2213.6531	7.7024	0.5779	32	70.0774	4.2496	0.0049
13	3000.3620	8.0065	0.7437	33	200.2886	5.2998	0.0232
14	1023.2941	6.9308	0.2375	34	94.1414	4.5448	0.0075
15	595.7251	6.3898	0.1135	35	268.8099	5.5940	0.0358
16	5033.9409	8.5239	0.9481	36	177.9667	5.1816	0.0195
17	6786.7041	8.8227	0.9903	37	17.6168	2.8689*	0.0006*
18	7311.4314	8.8972	0.9944	38	196.9976	5.2832	0.0226
19	1260.5173	7.1393	0.3098	39	43.4578	3.7718	0.0024
20	3577.9860	8.1826	0.8301	40	124.6388	4.8254	0.0114

the performance of the control charts. Moreover, some practical aspects to highlight the abilities of different proposed charts in various situations have also been discussed in this chapter. From our simulation study as well as from illustrative applications, it is evident that our proposals work efficiently.

In this chapter, we assumed the exponential distribution for the magnitude. However, in the real applications, this may not be well fitted to a situation under study, and some other suitable distributions could be considered for the construction of control charts. For this purpose, one can use our mathematical formulation and algorithms designed for the numerical computations. In the future, development of the time and magnitude charts using the nonparametric approach would be an interesting study. A comprehensive study is required to see the effect of parameter estimation on the time and magnitude control chart' performance. More advanced control charts like CUSUM and EWMA, can also be developed within the renewal reward framework to monitor the time and the magnitude. Furthermore, we assumed that X and M are independent; however, these might be dependent in some application. Therefore, the current work could also be extended to such situations.

In the next chapter, we extend the current work to a random threshold (cf. Chapter-5) scenario.

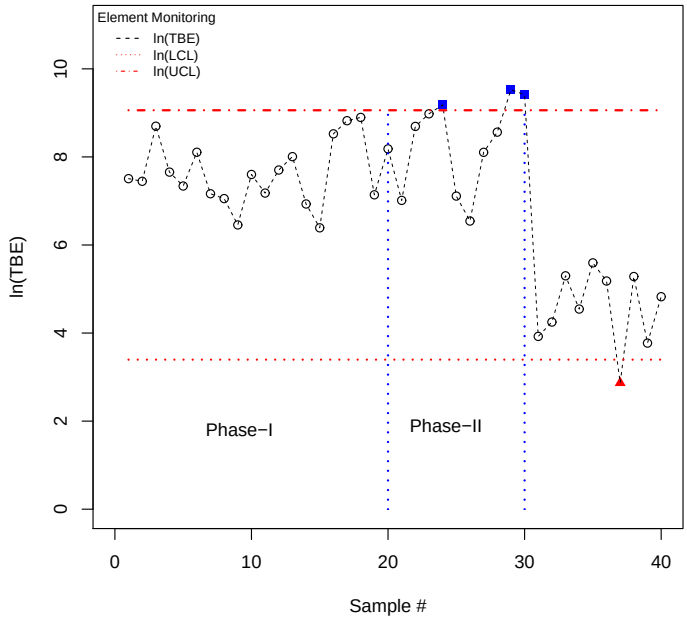

(a) Cumulative Quantity Control Chart

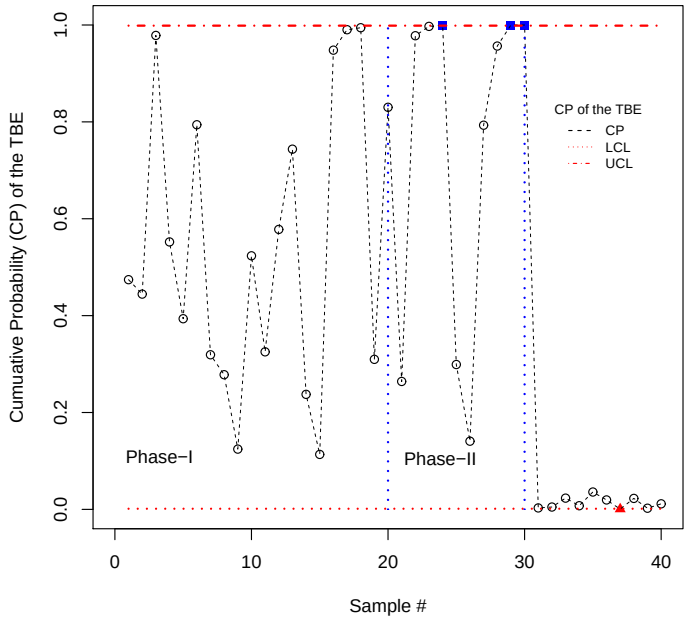

(b) Cumulative Probability Control Chart

Figure 4.6: Control Chart for the NHPP Independent Process

Appendix

Appendix A: Some Details

Since $E[N(t)] = \sum_{n=1}^{\infty} Pr[N(t) \geq n]$ (cf. Section-4.2) but the event $N(t) \geq n$ is same as $S_n \leq t$. Therefore, $E[N(t)]$ could be expressed in terms of the distribution function of $S_n, n \geq 1$ as $E[N(t)] = \sum_{n=1}^{\infty} Pr[S_n \leq t]$. Although this expression looks fairly simple, it becomes increasingly complex with the increasing t. As t increases, there is an increasing set of values of n for which $Pr(S_n \leq t)$ is significant, and $Pr(S_n \leq t)$ itself is not easy to calculate if the inter-arrival distribution $F_X(x)$ is complex/complicated.

We know that $S_n = S_{n-1} + X_n$ for each $n \geq 1$ (with $S_0 = 0$), and since X_n and S_{n-1} are independent by definition, we can use convolution to get $Pr(S_n \leq t) = \int_{x=0}^{t} Pr(S_{n-1} \leq t - x) dF_X(x)$ for $n \geq 2$. Therefore,

$$E[N(t)] = F_X(t) + \int_{x=0}^{t} \sum_{n=2}^{\infty} Pr(S_{n-1} \leq t - x) dF_X(x) \tag{A.1}$$

$$= F_X(t) + \int_{x=0}^{t} \sum_{n=1}^{\infty} Pr(S_n \leq t - x) dF_X(x) = F_X(t) + \int_{x=0}^{t} E[N(t-x)] dF_X(x)$$

for $t > 0$.

If we assume that X has density $f_X(x)$, and this density has a Laplace transform $L_x(s) = \int_0^{\infty} f_X(x) \exp(-sx) dx$, then the Laplace transform of $E[N(t)]$ is $L_m(s) = \frac{L_X(s)}{s} + L_m(s) L_X(s)$. Therefore, we have $L_m(s) = \frac{L_X(s)}{s[1 - L_X(s)]}$.

Note that $\sum_{n=0}^{\infty} G^n = \frac{1}{1-G}$, $\sum_{n=0}^{\infty} G^n F^{n+1} = \frac{F}{1-FG}$ and $\sum_{n=0}^{\infty} G^{n+1} F^{n+1} = \frac{FG}{1-FG}$.

Appendix B: An Alternative Representation of First Passage Distribution of the Cumulative Process

Note that $\exp(-\lambda t s/(s+\theta))$ (cf. Section-4.3) can be written as $\exp(-\lambda t s/(s+\theta)) = \sum_{n=0}^{\infty} \frac{(-1)^n (\lambda t)^n s^n}{n!(s+\theta)^n}$ and it's inverse LS is: $\sum_{n=0}^{\infty} \frac{(-1)^n (\lambda t)^n}{n!} \{-n\lambda_1 {}_1F_1[1+n, 2, -t\lambda]\}$, where ${}_1F_1[a, b, z]$ denotes the Kumer Confluent Hypergeometric function.

The general form of the Kumer Confluent Hypergeometric function can be defined as ${}_1F_1[a, b, z] = \sum_{k=0}^{\infty} (a)_k / (b)_k z^k / k!$, where $(.)_k$ denotes the rising factorial, i.e., $(d)_k = d(d+1)(d+2)\cdots(d+n-1)$. Thus, using the Hypergeometric function, we have an alternative representation of the inverse of the LS transform. An integral representation of the Hypergeometric function was given by Abramowitz and Stegun [1974] (pp. 505) which is defined as: ${}_1F_1[a, b, z] = \frac{\Gamma(b)}{\Gamma(b-a)\Gamma(a)} \int_0^1 \exp(zt) t^{a-1} (1-t)^{b-a-1} dt$. Moreover, one can also define it in terms of the Laplace integral, i.e., ${}_1F_1[a, b, z] = \frac{1}{\Gamma(a)} \int_0^{\infty} \exp(-zt) t^{a-1} (1-t)^{b-a-1} dt$.

In mathematics, a confluent hypergeometric function is a solution of the confluent

hypergeometric equation, which is a degenerate form of the hypergeometric differential equation $w(z)$: $z\frac{d^2w}{dz^2} + (b-z)\frac{dw}{dz} - aw$, where two of the three regular singularities merge into an irregular singularity.

The Bessel function is a solution of the differential equation $z^2\frac{d^2w}{dz^2} + z\frac{dw}{dz} - (z^2 - v^2)w$ where v denotes the order of the Bessel function. By using the Taylor series, it can be written as $J_v(z) = \sum_{n=0}^{\infty} \frac{(-1)^n (z/2)^{2n+v}}{n!\Gamma(n+v+1)}$. It has also an integral representation which can be written as: $J_v(z) = \frac{1}{\pi}\int_0^{\pi} \exp(vt - z\sin(t))dt - \frac{\sin(v\pi)}{\pi}\int_0^{\infty} \exp(-z\sinh(t) - vt)dt$. Moreover, one can also define it with the imaginary argument, i.e., $I_v(z) = -\iota^{-v}J_v(\iota z) = \sum_{n=0}^{\infty} \frac{(z/2)^{2n+v}}{n!\Gamma(n+v+1)}$ whereas the integral form is: $I_v(z) = \frac{1}{\pi}\int_0^{\pi} \exp(z\cos(\theta))\cos(v\theta)d\theta - \frac{\sin(v\pi)}{\pi}\int_0^{\infty} \exp(-z\cosh(t) - vt)dt$, i.e., we have differential equation $z^2\frac{d^2w}{dz^2} + z\frac{dw}{dz} - (z^2 + v^2)w$.

A relation of the Kummer Confluent Hypergeometric with the Bessel function was given by Olver et al. [2010] (pp. 255) and defined as

$$J_v(z) = \frac{(z/2)^v}{\Gamma(v+1)}{}_0F_1(v+1; z^2/4) = \frac{(z/2)^v}{\Gamma(v+1)}\exp(-z){}_1F_1[v+0.5, 2v+1, 2z] \qquad \text{(B.1)}$$

where ${}_0F_1[a, z]$ is called the confluent hypergeometric function given by ${}_0F_1[a, z] = \sum_{k=0}^{\infty} \frac{z^k}{(a)_k k!}$.

Appendix C: Estimation of Parameters

In this appendix, we shall derive the probability density function and especially the partial derivatives to find maximum likelihood estimators of the parameters.

Cumulative Process (Model 1):

Assume that both the time and magnitude have the exponential distribution with the rate parameter λ and θ, respectively. Therefore, for the cumulative process, the cumulative density function of the first passage distribution is given below:

$$Pr\{Z \le t\} = 1 - \exp(-\lambda t)\big[1 + \sqrt{\lambda\theta t}\int_0^K \exp(-\theta w)w^{-0.5}I_1(2\sqrt{\lambda\theta t w})dw\big] \qquad \text{(C.1)}$$

where I_i is the Bessel function of order i for the imaginary argument defined by $I_i(x) = \sum_{k=0}^{\infty} \frac{(x/2)^{2k+1}}{k!(k+i)!}$. After differentiating with respect to t, we have the density function

$$f(t) = \frac{\sqrt{\lambda}\exp(-t\lambda)}{2\sqrt{t\theta}}\Bigg[\theta(2t\lambda - 1)\int_0^K \exp(-\theta w)w^{-0.5}I_1(2\sqrt{\lambda\theta t w})dw + 2\Bigg(\sqrt{t\theta\lambda} - \frac{\sqrt{t\lambda}\theta^{1.5}}{2}\int_0^K \exp(-\theta w)\big\{I_0(2\sqrt{\lambda\theta t w}) + I_2(2\sqrt{\lambda\theta t w})\big\}dw\Bigg)\Bigg] \qquad \text{(C.2)}$$

Independent Process (Model 2):

Suppose that both the time and magnitude have the exponential distribution with the rate parameter λ and θ, respectively. Thus, for the independent process, the cumulative density function of the first passage distribution is given as:

$$Pr\{Z \leq t\} = 1 - \exp(-\lambda t \exp(-\theta K)) \tag{C.3}$$

and density function is

$$f(t) = \lambda \exp\big(-\theta K - \lambda t \exp(-\theta K)\big) \tag{C.4}$$

Therefore, the log-likelihood function of the first passage distribution is given below:

$$l(.) = n \ln(\lambda) - n\theta K - \lambda \sum_{i=1}^{n} t_i \exp(-\theta K) \tag{C.5}$$

and

$$\frac{\partial l(.)}{\partial \lambda} = \frac{n}{\lambda} - \sum_{i=1}^{n} t_i \exp(-\theta K) = 0 \Longrightarrow \hat{\lambda} = \frac{n \exp(\theta K)}{\sum_{i=1}^{n} t_i} \tag{C.6}$$

$$\frac{\partial l(.)}{\partial \theta} = -nK + \lambda K \exp(-\theta K) \sum_{i=1}^{n} t_i = 0 \Longrightarrow \hat{\theta} = \frac{1}{K} \ln\big(\frac{\lambda \sum_{i=1}^{n} t_i}{n}\big) \tag{C.7}$$

$$\frac{\partial^2 l(.)}{\partial \lambda^2} = -\frac{n}{\lambda^2} \tag{C.8}$$

$$\frac{\partial^2 l(.)}{\partial \lambda \partial \theta} = K \sum_{i=1}^{n} t_i \exp(-\theta K) \tag{C.9}$$

$$\frac{\partial^2 l(.)}{\partial \theta^2} = -\lambda K^2 \exp(-\theta K) \sum_{i=1}^{n} t_i \tag{C.10}$$

Independent Process with NHPP intensity (Model 3):

Assume that the time follows NHPP with power law intensity and magnitude has the exponential distribution with the rate parameter θ. Then, for the independent process, the cumulative density function of the first passage distribution is given below:

$$Pr\{Z \leq t\} = 1 - \exp\Big(-\exp(-K\theta)(\lambda t)^{\beta}\Big) \tag{C.11}$$

and it has density function given by

$$f(t) = \beta \lambda^{\beta} t^{\beta - 1} \exp\big(-\theta K - \exp(-\theta K)(\lambda t)^{\beta}\big) \tag{C.12}$$

The log-likelihood can be written as

$$l(.) = n\ln(\beta) + n\beta\ln(\lambda) + (\beta-1)\sum_{i=1}^{n}\ln(t_i) - n\theta K - \lambda^{\beta}\exp(-\theta K)\sum_{i=1}^{n}t_i^{\beta} \tag{C.13}$$

and the normal equations to find the likelihood estimators are

$$\frac{\partial l(.)}{\partial\theta} = -nK + \lambda^{\beta}K\exp(-\theta K)\sum_{i=1}^{n}t_i^{\beta} = 0 \Longrightarrow \hat{\theta} = \frac{1}{K}\ln\left(\frac{\lambda^{\beta}\sum_{i=1}^{n}t_i^{\beta}}{n}\right) \tag{C.14}$$

$$\frac{\partial l(.)}{\partial\lambda} = \frac{n\beta}{\lambda} - \beta\lambda^{\beta-1}\exp(-\theta K)\sum_{i=1}^{n}t_i^{\beta} = 0 \Longrightarrow \hat{\lambda} = \left(\frac{n\exp(\theta K)}{\sum_{i=1}^{n}t_i^{\beta}}\right)^{1/\beta} \tag{C.15}$$

$$\frac{\partial l(.)}{\partial\beta} = \frac{n}{\beta} + n\ln(\lambda) + \sum_{i=1}^{n}t_i - \lambda^{\beta}\exp(-\theta K)\{\ln(\lambda)\sum_{i=1}^{n}t_i^{\beta} + \sum_{i=1}^{n}t_i^{\beta}\ln(t_i)\} \Longrightarrow$$

$$\hat{\beta} = h(\beta) = \frac{n}{\lambda^{\beta}\exp(-\theta K)\{\ln(\lambda)\sum_{i=1}^{n}t_i^{\beta} + \sum_{i=1}^{n}t_i^{\beta}\ln(t_i)\} - n\ln(\lambda) - \sum_{i=1}^{n}t_i} \tag{C.16}$$

$$\frac{\partial^2 l(.)}{\partial\theta^2} = -K^2\lambda^{\beta}\exp(-\theta K)\sum_{i=1}^{n}t_i^{\beta} \tag{C.17}$$

$$\frac{\partial^2 l(.)}{\partial\theta\partial\lambda} = K\beta\lambda^{\beta-1}\exp(-\theta K)\sum_{i=1}^{n}t_i^{\beta} \tag{C.18}$$

$$\frac{\partial^2 l(.)}{\partial\theta\partial\beta} = K\lambda^{\beta}\exp(-\theta K)\{\ln(\lambda)\sum_{i=1}^{n}t_i^{\beta} + \sum_{i=1}^{n}t_i^{\beta}\ln(t_i)\} \tag{C.19}$$

$$\frac{\partial^2 l(.)}{\partial\lambda^2} = -\frac{n\beta}{\lambda^2} - \beta(\beta-1)\lambda^{\beta-2}\exp(-\theta K)\sum_{i=1}^{n}t_i^{\beta} \tag{C.20}$$

$$\frac{\partial^2 l(.)}{\partial\lambda\partial\beta} = \frac{n}{\lambda} - \lambda^{\beta-1}\exp(-\theta K)\sum_{i=1}^{n}t_i^{\beta} - \beta\lambda^{\beta-1}\ln(\lambda)\exp(-\theta K)\sum_{i=1}^{n}t_i^{\beta} - \tag{C.21}$$

$$\beta\lambda^{\beta-1}\exp(-\theta K)\sum_{i=1}^{n}t_i^{\beta}\ln(t_i)$$

$$\frac{\partial^2 l(.)}{\partial\beta^2} = -\frac{n}{\beta^2} - \lambda^{\beta}(\ln\lambda)^2\exp(-\theta K)\sum_{i=1}^{n}t_i^{\beta} - 2\lambda^{\beta}\ln(\lambda)\exp(-\theta K)\sum_{i=1}^{n}t_i^{\beta}\ln(t_i) \tag{C.22}$$

$$-\lambda^{\beta}\exp(-\theta K)\sum_{i=1}^{n}t_i^{\beta}\{\ln(t_i)\}^2$$

Chapter 5

Monitoring the Time and Magnitude based on the Renewal Reward Process with a Random Failure Threshold

In the previous chapter, i.e., Chapter-4, we have proposed some monitoring strategies for the cumulative and the independent processes by assuming a fixed threshold. However, in many situations, this assumption of the fixed threshold is not suitable, e.g., radioactivity or disease monitoring, and one needs to replace it with a random threshold. Therefore, contrary to Chapter 4, here we shall consider the case of a random failure threshold to develop a new monitoring strategy. Some comparison studies are also given in this chapter to show the effectiveness of our proposal.

5.1 Introduction

In Chapter 4, we assumed that a fixed critical threshold/failure level for the process monitoring. However, there are many situations where the assumption of the fixed critical threshold is not valid. We quote here some motivational examples from such complex fields:

Example 1: Radioactivity An atomic power station normally emits a daily amount of the radioactivity, which after some (large) time may cause a higher rate of the cancer in the nearby population. Similarly, a fault in the nuclear plant is either cause of cumulative damages or sudden deadly shock. Since, the nuclear systems are not readily accessible for inspection due to high levels of radiation, i.e., each shock is not directly observable, the time when damage exceeds the critical point

may be recorded. A maintenance engineer keeps the record of these critical points of different plants. There could be natural and un-natural causes of a plant failure and monitoring of such events, is a real challenge. Moreover, the risk of the radioactivity can vary with time, i.e., stochastic effect of radiation, and every authority tries to minimize it as much as possible.

Example 2: Cardiac monitoring Cardiac monitoring generally refers to continuous monitoring of the heart activity, usually by an electrocardiography. Currently, a handy device is used to monitor the heart rate, which displays an assessment of patients condition relative to their cardiac rhythm. A medical doctor knows the critical threshold of the normal rhythm of a heart and may use it to see the effectiveness of a treatment on the patient's health. For example, in hypertension case, a patient heart beat gradually or suddenly starts changing from normal to an abnormal rhythm, and many peaks would cross the normal threshold. This phenomenon is significantly dependent on the patient's medical history. If a medicine/treatment is an effective, then the risk of hypertension should be decreased with the passage of time, and vice versa. Note that the heart rhythm might change due to the cumulative or independent effect of a series of events. Moreover, the critical value of a normal heart's rhythm is also dependent on different factors, e.g., age, sex, smoking, diet and exercise, etc. Therefore, to develop an efficient monitoring strategy, the random critical threshold makes more sense than a fixed threshold for different patients.

Similar examples of the random failure threshold could be found in terrorism surveillance, flood or dam's water level monitoring, etc. Therefore, in such situations, one should consider process monitoring with a random threshold instead of a fixed threshold. In this chapter, we assumed a random failure threshold for the renewal reward process and proposed control charts. Note that we will use the same notations as discussed in Chapter 4. The rest of the chapter is organized as follows: We present definitions of the cumulative and the independent processes by assuming random threshold in Section 5.2. Discussion about the compound Poisson process assuming the random threshold is also given in the same Section 5.2. The control chart construction is given in 5.3 while the assessment of the control charts by the performance measure ARL, is given in Section 5.4. The implementation of proposals in the real-life situations, is discussed in Section 5.5. Finally, we conclude the chapter in Section 5.6.

5.2 Random Failure Threshold

As we have explained in the introduction (cf. Section-5.1) that in many situations, the failure threshold K may varies with time, i.e., dependent on the operating environment.

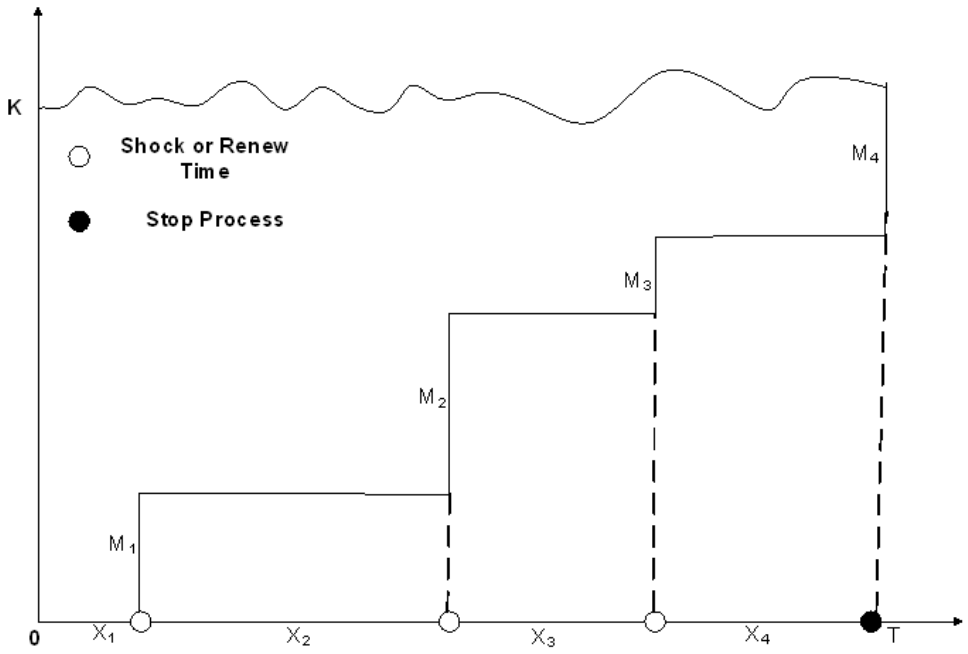

Figure 5.1: Process for a standard cumulative damage model with random failure threshold

Therefore, the idea of a constant failure threshold is not suitable in many situations and one needs to replace the constant failure threshold with a random threshold. For this purpose, let $D(k)$ be the distribution of failure threshold such that $D(0) = 0$. In this chapter, we are interested in finding the distribution of a first passage time to a random failure threshold and develop a monitoring scheme. The idea is to replace K with its distribution $D(k)$. Therefore, we shall use Equation-4.7 in the next section to get the first passage distribution.

5.2.1 Random Failure Threshold for the Cumulative Damage Model

To define the first passage distribution with a random failure threshold for the cumulative damage, we replace the constant K with its distribution in Equation-4.7, i.e., replace K with $D(k)$ (cf. Esary et al. [1973]). Thus, we have

$$Pr\{Z \leq t\} = \sum_{n=0}^{\infty} F^{(n+1)}(t) \int_0^{\infty} [G^{(n)}(k) - G^{(n+1)}(k)] dD(k) \tag{5.1}$$

the first passage distribution with a random threshold. To understand better the cumulative damage with a random failure threshold, a graphical presentation is given in Figure-5.1. The mean time to a random critical threshold can be written as: $E(Z) = \mu \int_0^{\infty} [1 + M_G(k)] dD(k)$.

5.2.2 Random Failure Threshold for the Compound Poisson Process

Consider a random failure threshold, i.e., K is not constant but has a distribution $D(k) = Pr\{K \leq k\}$, for the cumulative damage. The first passage distribution to a random critical threshold of the compound Poisson process, can be derived as:

$$Pr\{Z \leq t\} = \sum_{n=0}^{\infty} \int_0^{\infty} \left[G^{(n)}(k) - G^{(n+1)}(k)\right] dD(k) \sum_{j=n+1}^{\infty} \frac{(\lambda t)^j}{j!} \exp(-\lambda t) \tag{5.2}$$

and it has the mean $E(Z) = \frac{1}{\lambda} \sum_{n=0}^{\infty} \int_0^{\infty} G^{(n)}(k) dD(k)$.

Example 1: If we suppose that a random failure threshold has the exponential distribution, i.e., $D(k) = 1 - \exp(-\beta k)$, then the LS transform of Equation- is

$$\int_0^{\infty} \exp(-st) dPr\{Z \leq t\} = \sum_{n=0}^{\infty} \left(\frac{\lambda}{s+\lambda}\right)^{n+1} \frac{\beta \theta^n}{(\theta+\beta)^{n+1}} = \frac{\lambda\beta}{s(\theta+\beta)+\lambda\beta} \tag{5.3}$$

i.e., $\int_0^{\infty} \left(G^{(n)}(k) - G^{(n+1)}(k)\right) dD(k) = \frac{\beta\theta^n}{(\theta+\beta)^{n+1}}$. To find the first passage distribution, we have the inverse LS transform of Equation-5.3 given as

$$Pr\{Z \leq t\} = 1 - \exp\left(-\frac{\lambda\beta t}{\theta+\beta}\right) \tag{5.4}$$

which is clearly exponential distribution with the rate parameter $\frac{\lambda\beta}{\theta+\beta}$. Therefore, we have $E(Z) = \frac{\theta+\beta}{\lambda\beta}$ and $Var(Z) = \left(\frac{\theta+\beta}{\lambda\beta}\right)^2$.

5.2.3 Random Failure Threshold for Independent Damage Model

In previous Section 5.2.1, we defined the cumulative damage model with a random failure threshold. However, in this section, we extend the same idea and define the independent damage model with a random threshold. Therefore, Equation-4.12 can be modified as given below:

$$Pr\{Z \leq t\} = \sum_{n=0}^{\infty} F^{(n+1)}(t) \int_0^{\infty} [G^n(k) - G^{n+1}(k)] dD(k) \tag{5.5}$$

and its mean time is $E(Z) = \mu \sum_{n=0}^{\infty} \int_0^{\infty} [G(k)]^n dD(k)$. The graphical presentation of the independent damage model with a random failure threshold is given in Figure-5.2.

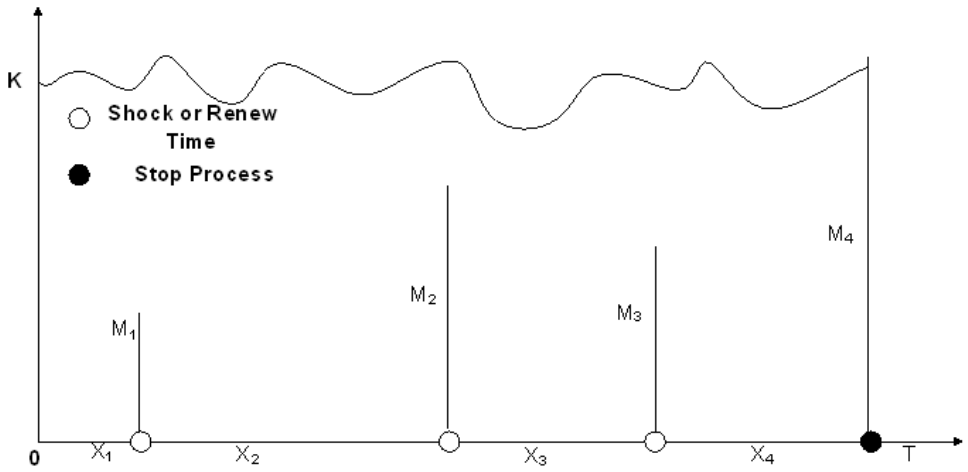

Figure 5.2: Process for a independent cumulative damage model

5.2.4 Random failure threshold for the Compound Poisson Process

To define the first passage distribution of the independent damage model to a random threshold, we consider the compound Poisson process for $N(t)$. Therefore,

$$Pr\{Z \leq t\} = \sum_{n=0}^{\infty} \int_0^{\infty} \left[G^n(k) - G^{n+1}(k)\right] dD(k) \sum_{j=n+1}^{\infty} \frac{(\lambda t)^j}{j!} \exp(-\lambda t) \tag{5.6}$$

which has the mean $E(Z) = \frac{1}{\lambda} \sum_{n=0}^{\infty} \int_0^{\infty} G^n(k) dD(k)$.

Example 2: Suppose that we have exponential distribution with the rate parameter β for the random failure threshold. To find the first passage distribution, Equation-5.6 can be written as:

$$\begin{aligned} Pr\{Z > t\} &= \int_0^{\infty} \exp(-\lambda t \exp(-\theta k)) \beta \exp(-\beta k) dk \\ &= \sum_{j=0}^{\infty} \frac{(-\lambda t)^j}{j!} \int_0^{\infty} \beta \exp(-(\beta + j\theta)k) dk = \sum_{j=0}^{\infty} \frac{(-\lambda t)^j}{j!} \frac{\beta}{\beta + j\theta} \\ &= \frac{\beta (t\lambda)^{-\beta/\theta}}{\theta} \Gamma(\beta/\theta, 0, t\lambda) \end{aligned} \tag{5.7}$$

where $\Gamma(\beta/\theta, 0, t\lambda) = \int_0^{t\lambda} k^{\beta/\theta - 1} \exp(-k) dk$ is the generalized incomplete gamma function (cf. Chaudhry and Zubair [1994]). Furthermore, the generalized gamma can be simplified as $\Gamma(\beta/\theta, 0, t\lambda) = \Gamma(\beta/\theta) - \Gamma(\beta/\theta, t\lambda)$. The mean time to a critical point is $E(Z) = \frac{1}{\lambda} \int_0^{\infty} \exp(\theta k) \beta \exp(-\beta k) dk = \frac{\beta}{\lambda(\beta - \theta)}$ for $\beta > \theta$, and it would be equal to ∞ for $\beta \leq \theta$.

5.3 Control Chart Construction

In this section, we are interested to develop control charts for the cumulative processes by assuming a random failure threshold. For this purpose, let α denotes the probability of the false alarm. To construct a two-sided control chart based on Equations-5.4 and 5.7, find $LCL = F^{-1}(\alpha/2)$ and $UCL = F^{-1}(1-\alpha/2)$, respectively, i.e., find the lower and upper percentiles of the first passage distribution at the specified false alarm probability to get the lower control limit (LCL) and the upper control limit (UCL). Similarly, a one-sided control chart can be designed by finding a lower percentile of the first passage distribution at α level to get only the LCL for the detection of a process deterioration. To monitor the process improvement, an upper-sided control chart can be designed by finding the $UCL = F^{-1}(1-\alpha)$ of the first passage distribution to a random critical point. The monitoring procedure using the proposed charts is the same as we have defined in Section-4.4. Moreover, one can also find the CPC charts, and procedure is exactly the same as we have described in Section-4.4 of Chapter-4.

By following the arguments of finding the adjusted parameter value as explained in Section-4.4, we have $\theta_1 = \beta_1\left[\frac{\lambda_0(\theta_0+\beta_0)}{\lambda_1\beta_0} - 1\right]$, $\lambda_1 = \frac{\lambda_0\beta_0(\theta_0+\beta_1)}{\beta_1(\theta_1+\beta_0)}$ and $\beta_1 = \frac{\theta_0\lambda_1\beta_0}{\lambda_0(\theta_1+\beta_0)-\lambda_1\beta_0}$ for the cumulative process with a random failure threshold. Similarly, for the independent process with a random failure threshold, we have $\theta_1 = \beta_1\left[\frac{\beta_0(\lambda_0-\lambda_1)+\lambda_1\theta_0}{\lambda_0\beta_0}\right]$, $\lambda_1 = \frac{\beta_1\lambda_0(\beta_0-\theta_1)}{\beta_0(\beta_1-\theta_0)}$ and $\beta_1 = \frac{\beta_0\lambda_0\theta_0}{\beta_0(\lambda_0-\lambda_1)+\lambda_1\theta_1}$.

To assess the performance of the proposed control charts, we use the ARL, quartiles of the run length distribution, the coefficient of variance of the run length and of the length of inspection distributions, respectively. We shall discuss these performances measures for the detection of a process deterioration and improvement using the one and the two sided control charts.

As we noticed in Chapter 4 that to get an explicit expression of the first passage distribution to a critical point is extremely difficult, if not impossible, for the construction of a control chart in general cases, e.g. considering the Weibull distribution for the time and the magnitude. Therefore, we propose the following Algorithm-5.1 to compute the control limits in general cases.

Similarly, we have Algorithm-5.2 for the ARL computation.

5.4 Discussion of ARL and ALI Study for Random Failure Threshold

In this section, we study the performance of the control charts proposed in Section-5.3. We suppose that TBE, damage and the random failure threshold follow exponential distributions with the rate parameters λ, θ and β, respectively.

Algorithm 5.1 Control Limits Computation for the First Passage Distribution' to a random Critical Threshold

Select $p = 1$ or $p = 2$ for the Process▷ where $p = 1$ - Cumulative, $p = 2$ - Independent
Choose parameters values to generate X, M, and K from F_X, G_M and D_K, respectively.
for $i = 1$ to S **do** ▷ where S is large, e.g., 10^6
    do
        Sample X_j, M_j and K_j, $j \geq 1$
        if $p == 1$ **then**
            $SM_j = \sum_{l=1}^{j} M_l$
        else
            $SM_j = M_j$
        end if
    while $SM_j < K_j$
    $Z_i = \sum_{l=1}^{j} X_l$
end for
Compute the Specified Quantiles of Z_i to find the LCL and UCL, respectively.

Algorithm 5.2 ARL Computation for the Two-Sided Chart based on the Renewal Reward Process with a random Critical Threshold

Select $p = 1$ or $p = 2$ for the Process▷ where $p = 1$ - Cumulative, $p = 2$ - Independent
Choose shifted parameters values to generate X, M and K from F_X, G_M and D_K
for $m = 1$ to S **do** ▷ where S is large, e.g., 10^6
    for $i = 1$ to S **do**
        do
            Sample X_j, M_j and K_j, $j \geq 1$
            if $p == 1$ **then**
                $SM_j = \sum_{l=1}^{j} M_l$
            else
                $SM_j = M_j$
            end if
        while $SM_j < K_j$
        $Z_i = \sum_{l=1}^{j} X_l$
        if $Z_i < LCL || Z_i > UCL$ **then**
            $RL_m = i$, break
        end if
    end for
end for
Compute Mean of RL_m.

5.4.1 Cumulative Compound Process

We are considering shifts for the following two cases:

A λ decreases from $\lambda_0 = 0.0005$ to $\lambda_1 \in \{0.0003, 0.0001, 0.00005\}$ while θ shifts from $\theta_0 = 0.001$ to $\theta_1 \in \{0.05, 0.01\}$ and β from $\beta_0 = 0.2$ to $\beta_1 \in \{0.1, 0.3\}$.

B λ increases from $\lambda_0 = 0.0005$ to $\lambda_1 \in \{0.005, 0.01, 0.1\}$ while θ shifts from $\theta_0 = 0.001$ to $\theta_1 \in \{0.0001, 0.01\}$ and β from $\beta_0 = 0.2$ to $\beta_1 \in \{0.1, 0.3\}$.

It is noticed that when there is no shift in the rate parameter of the time, magnitude/damage and the random failure distributions, the ARL is equal to the nominal value, i.e., 370.

Case A: an increase in θ (or decrease in λ): When a system improves, the damage becomes small and therefore, the system takes long time to cross a critical threshold. This improvement effect is reflected by the rate parameter of the first-passage distribution, i.e., it decreases, and the system fails occasionally. In our study, we fixed the magnitude distribution's rate parameter $\theta_0 = 0.001$ (for in-control process) while $\theta_1 \in \{0.05, 0.01\}$ to represent the out-of-control situation. The in-control parameter of the random threshold, exponential distribution with the rate parameter β, is $\beta_0 = 0.2$ while let the $\beta_1 \in \{0.1, 0.3\}$ to represent out-of-control situation. Similarly, the rate parameter of the time shifted from $\lambda_0 = 0.0005$ to $\lambda_1 \in \{0.0003, 0.0001, 0.00005\}$. When the system improves, an engineer is generally more concerned in the process improvement detection and for this purpose, the Upper-sided control chart should be used. We have computed the ARL values for the two-sided and the upper-sided charts in Table-5.1. The coefficient of variation (CV) values of the run length and of the length of inspection have also been reported below the ARL.

From Table-5.1, it is noticed that the one-sided chart is efficient in the detection of the shift than the two-sided control chart. However, the superiority of the one-sided chart is undermined when the random threshold distribution's rate parameter shifted from $\beta_0 = 0.2$ to $\beta_1 = 0.1$ for $\theta_0 = 0.001$. The large-size shifts, whether in the rate parameter of the time, failure threshold or magnitude distribution could be detected quickly as opposite to small shifts. The effectiveness of the one-sided chart could also be assessed by the coefficient of variation values. For the fixed λ and θ, the ARL decreases with the size of a shift in the rate parameter of the random failure threshold. Moreover, we observed that the CVLI (scale dependent) was noninformative as compared to the CV of run length distribution. The quartiles of the run length distribution have also been computed (not reported here for the sake of space), and we observed that for small to moderate shifts, the ARL values were smaller than Q_3 while for large shifts, the ARL was greater than Q_3.

Case B: a decrease in θ (or an increase in λ): This is the most important case because it detects the process deterioration. In this case, the rate parameter of the magnitude/damage would increase and lead to cross the threshold more often. Therefore, the time between event's occurrences decrease and result into an increased rate parameter of the first-passage distribution. In our study, we fixed the rate parameter of the magnitude distribution $\theta_0 = 0.001$ (for in-control process) while $\theta_1 \in \{0.0001, 0.01\}$ to represent the out-of-control situation. The rate parameter of the TBE distribution shifted from $\lambda_0 = 0.0005$ to $\lambda_1 \in \{0.005, 0.01, 0.1\}$. Similarly, the rate parameter of the random failure threshold is $\beta_0 = 0.2$ for the in-control situation while $\beta_1 \in \{0.1, 0.3\}$ for the out-of-control situation. When the system deteriorates, a practitioner or an engineer needs to use the lower-sided control chart instead of the upper-sided chart. Thus, in Table-5.2, we have presented the ARL values for the lower and the two sided control charts.

In this case, the lower-sided chart is efficient than the two-sided chart in the detection of a process deterioration, especially when θ decreases. However, if θ increases, i.e., damage becomes the small, then two-sided control would be very effective. This behavior is according to expectation because when θ decreases, the system will show improvements signs, and therefore, the use of the lower-sided chart must be avoided. Since the two-sided chart has UCL, its performance is good as compared to the one-sided chart. The ARL values get smaller as the shift in the rate parameter of the time distribution occurs, and this pattern can be verified from the CV values. For fixed λ and β, when a shift occurs in θ, it slightly improves the detection ability of the chart. Therefore, this behavior suggests that with a random failure threshold, the original distribution of the TBE plays an important role than the damage or random failure threshold. From the quartiles' computations, we observed that the ARL values were smaller than Q_3, but greater than the median, i.e., Q_2. Therefore, the run-length distribution is not highly skewed as we observed in the case of process improvement.

Table 5.1: ARL using $\alpha = 0.0027$ $\lambda_0 = 0.0005, \beta_0 = 0.2, \theta_0 = 0.001$ and $\lambda_1 \in \{0.0003, 0.0001, 0.00005\}$, $\beta_1 \in \{0.1, 0.3\}, \theta_1 \in \{0.05, 0.01\}$ for upper and two sided charts based on compound (cumulative) process with random failure threshold.

β	θ	λ	Upper Sided				Two Sided			
			0.0005	0.0003	0.0001	0.00005	0.0005	0.0003	0.0001	0.00005
0.1	0.001	ARL	359.683	34.1627	3.24477	1.80132	365.202	49.6078	3.72098	1.92945
			0.998609	0.985255	0.831752	0.666973	0.99863	0.98987	0.855134	0.694059
		CVLI	1.0000	1.0000	1.0000	1.0000	1.0000	1.0000	1.0000	1.0000
	0.01	ARL	222.228	25.5906	2.94686	1.71664	276.074	36.411	3.34201	1.82846
			0.997748	0.980267	0.812808	0.646117	0.998187	0.986172	0.837125	0.673121
		CVLI	1.0000	1.0000	1.0000	1.0000	1.0000	1.0000	1.0000	1.0000
	0.05	ARL	52.6001	10.7793	2.20901	1.48627	77.7999	14.1338	2.42295	1.55671
			0.990449	0.952486	0.739803	0.571993	0.993552	0.963975	0.766342	0.598011
		CVLI	1.0000	1.0000	1.0000	1.0000	1.0000	1.0000	1.0000	1.0000
0.2	0.001	ARL	370.37	34.7682	3.26383	1.80661	370.37	50.5407	3.74536	1.93577
			0.998649	0.985514	0.832833	0.668189	0.998649	0.990058	0.856156	0.695276
		CVLI	1.0000	1.0000	1.0000	1.0000	1.0000	1.0000	1.0000	1.0000
	0.01	ARL	287.443	29.8628	3.10249	1.76139	324.243	42.9819	3.53947	1.88175
			0.998259	0.983114	0.823212	0.657469	0.998457	0.988299	0.847037	0.684529
		CVLI	1.0000	1.0000	1.0000	1.0000	1.0000	1.0000	1.0000	1.0000
	0.05	ARL	116.194	17.3424	2.58843	1.60886	166.254	23.852	2.89181	1.70075
			0.995688	0.970741	0.783368	0.615176	0.996988	0.978813	0.808824	0.641892
		CVLI	1.0000	1.0000	1.0000	1.0000	1.0000	1.0000	1.0000	1.0000
0.3	0.001	ARL	374.027	34.9737	3.27025	1.80838	372.092	50.8574	3.75358	1.93789
			0.998662	0.9856	0.833194	0.668595	0.998655	0.99012	0.856497	0.695683
		CVLI	1.0000	1.0000	1.0000	1.0000	1.0000	1.0000	1.0000	1.0000
	0.01	ARL	314.924	31.5445	3.15967	1.77754	341.162	45.5728	3.6123	1.90103
			0.998411	0.984022	0.826747	0.661382	0.998533	0.988968	0.850393	0.688455
		CVLI	1.0000	1.0000	1.0000	1.0000	1.0000	1.0000	1.0000	1.0000
	0.05	ARL	163.191	21.2627	2.77038	1.66445	220.468	29.7908	3.11952	1.76649
			0.996931	0.976201	0.799399	0.631822	0.99773	0.983073	0.82428	0.658716
		CVLI	1.0000	1.0000	1.0000	1.0000	1.0000	1.0000	1.0000	1.0000

Table 5.2: ARL using $\alpha = 0.0027$ $\lambda_0 = 0.0005, \beta_0 = 0.2, \theta_0 = 0.001$ and $\lambda_1 \in \{0.005, 0.01, 0.1\}$, $\beta_1 \in \{0.1, 0.3\}, \theta_1 \in \{0.0001, 0.01\}$ for lower and two sided charts based on compound (cumulative) process with random failure threshold.

β	θ	λ	Lower Sided				Two Sided			
			0.0005	0.005	0.01	0.1	0.0005	0.005	0.01	0.1
0.1	0.0001	ARL	368.898	37.3421	18.9244	2.38701	374.502	74.2306	37.367	4.20905
			0.998644	0.986519	0.973221	0.762277	0.998664	0.993241	0.986528	0.873165
		CVLI	1.0000	1.0000	1.0000	1.0000	1.0000	1.0000	1.0000	1.0000

		ARL	372.211	37.6733	19.09	2.40317	365.202	74.8935	37.6984	4.24199
	0.001		0.998656	0.986639	0.973456	0.764123	0.99863	0.993301	0.986648	0.874221
		CVLI	1.000	1.0000	1.0000	1.0000	1.0000	1.0000	1.0000	1.0000
		ARL	405.333	40.9854	20.7458	2.56517	276.074	81.5224	41.0127	4.57162
	0.01		0.998766	0.987725	0.975601	0.781129	0.998187	0.993848	0.987733	0.883889
		CVLI	1.0000	1.0000	1.0000	1.0000	1.0000	1.0000	1.0000	1.0000
		ARL	368.714	37.3237	18.9152	2.38611	375.018	74.1937	37.3486	4.20722
	0.0001		0.998643	0.986513	0.973207	0.762173	0.998666	0.993238	0.986522	0.873106
		CVLI	1.0000	1.0000	1.0000	1.0000	1.0000	1.0000	1.0000	1.0000
0.2		ARL	370.37	37.4893	18.998	2.39419	370.37	74.5252	37.5143	4.22369
	0.001		0.998649	0.986573	0.973326	0.763101	0.998649	0.993268	0.986582	0.873636
		CVLI	1.0000	1.0000	1.0000	1.0000	1.0000	1.0000	1.0000	1.0000
		ARL	386.932	39.1453	19.8259	2.4751	324.243	77.8397	39.1714	4.38845
	0.01		0.998707	0.987144	0.974454	0.771994	0.998457	0.993556	0.987153	0.878709
		CVLI	1.0000	1.0000	1.0000	1.0000	1.0000	1.0000	1.0000	1.0000
		ARL	368.653	37.3175	18.9122	2.38581	375.19	74.1815	37.3424	4.20661
	0.0001		0.998643	0.98651	0.973203	0.762139	0.998666	0.993237	0.98652	0.873086
		CVLI	1.0000	1.0000	1.0000	1.0000	1.0000	1.0000	1.0000	1.0000
0.3		ARL	369.757	37.4279	18.9674	2.3912	372.092	74.4024	37.4529	4.21759
	0.001		0.998647	0.986551	0.973282	0.762758	0.998655	0.993257	0.98656	0.87344
		CVLI	1.0000	1.0000	1.0000	1.0000	1.0000	1.0000	1.0000	1.0000
		ARL	380.798	38.532	19.5193	2.44511	341.162	76.6121	38.5577	4.32742
	0.01		0.998686	0.986938	0.974048	0.768779	0.998533	0.993452	0.986947	0.876878
		CVLI	1.0000	1.0000	1.0000	1.0000	1.0000	1.0000	1.0000	1.0000

5.4.2 Independent Random Failure Threshold: Compound Poisson Process

We consider the shifts for the following two cases:

A λ decreases from $\lambda_0 = 0.0005$ to $\lambda_1 \in \{0.0003, 0.0001, 0.00005\}$ while θ shifts from $\theta_0 = 0.001$ to $\theta_1 \in \{0.04, 0.01\}$ and β from $\beta_0 = 0.2$ to $\beta_1 \in \{0.1, 0.3\}$.

B λ increases from $\lambda_0 = 0.0005$ to $\lambda_1 \in \{0.005, 0.01, 0.1\}$ while θ shifts from $\theta_0 = 0.001$ to $\theta_1 \in \{0.0001, 0.01\}$ and β from $\beta_0 = 0.2$ to $\beta_1 \in \{0.1, 0.3\}$.

It is observed from the ARL study that when the process is in-control, i.e., no shift in the process parameters, the ARL value is equal to the specified in-control ARL value, i.e., 370.

Case A: an increase in θ (or decrease in λ): When the system improves, the damage/magnitude associated with each event becomes small and system takes a long time to cross random threshold and therefore, this leads to a decrease in the rate parameter of the first passage distribution, i.e., the system fails occasionally. In our study, we fixed the magnitude' rate parameter $\theta_0 = 0.001$ (for in-control process) while $\theta_1 \in \{0.04, 0.01\}$ to represent an out-of-control situation. The in-control rate parameter of the random failure threshold, i.e., exponential distribution with the rate β, shifted from $\beta_0 = 0.2$ to $\beta_1 \in \{0.1, 0.3\}$. The rate parameter of the time distribution shifted from $\lambda_0 = 0.0005$ to $\lambda_1 \in \{0.0003, 0.0001, 0.00005\}$. Here again, we shall use the upper-sided control chart for detection of the process improvement. In Table-5.3, we have computed the ARL values for the two-sided and the upper-sided charts. The CVs of the run-length and of the length of inspection distributions have also been reported in Table-5.3.

From Table-5.3, it is clear that the one-sided chart is more efficient in the detection of shifts than the two-sided control chart. The superiority of the upper-sided chart is also evident when a shift occurs either in λ or θ for the fixed β. However, the effect of a shift on β is minor, especially when $\beta_1 < \beta_0$ as compared to the case $\beta_1 > \beta_0$. The large shifts either in the rate parameter of the time, random failure threshold or the magnitude distribution would be detected quickly as compared to the small shifts. The said effectiveness of the one-sided chart could also be assessed by the coefficient of variance values of the run length and of the length of inspection distributions. The CVs of the run length and of the length of inspection distributions, and quartiles of the run-length distribution also advocate the superiority of the upper-sided chart over the two-sided chart. It has been noticed from the quartiles' study that as a large shift in the time distribution occurs, the run-length distribution becomes highly skewed and therefore, the ARL gets greater than Q_3.

Case B: a decrease in θ (or an increase in λ): This is an important case as it detects the process deterioration. In this case, the damage/magnitude increases, and

it leads to cross the random threshold more frequently. This in turn shorten the time between the system failure and thus, the system would be prone to frequent failure. In our study, we fixed the rate parameter of the magnitude distribution $\theta_0 = 0.001$ (for an in-control process) while $\theta_1 \in \{0.0001, 0.01\}$ to represent out-of-control situation. The rate parameter of the time distribution shifts from $\lambda_0 = 0.0005$ to $\lambda_1 \in \{0.005, 0.01, 0.1\}$. Similarly, the rate parameter of the random failure threshold was fixed $\beta_0 = 0.2$ for in-control situation while $\beta_1 \in \{0.1, 0.3\}$ to represent out-of-control situation. Once again, we would use the lower-sided control chart to detect the process deterioration and further it would be compared with the two-sided control chart. The ARL values of the lower and two sided control charts have been reported in Table-5.4. Moreover, the CVs of the run-length and of the length of inspection distributions have also been computed in Table-5.4. One can easily recover the standard deviation of the run-length distribution using the ARL and the CV values.

Again, the one-sided chart is efficient in the detection of process deterioration than the two-sided chart. However, the said superiority is subject to the rate parameter of the time distribution, i.e., both charts compete each other, especially when $\lambda = 0.0005$. We observed that the detection ability of the both charts was greatly improved as a shift in the rate parameter of the time distribution was occurred. This behavior could also be verified from the CV of the run-length distribution. However, it is also observed that the effect of the magnitude is very significant as compared to the random failure distribution (cf. Table-5.4). A shift of large size would be detected quickly than the small to moderate size of the shift. When $\theta_1 > \theta_0$ and $\lambda_0 = 0.0005$, it has been noticed that the ARL is greater than its nominal value, and two-sided chart outperforms than the lower-sided chart. However, one should be very careful in interpretation because it is not the violation of the ARL's unbiasedness property. This is happening because when the damage decreases the chart would take long time to cross a threshold, and the use of LCL is inappropriate in such a situation. Since the two-sided chart has the UCL, its performance is better than the lower-sided control chart. Therefore, to design a control chart one must be very careful about the choice of parameters, especially in estimation as the parameters have a significant effect on the control chart performance (cf. Table-5.4). The examination of the quartiles reveals that for the large shifts, the ARL values are smaller than Q_3 (but are greater than median, i.e., Q_2). Therefore, the run-length distribution becomes highly skewed with the size of a shift.

Table 5.3: ARL using $\alpha = 0.0027$ $\lambda_0 = 0.0005, \beta_0 = 0.2, \theta_0 = 0.001$ and $\lambda_1 \in \{0.0003, 0.0001, 0.00005\}$, $\beta_1 \in \{0.1, 0.3\}, \theta_1 \in \{0.04, 0.01\}$ for upper and two sided charts based on compound (independent) process with random failure threshold.

β	θ	λ	Upper Sided				Two Sided			
			0.0005	0.0003	0.0001	0.00005	0.0005	0.0003	0.0001	0.00005
0.1	0.001	ARL	359.207	34.1503	3.24483	1.80137	364.892	49.5862	3.72107	1.92951
			0.998607	0.98525	0.831756	0.666984	0.998629	0.989865	0.855138	0.694071
		CVLI	0.998607	0.985252	0.831775	0.667027	0.998629	0.989866	0.855154	0.694109
	0.01	ARL	189.434	24.3157	2.93205	1.71457	239.82	34.1754	3.32094	1.8257
			0.997357	0.979221	0.811752	0.645572	0.997913	0.985261	0.835991	0.672506
		CVLI	0.99739	0.979484	0.814374	0.651194	0.997939	0.985447	0.838239	0.677577
	0.04	ARL	26.9025	9.16146	2.25974	1.51642	33.7868	11.2518	2.47344	1.59023
			0.981238	0.943847	0.74664	0.583568	0.98509	0.954529	0.771819	0.609229
		CVLI	0.996276	0.989024	0.954722	0.931724	0.997036	0.991073	0.958718	0.935004
0.2	0.001	ARL	370.37	34.7719	3.26406	1.80668	370.37	50.5472	3.74569	1.93586
			0.998649	0.985516	0.832846	0.668205	0.998649	0.990059	0.85617	0.695295
		CVLI	0.998649	0.985516	0.832851	0.668216	0.998649	0.990059	0.856174	0.695304
	0.01	ARL	275.419	29.4414	3.09809	1.76081	314.019	42.2419	3.53319	1.88098
			0.998183	0.98287	0.822934	0.657328	0.998406	0.988093	0.846741	0.68437
		CVLI	0.998188	0.982918	0.823479	0.658527	0.998411	0.988126	0.847205	0.685448
	0.04	ARL	87.4395	16.748	2.6532	1.63518	117.866	22.3928	2.9664	1.731
			0.994265	0.969686	0.789365	0.623255	0.995749	0.977416	0.814181	0.649846
		CVLI	0.994649	0.971737	0.805123	0.655146	0.996033	0.827868	0.854142	0.678832
0.3	0.001	ARL	374.119	34.9805	3.27051	1.80846	372.149	50.8693	3.75396	1.93799
			0.998663	0.985603	0.833209	0.668613	0.998656	0.990122	0.856513	0.695703
		CVLI	0.998663	0.985603	0.833211	0.668617	0.998656	0.990122	0.856515	0.695707
	0.01	ARL	308.996	31.3433	3.15771	1.77731	336.632	45.2202	3.6095	1.90072
			0.998381	0.983918	0.826629	0.661326	0.998514	0.988881	0.850267	0.688392
		CVLI	0.998382	0.983938	0.826857	0.661832	0.998515	0.988894	0.850461	0.688847
	0.04	ARL	145.782	21.4072	2.8316	1.68629	192.068	29.6081	3.19288	1.79192
			0.996564	0.976364	0.804266	0.637951	0.997393	0.982968	0.828736	0.664785
		CVLI	0.996648	0.976944	0.809571	0.64912	0.997457	0.983384	0.833304	0.674884

Table 5.4: ARL using $\alpha = 0.0027$ $\lambda_0 = 0.0005, \beta_0 = 0.2, \theta_0 = 0.001$ and $\lambda_1 \in \{0.005, 0.01, 0.1\}$, $\beta_1 \in \{0.1, 0.3\}, \theta_1 \in \{0.0001, 0.01\}$ for lower and two sided charts based on compound (independent) process with random failure threshold.

β	θ	λ	Lower Sided				Two Sided			
			0.0005	0.005	0.01	0.1	0.0005	0.005	0.01	0.1
0.1	0.0001	ARL	368.898	37.3421	18.9244	2.38701	374.6	74.2306	37.367	4.20905
			0.998644	0.986519	0.973221	0.762277	0.998664	0.993241	0.986528	0.873165
		CVLI	0.998644	0.986519	0.973221	0.762277	0.998664	0.993241	0.986529	0.873165

		ARL	372.211	37.6733	19.09	2.40322	364.892	74.8935	37.6985	4.24204
	0.001		0.998656	0.986639	0.973456	0.764128	0.998629	0.993301	0.986648	0.874222
		CVLI	0.998656	0.98664	0.973459	0.764156	0.998629	0.993302	0.986649	0.874236
		ARL	405.337	40.9895	20.7499	2.56935	239.82	81.5266	41.0169	4.57582
	0.01		0.998766	0.987726	0.975606	0.781535	0.997913	0.993848	0.987735	0.884002
		CVLI	0.998781	0.987881	0.975915	0.784642	0.997939	0.993925	0.987889	0.885546
		ARL	368.714	37.3237	18.9152	2.38611	375.12	74.1937	37.3486	4.20722
	0.0001		0.998643	0.986513	0.973207	0.762173	0.998666	0.993238	0.986522	0.873106
		CVLI	0.998643	0.986513	0.973207	0.762174	0.998666	0.993238	0.986522	0.873106
0.2		ARL	370.37	37.4893	18.998	2.39421	370.37	74.5252	37.5143	4.2237
	0.001		0.998649	0.986573	0.973326	0.763102	0.998649	0.993268	0.986582	0.873637
		CVLI	0.998649	0.986573	0.973326	0.763109	0.998649	0.993268	0.986582	0.87364
		ARL	386.933	39.1464	19.827	2.47622	314.019	77.8408	39.1726	4.38959
	0.01		0.998707	0.987145	0.974456	0.772114	0.998406	0.993556	0.987153	0.878743
		CVLI	0.998711	0.987181	0.974528	0.77284	0.998411	0.993574	0.987189	0.879103
		ARL	368.653	37.3175	18.9122	2.38581	375.292	74.1815	37.3424	4.20661
	0.0001		0.998643	0.98651	0.973203	0.762139	0.998667	0.993237	0.98652	0.873086
		CVLI	0.998643	0.986511	0.973203	0.762139	0.998667	0.993237	0.98652	0.873086
0.3		ARL	369.757	37.4279	18.9674	2.39121	372.149	74.4024	37.4529	4.2176
	0.001		0.998647	0.986551	0.973282	0.762759	0.998656	0.993257	0.98656	0.87344
		CVLI	0.998647	0.986551	0.973282	0.762762	0.998656	0.993257	0.98656	0.873442
		ARL	380.798	38.5325	19.5198	2.44563	336.632	76.6126	38.5582	4.32794
	0.01		0.998686	0.986939	0.974048	0.768835	0.998514	0.993452	0.986947	0.876894
			0.998688	0.986954	0.97408	0.769151	0.998515	0.99346	0.986963	0.877051

5.5 Real life examples

In this section, we discuss two illustrative examples for the implementation of the proposed control charts. Note that we use $\alpha = 0.0027$ to develop these control charts.

5.5.1 Cardiac Monitoring-Cumulative Process with Random Failure Threshold

In the introduction section (cf. Section-5.1), we have given a motivational example (see example 2) about the cardiac monitoring. To study such events, i.e., to monitor the time to a critical threshold and see treatment effectiveness, we propose here the cumulative process with a random failure threshold. The random failure threshold is assumed because each event has a different level of severity, and it is hard to fix the threshold without having some knowledge about person's health. In other words, the critical point cannot be fixed in advanced. We are interested to decide whether the treatment of hypertension is effective or not. Mostly, the effect of a treatment on the patient health is additive; therefore, the doctor has to wait for a few time periods to decide whether new treatment is effective or not. That's why we are advocating the use of the cumulative process with a random threshold.

To monitor a person's heart condition with two hypertension treatments, we generated 40 observations using the cumulative process with a random failure threshold. The first 20 in-control observations (cf. Table-5.5) have been generated using $\beta = 0.2, \lambda = 0.0005, \theta = 0.001$, the next 10 (i.e., adopting the first hypertension treatment) from $\lambda = 0.00005, \theta = 0.001, \beta = 0.1$ and the last 10 (i.e., using the second treatment) from $\lambda = 0.1, \theta = 0.0001, \beta = 0.2$. The bold values given in Table-5.5 denote the occurrences of the shift while the values with a $\star$ represent the detection of the shift at that particular sample point by the control chart. Using the first 20 observations, the control limits are: $LCL = \ln(2.71533) = 0.998913$ and $UCL = \ln(13281.4) = 9.494119$. In Figure-5.3a, the natural logarithm of the data and of the control limits is taken for a better presentation of the chart. From Figure-5.3a it is clear that for the first 20 observations, the process was statistically in-control. A shift of the process improvement occurred at the sample number 21 which was efficiently detected. Again, another shift occurred at the sample number 31 which was detected at the sample number 33, i.e., an indication that treatment is not effective (process deterioration). A CPC chart has also been developed in Figure-5.3b, and we support the same conclusion as we have in the case of CQC chart. Note that here a process improvement means the new treatment is effective, i.e., hypertension is under control, and the patient heart rhythm performing well while a process deterioration

Table 5.5: Simulated failure time data of the Cumulative Random Process

Failure #	Inter-failure time (X)	ln(X)	Cumulative Probability	Failure #	Inter-failure time (X)	ln(X)	Cumulative Probability
1	1358.6356	7.2142	0.4913	21	14621.1015	**9.5902***	0.9993
2	1455.9690	7.2834	0.5154	22	31992.3574	10.3733*	1
3	1190.2321	7.0819	0.4469	23	806.2818	6.6924	0.3304
4	171.7995	5.1463	0.0819	24	4653.1388	8.4453	0.9012
5	213.2174	5.3623	0.1007	25	4678.5287	8.4507	0.9025
6	549.4725	6.3089	0.2392	26	9464.1135	9.1553	0.9909
7	769.6276	6.6459	0.3181	27	16041.8204	9.6829*	0.9997*
8	92.6176	4.5285	0.0450	28	19609.4364	9.8838*	0.9999*
9	2232.0274	7.7107	0.6706	29	18912.2774	9.8476*	0.9999*
10	5647.7267	8.6390	0.9398	30	16712.0086	9.7239*	0.9998*
11	139.1173	4.9353	0.0669	31	46123.4917	**10.7391**	1*
12	5.0298	1.6154	0.0025	32	16.8552	2.8247	0.0084
13	1688.7102	7.4317	0.5684	33	1.8656	0.6236*	0.0009*
14	5304.9566	8.5764	0.9286	34	1.6743	0.5154*	0.0008*
15	2971.2229	7.9967	0.7719	35	1.2551	0.2272*	0.0006*
16	250.7712	5.5245	0.1173	36	8.5577	2.1469	0.0043
17	913.7152	6.8175	0.3653	37	5.2704	1.6621	0.0026
18	573.7196	6.3521	0.2483	38	3.3900	1.2208	0.0017
19	5494.8959	8.6116	0.9350	39	1.1046	0.0995*	0.0006*
20	2603.9642	7.8648	0.7262	40	13.6607	2.6145	0.0068

means the treatment is not effective and heat rhythm has increased than a normal rate.

5.5.2 Radiation Monitoring-Independent Process with Random Failure Threshold

As we have quoted an example of radioactivity in the introduction section (cf. Example-1 in Section-5.1), and we are interested in monitoring its level near a nuclear plant. Note that there could be natural and un-natural causes of radioactivity and monitoring of such events, is really a challenge. Here, we propose the independent process with a random failure threshold to monitor radioactivity level. We consider the independent process as the radioactivity level changes over time.

The first 20 in-control observations in Table-5.6, are generated using $\beta = 0.2, \lambda = 0.0005, \theta = 0.001$, the next 10 (i.e., radioactivity level decreased and the process has been improved) from $\lambda = 0.0001, \theta = 0.001, \beta = 0.2$ and the last 10 (i.e., process deterioration means that the radioactivity level has been increased) from $\lambda = 0.01, \theta = 0.001, \beta = 0.2$. The bold values given in Table-5.6 denote the occurrence of the shift while the values with a $\star$ represent the detection of a shift. Using the first 20 observations, the control limits are: $LCL = \ln(2.71533) = 0.998913$ and $UCL = \ln(13282.5) = 9.494203$. A shift of the process improvement was occurred at the sample number 21, and detected by the control chart at the sample number 22. Again, another process deterioration shift occurred at the sample number 31 which was detected at the sample number 36. In Figure-5.4a, the natural logarithm of the data and of the control limits is taken for a better presentation of

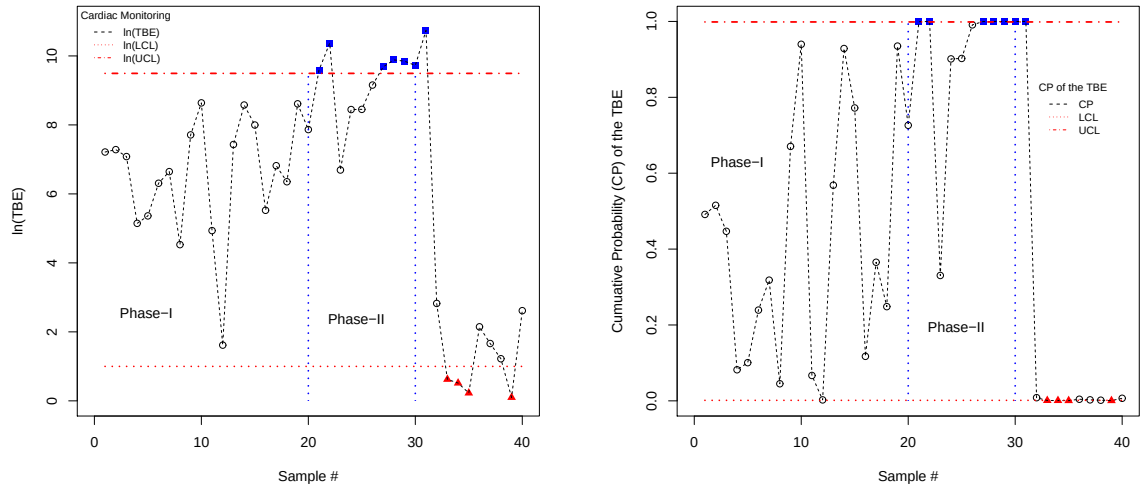

(a) Cumulative Quantity Control Chart (b) Cumulative Probability Control Chart

Figure 5.3: Control Chart for the Cumulative Process with Random Failure Threshold

the chart. Clearly, first the process improves, i.e., radioactivity level has been decreased, while in the last 10 observations, the process has been deteriorated, i.e., radioactivity level has been increased. Moreover, the same conclusion is supported by the CPC chart (cf. Figure-5.4b).

5.6 Conclusion

In this chapter, we have proposed two different control charts assuming a random failure threshold based on the renewal reward process. Although after defining a general mathematical setup of the renewal reward process with a random failure threshold, we resorted ourselves to the compound Poisson process. The compound Poisson process was assumed just for illustration purposes, i.e., to get an explicit distribution of the first passage time. However, we have also purposed a computational algorithm to find the first passage distribution by any lifetime distribution of the time, damage and threshold. Therefore, this work is actually a generalization of the previous chapter, i.e., Chapter 4, where we assumed a fixed failure threshold.

The effective performance of proposed charts lies in their sensitivity to detect the simultaneous shifts of TBE, magnitude/damage and the random threshold. The ARL study with the CVs of the run-length and of the length of inspection distributions have been conducted to assess the performance of the control charts under different conditions. For our assumed parameter values, we noticed that the effect of a random threshold or the magnitude distribution was less significant than the TBE distribution itself. Therefore, one must be very careful about the choice of different parameters, especially in estima-

Table 5.6: Simulated failure time data of the Independent Failure Process

Failure #	Inter-failure time (X)	ln(X)	Cumulative Probability	Failure #	Inter-failure time (X)	ln(X)	Cumulative Probability
1	1409.92	7.2513	0.5041	21	3266.91	**8.0916**	0.8032
2	3674.38	8.2091	0.8393	22	31807.2	10.3675*	1*
3	2698.71	7.9005	0.7388	23	1354.41	7.2111	0.4903
4	2541.87	7.8407	0.7177	24	17142.8	9.7493*	0.9998*
5	1304.95	7.1739	0.4776	25	10110.3	9.2213	0.9935
6	2219.62	7.7051	0.6686	26	9193.45	9.1263	0.9897
7	463.459	6.1387	0.2059	27	1262.78	7.1411	0.4665
8	3634.95	8.1984	0.8361	28	746.301	6.6151	0.3102
9	1170.39	7.0651	0.4414	29	31628.3	10.3618*	1*
10	2456.87	7.8066	0.7198	30	1832.02	7.5132	0.5981
11	915.5	6.8195	0.3659	31	14.4584	**2.6713**	0.0072
12	788.862	6.6706	0.3246	32	17.5116	2.8629	0.0087
13	1741.02	7.4622	0.5794	33	86.9144	4.4649	0.0414
14	2410.72	7.7877	0.6886	34	5.5391	1.7118	0.0028
15	3433.98	8.1415	0.8189	35	92.418	4.5263	0.0449
16	3174.49	8.0629	0.7939	36	2.5434	0.9335*	0.0013*
17	611.132	6.4153	0.2622	37	155.455	5.0464	0.0744
18	2939.43	7.9859	0.7683	38	129.656	4.8649	0.0625
19	1460.29	7.2864	0.5164	39	145.026	4.9769	0.0696
20	3055.25	8.0246	0.7813	40	514.848	6.2439	0.2259

tion. The run-length distribution becomes highly skewed for the large shifts either in the time, magnitude or random threshold' rate parameter. Moreover, the one-sided charts outperform than the two-sided charts in almost all cases. It is worth mentioning that there are few exceptions where the superiority of the one-sided chart is undermined, but these cases are specific to damage/magnitude distribution. The shift in the rate parameter of the damage distribution plays an important role in the choice of the chart. It is clear from our simulation study as well as from the real-life applications that the proposed monitoring strategies are efficient in the detection of different size shifts simultaneously.

In this chapter, we assumed the exponential distribution for the magnitude and random failure threshold. However, in the real applications, this distribution may not be well fitted to a situation, and thus some other suitable distributions can be considered for the analysis with our defined general procedure. A nonparametric approach could be considered, which is an alternative interesting option to parametric charts, for the time and magnitude charts. More advanced control charts like CUSUM and EWMA, are an open issue for the new proposal.

In the next chapter, we introduce a TBE chart based on nonhomogeneous Poisson process for sequential process monitoring (cf. Chapter-6).

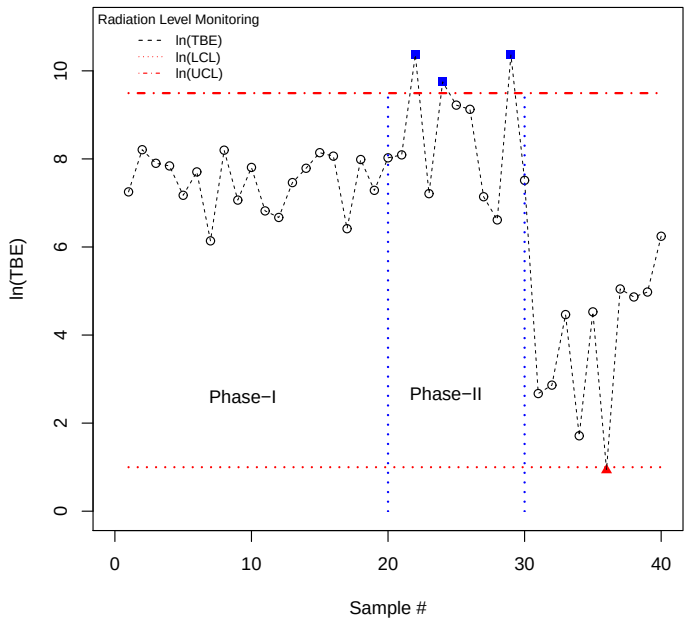

(a) Cumulative Quantity Control Chart

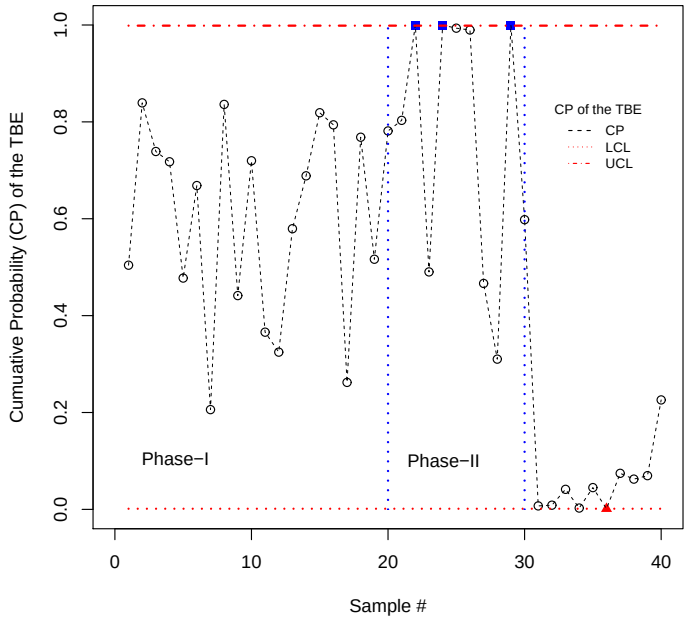

(b) Cumulative Probability Control Chart

Figure 5.4: Control Chart for the Independent Process with Random Failure Threshold

Appendix

In this appendix, we derive the probability density function and partial derivatives to find the maximum likelihood estimates of the unknown parameters.

Appendix A: Cumulative Process with random failure threshold (Model 1):

Suppose that the time, magnitude and random failure threshold are exponentially distributed with the rate parameters λ, θ and β, respectively. The distribution function of the first passage distribution for the cumulative process is:

$$Pr\{Z < t\} = 1 - \frac{\beta(t\lambda)^{-\beta/\theta}}{\theta}\Gamma(\beta/\theta, 0, t\lambda) \tag{1}$$

where $\Gamma(\beta/\theta, 0, t\lambda) = \int_0^{t\lambda} x^{\beta/\theta-1}\exp(-x)dx$ is the generalized incomplete gamma function (cf. Chaudhry and Zubair [1994]). Further, it can be written as $\Gamma(\beta/\theta, 0, t\lambda) = \Gamma(\beta/\theta) - \Gamma(\beta/\theta, t\lambda)$. Therefore, the density function is:

$$f(t) = \frac{\beta[-\theta\exp(-t\lambda) + \beta(t\lambda)^{-\beta/\theta}\Gamma(\beta/\theta, 0, t\lambda)]}{t\theta^2} \tag{2}$$

Appendix A: Independent Process with random failure threshold (Model 2):

To derive a first passage distribution for the independent process, suppose that the time, the magnitude and the random failure threshold are exponentially distributed with the rate parameters λ, θ and β, respectively. The cumulative distribution function of the first passage distribution is given as:

$$Pr\{Z \leq t\} = 1 - \exp\left(-\frac{\lambda\beta t}{\theta+\beta}\right) \tag{3}$$

and it has pdf

$$f(t) = \frac{\lambda\beta}{\theta+\beta}\exp\left(-\frac{\lambda\beta t}{\theta+\beta}\right) \tag{4}$$

The log-likelihood function is

$$l(.) = n\ln(\lambda) + n\ln(\beta) - n\ln(\theta+\beta) - \frac{\lambda\beta}{\theta+\beta}\sum_{i=1}^{n} t_i \tag{5}$$

and we have the normal equations:

$$\frac{\partial l(.)}{\partial \lambda} = \frac{n}{\lambda} - \frac{\beta}{\theta+\beta}\sum_{i=1}^{n} t_i = 0 \Longrightarrow \hat{\lambda} = \frac{n(\theta+\beta)}{\beta\sum_{i=1}^{n} t_i} \tag{6}$$

$$\frac{\partial l(.)}{\partial \beta} = \frac{n}{\beta} - \frac{n}{\theta+\beta} - \frac{\lambda\theta\sum_{i=1}^{n} t_i}{(\theta+\beta)^2} = 0 \Longrightarrow \hat{\beta} = \frac{n\theta}{\lambda\sum_{i=1}^{n} t_i - n} \tag{7}$$

$$\frac{\partial l(.)}{\partial \theta} = -\frac{n}{\theta+\beta} + \frac{\lambda\beta\sum_{i=1}^{n} t_i}{(\theta+\beta)^2} = 0 \Longrightarrow \hat{\theta} = \frac{\beta(\lambda\sum_{i=1}^{n} t_i - n)}{n} \tag{8}$$

$$\frac{\partial^2 l(.)}{\partial \lambda^2} = -\frac{n}{\lambda} \tag{9}$$

$$\frac{\partial^2 l(.)}{\partial \lambda \partial \theta} = \frac{\beta\sum_{i=1}^{n} t_i}{(\theta+\beta)^2} \tag{10}$$

$$\frac{\partial^2 l(.)}{\partial \lambda \partial \beta} = -\frac{\theta\sum_{i=1}^{n} t_i}{(\theta+\beta)^2} \tag{11}$$

$$\frac{\partial^2 l(.)}{\partial \beta^2} = -\frac{n}{\beta^2} + \frac{n}{(\theta+\beta)^2} + \frac{2\lambda\theta\sum_{i=1}^{n} t_i}{(\theta+\beta)^3} \tag{12}$$

$$\frac{\partial^2 l(.)}{\partial \beta \partial \theta} = \frac{n}{(\theta+\beta)^2} - \frac{\lambda(\beta-\theta)\sum_{i=1}^{n} t_i}{(\theta+\beta)^3} \tag{13}$$

$$\frac{\partial^2 l(.)}{\partial \theta^2} = \frac{n}{(\theta+\beta)^2} - \frac{2\lambda\beta\sum_{i=1}^{n} t_i}{(\theta+\beta)^3} \tag{14}$$

Chapter 6

Time-Between-Events Monitoring using Nonhomogeneous Poisson Process with Power Law Intensity

In Chapters 3-5, we have introduced TBE control charts for the renewal and the renewal reward processes. However, there are many situations where we need an adaptive monitoring, e.g. health, flood, food, system or terrorist surveillance. Therefore, the proposed charts are not useful, especially in sequential monitoring. The aim of this chapter is to introduce an adaptive TBE chart. Therefore, we introduce a new time-between-events control chart for high-quality processes based on nonhomogeneous Poisson process by assuming the Power law process (commonly known as the Weibull process). Since the control limits of the proposal are sequentially updated, our proposed chart is suitable for the online process monitoring. The performance of the proposed control chart is evaluated in terms of some standard measures, including the average run length (ARL), coefficient of variation (CV) of the run length distribution, expected quality loss (EQL) and the relative ARL (RARL). The study also presents three examples to highlight the practical aspects of the proposal.

6.1 Introduction

From Chapter 2 (particularly Section-2.11), it is evident that the available continuous TBE charts are developed using the Poisson process. In the homogeneous Poisson process, the underlying distribution of time is exponential, which has a constant hazard rate. However, in many applied fields, it is difficult to verify that each unit has the same risk level and therefore, it may be realistic to assume (depending upon situation) that the items/products/systems have different levels of risk, which may vary with time, e.g. health surveillance. To generalize the existing TBE charts, we used the renewal (cf. Chapter 3)

and the renewal reward (cf. Chapters 4 & 5) processes. However, these charts are suitable only if the risk level is fixed. Moreover, the introduced charts are not adaptive. There are many situations where we need an adaptive monitoring, e.g. an old system would be prone to more failures than a new one. Similar examples could be found in the fields of health, flood, food, system or terrorist surveillance, etc. Recently, Purdy et al. [2014] noticed that it is useful to develop risk varying control charts in a health surveillance because the number of patients in the hospital may stay constant over time, but the age distribution among the population (patients) may change, which result into an increase risk of the sick population. Therefore, one needs to consider some alternative classes of underlying processes such as a nonhomogeneous Poisson process.

The main aim of this chapter is to introduce an adaptive process monitoring strategy. Therefore, we consider a nonhomogeneous Poisson process with Power law intensity to develop the TBE control charts. A nonhomogeneous Poisson process with the power law intensity is also commonly known as the power law process. Note that there are different names of the power law process such as the Weibull process, the AMSAA model (name due to its adoption by the United States army for material testing, i.e., United States Army Material Systems Analysis Activity), and Duane's model, etc. Since the control limits of the proposed chart are sequentially updated, the proposed control chart is adaptive and suitable for online process monitoring. In the existing state of the art, the nonhomogeneous/inhomogeneous Poisson process has been used to describe numerous random phenomena, including cyclone prediction, arrival times of calls to a call center in a hospital laboratory, arrival times of aircraft to the airspace around an airport and database transaction times, etc.

The rest of the chapter is organized as follows: In Section 6.2, some definitions related to nonhomogeneous Poisson, Lévy and power law processes, are given. The design of the power law process TBE chart is described in Section 6.3. In Section 6.4, some performance criteria for the evaluation of control charts effectiveness are discussed. These performance criteria include: average run length, coefficient of variance of the run length distribution, expected quadratic loss and the relative average run length. Some experiments related to random and sustained (fixed) shifts are also discussed in Section 6.4. The Bayesian and the classical methods for the estimation of unknown parameters are discussed in Section 6.5. The optimal stopping time based on two types of maintenance is also studied in the same Section 6.5. In Section 6.6, some goodness of fit tests are discussed. In Section 6.7, we discuss three illustrative examples to explain how the proposed methodology can be implemented in practical situations. Finally, we conclude the chapter in Section 6.8.

6.2 Some Preliminaries

In this section, we provide some necessary information for the further developments. We have defined HPP in Theorem-1.1.3. It is worth mentioning once again that the distribution of TBE in the HPP is exponential. This limits its application to many complex problems. Therefore, an alternative of the HPP is the NHPP. The NHPP is defined as:

Theorem 6.2.1 *(Insua et al. [2012]) A process $N(t)_{t\geq 0}$ be an increasing, right-continuous integer valued processes starting from zero. Let $0 < \lambda(t) < \infty$, then it is called nonhomogeneous Poisson process (NHPP) if:*

1. *N(0)=0 i.e. no event at time zero.*
2. *the number of events $N(s_2) - N(s_1)$ and $N(t_2) - N(t_1)$ in disjoint intervals $(s_1, s_2]$ and $(t_1, t_2]$ are independent random variables (independent increments).*
3. *there exists a function $\lambda(t)$ such that $\lim_{\Delta t\to 0} \frac{Pr(N(t+\Delta t)-N(t)=1)}{\Delta t} = \lambda(t)$.*
4. *for each $t > 0$, $\lim_{\Delta t\to 0} \frac{Pr(N(t+\Delta t)-N(t)=\geq 2)}{\Delta t} = 0$.*

If $N(t)_{t\geq 0}$ satisfies these conditions then it is called a nonhomogeneous Poisson process of rate $\lambda(t)$.

An important consequence of Theorem-6.2.1, i.e., conditions (i-iv), is that the number of failures in the interval $(s, t]$ where $t > s$, has the Poisson distribution with the parameter $\int_s^t \lambda(u)du$, i.e.,

$$Pr(N(t) - N(s) = k) = \frac{(\int_s^t \lambda(u)du)^k}{k!} exp\Big(-\int_s^t \lambda(u)du\Big). \tag{6.1}$$

Moreover, the stationarity assumption of the HPP has also been relaxed here. The function $\lambda(t)$ and $\Lambda(t) = \int_0^t \lambda(u)du$ are called the intensity function, and the cumulative intensity function of the NHPP process, respectively. Also, if $\lambda(t) = \lambda$, then the $NHPP(\lambda(.))$ is reduced to the homogeneous Poisson process $HPP(\lambda)$. Moreover, $\int_s^t \lambda(u)du$ is the mean and the variance of the NHPP, i.e., mean and variance of the time interval s to t. The following are the properties of the NHPP:

- *Conditioning on the Numbers:* Given the total number of arrivals $N(t) = n$ in the interval $(0, t]$ from a NHPP, the arrival instants of these n arrivals are distributed independently in the interval $(0, t]$ with the density function $\frac{\lambda(t)}{\int_s^t \lambda(u)du}$.
- *Superposition:* The superposition of the two NHHP with intensities $\lambda_1(t)$ and $\lambda_2(t)$ is a NHPP with intensity $\lambda(t) = \lambda_1(t) + \lambda_2(t)$.

- *Random Selection:* A random selection from NHPP with intensity $\lambda(t)$ such that each interval is selected, independent of others with the probability $p(t)$ (may depend on time) results in NHPP with intensity $p(t)\lambda(t)$.
- *Random Split:* If a NHPP with intensity $\lambda(t)$ is randomly split into two sub-processes with probabilities $p_1(t)$ and $p_2(t)$ with $p_1(t) + p_2(t) = 1$ then the resulting sub-processes are independent NHPP with intensities $p_1(t)\lambda(t)$ and $p_2(t)\lambda(t)$ respectively.

Since NHPP is characterized by an intensity function that varies over time, allowing events to be more or less likely at different time periods. As a consequence, the NHPP has no stationary increments unlike the HPP. Therefore, this property make NHPP suitable to describe rare (or high-quality) events whose rate of occurrence evolves over time (cf. Insua et al. [2012]). A typical example can be given by the life cycle of a new product, which is subject to an initial greater number of failures,followed by a steady rate of failures until they start occurring more and more, i.e., wear-out of the product.

Simulation of NHPP: The following is the steps of the NHPP generation using the random sampling or thinning approach.

1. Set t=0, n=0 and fix T.
2. Generate a random number $U \sim U(0,1)$.
3. Set $X = -\frac{1}{\lambda}\ln(u)$.
4. $t = t + X$ and if $t > T$ then stop.
5. Generate a random number $U \sim U(0,1)$.
6. If $U \leq \frac{\lambda(t)}{\lambda}$, set $n = n + 1, T_n = t$.
7. Go to step 2.

Note that n denotes the number of events in the time interval $(0, T]$ and $T_1, \cdots, T_n$ are the successive n event times of the NHPP($\lambda(t)$) in this time interval.

6.2.1 Power Law Process (PLP)

The NHPP($\lambda(.)$) for which $\lambda(t) = \lambda(t; \lambda, \beta) = \beta\lambda^\beta t^{\beta-1}$, where λ and $\beta > 0$ are the rate and the shape parameters, is called the power law process (PLP) and denoted by $PLP(\lambda, \beta)$.

Simulation of the PLP: To simulate event times of the PLP(λ, β) until a given number of jumps (failure), the following formula is commonly used.

$$T_i = T_{i-1} + \frac{1}{\lambda}\Big[\ln\frac{1}{1-u}\Big]^{\frac{1}{\beta}} \tag{6.2}$$

for $i = 1, 2, \ldots; T_0 = 0$ and u_i are the random numbers from $U(0, 1)$.

6.2.2 Infinitely Divisible (ID) Distribution

Consider a random variable T in a probability space $(\Omega, \mathcal{B}(\mathbb{R}), \mu)$ and its characteristic function is given by $\phi(u) = \mathbb{E}_\mu[\exp(\iota u T)] = \mathbb{E}_\mu[\cos uT] + \iota \mathbb{E}_\mu[\sin uT]$ *where* $\iota = \sqrt{-1}$ *and* $u \in \mathbb{R}$, then we state the following:

Definition 6.2.2.1 *The law μ is called infinitely divisible (ID) if for any integer $n > 0$, there exists a probability measure μ_n such that $\phi_\mu(u) = [\phi_{\mu_n}(u)]^n$.*

In other words, μ can be expressed as the n-th convolution power of μ_n and T as the sum $T(\omega) \overset{D}{\equiv} \sum_{i=1}^{n} T_i(\omega)$ for $\omega \in \Omega$, where $\{T_i\}_{i=1,\cdots,n}$ is a family of i.i.d. random variables having a common law μ_n. It is interesting to note that the family of all infinitely divisible distributions is closed under linear transformation, convolutions and limits.

Theorem 6.2.2.2 *The NHPP is a infinitely divisible (ID).*

Proof : *Since,*

$$\begin{aligned}\phi_{N(t)}(u) = \mathbb{E}_{\mu_k}[\exp(uk\iota)] &= \sum_{k=0}^{\infty} \exp(-\Lambda(t)) \frac{\Lambda(t)^k}{k!} \exp(uk\iota) \\ &= \exp\Big(\Lambda(t)\big(\exp(u\iota) - 1\big)\Big) \\ &= \Big[\exp\Big(\frac{\Lambda(t)}{n}\big(\exp(u\iota) - 1\big)\Big)\Big]^n\end{aligned}$$

Note that $\phi_{N(t)}(u) = \exp(\Psi_\mu(u))$, where $\Psi_\mu(u) = \Lambda(t)\big(\exp(u\iota) - 1\big)$. Hence, NHPP is ID.

6.2.3 Nonhomogeneous Lévy Process (NHLP)

NHLP is a general class of processes as compared to the homogeneous Lévy process where one can replace the assumption of stationary increments with non-stationary increments. To define it, let's assume that a stochastic basis $(\Omega, \mathcal{F}, \mathbb{F}, \mathbf{P})$, i.e., a probability space is equipped with the filtration $\mathbb{F} = \mathcal{F}_t = N(t)_{t \geq 0}$. Here, filtration means an increasing and right continuous family of sub-σ-fields of $\mathbb{F}$.

Definition 6.2.3.1 *(Andersen [2008]) An adapted, right continuous process $N(t)_{t \geq 0}$ with $N(0) = 0$ almost surely (a.s.) is a nonhomogeneous Lévy process if*

- N *has increments independent of the past, i.e., $N(t) - N(s)$ is independent of $\mathcal{F}_t; 0 \leq < t < \infty$;*
- N *is continuous in probability, i.e., $\forall \epsilon > 0, lim_{s \to 0} Pr(|N(t+s) - N(t)| \geq \epsilon) = 0$*

Theorem 6.2.3.2 *(Cont and Tankov [2004]) Consider a collection of triples* $(a, \Sigma, v) \equiv \{(a_t, \Sigma_t, v_t), t \geq 0\}$, *such that*

1. *For all* t; a_t *is a* $d \times 1$ *vector,* Σ_t *is a positive definite* $d \times d$ *matrix and* v_t *is positive measure on* $\mathbb{R}_0^d \equiv (\mathbb{R} \setminus \{0\})^d$ *with* $\int_{\mathbb{R}_0^d}(1 \wedge absx^2)v_t(dx) < \infty$.
2. *Positiveness:* $a_0 = 0, \Sigma_0 = 0, v_0 = 0$ *and for all* s, t *such that for* $s \leq t$; $A_t - A_s$ *is a positive definite* $d \times d$ *matrix and* $v_t(A) \geq v_s(A)$ *for all measurable sets* $A \in \mathcal{B}(\mathbb{R}^d)$.
3. *Continuity: If* $s \to t$ *then* $a_s \to a_t, \Sigma_s \to \Sigma_t$ *and* $v_s(A) \to v_t(A)$ *for all measurable sets* $A \in \mathcal{B}(\mathbb{R}^d)$ *such that* $A \subset \{x : |x| > \epsilon\}$ *for some* $\epsilon > 0$

then by considering N *be a* $d-$*dimensional nonhomogeneous Lévy process, one can write the Lévy Khintchine formula as follows:*

$$\psi_N(u, t) = \mathbb{E}[\exp(\iota u^T N_t)] = \exp(\Psi(u, t))$$

where

$$\Psi(u, t) = \iota u^T a_t - 0.5 u^T \Sigma_t u + \int_{\mathbb{R}_0^d} [\exp(\iota u^T N) - 1 - \iota u^T N 1_{\{|x|<1\}}] v_t(dx)$$

The triplet (a_t, Σ_t, v_t) *characterizes the process and knows as a Lévy triplet or spot characteristics.*

The standard version of the Lévy-Khintchine formula is naturally obtained as a special case when $a_t = bt, \Sigma_t = \Gamma t, v_t = \mu t$, i.e., characteristic triplet of the homogeneous Lévy process will be (b, Γ, μ) (cf. Kluge [2005]).

Theorem 6.2.3.3 *The NHPP is NHLP.*

Proof : *From Lévy-Khintchine nonhomogeneous formulation, one can get* $a_t = 0, \Sigma_t = 0$ *and* $v_t = \Lambda(t)\delta_t$ *where* δ_t *is the Dirac measure supported on* $\{1\}$. *Thus, it is a NHLP.*

6.3 Control Charts for the Power Law Process

In this section, we introduce a new TBE control chart using the PLP. Before proceeding further, we give joint and conditional distributions of the n successive times.

Let $T_1, T_2, \cdots, T_n$ denote the first n successive times of the occurrence of the failures from the PLP. We assume the following form of the failure rate: $\lambda(t) = \beta\lambda^\beta t^{\beta-1}$, where λ and β are the rate and the shape parameters, respectively. The joint probability density function of $T_1, T_2, \cdots, T_n$ can be written as (cf. Muralidharan et al. [2008]):

$$f(t_1, t_2, \cdots, t_n) = (\beta\lambda^\beta)^n \prod_{i=1}^{n} t_i^{\beta-1} \exp\left(-(t_n\lambda)^\beta\right) \tag{6.3}$$

for $0 < t_1 < t_2 < \cdots < t_n < \infty$ and $\lambda, \beta > 0$. For a known β, t_n is a complete sufficient statistic for λ. The following densities can easily be derived by suitably integrating Equation-6.3 as follows:

$$\begin{aligned} f(t_i) &= \int_{t_1}\int_{t_2}\int_{t_3}\cdots\int_{t_{i-1}}\int_{t_{i+1}}\cdots\int_{t_n} f(t_1, t_2, \cdots, t_n)dt_1dt_2\cdots dt_{i-1}dt_{i+1}\cdots dt_n \\ &= \frac{\beta\lambda^{i\beta}}{\Gamma(i)}t_i^{i\beta-1}\exp\big(-(t_i\lambda)^{\beta}\big), \qquad 0 < t_i < \infty \end{aligned} \tag{6.4}$$

$$\begin{aligned} f(t_i, t_n) &= \int_{t_1}\int_{t_2}\int_{t_3}\cdots\int_{t_{i-1}}\int_{t_{i+1}}\cdots\int_{t_{n-1}} f(t_1, t_2, \cdots, t_n)dt_1dt_2\cdots dt_{i-1}dt_{i+1}\cdots dt_{n-1} \\ &= \frac{\beta^2\lambda^{n\beta}}{\Gamma(i)\Gamma(n-i)}t_i^{i\beta-1}t_n^{\beta-1}(t_n^{\beta}-t_i^{\beta})^{n-i-1}\exp\big(-(t_n\lambda)^{\beta}\big), \quad 0 < t_i < t_n < \infty \end{aligned} \tag{6.5}$$

and

$$f(t_n) = \frac{\beta\lambda^{n\beta}}{\Gamma(n)}t_n^{n\beta-1}\exp\big(-(t_n\lambda)^{\beta}\big), \qquad 0 < t_n < \infty$$

Moreover, the conditional distribution of t_i given t_n is

$$f(t_i|t_n) = \frac{\Gamma(n)}{\Gamma(i)\Gamma(n-i)}\frac{\beta}{t_n}\left(\frac{t_i}{t_n}\right)^{i\beta-1}\left[1-\left(\frac{t_i}{t_n}\right)^{\beta}\right]^{n-i-1} \qquad 0 < t_i < t_n < T < \infty$$

Thus, the true reliability of this process depends on the entire history of the failures process. Moreover, the reliability of the process at time t based on the distribution of $T_i = t_i$ can be written as follows:

$$R_i(t) = P(T_i > t) = \int_t^{\infty} f(t_i)dt_i = \frac{\Gamma(i, t^{\beta}\lambda^{\beta})}{\Gamma(i)}, \quad i > 0 \tag{6.6}$$

This reliability will depend on the i-th realizations of the process. If $i = n$ then the reliability will be based on the first n realizations (cf. Muralidharan et al. [2008]). Note that for a PLP process, apart from the time to first failure, intervals between points are not Weibull-distributed.

As we have explained in the introduction section (cf. Section-6.1) that in many applications, the event rate varies (or drifts) over time, and thus the time T may be assumed to follow a PLP. We know that for the PLP, the event rate is proportional to a power of the time. This power is equal to the shape parameter minus one. As a result, a value of the shape parameter greater than one indicates that the event rate will increase with time. This happens if events are more likely to occur as time goes on. Similarly, the shape parameter less than indicates that the event rate will decrease with time, i.e., the system

improves.

To develop a TBE chart using the PLP, we need to work out the conditional density of T_i given T_{i-1} for $i \geq 1$ and $T_0 = 0$. Thanks to the independent increments property of the NHPP (cf. Theorem-6.2.1), the conditional distribution function of T_i given T_{i-1} can be derived as follows:

$$\begin{aligned} P(T_i \leq t_i | T_{i-1} = t_{i-1}) &= 1 - P(N(t_i) - N(T_{i-1}) = 0 | T_{i-1} = t_{i-1}) \\ &= 1 - P(N(t_i) - N(t_{i-1}) = 0) = 1 - \exp\big(\Lambda(t_i) - \Lambda(t_{i-1})\big) \end{aligned} \tag{6.7}$$

where $T_i = T_{i-1} + X_i$, i.e., $X_i = T_i - T_{i-1}$, and by letting $X_i = x$ it becomes $T_i = T_{i-1} + x$. Therefore,

$$P(X_i \leq x) = 1 - \exp\big(-\Lambda(t_{i-1} + x) + \Lambda(t_{i-1})\big) \tag{6.8}$$

In particular, for the PLP, i.e., $\lambda(t) = \beta\lambda^\beta t^{\beta-1}$, the waiting time to the next failure given a failure at a time t_{i-1}, has the distribution function

$$F_{X_i}(x | T_{i-1} = t_{i-1}) = P(X_i \leq x) = 1 - \exp\left(-\lambda^\beta \left[(t_{i-1} + x)^\beta - t_{i-1}^\beta\right]\right) \tag{6.9}$$

To derive the mean time between failure for the PLP, we need:

$$f(x | t_{i-1}) = \frac{d}{dt_i} F(x | t_{i-1}) = \beta\lambda^\beta (t_{i-1} + x)^{\beta-1} \exp\big(-\lambda^\beta \left[(t_{i-1} + x)^\beta - t_{i-1}^\beta\right]\big) \tag{6.10}$$

Thus,

$$\begin{aligned} E(X) &= \int_0^\infty x f(x | t_{i-1}) dx = (\lambda t_{i-1})^{\beta-1} \exp\big(\lambda t_{i-1}\big)^\beta \times R \\ &= (\lambda t_{i-1})^{\beta-1} \exp\big(\lambda t_{i-1}\big)^\beta \left[\frac{1}{\lambda}\Gamma\big(2\beta^{-1}, (\lambda t_{i-1})^\beta\big) - t_{i-1}\Gamma\big(1\beta^{-1}, (\lambda t_{i-1})^\beta\big)\right] \end{aligned} \tag{6.11}$$

where $R = \left[\frac{1}{\lambda}\int_{(\lambda t_{i-1})^\beta}^\infty u^{2/\beta-1}\exp(-u)du - t_{i-1}\int_{(\lambda t_{i-1})^\beta}^\infty u^{1/\beta-1}\exp(-u)du\right]$ and $\Gamma(.)$ is the incomplete gamma function, i.e., $\Gamma(a, x) = \int_x^\infty v^{a-1}\exp(-v)dv$.

A two-sided TBE power law quantity control (PLQC) chart can be constructed by evaluating the specified percentiles of Equation-6.9, i.e., find the $LCL = F^{-1}(\alpha/2 | T_{i-1} = t_{i-1})$ and $UCL = F^{-1}(1 - \alpha/2 | T_{i-1} = t_{i-1})$ to get the lower control limit (LCL) and upper control limit (UCL), respectively. Note that α is the pre-specified false alarm probability. The simplified form of the control limits for the PLP can be expressed as follows: $LCL_i = \left[t_{i-1}^\beta + \frac{1}{\lambda^\beta}\ln\frac{2}{2-\alpha}\right]^{\frac{1}{\beta}} - t_{i-1}$, $CL_i = \left[t_{i-1}^\beta + \frac{1}{\lambda^\beta}\ln(2)\right]^{\frac{1}{\beta}} - t_{i-1}$, and $UCL_i = \left[t_{i-1}^\beta + \frac{1}{\lambda^\beta}\ln\frac{2}{\alpha}\right]^{\frac{1}{\beta}} - t_{i-1}$.

The decision criterion for the PLQC chart is as follows: For the two-sided PLQC chart, the plotting statistic X, i.e., TBE, is plotted against the failure number whenever

a defect is observed. If a point is plotted below the LCL, then it is a signal that the process has (statistically) deteriorated. Similarly, if a point is plotted above the UCL, then it is a sign that the process may have improved. It is interesting to note that the above reported control limits are sequentially updated with the step $i-1$ observed failure time. Therefore, the proposal is appropriate not only for the off-line process monitoring, but also for the online process monitoring. However, this flexibility has a price that will be discussed in the next section. To detect only the process deterioration, a single limit PLQC chart can be obtained by finding $LCL = F^{-1}(\alpha|T_{i-1} = t_{i-1})$, i.e., $LCL_{one-sided} = \left[t_{i-1}^{\beta} + \frac{1}{\lambda^{\beta}} \ln \frac{1}{1-\alpha}\right]^{\frac{1}{\beta}} - t_{i-1}$, without the UCL, or $UCL = +\infty$.

6.3.1 An extension of the PLQC chart

As we have noticed in Section-3.4 that sometime the interpretation of the TBE control chart is difficult, and an alternative was suggested by Chan et al. [2002], i.e., CPC chart. We define a power law cumulative probability control (PLCPC) charts by plotting Equation-6.9 against the $LCL = \alpha/2$ and the $UCL = 1 - \alpha/2$, respectively.

6.4 Performance Evaluation

In this section, we use the average run length (ARL), the coefficient of variance of the run length distribution (CV), expected quality loss (EQL) and the relative average run length (RARL) to assess the control chart performance (cf. Section-3.4).

6.4.1 Average Run Length (ARL)

The average of the number of samples taken from a process until the monitoring statistic falls outside the control limits is known as the ARL (cf. Section-3.4). To assess the ARL performance of the PLQC charts, a simulation study has been conducted, and results are given in Tables 6.1-6.2, and Figure-6.1. We used 0.0027 as the false alarm probability to calculate the ARL values, i.e., the in-control ARL is 370. Note that first we would study the chart performance by using one-step ahead control limits and then extend to full sequential settings. We generated data by introducing different size of shifts, as mentioned in Tables 6.1-6.2/Figure-6.1, and monitored with the one-step ahead control limits. The index when the control limits detected an out-of-control signal was noted. This process was repeated a large number of times, e.g. 10^6, and the average of the out-of-control indexes or failure numbers have been given in Tables 6.1-6.2/ Figure-6.1. Moreover, the CV values have also been tabulated in Tables 6.1-6.2.

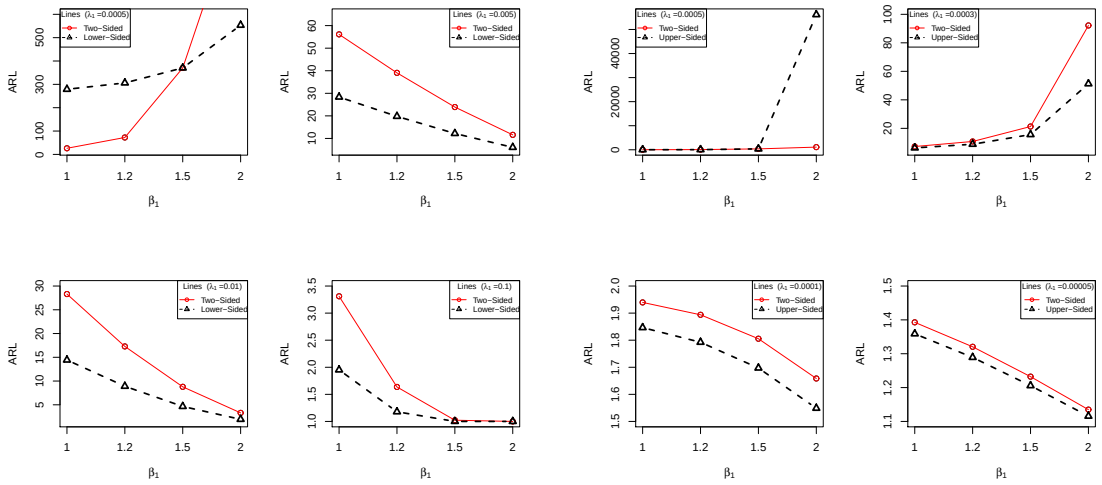

(a) Two sided versus Lower sided (b) Two sided versus Upper sided

Figure 6.1: One step ahead ARL for process deterioration detection at $\alpha = 0.0027$

6.4.2 Discussion on the ARL study (one-step ahead)

We considered the shifts for the following two cases:

A λ decreases from $\lambda_0 = 0.0005$ to $\lambda_1 \in \{0.0003, 0.0001, 0.00005\}$ while β shifts from $\beta_0 = 1.5$ to $\beta_1 \in \{1, 1.2, 1.5, 2\}$ (i.e., PI-IHR).

B λ increases from $\lambda_0 = 0.0005$ to $\lambda_1 \in \{0.005, 0.01, 0.1\}$ and β shifts from $\beta_0 = 1.5$ to $\beta_1 \in \{1, 1.2, 1.5, 2\}$ (i.e., TD-IHR).

When the process is in-control, i.e., $\lambda_1 = \lambda_0$ and $\beta_1 = \beta_0$, the ARL value is equal to the nominal value, i.e., 370.

Case A- a decrease in λ: When the rate parameter decreases from its nominal value, the system shows some improvement signs. Therefore, the role of an expert in such a situation would be to maintain that position for the system stability. Since the shape parameter β is greater than one, the overall system performance deteriorates, and it could be labeled as a partial improvement (PI). The PI occurs when some temporary actions are taken to improve a system reliability or to stop its deterioration, e.g. replace some components of a system for its temporary functioning. In our study, we fixed the shape parameter $\beta_0 = 1.5$ (for in-control process) while $\beta_1 \in \{1, 1.2, 1.5, 2\}$ to represent the out-of-control situation. The rate parameter shifted from $\lambda_0 = 0.0005$ to $\lambda_1 \in \{0.0003, 0.0001, 0.00005\}$. To check the PD, we have used the upper-sided control chart and further it is compared with the two-sided chart. Therefore, in Table-6.1/Figure-6.1b, we compared the ARL values for the two-sided and the upper-sided charts. The CV values have also been reported below the ARL, and one could easily recover the standard deviation of the run length distribution using the CV and the ARL values.

It is observed from Table-6.1/Figure-6.1b that the ARL values increase as the size of the shift in the shape parameter increase, and therefore, we conclude that the shape parameter has a significant impact on the control chart performance. The large shifts in the shape parameter could be detected quickly as compared to the small shifts. For the fixed β, if a shift occurred in the rate parameter, i.e. λ, the upper-sided chart would detect it quickly as compared to the two-sided chart. However, the said detection ability of the chart is also dependent on the size of a shift, i.e., the large shifts in λ will be detected quickly in contrast to the small shifts. For the $\beta < 1.5$, the ARL values are smaller than the case when we have $\beta > 1.5$. Moreover, it has been observed that the CV values decrease with the size of shifts in the rate parameter.

Case B- an increase in λ: This is an important case where we are concerned in the process deterioration detection, and it could be labeled as a total deterioration (TD), i.e., $\beta > 1$ and λ increases from its nominal value. In our study, we fixed the shape parameter $\beta_0 = 1.5$ (for in-control process) while we let $\beta_1 \in \{1, 1.2, 1.5, 2\}$ to represent the out-of-control situation. The rate parameter shifted from $\lambda_0 = 0.0005$ to $\lambda_1 \in \{0.005, 0.01, 0.1\}$. When the system deteriorates, the practitioner needs to use the lower-sided control chart, therefore, we compare the lower-sided chart with the two-sided chart in Table-6.2/Figure-6.1a.

For the TD case, when the shape parameter is less than its nominal value, i.e., $\beta < 1.5$, the ARL values are greater than the case $\beta > 1.5$. Thus, an upward shift in the shape parameter would be detected efficiently than the downward shifts. Note that an upward shift means the case where β is greater than its nominal in-control value. Similarly, a downward shift implies the case where β is smaller than its fixed in-control value. The lower-sided chart is more sensitive to detect an out-of-control situation, and it outperforms than the counterpart, i.e., two-sided chart. For the fixed shape parameter, the occurrence of a shift in the rate parameter λ is detected quickly by the lower-sided chart except the case when $\lambda = 0.0005$. The detection of a shift in the shape parameter is quite slow using the lower-sided chart than the two-sided chart. However, this behavior is specific to the case when $\lambda = 0.0005$, otherwise the detection ability of the lower-sided chart has no question mark. The values of the ARL for $\beta < 1.5$ are greater as compared to the case $\beta > 1.5$, i.e., ARL is biased. The CV values have an inverse relationship with the size of shifts in the rate parameter, i.e., the CV decreases with the increase of a shift in λ. Moreover, the CV values approach to one for small to moderate shifts, i.e., either in the shape or the rate parameter.

Table 6.1: ARL study of the PI-IHR case using $\alpha = 0.0027, \lambda_0 = 0.0005, \beta_0 = 1.5, t_1 = 500$ and $\lambda_1 \in \{0.0003, 0.0001, 0.00005\}$, $\beta_1 \in \{1, 1.2, 1.5, 2\}$ for the upper and two-sided PLQC charts.

β	λ	Two-Sided				Upper-Sided			
		0.0005	0.0003	0.0001	0.00005	0.0005	0.0003	0.0001	0.00005
1	ARL	26.239	7.25337	1.93946	1.39278	21.4646	6.29555	1.84648	1.35885
	CV	0.980759	0.928511	0.695983	0.531048	0.976428	0.917146	0.677074	0.513892
1.2	ARL	72.4083	10.7888	1.89376	1.3205	56.0121	8.85307	1.79235	1.28917
	CV	0.993071	0.952529	0.686986	0.492657	0.991033	0.941831	0.664887	0.473609
1.5	ARL	370.37	21.2746	1.80541	1.23232	370.37	15.6241	1.69725	1.20567
	CV	0.998649	0.976215	0.667914	0.434193	0.998649	0.967469	0.640946	0.413018
2	ARL	1104.94	92.184	1.65858	1.13484	56164.4	51.2632	1.54874	1.11556
	CV	0.999547	0.994561	0.630138	0.344705	0.999991	0.990198	0.595243	0.321858

Table 6.2: ARL study of the TD-IHR case using $\alpha = 0.0027, \lambda_0 = 0.0005, \beta_0 = 1.5, t_1 = 500$ and $\lambda_1 \in \{0.0003,\ 0.0001, 0.00005\}$, $\beta_1 \in \{1, 1.2, 1.5, 2\}$ for the lower and two-sided PLQC charts.

β	λ	Two-Sided				Lower-Sided			
		0.0005	0.005	0.01	0.1	0.0005	0.005	0.01	0.1
1	ARL	26.239	56.1192	28.3119	3.31079	278.897	28.3427	14.4258	1.95134
	CV	0.980759	0.99105	0.982181	0.835438	0.998206	0.9822	0.964717	0.698235
1.2	ARL	72.4083	39.0618	17.289	1.63655	306.185	19.7917	8.90525	1.17841
	CV	0.993071	0.987117	0.970649	0.623664	0.998366	0.974409	0.942182	0.389102
1.5	ARL	370.37	23.912	8.78621	1.0224	370.37	12.2034	4.65541	1.00048
	CV	0.998649	0.978867	0.941374	0.14801	0.998649	0.958152	0.886113	0.0218503
2	ARL	1104.94	11.5912	3.30093	1.00001	553.322	6.04328	1.94183	1.0
	CV	0.999547	0.955891	0.834898	0.00	0.999096	0.913525	0.696435	0.0

6.4.3 Complete Performance Evaluation

As we have mentioned earlier that the control limits of the PLQC charts are sequentially updated with the observed failure time. Therefore, every in-control or out-of-control observation will essentially contribute to the uncertainty of the sequential control limits and consequently, only a very large shift will be detected efficiently. Since extreme false alarm probabilities are involved in the construction of the control limits in adaptive setup, the control limits deteriorate/drift (cf. Figure-6.2). The control chart will be insensitive even though one might have the knowledge of a shift in the process. Note that an exception of the detection of a very large shift is guaranteed in the above setup. Therefore, to check control limits for a possible trend, we propose $F(x|T_{i-1}) \leq C_D$ and $F(x|T_{i-1}) \geq C_I$, where C_D and C_I denote the stopping criteria for the process deterioration and improvement, respectively. We used $C_D = 0.11$ and $C_I = 0.89$ as the stopping criteria in our study. A similar rule has been used by Toubia-Stucky et al. [2012] for the sequential monitoring of the geometric chart. Note that the proposed stopping criteria may give frequent false alarms, which could be adjusted by choosing appropriate (small) values of C_D and C_I.

We extend the definitions presented in Section-3.4.3 and propose the following four definitions for the PLP monitoring.

Definition 6.4.3.1 *For the PLP, if $\beta > 1$, i.e., increasing hazard rate (IHR), and λ is decreasing then the system is partial improving (PI). We label this situation as the PI-IHR.*

Definition 6.4.3.2 *For the PLP, if $\beta > 1$, i.e., increasing hazard rate (IHR), and λ is increasing then system is totally deteriorating (TD). We label this situation as the TD-IHR.*

Definition 6.4.3.3 *For the PLP, if $\beta < 1$, i.e., decreasing hazard rate (DHR), and λ is decreasing then system is totally improving (TI). We label this situation as the TI-DHR.*

Definition 6.4.3.4 *For the PLP, if $\beta < 1$, i.e., decreasing hazard rate (DHR), and λ is increasing then system is partially deteriorating (PD). We label this situation as the PD-DHR.*

To study the control chart performance we considered shifts for the following cases:

A Increasing Hazard Rate (IHR), i.e., $\beta > 1$

1. λ decreases from $\lambda_0 = 0.0005$ to $\lambda_1 \in \{0.00045, 0.0003, 0.0002, 0.0001\}$ while β shifts from $\beta_0 = 1.5$ to $\beta_1 \in \{1, 1.2, 1.45, 1.55, 2\}$ [i.e., Partial Improvement (PI)].

2. λ increases from $\lambda_0 = 0.0005$ to $\lambda_1 \in \{0.00055, 0.0008, 0.005, 0.01\}$ and β shifts from $\beta_0 = 1.5$ to $\beta_1 \in \{1, 1.2, 1.45, 1.55, 2\}$ [i.e., Total Deterioration (TD)].

B Decreasing Hazard Rate (DHR), i.e., $\beta < 1$

1. λ decreases from $\lambda_0 = 0.0005$ to $\lambda_1 \in \{0.00045, 0.0003, 0.0002, 0.0001\}$ and β shifts from $\beta_0 = 0.5$ to $\beta_1 \in \{0.2, 0.45, 0.55, 0.7, 0.9, 1.0\}$ [i.e., Total Improvement (TI)].
2. λ increases from $\lambda_0 = 0.0005$ to $\lambda_1 \in \{0.00055, 0.0008, 0.005, 0.01\}$ andβ shifts from $\beta_0 = 0.5$ to $\beta_1 \in \{0.2, 0.45, 0.55, 0.7, 0.9, 1.0\}$ [i.e., Partial Deterioration (PD)].

Case A-1 a decrease in λ: When the shape parameter β of the PLP is greater than one and λ decreases from its nominal value, we expect that the overall performance of the system will deteriorate. However, one could observe some temporary improvements due to a decrease in the rate parameter λ, e.g. some components of a machine could be replaced to get an acceptable output. A possible task of an expert could be to stabilize such improvements and achieve the long-run stability of the process, i.e., permanent improvement. Thus, we labeled this case as the partial improvement (PI). We compare the upper-sided chart with the two-sided chart in this study. We fixed the shape parameter $\beta_0 = 1.5$ (for in-control process) while $\beta_1 \in \{1, 1.2, 1.45, 1.55, 2\}$ to represent the out-of-control situation. The rate parameter shifted from $\lambda_0 = 0.0005$ to $\lambda_1 \in \{0.00045, 0.0003, 0.0002, 0.0001\}$. From Table-6.3, we noticed that when $\beta = 1.5$ and $\lambda = 0.0005$, the ARL of the upper-sided chart is approximately equal to the desired in-control ARL. However, the in-control performance of the two-sided chart is not appreciable as compared to the out-of-control performance. Both, the upper-sided and the two-sided charts detect efficiently the large shifts, either in the shape parameter or the rate parameter, as compared to small-to-moderate shifts. However, it does not mean that a small shift cannot be detected efficiently. From Table-6.3, one can observe that small shifts can also be detected without a great loss of efficiency using the proposed criteria. For the fixed β, the small shifts in λ would take more data points to raise an out-of-control signal. Moreover, the CV of the two-sided chart is smaller than the upper-sided chart, and therefore, we support the superiority of the two-sided chart.

Case A-2 an increase in λ: This is an important case because we are concerned in the detection of a process deterioration. Since the shape parameter β is greater than one while the rate parameter increases from its nominal value, the system could be labeled as total deterioration (TD). To study this case, we fixed the shape parameter $\beta_0 = 1.5$ (for in-control process) while we let $\beta_1 \in \{1, 1.2, 1.45, 1.55, 2\}$ to represent the out-of-control situation. The rate parameter shifted from $\lambda_0 = 0.0005$ to $\lambda_1 \in \{0.00055, 0.0008, 0.005, 0.01\}$. A comparison study of the lower-sided and two-sided charts has been given in Table-6.4.

From Table-6.4, we notice that the downward shifts in the shape parameter, i.e. $\beta < 1.5$, are detected quickly as compared to the upward shifts, i.e. $\beta > 1.5$. For a fixed β, a small shift in λ takes large data points to produce an out-of-control alarm as compared to a large shift (cf. Table-6.4). The same argument is valid for the case when λ is fixed, and a shift occurs in β. Thus, the two-sided chart is superior than the lower-sided chart based on the ARL and the CV values.

Case B-1 a decrease in λ: This is again another important case because here we consider the case when λ decreases, and $\beta < 1$. Therefore, it is a sign that the system failures becoming less frequent, i.e., the system improves, and can be labeled as a total improvement (TI). We suggest the use of the upper-sided chart for the detection of a process improvement. To study the TI, we fixed the shape parameter $\beta_0 = 0.5$ (for in-control process) while $\beta_1 \in \{0.2, 0.45, 0.55, 0.7, 0.9, 1.0\}$ to represent the out-of-control situation. The rate parameter shifted from $\lambda_0 = 0.0005$ to $\lambda_1 \in \{0.00045, 0.0003, 0.0002, 0.0001\}$. In Table-6.5, we have computed the ARL values of the two-sided and the upper-sided charts. We skipped the standard deviation of the run length (SDRL) distribution and reported only the CV values as the $SDRL = ARL * CV$. In this case, the downward shifts, i.e. $\beta < 0.5$, are detected more quickly as compared to the upward shifts, i.e., $\beta > 0.5$. This comment is not specific only to the upper-sided chart, but also true for the two-sided chart. For a fixed β, both the upper-sided and the two-sided charts are good in the detection of a large shift in λ. Moreover, one can observe that the detection ability of both charts has been greatly improved with our proposed check.

Case B-2 an increase in λ: In this case, since the shape parameter β is less than one and the events' occurrence rate is assumed to increase, one could label this situation as a partial deterioration (PD). This type of situation in a reality occurs when the system improves overall, but due to some changes, i.e., change in material, change in the labor force or some other environmental stress, etc., we observe a temporary deterioration. Since a practitioner in such cases wants to stop the deterioration as soon as possible, we suggest the use of the lower-sided chart for the PD detection. To study the PI, we fixed the shape parameter $\beta_0 = 0.5$ (for in-control process) while $\beta_1 \in \{0.2, 0.45, 0.55, 0.7, 0.9, 1.0\}$ to represent the out-of-control situation. The rate parameter allowed to shift from $\lambda_0 = 0.0005$ to $\lambda_1 \in \{0.00055, 0.0008, 0.005, 0.01\}$. The ARL study has been tabulated to assess the effectiveness of the lower-sided and the two-sided charts. Moreover, the CVRL values have also been computed in Table-6.6. From Table-6.6, it is observed that the proposed charts detect the different size of shifts very efficiently.

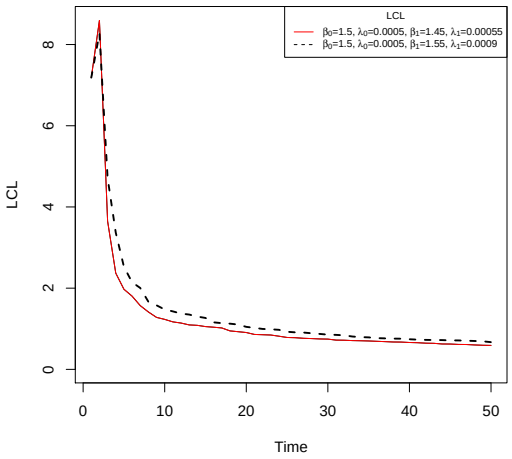

(a) Control limits of the lower-sided PLQC chart

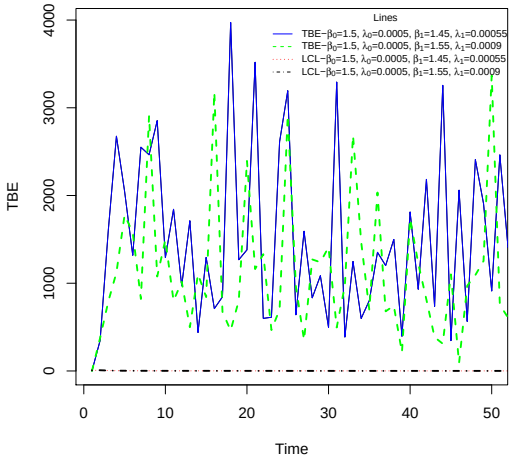

(b) Control limits with TBE data of the lower sided PLQC chart

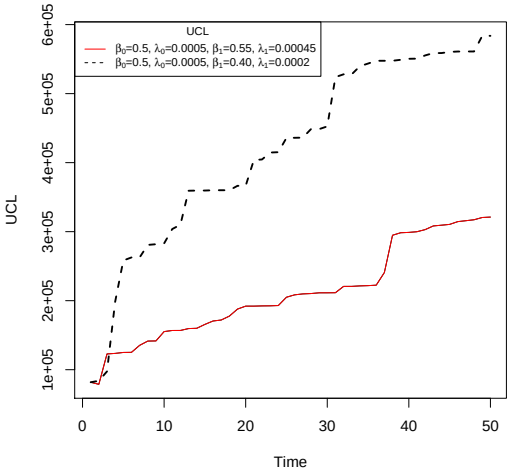

(c) Control limit of the upper sided PLQC chart

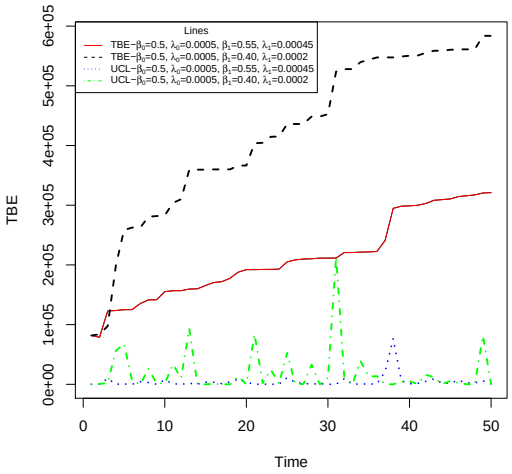

(d) Control limits with TBE data of an upper sided PLQC chart

Figure 6.2: Control Limits' Drift/Deterioration for the PLP using $\alpha = 0.0027$

Table 6.3: ARL study of the PI-IHR case based on $\alpha = 0.0027, \lambda_0 = 0.0005, \beta_0 = 1.5, t_1 = 500$ and $\lambda_1 \in \{0.00045, 0.0003, 0.0002, 0.0001\}$, $\beta_1 \in \{1, 1.2, 1.45\ , 1.5, 1.55, 2\}$ for the upper and two-sided PLQC charts.

β	λ	Two-Sided					Upper-Sided				
		0.0005	0.00045	0.0003	0.0002	0.0001	0.0005	0.00045	0.0003	0.0002	0.0001
1.0	ARL	2.76508	2.60774	2.03478	1.64707	1.30081	7.4053	6.43866	3.9809	2.71166	1.73256
	CV	0.798039	0.783969	0.713585	0.627254	0.480557	0.593461	0.603243	0.637749	0.642405	0.579003
1.2	ARL	3.42249	3.09178	2.14779	1.6339	1.24192	8.44924	7.15568	4.14735	2.69093	1.63697
	CV	0.832643	0.818712	0.730111	0.621278	0.441145	0.525365	0.545895	0.592979	0.610921	0.547568
1.45	ARL	4.41562	3.7687	2.2187	1.57529	1.18462	9.57078	8.03193	4.32932	2.64269	1.53934
	CV	0.850037	0.839758	0.742010	0.604632	0.394823	0.460285	0.481649	0.544787	0.576214	0.515929
1.5	ARL	4.61784	3.89819	2.23176	1.55999	1.17155	9.78106	8.1484	4.36549	2.62957	1.51878
	CV	0.844822	0.837337	0.740214	0.601753	0.383938	0.449371	0.467718	0.537472	0.569986	0.50611
1.55	ARL	4.87504	4.05792	2.22552	1.54607	1.16582	9.99865	8.32052	4.39821	2.62674	1.50011
	CV	0.843439	0.836550	0.742875	0.594975	0.376525	0.440578	0.460670	0.523574	0.562432	0.502926
2.0	ARL	7.24768	5.4279	2.22726	1.43335	1.09384	11.55485	9.41566	4.61587	2.57323	1.38307
	CV	0.768301	0.807712	0.737603	0.550407	0.292026	0.365794	0.383242	0.452513	0.512749	0.455216

Table 6.4: ARL study of the TD-IHR case using $\alpha = 0.0027, \lambda_0 = 0.0005, \beta_0 = 1.5, t_1 = 500$ and $\lambda_1 \in \{0.000055, 0.0008, 0.005, 0.01\}$, $\beta_1 \in \{1, 1.2, 1.45, 1.5,\ 1.55, 2\}$ for the lower and two-sided PLQC charts.

β	λ	Two-Sided					Lower-Sided				
		0.0005	0.00055	0.0008	0.005	0.01	0.0005	0.00055	0.0008	0.005	0.01
1	ARL	2.77029	2.93175	3.30734	1.28847	1.05352	7.13715	6.57216	4.69799	1.2878	1.05174
	CV	0.796581	0.810449	0.832053	0.472346	0.224333	0.927055	0.924629	0.888609	0.471286	0.222016
1.2	ARL	3.4344	3.73137	4.48907	1.24557	1.0249	10.17999	9.26196	6.0577	1.24564	1.02393
	CV	0.833410	0.841793	0.872314	0.442941	0.156053	0.950986	0.948720	0.912047	0.443015	0.153482
1.45	ARL	4.38397	5.04923	6.714	1.19643	1.00724	16.08578	14.11715	8.44837	1.19651	1.00712
	CV	0.845361	0.852602	0.875454	0.402399	0.084521	0.969507	0.963519	0.939252	0.407040	0.083839
1.5	ARL	4.63317	5.35429	7.27372	1.19141	1.00528	17.62839	15.53338	8.98598	1.18936	1.00589
	CV	0.846623	0.847747	0.868579	0.401056	0.072365	0.972214	0.963354	0.942952	0.397814	0.076848
1.55	ARL	4.84745	5.68234	7.84248	1.18253	1.00428	19.35293	16.83149	9.66755	1.18031	1.0044
	CV	0.841624	0.842662	0.865811	0.392049	0.065156	0.975161	0.968993	0.947149	0.388843	0.066047
2	ARL	7.25932	9.293	14.75946	1.12066	1.00016	44.81022	37.37428	17.84751	1.119	1.00018
	CV	0.765642	0.724668	0.770523	0.327015	0.012646	0.990744	0.983135	0.974265	0.325517	0.013413

Table 6.5: ARL study of the TI-DHR case based on $\alpha = 0.0027, \lambda_0 = 0.0005, \beta_0 = 0.5, t_1 = 500$ and $\lambda_1 \in \{0.00045, 0.0003, 0.0002, 0.0001\}$, $\beta_1 \in \{0.2, 0.45, 0.5, 0.55, 0.7, 0.9, 1\}$ for the upper and two-sided PLQC charts.

β	λ	Two-Sided					Upper-Sided				
		0.0005	0.00045	0.0003	0.0002	0.0001	0.0005	0.00045	0.0003	0.0002	0.0001
0.2	ARL	1.38963	1.38426	1.38704	1.37664	1.3682	4.41575	4.24592	3.78954	3.42081	2.91266
	CV	0.529876	0.528687	0.528363	0.521653	0.520828	0.876652	0.872281	0.858253	0.840388	0.812624
0.45	ARL	2.31502	2.32613	2.32657	2.25503	2.02751	11.22149	10.01608	6.76986	4.95017	3.2115
	CV	0.755915	0.761312	0.750697	0.743738	0.711940	0.954690	0.953308	0.923728	0.889331	0.825991
0.5	ARL	2.59214	2.616	2.6155	2.51889	2.16707	14.39046	12.51068	7.85791	5.37231	3.29469
	CV	0.782320	0.785106	0.783241	0.774954	0.729714	0.970043	0.957811	0.928341	0.898162	0.834950
0.55	ARL	2.90924	2.93246	2.97054	2.79956	2.32067	18.82523	15.97906	9.1675	5.90478	3.36477
	CV	0.806299	0.813713	0.813130	0.798745	0.752748	0.975596	0.963383	0.941815	0.908575	0.839918
0.7	ARL	4.06941	4.19491	4.35625	3.95384	2.79032	51.11765	38.7715	15.686	7.92776	3.57451
	CV	0.866796	0.869932	0.875035	0.863316	0.800717	0.994439	0.982101	0.966045	0.933496	0.848293
0.9	ARL	6.13209	6.57307	7.67814	6.62031	3.4032	338.0195	199.3241	39.4575	12.90469	3.93794
	CV	0.913859	0.923357	0.928717	0.918861	0.842021	0.997038	0.998043	0.989995	0.952259	0.861219

Table 6.6: ARL study of the PD-DHR case using $\alpha = 0.0027, \lambda_0 = 0.0005, \beta_0 = 0.5, t_1 = 500$ and $\lambda_1 \in \{0.000055,$ $0.0008, 0.005, 0.01\}$, $\beta_1 \in \{0.2, 0.45, 0.5, 0.55, 0.7, 0.9, 1\}$ for the lower and two-sided PLQC charts.

β	λ	Two-Sided					Lower-Sided				
		0.0005	0.00055	0.0008	0.005	0.01	0.0005	0.00055	0.0008	0.005	0.01
0.2	ARL	1.38587	1.38624	1.38458	1.32415	1.2877	2.03059	1.99691	1.90246	1.51242	1.41298
	CV	0.526873	0.525211	0.525949	0.494343	0.471219	0.707098	0.699077	0.685285	0.580538	0.539745
0.45	ARL	2.32116	2.29415	2.19621	1.44292	1.24629	2.93999	2.81862	2.46423	1.44323	1.25179
	CV	0.757905	0.746354	0.739504	0.553577	0.444069	0.806688	0.803576	0.772457	0.554695	0.447769
0.5	ARL	2.5927	2.55867	2.40518	1.42919	1.22677	3.16604	3.04591	2.61596	1.42893	1.22193
	CV	0.783077	0.781615	0.762896	0.549702	0.431343	0.826634	0.821178	0.788582	0.547715	0.425525
0.55	ARL	2.90859	2.8547	2.61292	1.41691	1.20039	3.41968	3.29526	2.76212	1.41995	1.19966
	CV	0.810367	0.808283	0.783849	0.542382	0.407840	0.842315	0.833708	0.797908	0.545081	0.408992
0.7	ARL	4.04563	3.92257	3.27449	1.37849	1.14131	4.40214	4.15516	3.31862	1.38048	1.14096
	CV	0.865182	0.866621	0.830904	0.520272	0.351309	0.880246	0.870938	0.831658	0.525627	0.350157
0.9	ARL	6.12448	5.69874	4.25654	1.33366	1.08131	6.24726	5.76195	4.24456	1.33048	1.08017
	CV	0.916181	0.908764	0.874114	0.497945	0.273185	0.920959	0.91033	0.872186	0.496851	0.272349

6.4.4 Some Other Experiments

In the previous section (cf. Section-6.4), we presented a detailed performance study of different proposed charts by assuming constant (sustained) shifts. We notice that a very large shift can be detected with the sequential control limits. Therefore, one should use our proposed check to get an efficient performance of the charts. Contrary to the previous section, in this section we are interested to investigate the performance of the PLP control charts by assuming a random shift scenario. In the existing literature, although most researchers have been focused on the constant/fixed shifts, the random shifts are very important, especially for on-line process monitoring, e.g. a company may buy material from other than regular material providers to fulfil more than expected requirements of demands/goods on a special occasion; hiring extra labour/workforce for a particular job, etc. The importance of the random shifts has recently been highlighted by Woodall and Driscoll [2015]. To study the control chart's performance by assuming the random shifts, we generated shifts from a uniform distribution (support of the uniform distribution for a shift generation has been mentioned in Figure-6.3). The resulting study has been summarized in Figure-6.3, where we depicted the histogram of the run length distribution. The red vertical line in Figure-6.3 represents the mean of the run length distribution, i.e., ARL, while blue line indicates the standard deviation of the run length distribution, i.e., SDRL. Note that we assumed uniform distribution just for illustration purposes and one can consider more realistic distributions for shifts. From Figure-6.3, we have observed that the proposed control charts are very efficient in the detection of random shifts and there is no need to use any deterioration/improvement check.

Another interesting experiment has been conducted and analyzed in this section, which is penalization of the lower control limit. The idea behind this penalization is to get an appropriate chart's performance in the presence of control limits drift and without using any check for it. For this purpose, we penalized the LCL by i^p, where p is the penalizing factor and i denotes the time index. From Figure-6.4a, it is observed that using $p = 0.01$, one can get a similar performance (cf. Figure-6.4b) as we have observed with the process deterioration check.

6.4.5 EQL and RARL for the PLP chart

To assess the overall performance of the control charts, expected quadratic loss (EQL) and the relative average run length (RARL) are commonly used measures (see Section-3.4.4 of Chapter-3). In this section, we compare the CQC chart and the PLP chart. The EQL and RARL with $\lambda_0 = 0.0005$ and $\beta = 1.5$ have been numerically computed using the statistical software R, R Core Team [2013], considering a uniform distribution for both parameter's shifts over the interval $[0.00005 < \lambda < 0.5]$ and $[0.5 < \beta < 2.5]$, respectively. The choice of uniform distribution has been done purely illustrative purposes, and one can consider

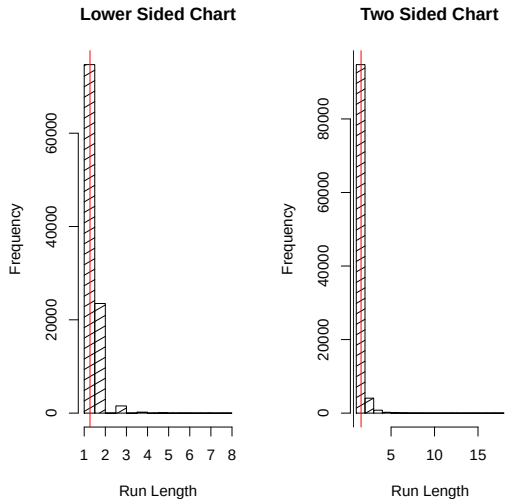

(a) Process deterioration detection for a random shift in the PLP parameters $(\lambda_0 = 0.0005, \beta_0 = 1.5, \lambda_1 = U[0.0005, 0.5], \beta_1 = [1, 2])$

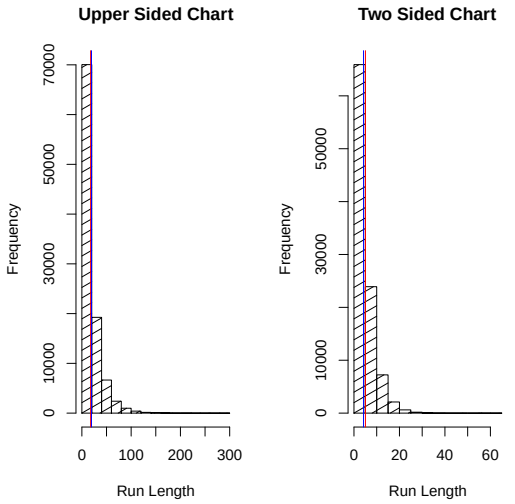

(b) Process improvement detection for a random shift in the PLP parameters $(\lambda_0 = 0.0005, \beta_0 = 0.5, \lambda_1 = U[0.0001, 0.0005], \beta_1 = [0, 1])$

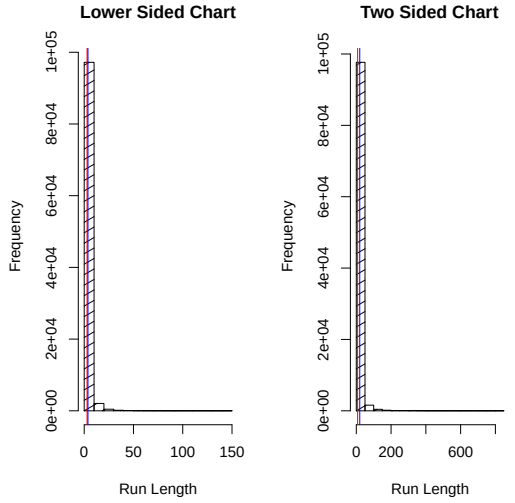

(c) Process deterioration detection for a random shift in the PLP parameters $(\lambda_0 = 0.0005, \beta_0 = 1.5, \lambda_1 = U[0.0001, 0.1], \beta_1 = [1, 2])$

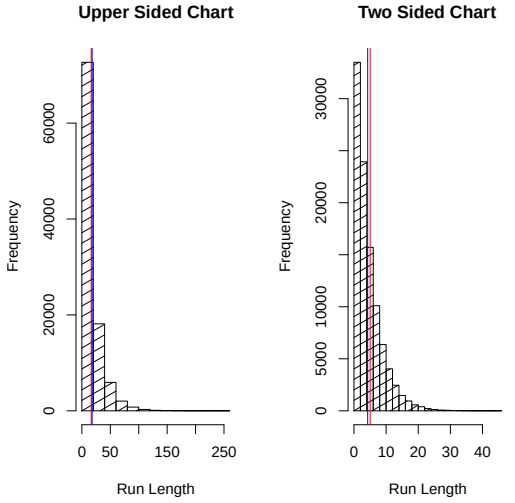

(d) Process improvement detection for a random shift in the PLP parameters $(\lambda_0 = 0.0005, \beta_0 = 0.5, \lambda_1 = U[0.0001, 0.0003], \beta_1 = [0, 1])$

Figure 6.3: Histograms of run-length distribution's for process deterioration and improvement detection with random shifts generated from Uniform distribution; red line-ARL, blue line-SDRL

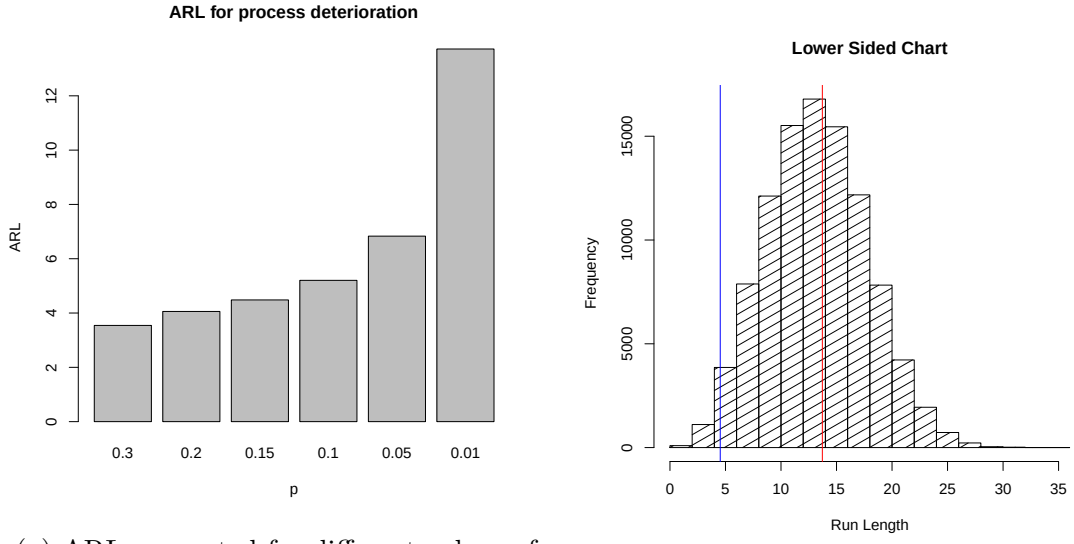

(a) ARL computed for different values of the penalized factor to detect process deterioration

(b) Histogram of the run length distribution using $p = 0.01$

Figure 6.4: ARL computation by penalizing LCL for different p at $\alpha = 0.0027$

Table 6.7: EQL and RARL estimation at different false alarm probability using $\beta_0 = 1.5, \lambda_0 = 0.0005$

ARL_0	EQL			RARL		
	Lower-Sided	Upper-Sided	Two-Sided	Lower-Sided	Upper-Sided	Two-Sided
20,000	1.80737	123.536728	3.42907	21.3663	98.350047	34.5724
2000	0.360584	116.667372	0.518554	4.27496	75.384899	6.97753
740.74	0.263751	113.677832	0.32024	2.25048	65.482489	3.51786
370.37	0.23674	19.6782976	0.26375	1.55762	58.573908	2.26604
200	0.225146	15.376355	0.238834	1.23652	52.433984	1.62434

some more realistic distributions for shifts. Note that for the RARL computation, we have considered the exponential chart as an alternative chart. Both, the EQL and the RARL shown a decreasing trend with the increase of false alarm probability (cf. Table-6.7). In the case of EQL, the loss associated with the upper-sided chart is high as compared to the lower and the two-sided charts. This behavior confirms that one should pay special attention to the upper side of the chart. From the RARL study, clearly the performance of the PLP control chart is very good for process monitoring.

6.5 Effect of Parameters estimation on the ARL

As we explained in Section-3.5 (Chapter-3) that in most of the process monitoring settings, parameters are assumed to be known. However, in reality, this assumption of known parameters is not true. When the parameters are unknown, these should be estimated from the phase-I data. Since control charts are very sensitive to a minor change in

Table 6.8: Comparison of the classical estimation methods for λ and β

Method	λ	Shift in λ	β	Shift in β
MLE	0.004054	0.810800	1.039605	0.693070
Unbiased	0.001377	0.275448	1.551724	1.034483
Linealy Unbiased	0.001489	0.297877	1.498216	0.998811

the design parameters, the parameter estimation has certain consequences. Thus, care should be taken in the selection of an appropriate method of estimation and particularly the sample size to overcome the estimation (approximation) error. To see the effect of estimation on the PLP chart' ARL, we examine two methods of estimation, i.e., the maximum likelihood and the Bayesian methods. Note that only results are reported here and for the derivations we refer to Appendix-6.8.

Case I: Method of Maximum Likelihood (ML): The maximum likelihood is the most commonly used method in statistics for the parameter estimation, and it has some very nice properties. To find the ML estimates of the PLP, we shall use the time truncated case, i.e., when testing stops at a predetermined time t and the number of failures ($N(t) = n$) are random (cf. Appendix-6.8). For example, we fixed the truncation time $t = 6500$ and generated 30 observations with $\lambda = 0.005$ and $\beta = 1.5$, which are: 97.2527, 365.4194, 495.7257, 828.4466, 1227.7677, 1253.6769, 1418.9199, 1760.2463, 1932.8454, 2076.6877, 2505.7932, 2648.6875, 2865.9049, 3045.3843, 3090.9136, 3439.4813, 3525.5849, 3550.1209, 3658.2228, 4082.5301, 4421.1550, 4644.5209, 4847.5839, 5444.9520, 5653.6917, 5883.6398, 6053.8922, 6240.5680, 6338.2454, 6396.9758. The estimated parameter values for the given data set are: $\beta = 1.039605 \quad (SD = 0.0384051)$ and $\lambda = 0.004054 \quad (SD = 0.0004873)$. The unbiased estimate of the β is 1.551724 with $SD = 0.051755$, and the linear unbiased estimate of β is 1.498216 with $SD = 0.050855$. To get an idea about the shift induced by using the ML, the unbiased and the linearly unbiased estimates, a comparative study has been reported in Table-6.8. It is observed from Table-6.8 that a shift in λ is high using the MLE method as compared to the unbiased or linear unbiased estimate. In contrast to λ case, we observed that the MLE introduced a smaller shift in β than in the other two methods.

Case II: Bayesian estimation: In Bayesian methodology, Bayes theorem is used to summarize the current and the prior knowledge. This updated form of the information is known as a posterior distribution. However, for parameter estimation in Bayesian, the choice of an appropriate loss function plays an important role (cf. Section-3.5). Therefore, we shall compare eight different loss functions, which have already been mentioned in Section-3.5 (cf. Chapter-3).

In the available literature, both informative and noninformative priors (Bar-Lev et al. [1992]) have been considered for the Bayesian estimation of the PLP. Several authors considered gamma prior for $\Lambda(t)$ and a variety of informative prior distributions such

Table 6.9: Estimates of the best decision d under various loss functions

LF	λ	Shift in λ	β	Shift in β	Cumulative Intensity
SELF	0.004817 (0.000010)	0.963400	1.660623 (0.052868)	1.107082	304.6001
WSELF	0.003592 (0.001225)	0.718400	1.628726 (0.031897)	1.085817	169.223
MSELF	0.002822 (0.214349)	0.564400	1.596763 (0.019625)	1.064509	104.0958
SLLF	0.004115 (0.290935)	0.823000	1.644713 (0.019393)	1.096475	222.6075
ELF	0.003592 (0.136089)	0.718200	1.628726 (0.009767)	1.085817	169.223
KLF	0.004159 (0.682066)	0.831800	1.644597 (0.039168)	1.096398	226.4476
DLF	0.006976 (0.309514)	1.395000	1.692459 (0.018811)	1.128306	636.1651
PLF	0.005797 (0.001959)	1.159400	1.676466 (0.031685)	1.117644	438.7839

as uniform (Guida et al. [1989]), beta (Calabria et al. [1992]), and gamma (Wang et al. [2010], Wang and Lu [2011]) for the shape parameter β. Zhao [2004, 2010] presented empirical Bayesian procedure for the PLP based on the two and three hyperparameters conjugate priors. Huang and Bier [1998] proposed a conjugate prior which consisted of four hyperparameters for the PLP and studied its properties for the current and the future intensities of the PLP. Recently, Yan-Ping and Zhen-Zhou [2015] extended the work of Huang and Bier [1998] and developed an importance sampling procedure using gamma prior.

Although the natural conjugate prior is a good choice for the Bayesian analysis of the PLP, the whole approach is somewhat difficult to implement in practice. This is because the posterior distribution of the PLP does not belong to any well-known family of distribution, and constitutes complicated integrals with no closed-form solution. Thus, Aminzadeh [2013] proposed a practical method for the posterior evaluation of the PLP. A full derivation of the posterior distribution has been given in Appendix-6.8. Moreover, a computational algorithm to compute Bayes estimates under different loss functions has also been mentioned in Appendix-6.8.

Bayes estimates of the shape and the rate parameters with cumulative intensity have been tabulated in Table-6.9. It is observed from Table-6.9 that the WSELF, MSELF and ELF are not-suitable for the analysis, especially for λ, i.e., parameter value is under-estimated. However, on the basis of minimum posterior risk for λ, we prefer the SELF, DLF and the PLF (in the case of λ) for further use. Similarly, for the estimation of β we suggest the use of the ELF, DLF, MSELF and SLLF, i.e., assuming minimum posterior risk.

6.5.1 Optimal Maintenance Time (τ)

Consider a repairable system modeled by the NHPP with an increasing intensity function subject to two types of repairs: either a minimal repair after a failure which restores the system, i.e., the intensity to exactly the same level as it was immediately before the failure or a preventive maintenance, which restores the system to be as good as new condition. If preventive maintenance is performed after every τ units of time, the expected cost per unit of time is

$$H(\tau) = \frac{C_{pm} + C_{mr} EN(\tau)}{\tau} = \frac{C_{pm} + C_{mr}\Lambda(\tau)}{\tau}$$

where C_{mr} and C_{pm} are the expected costs associated with the two types of repair actions. It can be shown that (cf. Barlow and Hunter [1960], Gilardoni and Colosimo [2007]) the periodicity τ which minimize $H(\tau)$, satisfies $\tau\lambda(\tau) - \Lambda(\tau) = C_{pm}/C_{mr}$. In the special case of the PLP, we have

$$\tau = \frac{1}{\lambda}\left[\frac{C_{pm}}{C_{mr}(\beta - 1)}\right]^{1/\beta}$$

Note that the inference about τ only makes sense when $\beta > 1$, leading to the necessity of truncated prior density for β. This can be done by protecting the conjugacy and truncating the prior $p(\beta, \xi)$ to set $\beta > 1$. Since, the term $(\beta - 1)^{1/\beta}$ in the denominator of τ makes the posterior density non-null as $\beta \to 1$ (cf. de Oliveira et al. [2012]). Therefore, posterior expectation of τ becomes infinite. However, under the truncated prior, one can use, for example, a maximum a posteriori estimate for the optimal time. An alternative formulation which leads to a finite expectation of the posterior τ is gamma distribution for $(\beta - 1)$. This choice of prior assigns less weight to value of β near to one. For the data set given in Section 6.5, let us assume that $C_{MR}/C_{PM} = 20$€, i.e., $C_{PM} = 3$€ and $C_{MR} = 60$€. For these specifications, we have $\tau = 43.088694$ (in hours) and expected cost per unit of time (per hours) is 0.208871€.

6.5.2 Discussion: Effect of Estimation on the ARL

The effect of parameter estimation on the control chart performance is multidimensional because it is not only a result of the accuracy and precision of parameter estimates, but also of the choice of the design parameter and of the size of a shift to be detected. In Table-6.10, or Figure-6.5, we have reported the estimated one-step ahead ARL. From Table-6.10, it is clear that the parameter estimation has a great effect on the ARL values (cf. Figure-6.5). The lower-sided chart is highly affected by the estimation error than the ARL of the upper and two-sided charts. We also noticed that the values of the ARL gradually decrease with the increase of a sample size (cf. Table-6.10/Figure-6.5). The upper and two-sided charts' performance is much inflated in the case of MLE. However, the lower and upper sided charts' performance is effected in the case of Bayesian estimation. The

CV of the run length distribution supports the effectiveness of the Bayesian methodology as compared to the MLE (cf. Table-6.10/Figure-6.5).

Next, we consider the effect of estimation on the full/sequential ARL instead of one-step ahead. We use the sample of different sizes (cf. Table-6.10/Figure-6.5) to estimate the ARL for the full performance assessment. However, in this case, we cannot recommend any effective sample size to overcome the estimation error. The reason for this conclusion is the dependency of the control limits on the observed failure data. However, using the deterioration (cf. Table-6.11/Figures 6.6a-6.6c)(improvement, cf. Table-6.12/Figures 6.6b-6.6d) check, a sample of the size 1000 will be sufficient to overcome the estimation error (cf. Table-6.11 and 6.12/Figure-6.5). The CV of the run length distribution suggests the use of Bayesian methodology for the parameter estimation (cf. Figures 6.5-6.6).

Table 6.10: Effect of parameter estimation on the ARL by the MLE and Bayesian methods using $\alpha = 0.0027, \lambda_0 = 0.005, \beta_0 = 1.5$ for the lower, the upper and the two-sided charts.

Method		MLE			Bayesian		
Sample Size		Two-Sided	Upper-Sided	Lower-Sided	Two-Sided	Upper-Sided	Lower-Sided
30	ARL	322.2269 (321.1203)	296.9341 (291.7979)	920.6105 (920.1104)	263.8332 (263.3324)	. (.)	1480.4873 (1479.9871)
	CV	0.9966	0.9827	0.9995	0.9981	.	0.9997
60	ARL	323.4106 (321.3049)	298.0492 (291.9147)	889.5205 (889.0204)	295.1725 (293.6711)	. (.)	1198.9543 (1198.4542)
	CV	0.9935	0.9794	0.9994	0.9949	.	0.9996
100	ARL	325.5047 (322.6401)	299.6756 (290.5435)	867.2767 (866.7765)	300.7845 (298.2803)	. (.)	1184.069 (1183.569)
	CV	0.9912	0.9695	0.9994	0.9917	.	0.9996
150	ARL	327.5913 (321.9567)	300.8731 (290.7427)	852.0437 (851.5436)	305.9618 (302.8466)	. (.)	927.1677 (926.7012)
	CV	0.9828	0.9663	0.9994	0.9898	.	0.9995
300	ARL	328.6361 (322.5355)	302.1211 (291.9229)	831.7735 (831.2734)	312.6656 (307.1071)	2940.64 (2388.875)	901.2386 (900.7386)
	CV	0.9814	0.9662	0.9994	0.9822	0.8124	0.9995
500	ARL	329.453 (323.3525)	302.7829 (291.6549)	820.0859 (819.5858)	321.0034 (314.2023)	2195.2001 (1780.3197)	841.9306 (841.4306)
	CV	0.9815	0.9632	0.9994	0.9788	0.8110	0.9994
700	ARL	331.9446 (325.4346)	310.2815 (296.7687)	815.0098 (814.5096)	329.6074 (317.7250)	1838.04 (1481.109)	804.2529 (803.7528)
	CV	0.9804	0.9565	0.9994	0.9639	0.8058	0.9994
1000	ARL	332.9565 (325.4465)	310.2939 (295.7812)	831.8689 (809.3112)	305.9618 (320.2743)	1761.609 (1415.83)	744.3651 (743.8650)
	CV	0.9774	0.9532	0.9994	0.9651	0.8037	0.9993
1500	ARL	333.9452 (326.4352)	312.8918 (296.7764)	805.7560 (805.2559)	338.0409 (323.0442)	1707.235 (1298.825)	658.2592 (657.7591)
	CV	0.9775	0.9485	0.9994	0.9556	0.7608	0.9992
2000	ARL	335.9368 (324.4267)	313.2568 (309.7438)	803.4259 (802.9258)	341.7729 (325.1711)	1680.524 (1609.409)	624.0508 (623.5507)
	CV	0.9657	0.9888	0.9994	0.9514	0.9577	0.9992

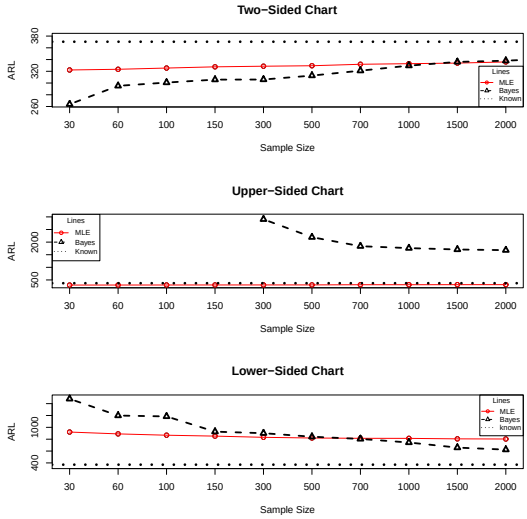

(a) ARL comparison of the MLE and Bayes

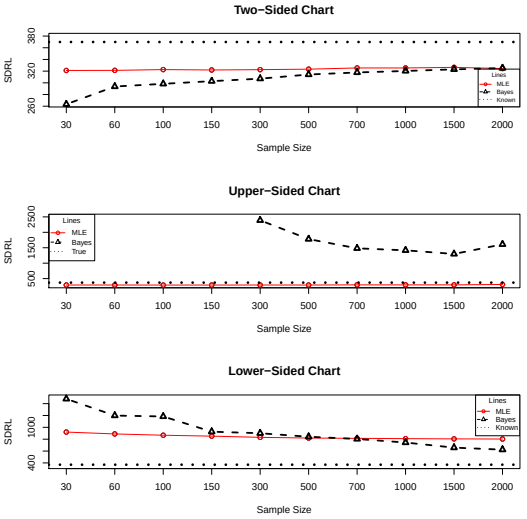

(b) SDRL comparison of the MLE and Bayes

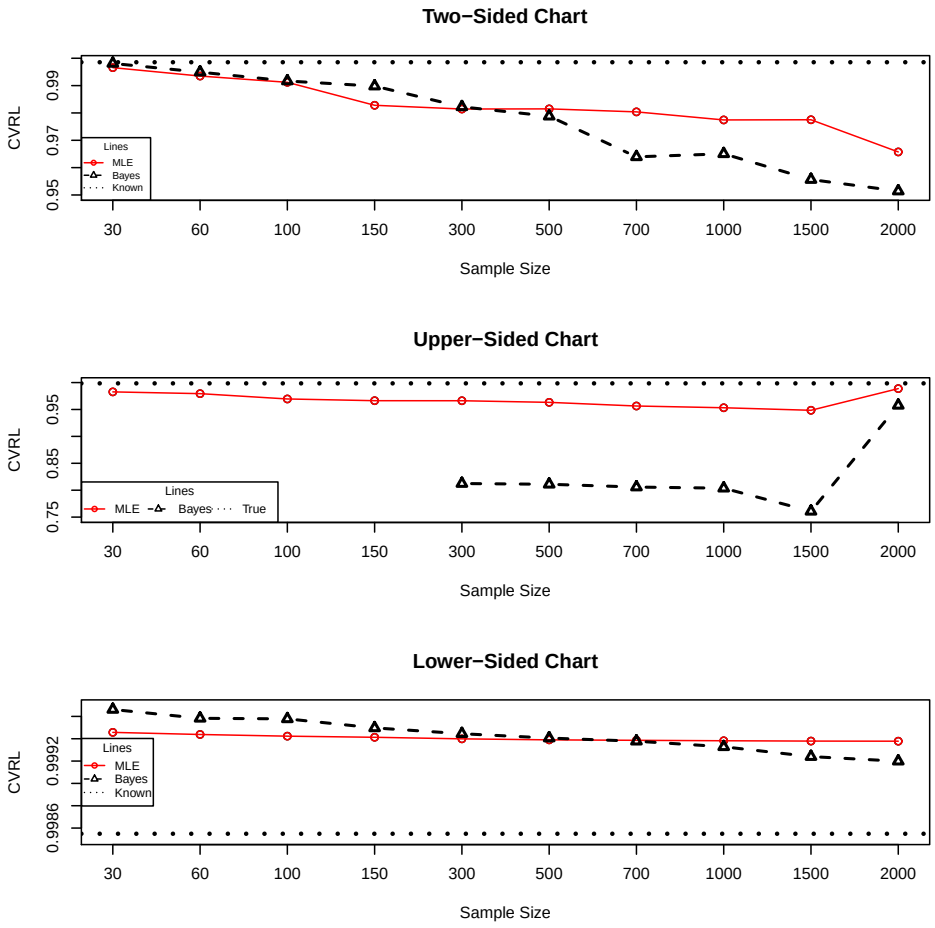

(c) CVRL comparison of the MLE and Bayes

Figure 6.5: Sample size requirement to minimize the effect of estimation for ARL and SDRL

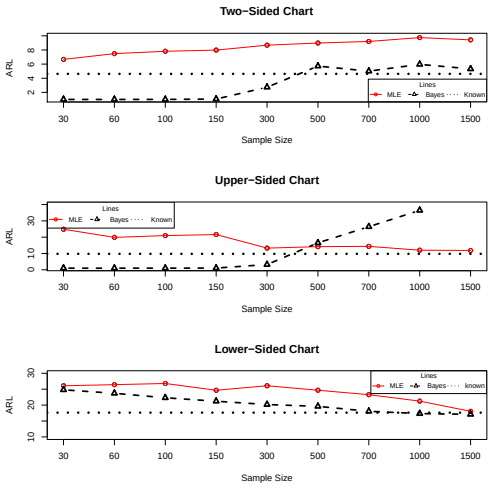

(a) Process Deterioration's ARL comparison of the MLE and Bayes

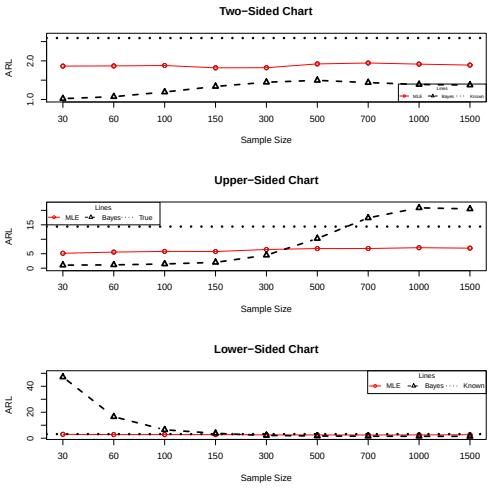

(b) Process Improvement's ARL comparison of the MLE and Bayes

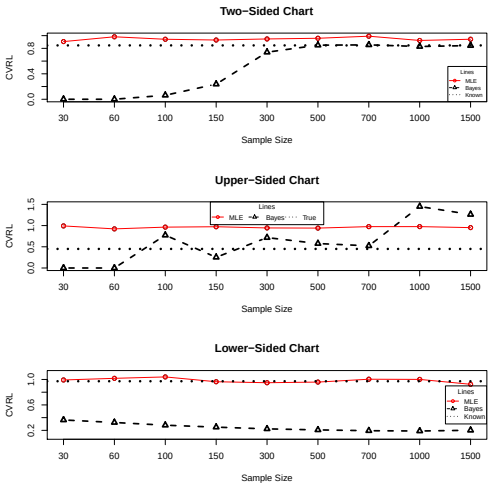

(c) Process Deterioration's CVRL comparison of the MLE and Bayes

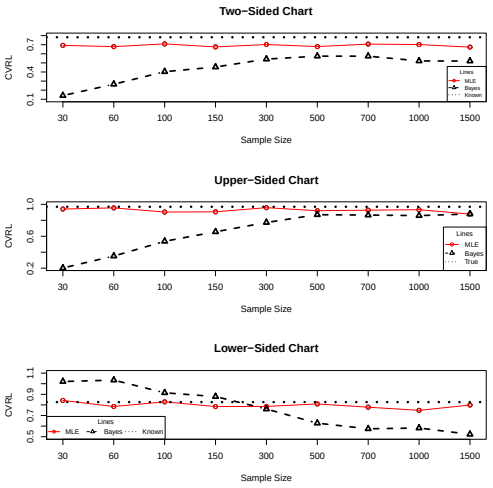

(d) Process Improvement's CVRL comparison of the MLE and Bayes

Figure 6.6: Sample size requirement to minimize the effect of estimation for the PLP with the CDC

Table 6.11: Effect of parameter estimation on the ARL by the MLE and Bayes methods using $\alpha = 0.0027, \lambda_0 = 0.005, \beta_0 = 1.5$ for the lower, the upper and the two-sided charts with the process deterioration check.

Method		MLE			Bayesian		
Sample Size		Two-Sided	Upper-Sided	Lower-Sided	Two-Sided	Upper-Sided	Lower-Sided
30	ARL	6.668	24.84774	26.072	1	1	24.805
	CV	0.906597	0.991951	0.992201	0	0	0.363336
60	ARL	7.481	9.888	26.43	1	1	23.71024
	CV	0.981972	0.921998	1.0179	0	0	0.323884
100	ARL	7.814	10.984	26.797	1.004	1.001	22.306
	CV	0.943047	0.963379	1.039913	0.062899	0.031591	0.281150
150	ARL	7.98	11.615	24.657	1.056	1.067	21.219
	CV	0.931212	0.972775	0.964465	0.237549	0.252496	0.250616
300	ARL	8.678	13.3	26.083	2.732	3.227	20.179
	CV	0.947808	0.944313	0.948773	0.739553	0.7165537	0.223473
500	ARL	8.983	14.201	24.67	5.717	26.50765	19.607
	CV	0.958676	0.940698	0.959079	0.850113	0.576332	0.207329
700	ARL	9.203	14.369	23.276	4.003	164.2526	18.049
	CV	0.991259	0.975341	1.003896	0.854881	0.522474	0.194508
1000	ARL	9.749	12.020134	21.247	2.962	162.3333	17.331
	CV	0.924238	0.975393	1.001134	0.799227	2.44949	0.189887
1500	ARL	9.427	14.843	18.043	2.320988	159.73621	17.09231
	CV	0.943308	0.951990	0.924234	0.743605	2.32103	0.201479

6.6 Goodness of Fit Tests

In this section, we give a brief discussion of the goodness-of-fit tests for the testing of the homogenous and the nonhomogeneous Poisson processes. A comprehensive detail can be found either in Rigdon and Basu [2000] or Lawless [2011]. Note that the goodness-of-fit tests for the time truncated case are similar to tests for the failure truncated case as given in Rigdon and Basu [2000]. Two transformations can be applied to see a trend in the original failure times. The first transformation is the *ratio power* and defined as $\hat{R}_i = \left(t_i/t\right)^{\beta}$. Therefore, to test H_0 : the failure times were governed by a PLP, the Cramér-Von Mises test statistic using ratio power transformation is

$$C_R^2 = \frac{1}{12n} + \sum_{i=1}^{n}\left(\hat{R}_i - \frac{2i-1}{2n}\right)^2$$

$C_R^2 > c$, where c is a critical value used to reject or accept the null hypothesis, and the tables of c can be found in Rigdon and Basu [2000]. Note that a critical value should be obtained by simulation if the parameter β of the PLP has been estimated from the data. A plot of $\hat{R}_i$ on the horizontal axis, against its expectation $E(\hat{R}_i) = \frac{2i-1}{2n}$ on the vertical axis can be constructed to see a departure from the PLP. For the PLP, this plot is expected to be approximately linear along the 45° line that goes through the origin $(0, 0)$.

The second transformation that leads to a goodness-of-fit test for the PLP is the *log-ratio* transformation and defined as: $w_j = \log\left(t/t_{n-j+1}\right)$, $j = 1, 2, \cdots, n$. If the PLP

Table 6.12: Effect of parameter estimation on the ARL by the MLE and Bayesian methods using $\alpha = 0.0027, \lambda_0 = 0.0005, \beta_0 = 0.5$ for the lower, the upper and the two-sided charts with the process improvement check.

Method		MLE			Bayesian		
Sample Size		Two-Sided	Upper-Sided	Lower-Sided	Two-Sided	Upper-Sided	Lower-Sided
30	ARL	2.995	5.147	1.865	1.045	1.021	47.13568
	CV	0.842392	0.941462	0.693007	0.202046	0.140505	1.020766
60	ARL	2.781	5.56	1.869	1.146	1.072	16.554
	CV	0.784995	0.955926	0.679202	0.351540	0.265321	1.033905
100	ARL	2.786	5.806	1.88	1.4535	1.192	6.494
	CV	0.828947	0.903932	0.70914	0.536944	0.403529	0.9144004
150	ARL	2.76	5.754	1.82	2.0061	1.337	3.753
	CV	0.784576	0.906701	0.675872	0.656033	0.454833	0.8786854
300	ARL	2.567	6.463	1.823	4.4892	1.446	2.133
	CV	0.785867	0.958621	0.702334	0.772497	0.541763	0.761163
500	ARL	2.53	6.784	1.921	10.251	1.495	1.68
	CV	0.809002	0.920387	0.679621	0.870592	0.574127	0.627888
700	ARL	2.478	6.8	1.945	17.382	1.437	1.534
	CV	0.778471	0.927214	0.706799	0.865716	0.574149	0.574856
1000	ARL	2.539	7.078	1.916	33.875	1.388	1.482
	CV	0.748750	0.933211	0.701931	0.859053	0.521516	0.582185
1500	ARL	2.669	6.919	1.891	60.49645	1.373	1.432
	CV	0.798850	0.878466	0.673648	0.879529	0.520328	0.522548

is a correct model, then w_j's are distributed as n order statistics from the exponential distribution with the mean $1/\lambda$. Thus, one can also test exponentiality as well as PLP using this test.

Another commonly used test is *Lilliefors' Kolmogorov type* test. This is defined as the largest difference between the empirical distribution function for w's

$$S_W(w) = \begin{cases} 0, & w < w_1; \\ \frac{j}{n}, & w_j \leq w \leq w_{j+1}; \\ 1, & w \geq w_n. \end{cases}$$

and the estimated cumulative distribution function (where w's are assumed to be exponentially distributed) $F^*_W(w) = 1 - \exp(-w/\mu_t)$ where $w > 0$ and $\mu_t = \sum_{i=1}^{n} w_i/n$. The largest (actually the supermum) difference between $S_W(w)$ and $F^*_W(w)$ can be found by taking the larger of the

$$T_1 = \max_{1\leq j\leq n} |F^*_W(w_j) - S_W(w_j)| = \max_{1\leq j\leq n} S^L_j$$

and

$$T_2 = \max_{1\leq j\leq n} |F^*_W(w_j) - S_W(w_{j-1})| = \max_{1\leq j\leq n} S^R_j$$

To test H_0 :PLP is a correct model, the statistic $T = \max(T_1, T_2)$ is compared with the critical values (cf. Rigdon and Basu [2000]). If the test-statistic value is larger than the critical value, we reject H_0.

It is worth mentioning that mostly goodness-of-fit tests are almost powerless for detecting a failure process when the failure time is more evenly spaced than expected. Thus, in such a situation an alternative is *Durbin's modified* test which utilizes spacing between two adjacent order statistics, i.e., $D_j = (n+1-j)(w_j - w_{j-1})$ for $j = 1, 2, \cdots, n$ where $w_0 = 0$ and D_j is exponentially distributed with mean $1/\lambda$ (cf. Rigdon and Basu [2000]). By plotting D_j-statistics on the y-axis against the empirical distribution function, $F_n(x_{(i)}) = i/n$ on the x-axis and by joining these points in a straight line we get a curve within the unit square of the (x, y)-plan, known as TTT-plot. Note that the TTT plot is also useful for testing exponentiality (cf. Section-8.3 of Chapter-8).

To test the hypothesis $H_0 : HPP$ versus $H_1 : NHPP$, the *Laplace test* is commonly used. The test-statistic of the Laplace test is given as follows: $U_L = \frac{\sum_{i=1}^{n} t_i/n - t/2}{t\sqrt{12n}}$. We reject H_0 either if $U_L > Z_{(1-\alpha/2)}$ or $U_L < Z_{(\alpha/2)}$, where Z denotes a critical value computed from a standard normal at the specified level of significance.

6.7 Applications

In this section, we present three case studies to show the implementation of the PLP chart. Note that we will use the terminologies as suggested by Chan et al. [2000].

Example#1: First data set is taken from Rigdon and Basu [2000] (page 179), and it is about the execution times (in 0.01 sec.) between software failure. Since we have no prior knowledge of the process, we prefer here classical analysis of this example. The estimated parameters are: $\hat{\beta} = 1.601699$ and $\hat{\lambda} = 0.000156$ and therefore, we have $\chi^2_{(\alpha/2,2n)} = \chi^2_{(0.025,172)} = 137.577799$ and $\chi^2_{(1-\alpha/2,2n)} = \chi^2_{(0.975,172)} = 210.207633$. The confidence interval for β is $1.281153 < \beta < 1.957497$. Note that this interval excludes 1, so there is evidence that the system reliability is deteriorating. To test hypotheses $H_0 : \beta = 1$ versus $H_1 : \beta \neq 1$, we would reject the null hypothesis if $\hat{\beta} > 1.250202$ or $\hat{\beta} < 0.818239$. Since we have $\hat{\beta} = 1.60$, we reject the null hypothesis in this example. Moreover, to test $H_0 : HPP$ versus $H_1 : NHPP$, we apply the Laplace test which gives $U_L = -0.003828$. We reject H_0 as $U_L > -1.95$.

Another test to check whether PLP is an appropriate model for this data or not, is Lilliefor's Kolmogorov type test (cf. Section-6.6 or Rigdon and Basu [2000]). Using this test, we have $\hat{\mu} = 0.624337$ and $T = \max(T_1, T_2) = 0.077173$ which is not greater than 0.116. Therefore, PLP is an adequate model for this data.

A software failure data set is given in Table-6.13, where X denotes the TBE of a software failure. The lower, central and the upper control limits have been computed using $\alpha = 0.0027$ as the false alarm probability. Note that, 'i.c', and 'n.d' stand for 'in-control', and 'no decision' in Table-6.13 (cf. Chan et al. [2000]). From Table-6.13, clearly, these software failures are statistically in-control at 0.0027 false alarm probability. Moreover, we

did not observe the software improvement sign (cf. Figure-6.7) and the CPC chart also has a similar conclusion (cf. Figure- 6.8). However, if we use the deterioration/improvement check, then there are many time points, which are out-of-control. We have marked the out-of-control observations in the last column of Table-6.13, where a $*$ has been used for the deterioration detection and $**$ to mark the improvement.

Table 6.13: Inspection of the Example 1 Data Set using PLQC charts

Sample#	T_i	X_i	LCL	CL	UCL	CP	Indication	Check
1	479	479	.	.	.	.	n.d.	.
2	745	266	25.374547	4695.231723	20403.84287	0.015995	i.c.	0.015996*
3	1022	277	19.605891	4502.410034	20169.56984	0.020745	i.c.	0.016739*
4	1576	554	16.259986	4319.633556	19933.77139	0.051452	i.c.	0.037286*
5	2610	1034	12.559371	3998.763741	19483.38101	0.123030	i.c.	0.079862*
6	3559	949	9.283669	3520.390542	18705.56738	0.141344	i.c.	0.071777*
7	4252	693	7.706546	3180.552716	18051.63285	0.120445	i.c.	0.048797**
8	4849	597	6.925313	2975.915037	17605.26692	0.114168	i.c.	0.040768*
9	4966	117	6.399519	2822.626797	17239.7078	0.024560	i.c.	0.006547*
10	5136	170	6.308463	2794.736441	17170.00197	0.036096	i.c.	0.009773*
11	5253	117	6.182106	2755.360438	17069.81055	0.025404	i.c.	0.006547*
12	6527	1274	6.098962	2729.020077	17001.59382	0.260707	i.c.	0.103750*
13	6996	469	5.352498	2476.88337	16295.52011	0.113856	i.c.	0.030624*
14	8170	1174	5.133751	2397.575565	16051.41415	0.276841	i.c.	0.093617*
15	8866	696	4.676469	2223.809681	15474.06059	0.186263	i.c.	0.049053*
16	10774	1908	4.452085	2134.638284	15152.80448	0.459545	i.c.	0.172727
17	10909	135	3.959567	1930.162512	14343.28111	0.045175	i.c.	0.007625*
18	11186	277	3.930019	1917.524651	14289.63163	0.091473	i.c.	0.016738*
19	11782	596	3.871186	1892.240114	14180.94927	0.190447	i.c.	0.040686*
20	12539	757	3.752173	1840.604319	13953.29463	0.242509	i.c.	0.054336*
21	12976	437	3.614219	1779.95168	13675.7605	0.152133	i.c.	0.028194*
22	15206	2230	3.540499	1747.196305	13521.16615	0.590922	i.c.	0.210019
23	15643	437	3.218333	1601.366447	12790.49911	0.168897	i.c.	0.028194*
24	15983	340	3.163940	1576.332007	12657.78842	0.135936	i.c.	0.021107*
25	16388	405	3.123276	1557.541456	12556.72153	0.161797	i.c.	0.025809*
26	16963	575	3.076609	1535.899673	12438.75281	0.225173	i.c.	0.038978*
27	17240	277	3.013437	1506.474199	12275.63147	0.117309	i.c.	0.016738*
28	17603	363	2.984214	1492.812607	12198.81866	0.152407	i.c.	0.022749*
29	18125	522	2.947038	1475.388072	12099.84534	0.214471	i.c.	0.034743*
30	18738	613	2.895678	1451.235113	11960.77731	0.250886	i.c.	0.042082*
31	19015	277	2.838309	1424.147007	11802.18816	0.124026	i.c.	0.016738*
32	20315	1300	2.813361	1412.331978	11732.1403	0.471085	i.c.	0.106423
33	21136	821	2.703624	1360.115725	11416.11551	0.339773	i.c.	0.060016*
34	21349	213	2.639943	1329.635416	11226.72352	0.103559	i.c.	0.012501*
35	22969	1620	2.624065	1322.015638	11178.80535	0.573790	i.c.	0.140506
36	24570	1601	2.511098	1267.581797	10829.77785	0.584873	i.c.	0.138427
37	24868	298	2.411335	1219.199149	10509.58675	0.154268	i.c.	0.018173*
38	25742	874	2.393908	1210.718776	10452.49275	0.392489	i.c.	0.064823*
39	26360	618	2.344671	1186.713645	10289.30247	0.301362	i.c.	0.042495*
40	29000	2640	2.311441	1170.476569	10177.59866	0.795827	i.c.	0.258749
41	29005	5	2.182441	1107.173132	9731.912144	0.003090	i.c.	0.000263*
42	29154	149	2.182215	1107.061687	9731.113236	0.088241	i.c.	0.008476*

43	30188	1034	2.175498	1103.754111	9707.379735	0.477372	i.c.	0.079862*
44	32629	2441	2.130354	1081.496801	9546.52677	0.795079	i.c.	0.234970
45	33089	460	2.032983	1033.330114	9191.629689	0.264318	i.c.	0.029936*
46	33654	565	2.015931	1024.873259	9128.365214	0.316515	i.c.	0.038170*
47	34773	1119	1.995499	1014.731934	9052.126414	0.534699	i.c.	0.088151*
48	35210	437	1.956611	995.4055088	8905.716037	0.261293	i.c.	0.028194*
49	36137	927	1.941964	988.117994	8850.128258	0.477923	i.c.	0.069719*
50	40599	4462	1.911836	973.114675	8735.034301	0.961921	i.c.	0.474114
51	41313	714	1.782493	908.503487	8229.511202	0.419563	i.c.	0.050598*
52	41494	181	1.763895	899.186761	8155.316561	0.129601	i.c.	0.010461*
53	42979	1485	1.759260	896.864869	8136.775799	0.684159	i.c.	0.125878
54	43736	757	1.722431	878.396053	7988.591126	0.449457	i.c.	0.054336*
55	46890	3154	1.704431	869.361137	7915.645022	0.922193	i.c.	0.320653
56	49005	2115	1.634496	834.207142	7629.026306	0.829941	i.c.	0.196575
57	49889	884	1.591679	812.646251	7451.080037	0.529677	i.c.	0.065740*
58	51926	2037	1.574649	804.062879	7379.793268	0.829480	i.c.	0.187531
59	53407	1481	1.537186	785.165942	7221.969227	0.730894	i.c.	0.125450
60	53966	559	1.511395	772.144589	7112.522576	0.394204	i.c.	0.037688*
61	54456	490	1.501955	767.376652	7072.307528	0.357200	i.c.	0.032242*
62	55049	593	1.493809	763.260851	7037.533207	0.416099	i.c.	0.040441*
63	56818	1769	1.484106	758.357345	6996.031761	0.803231	i.c.	0.157019
64	56903	85	1.456129	744.211797	6875.875854	0.075861	i.c.	0.004676*
65	59739	2836	1.454819	743.549629	6870.235592	0.930931	i.c.	0.282315
66	59952	213	1.412863	722.315589	6688.637377	0.184438	i.c.	0.012501*
67	61818	1866	1.409840	720.785119	6675.494389	0.835471	i.c.	0.167952
68	62308	490	1.384078	707.735419	6563.139005	0.380842	i.c.	0.032242*
69	63795	1487	1.377519	704.411441	6534.437872	0.769777	i.c.	0.126092
70	68117	4322	1.358109	694.572426	6449.288804	0.987549	i.c.	0.458303
71	69535	1418	1.305585	667.926056	6217.263446	0.771538	i.c.	0.118748
72	70558	1023	1.289499	659.759509	6145.746835	0.659196	i.c.	0.078804*
73	76048	5490	1.278218	654.029942	6095.460445	0.997359	i.c.	0.583320
74	77568	1520	1.221869	625.393511	5842.790207	0.815591	i.c.	0.129637
75	80849	3281	1.207406	618.038002	5777.538871	0.975703	i.c.	0.335941
76	83565	2716	1.177681	602.914555	5642.941652	0.957012	i.c.	0.267875
77	85740	2175	1.154499	591.114262	5537.522207	0.923072	i.c.	0.203574
78	89245	3505	1.136788	582.095285	5456.720664	0.985244	i.c.	0.362796
79	89970	725	1.109710	568.301878	5332.769912	0.587176	i.c.	0.051548*
80	91933	1963	1.104321	565.555823	5308.040152	0.910815	i.c.	0.179014
81	95912	3979	1.090072	558.294158	5242.561399	0.993228	i.c.	0.418802
82	97002	1090	1.062633	544.305479	5116.090145	0.751032	i.c.	0.085301*
83	97247	245	1.055432	540.633505	5082.820356	0.269355	i.c.	0.014594*
84	98441	1194	1.053831	539.817181	5075.420101	0.784810	i.c.	0.095624*
85	99435	994	1.046122	535.885229	5039.75545	0.724039	i.c.	0.076031*
86	103337	3902	1.039817	532.669361	5010.561359	0.994077	i.c.	0.409803
87	.	.	1.016011	520.524325	4900.110282	.	n.d.	.

Example#2: Zhou and Weng [1992] (page $51-52$) reported a total of 37 failures for an engine undergoing development testing in the time interval $(0, 8500]$. The estimated parameters of the PLP are: $\hat{\beta} = 1.888215$ and $\hat{\lambda} = 0.000796$, while $\chi^2_{(\alpha/2,2n)} = \chi^2_{(0.025,74)} = 52.102829$ and $\chi^2_{(1-\alpha/2,2n)} = \chi^2_{(0.975,74)} = 99.678349$. Thus, the confidence interval for β

is $1.329478 < \beta < 2.543434$. Since this interval excludes 1, there is evidence that the engine reliability is deteriorating. To test $H_0 : \beta = 1$ versus $H_1 : \beta \neq 1$, we reject a null hypothesis if either $\hat{\beta} > 1.420268$ or $\hat{\beta} < 0.742388$ is true. Therefore, we reject the null hypothesis in this example, i.e., $\hat{\beta} = 1.888215 > 1.420268$.

To test $H_0 : HPP$ versus $H_1 : NHPP$, we apply the Laplace test (cf. Section-6.6 or Rigdon and Basu [2000]), and obtain $U_L = -0.002517$. Since $U_L > -1.96$, we reject H_0 in the favor of H_1. To apply Lilliefor's Kolmogorov type test, we calculated $\hat{\mu} = 0.529601$ and $T = \max(T_1, T_2) = 0.132486$, which is not greater than 0.175 at $\alpha = 0.05$. Thus, we conclude that the PLP is an adequate model for this data.

The process monitoring has been given in Table-6.14, and it is clear that the engine was statistically the out-of-control at the sample points, 13, 16, 31 and 33, respectively. Moreover, we notice an improvement signal at the sample point 28. The CPC chart also confirms this conclusion (cf. Figure-6.7 and Figure-6.8). However, if we use the deterioration/improvement check, then there are many observations at which the engine was statistically the out-of-control. We have marked the out-of-control observations in the last column of Table-6.14, where a $*$ has been used for the deterioration detection and $**$ for the process improvement.

Note that the behavior of the adaptive control limits of the PLP chart is significantly dependent on the value of the shape parameter β. For both examples, we considered data sets where $\hat{\beta} > 1$. However, the following example is given where $\hat{\beta} < 1$ and control limits drift up with the observed failure time.

Example#3: To see increasing control limits, let's consider a data set given by Rigdon and Basu [2000] (page: 139, example 4.17). In this example, truncation time is $t = 2000$ and the estimated parameters are: $\hat{\beta} = 0.375$ and $\hat{\lambda} = 0.175233$. Rigdon and Basu [2000] applied test for appropriateness of PLP and found that PLP is a suitable process for this data set. We apply the PLP control chart on this data set to detect any deterioration or improvement. The results have been tabulated in Table-6.15, and one can observe that the system is statistically in-control using both, the PLQC and the PLCP charts (cf. Figure-6.7 and Figure-6.8). However, if we use the deterioration/improvement check, then three observations, i.e., 3, 5 and 7, have been found statistically deteriorated while the system was statistically improved at 8-th sample point. We have marked these observations in the last column of Table-6.15, where a $*$ has been used for the process deterioration and $**$ for the process improvement.

6.8 Some Final Remarks

In this chapter, we introduced a new TBE control chart based on the power law process. The proposed chart is suitable for adaptive process monitoring especially real time moni-

Table 6.14: Inspection of the Example 2 Data Set using PLQC charts

Sample#	T_i	X_i	LCL	CL	UCL	CP	Indication	Check
1	171	171	.	.	.	.	n.d.	.
2	234	63	5.208966	881.356654	3248.801506	0.018551	i.c.	0.041691*
3	274	40	3.965829	832.83745	3190.912752	0.014439	i.c.	0.026150*
4	377	103	3.453756	803.965425	3154.878023	0.045595	i.c.	0.069501*
5	530	153	2.607863	736.001912	3064.57364	0.088861	i.c.	0.105466*
6	533	3	1.929822	650.099241	2936.76712	0.002099	i.c.	0.001920*
7	941	408	1.920204	648.575589	2934.334284	0.317285	i.c.	0.299988
8	1074	133	1.160211	486.029359	2627.992441	0.151633	i.c.	0.090936*
9	1188	114	1.031794	447.856399	2538.006069	0.144613	i.c.	0.077307*
10	1248	60	0.943432	419.306172	2464.446815	0.084063	i.c.	0.039645*
11	2298	1050	0.903063	405.612954	2427.006616	0.882551	i.c.	0.724248
12	2347	49	0.525189	256.806077	1893.677095	0.119459	i.c.	0.032190*
13	2347	0	0.515441	252.480989	1873.590579	0.0	o.c.	0*
14	2381	34	0.515441	252.480989	1873.590579	0.085771	i.c.	0.022154*
15	2456	75	0.508899	249.565928	1859.865847	0.182787	i.c.	0.049935*
16	2456	0	0.495075	243.371876	1830.193229	0.0	o.c.	0*
17	2500	44	0.495075	243.371876	1830.193229	0.113972	i.c.	0.028827*
18	2913	413	0.487329	239.881807	1813.162648	0.707198	i.c.	0.303852*
19	3022	109	0.425456	211.511246	1665.896667	0.296592	i.c.	0.073751*
20	3038	16	0.411799	205.136465	1630.521201	0.051249	i.c.	0.010319*
21	3728	690	0.409873	204.233932	1625.441669	0.918047	i.c.	0.509109
22	3873	145	0.341748	171.844448	1430.898333	0.441802	i.c.	0.099632*
23	4724	851	0.330360	166.344871	1395.39815	0.978000	i.c.	0.614240
24	5147	423	0.276932	140.249189	1216.666432	0.882954	i.c.	0.311573
25	5179	32	0.256622	130.212964	1143.321549	0.155420	i.c.	0.020827*
26	5587	408	0.255213	129.514625	1138.122254	0.893002	i.c.	0.299988
27	5626	39	0.238591	121.254317	1075.679286	0.198684	i.c.	0.025482*
28	6824	1198	0.237121	120.522290	1070.061982	0.999428	im.	0.790845
29	6983	159	0.199758	101.822152	922.023488	0.662563	i.c.	0.109860*
30	7106	123	0.195713	99.787981	905.403355	0.574987	i.c.	0.083740*
31	7106	0	0.192702	98.272265	892.955045	0.0	o.c.	0*
32	7568	462	0.192702	98.272265	892.955045	0.964280	i.c.	0.341568
33	7568	0	0.182217	92.988346	849.136316	0.0	o.c.	0*
34	7593	25	0.182217	92.988346	849.136316	0.169406	i.c.	0.016207*
35	7642	49	0.181684	92.719459	846.889121	0.306068	i.c.	0.032190*
36	7928	286	0.180649	92.197183	842.519478	0.886303	i.c.	0.205638
37	8063	135	0.174849	89.268659	817.902468	0.650379	i.c.	0.092380*
38	.	.	0.172246	87.953504	806.784211	.	n.d.	.

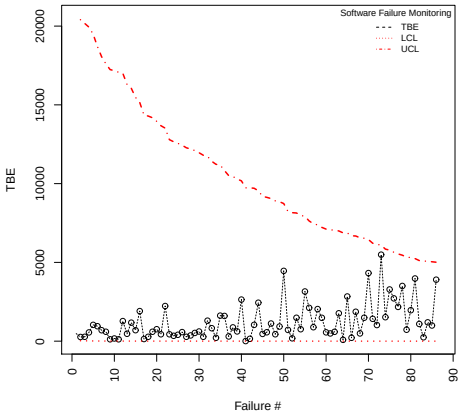

(a) Process improvement and deterioration Monitoring of Example 1 data set

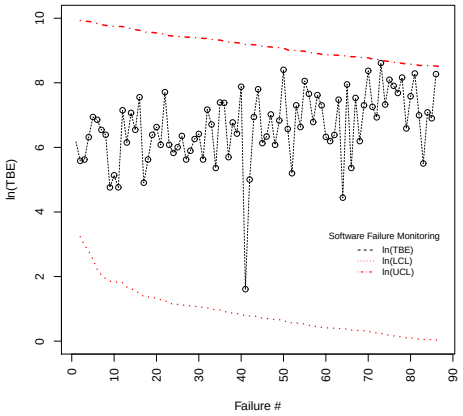

(b) Process improvement and deterioration Monitoring of Example 1 data set

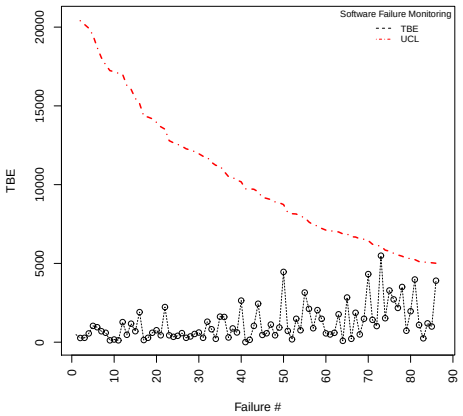

(c) Process improvement Monitoring of Example 1 data set

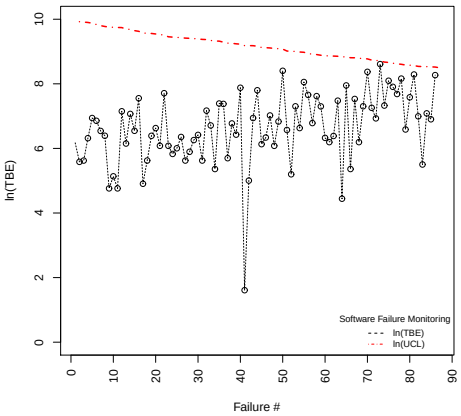

(d) Process improvement Monitoring of Example 1 data set

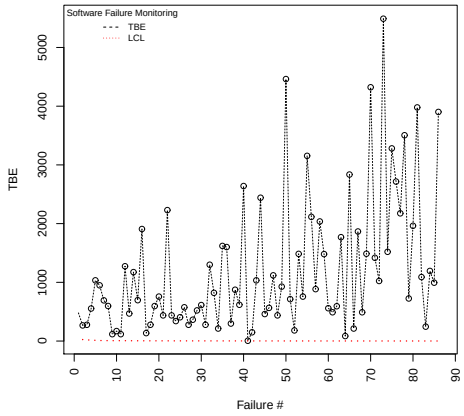

(e) Process deterioration Monitoring of Example 1 data set

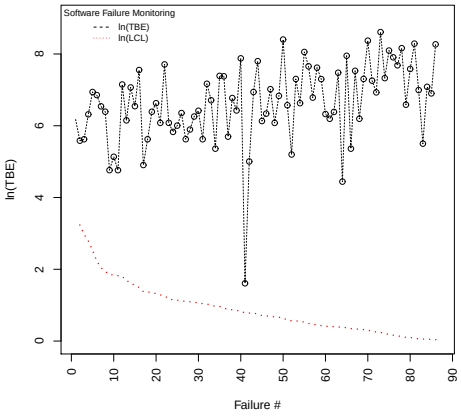

(f) Process deterioration Monitoring of Example 1 data set

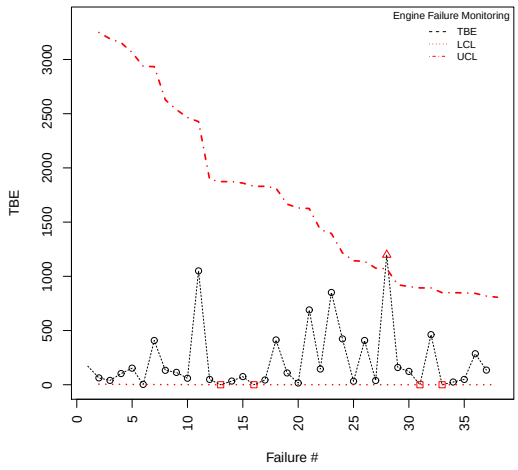

(g) Process improvement and deterioration Monitoring of Example 2 data set

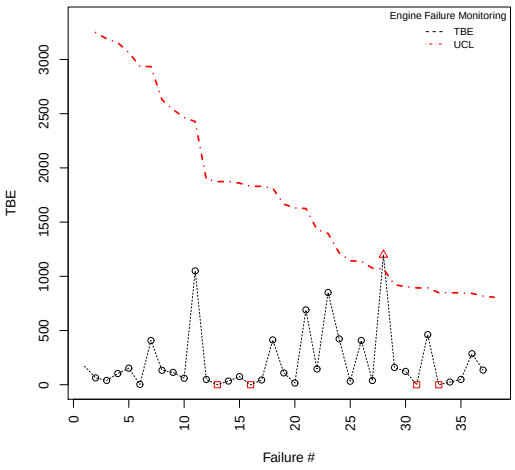

(h) Process improvement Monitoring of Example 2 data set

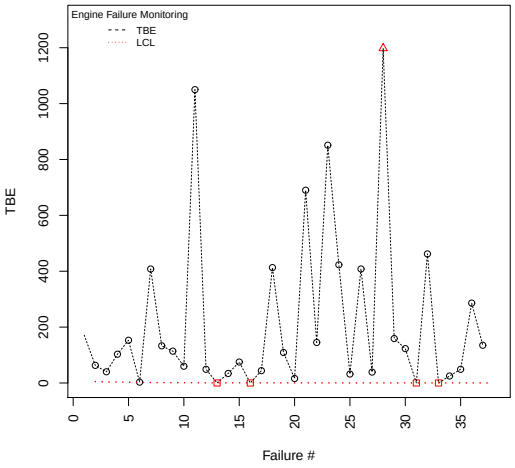

(i) Process deterioration Monitoring of Example 2 data set

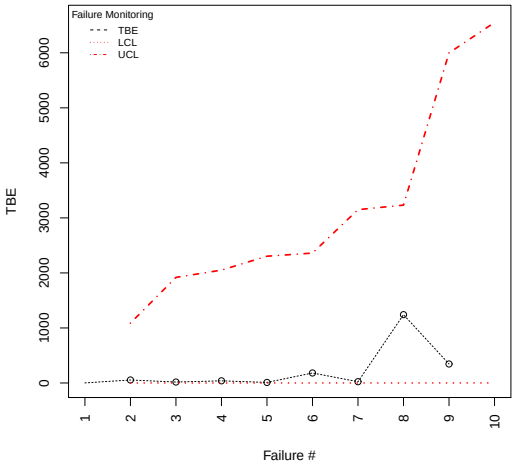

(j) Process improvement Monitoring of Example 3 data set

Figure 6.7: Power Law Process monitoring for Real Data Sets using $\alpha = 0.0027$

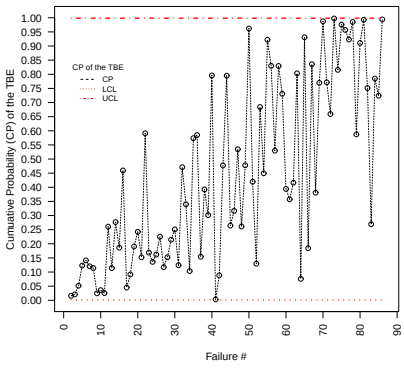

(a) Process improvement and deterioration Monitoring of the Example 1 data set

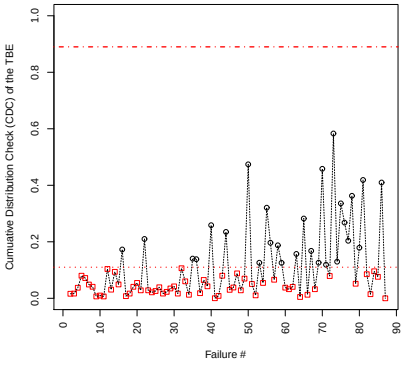

(b) Process improvement and deterioration Monitoring with CDC of the Example 1 data set

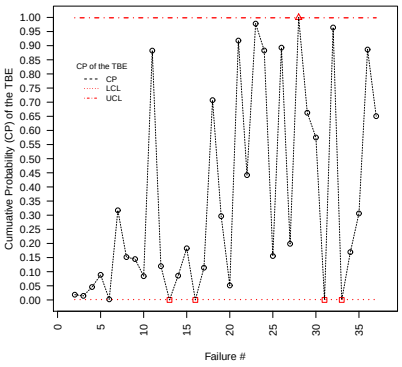

(c) Process improvement and deterioration Monitoring of Example 2 data set

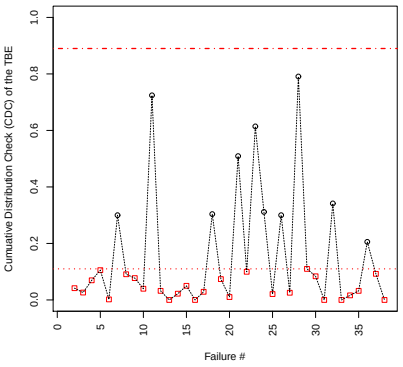

(d) Process improvement and deterioration Monitoring with CDC of Example 2 data set

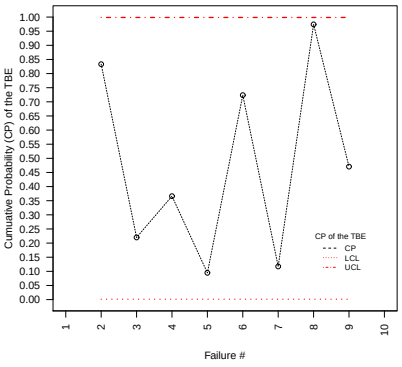

(e) Process improvement and deterioration Monitoring of Example 3 data set

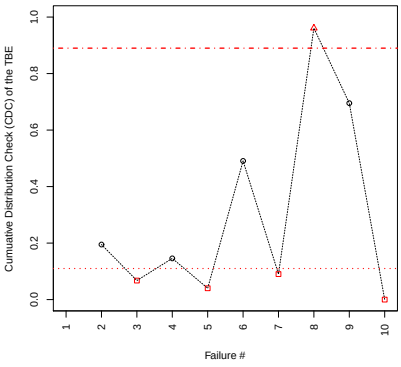

(f) Process improvement and deterioration Monitoring with CDC of Example 3 data set

Figure 6.8: Power Law Process monitoring using the CPC Charts of Real Data Sets using $\alpha = 0.0027$

Table 6.15: Inspection of Example 3 Data Set using PLQC charts

Sample#	T_i	X_i	LCL	CL	UCL	CP	Indication	CDC
1	1.2	1.2	.	.	.	.	n.d.	.
2	55.6	54.4	0.007773	9.155639	1087.588674	0.833220	i.c.	0.194884
3	72.7	17.1	0.085333	55.217712	1918.421264	0.219974	i.c.	0.067351*
4	111.9	39.2	0.100899	63.927896	2050.735925	0.366075	i.c.	0.145851
5	121.9	10	0.132105	81.214142	2303.655624	0.094775	i.c.	0.040133*
6	303.6	181.7	0.139363	85.208579	2360.622352	0.723674	i.c.	0.490824
7	326.9	23.3	0.246484	143.456753	3149.91387	0.117319	i.c.	0.090295*
8	1568.4	1241.5	0.258140	149.739152	3231.638196	0.974079	i.c.	0.960837**
9	1913.5	345.1	0.687796	378.126580	5998.514345	0.470679	i.c.	0.695255
10	.	.	0.778821	426.082126	6550.64807	.	n.d.	.

toring. Since the control limits of the proposal are sequentially updated, every observation will contribute to uncertainty of the control limits. Therefore, one may observe a drift in the control limits of the PLP chart. In such a situation, one cannot observe the actual performance of the system. Hence, to test the possible deterioration (improvement)/drift of the control limits, we proposed a check. By the simulation study and the real data examples, it has been shown that the proposed test improves the performance of the PLP control charts. Moreover, the proposed control charts not only studied in the case of constant shifts but also for the random shifts. The reason of considering random shifts is, since the control limits are sequentially updated, if there is a constant shift, then the monitoring design may adopt a trend, and the out-of-control observation could be considered as the in-control. It is observed that the PLP chart outperforms for a random shift scenario without deterioration/improvement (drift) check. We have assessed the superiority of the PLP chart by different performance measures, i.e., the ARL, CVRL, EQL, and the RARL.

The effect of parameter estimation has been discussed in this study. Two different methods for the parameter estimation, namely the maximum likelihood and the Bayesian methods, have been used to estimate the parameters of the PLP. We found that the effect of parameter estimation on the ARL is very significant and with a minor estimation error, the control chart performance could be seriously inflated. In the future, this work could be extended to design more advanced control charts, like the CUSUM and the EWMA.

In this chapter, we again noticed that a large phase-I data is required to estimate the unknown parameters of the PLP process. Phase-I data poses a problem to a situation where the sampling is expensive or one may have a short-run production process. Therefore, in the next chapter, we introduce a TBE chart for sequential and adaptive monitoring using the Bayesian predictive approach (cf. Chapter-7).

Appendix

In this appendix, we shall discuss some methods of the parameter estimation of the PLP (cf. Section-6.5).

Case-1: The Method of Maximum Likelihood (ML) Let $T_1 < T_2 < \cdots < T_N < t$ denote the observed failure times before time t, i.e., no failure at t. Since the number of failures N is random, one should take into account both types of randomness, i.e., failure time and the number of failures. The likelihood equation for the time truncated case can be derived as follows:

The joint density of $(N, T_1, T_2, \cdots, T_N)$ is:

$$f(n, t_1, t_2, \cdots, t_n) = \begin{cases} f_N(n) f(t_1, t_2, \cdots, t_n|n), & n \geq 1; \\ f_N(0), & \text{n=0.} \end{cases}$$

The random variable N has a Poisson distribution with mean $(\lambda t)^\beta$, i.e.,

$$f_N(n) = \frac{(\lambda t)^{n\beta} \exp(-(\lambda t)^\beta)}{n!}, \qquad n = 0, 1, \cdots$$

The conditional distribution of $T_1 < T_2 < \cdots < T_N$ given $N = n$ is distributed as the n-th order statistics with the cumulative density function (cf. Rigdon and Basu [2000], Theorem 26 of Chapter 2, page 59)

$$G(z) = \begin{cases} 0, & z < 0; \\ \frac{\Lambda(z)}{\Lambda(t)}, & 0 \leq z \leq t; \\ 1, & z > t. \end{cases}$$

For PLP, we have the cumulative density function $G(z) = \left(\frac{z}{t}\right)^\beta$ and therefore, the density function corresponding to G is $g(z) = \frac{\beta}{t^\beta} z^{\beta-1}$ for $0 \leq z \leq t$. Given $N = n$, the distribution of $T_1 < T_2 < \cdots < T_n$ is therefore

$$f(t_1, t_2, \cdots, t_n|n) = n! \prod_{i=1}^{n} G'(t_i) = n! \prod_{i=1}^{n} \frac{\beta}{t} \left(\frac{t_i}{t}\right)^{\beta-1}, \qquad 0 < t_1 < \cdots < t_n < t$$

The joint density of N and $T_1 < T_2 < \cdots < T_n$ is

$$f(t_1, t_2, \cdots, t_n, n) = \lambda^{n\beta} \beta^n \Big(\prod_{i=1}^{n} t_i\Big)^{\beta-1} \exp\big(-(t\lambda)^\beta\big), \qquad n \geq 1 \tag{A.1}$$

and $f(0) = \exp\big(-(t\lambda)^\beta\big)$ for $n = 0$. Note that this is nearly identical to the likelihood function from for the failure truncation case, although we adopted a completely different

approach for the likelihood derivation. The log-likelihood function is given as

$$\ln f(\beta,\lambda|n,\mathbf{t}) = l(\beta,\lambda|n,\mathbf{t}) = n\ln\beta + n\beta ln(\lambda) + (\beta-1)\sum_{i=1}^{n}\ln t_i - (t\lambda)^{\beta} \qquad (A.2)$$

To obtain the maximum likelihood estimators, the partial derivative with respect to λ is

$$\frac{\partial l(.)}{\partial\lambda} = \frac{n\beta}{\lambda} - t^{\beta}\beta\lambda^{\beta-1} = 0 \Longrightarrow \hat{\lambda} = \frac{n^{1/\beta}}{t}$$

The profile log-likelihood, i.e., after replacing the value of $\hat{\lambda}$, is given by

$$l_p(\hat{\lambda},\beta|n,\mathbf{t}) = n\ln\beta + n\ln(n) - n\beta\ln(t) + (\beta-1)\sum_{i=1}^{n}\ln t_i - n \qquad (A.3)$$

and

$$\frac{\partial l_p(.)}{\partial\beta} = \frac{n}{\beta} - n\ln(t) + \sum_{i=1}^{n}\ln t_i = 0 \Longrightarrow \hat{\beta} = \frac{n}{\sum_{i=1}^{n}\ln\left(\frac{t}{t_i}\right)}$$

To compute the Fisher information, we have the following expected values of the second partial derivatives. $-E\left[\frac{\partial^2 l(.)}{\partial\beta^2}\right] = \frac{n}{\beta^2} - (t\lambda)^{\beta}\big[\ln(t\lambda)\big]^2$, $-E\left[\frac{\partial^2 l(.)}{\partial\lambda\partial\beta}\right] = t^{\beta}\lambda^{\beta-1}\big[1 + \beta\ln(\beta) + \beta\ln(\lambda)\big] - \frac{n}{\lambda}$, and $-E\left[\frac{\partial^2 l(.)}{\partial\lambda^2}\right] = t^{\beta}\beta(\beta-1)\lambda^{\beta-2} - \frac{n\beta}{\lambda^2}$. Since the PLP reduces to the HPP when $\beta = 1$, it is often interesting to see if $\beta = 1$ is in the confidence interval. To do this, we know that by conditioning on $N = n$, the random variables $T_1 < T_2 < \cdots < T_n < t$ are distributed as the n-th order statistics from the distribution having the cdf $G(z) = \left(\frac{z}{t}\right)^{\beta}$. Therefore, the random variable Z is uniformly distributed, i.e., $(z/t)^{\beta}$, over the interval $[0,1]$. Consequently, $\left(t_i/t\right)^{\beta}$, $i = 1,2,\cdots,n$, are distributed as the n-th order statistics from the uniform distribution over the interval $[0,1]$. Thus, $\sum_{i=1}^{n} -\ln\left(t_i/t\right)^{\beta} = -\beta\sum_{i=1}^{n}\ln\left(t_i/t\right)$ has a gamma distribution $\Gamma(n,1)$. Note that, $2n\beta/\hat{\beta} = -2\beta\sum_{i=1}^{n}\ln\left(t_i/t\right)$ has a Chi-Square distribution with $2n$ degree of freedom. Therefore, a $100(1-\alpha)\%$ confidence interval for β is given by $\frac{\chi^2_{(\alpha/2,2n)}\hat{\beta}}{2n} < \beta < \frac{\chi^2_{(1-\alpha/2,2n)}\hat{\beta}}{2n}$. To test $H_0 : \beta = \beta_0$ vs $H_1 : \beta \neq \beta_0$, the rule is to reject H_0 if $2n\beta_0/\hat{\beta} < \chi^2_{(\alpha/2,2n)}$ or $2n\beta_0/\hat{\beta} > \chi^2_{(1-\alpha/2,2n)}$.

Theorem A.1 *The conditionally unbiased estimator of β for $n \geq 1$ is $\bar{\beta} = \frac{n-1}{n}\hat{\beta}$.*

To prove this we need the following lemma.

Lemma A.2 *Let Y be χ^2-distributed with n degree of freedom, then $E(Y^k) = 2^k\frac{\Gamma(n/2+k)}{\Gamma(n/2)}$ where k is an integer such that $\frac{n}{2} + k > 0$. Moreover, $E(Y) = n$, $E(1/Y) = \frac{1}{n-2}$,*

$E(Y^2) = n^2 + 2n$ *and* $E(1/Y^2) = \frac{1}{(n-2)(n-4)}$.

Proof : *By Lemma-A.2, we have* $E(\hat{\beta}) = 2n\beta E\big(1/\chi^2_{2n}\big) = \frac{n\beta}{n-1}$ *which implies that* $\bar{\beta} = E\big(\frac{n-1}{n}\hat{\beta}\big) = \beta$. *To find the variance of MLE, we need* $E(\hat{\beta}^2) = E\big(2n\beta/\chi^2_{2n}\big)^2 = \frac{4n^2\beta^2}{(2n-2)(2n-4)} = \frac{n^2\beta^2}{(n-1)(n-2)}$ *and* $Var(\hat{\beta}) = \frac{n^2\beta^2}{(n-1)^2(n-2)}$ *while* $Var(\bar{\beta}) = \frac{\beta^2}{n-2}$.

We refer to Bain and Engelhardt [1991], and Calabria et al. [1987], for some additional properties of the unbiased estimator of β. In Qiao and Tsokos [1998], it has been shown that there exists a linearly best efficient estimator of β denoted by β', which is more efficient. Qiao and Tsokos [1998] define the following theorem to claim the efficiency of the β'.

Theorem A.3 *Assume* $\bar{\theta}$ *is an unbiased estimator of* θ, *and also* $\bar{\theta}$ *has a finite variance, then there exists a unique* ϕ_0 *such that the mean square error* $MSE(\phi_0\bar{\theta}) = \min_\phi MSE(\phi\bar{\theta})$. *Moreover,* $\phi_0 = \frac{\theta^2}{\theta^2 + Var(\theta)}$.

Thus, for PLP, we have $\phi_0 = \frac{n-2}{n-1}$ and the best efficient estimate of β is $\beta' = \frac{n-2}{n-1}\bar{\beta} = \frac{n-2}{\sum_{i=1}^{n}\ln(t/t_i)}$. We also have $MSE(\phi_0\bar{\beta}) = \phi_0^2 Var(\bar{\beta}) + (\phi_0 - 1)^2\beta^2 = \frac{\beta^2}{n-1}$. The efficiency comparison of the MLE $\hat{\beta}$, the unbiased estimator $\bar{\beta}$ and the linearly best estimator β' is:

$$\text{Efficiency}(\beta'/\bar{\beta}) = \frac{MSE(\beta')}{MSE(\bar{\beta})} = \frac{n-2}{n-1} < 1$$
$$\text{Efficiency}(\beta'/\hat{\beta}) = \frac{MSE(\beta')}{MSE(\hat{\beta})} = \frac{n-2}{n^2} < 1$$
$$\text{Efficiency}(\bar{\beta}/\hat{\beta}) = \frac{MSE(\bar{\beta})}{MSE(\hat{\beta})} = \frac{n-1}{n^2} < 1$$

Therefore, the linearly best estimator β' has the greatest efficiency while the unbiased estimator $\bar{\beta}$ has a better efficiency than the MLE $\hat{\beta}$.

Case-II: Bayesian Estimation Following the idea of Aminzadeh [2013], and de Oliveira et al. [2012], let $\xi = \Lambda(t) = (t\lambda)^\beta$ which simplifies $\lambda = \frac{\xi^{1/\beta}}{t}$. Thus, the likelihood given in Equation-A.1 can be written as follows

$$L(\beta, \xi|\mathbf{t}, n) = C\big[\xi^n \exp(-\xi)\big]\big[\beta^n \exp(-n\beta/\hat{\beta})\big] \tag{A.4}$$

where $C = \prod_{i=1}^{n} t_i^{-1}$ and $\hat{\beta} = \frac{n}{\sum_{i=1}^{n}\ln(t/t_i)}$. Hence, both ξ and β belong to a gamma family. Assuming independent gamma prior both for β and ξ, we have the joint prior density given as $p(\beta, \xi) = \gamma(\beta|a, b)\cdot\gamma(\xi|c, d)$ and $\gamma(.|A, B) = \frac{B^A}{\Gamma(A)}(.)^{A-1}\exp(-B(.))$ where the hyperparameters, i.e., a, b, c and d, all must be positive. The resulting posterior distribution is given as

$$\Pi(\beta, \xi|\mathbf{t}, t, n) \propto \gamma(\beta|n + a, b + n/\hat{\beta}) \times \gamma(\xi|c + n, d + 1) \tag{A.5}$$

i.e. both, a priori and a posteriori of the β and ξ are independent and each follows a gamma distribution. Therefore, the intensity function can be written as $\lambda(t) = \frac{\xi\beta}{t}$. This transformation of β and ξ may be facilitated in view of that both β and ξ have clear operational interpretations, i.e., $\frac{d\Lambda(t)/\Lambda(t)}{dt/t} = t\frac{\Lambda^{'}(t)}{\Lambda(t)} = \beta$. Therefore, β is the elasticity of the mean number of event $\lambda(t)$ with respect to time, i.e., the relative change in Λ due to relative change in t. Indeed, the PLP is characterized by the fact that this elasticity is constant over time. On the other hand, $\xi = \Lambda(t) = E[N(t)]$ is the expected number of events during the observed period of the process.

To derive Bayes estimator of $\lambda(t)$ using SELF, we proceed as follows:

$$E[\lambda(t)|\mathbf{t}, n] = E\big[\frac{\beta\xi}{t}|\mathbf{t}, n\big] = \frac{1}{t}E[\beta|\mathbf{t}]E[\xi|\mathbf{t}] = \frac{1}{t}\cdot\frac{a+n}{b+n/\hat{\beta}}\cdot\frac{c+n}{d+1} \tag{A.6}$$

An alternative to Bayes estimator under SELF is a maximum posteriori estimator. In this case, the mode of the posterior density is attained at $\beta^m = \frac{a+n-1}{b+n/\hat{\beta}}$ and $\xi^m = \frac{c+n-1}{d+1}$ respectively, where m denotes the maximum posteriori estimator. Hence, an alternative estimate for $\lambda(t)$ can be written as $\lambda^m(t) = \frac{1}{t}\beta^m\xi^m = \frac{1}{t}\frac{a+n-1}{b+n/\hat{\beta}}\frac{c+n-1}{d+1}$.
A simulation based consistent estimate of $E(g(\xi,\beta)) = \theta$ can be obtained by repeating the following steps:

1. Using $t_1, t_2, \cdots, t_n$, repeat steps (2-5) D times.
2. Generate β_k from $\Pi(\beta|\mathbf{t}, n)$ from $\Gamma(\beta|n+a, b+n/\hat{\beta})$ for $k = 1, \cdots, D$.
3. Generate ξ_k from $\Pi(\xi|\mathbf{t}, n)$ from $\Gamma(\beta|n+c, d+1)$ for $k = 1, \cdots, D$.
4. Compute $\theta_{(j,k)}$ based on the kth sample, $k = 1, \cdots, D$; $j = 1, \cdots, N$.
5. Find $\bar{\beta}_{(j)} = \sum_{k=1}^{D}\theta_{(j,k)}/D$ $j = 1, \cdots, N$.
6. To find Bayes estimate of λ, compute $\lambda_{(j)} = \frac{\xi^{1/\bar{\beta}_j}}{t}$.

Similarly, the Bayes estimates and the respective posterior risks for the other loss functions (cf. Table-3.10) can be computed. To choose hyperparameters values, the idea is to select them in such a way that the mean of the corresponding prior distribution is close to the selected value of ξ and β (cf. Aminzadeh [2013]). For example, for the case of $\lambda = 0.005$, $\beta = 1.5$ and $T = 6500$, the "true" value of ξ is 185.2785, therefore $a = 18$ and $b = 0.01$ is close to ξ value (as the mean of the prior is a/b). Also, with $c = 7, d = 4$, we get the mean of the prior $c/d = 1.75$ which is also close to β's value.

Chapter 7

Bayesian Sequential (Adaptive) Process Monitoring

We are becoming more and more machine dependent and therefore, quality practitioners are now interested in online process monitoring. In Chapter 6, we have introduced a TBE control chart for the sequential process monitoring. However, we observed in Chapter 6 that a large Phase-I data was required to estimate the unknown parameters. This assumption is problematic, especially when the sampling is expensive or when limited Phase-I data are available. In the case of sequential and adaptive monitoring, since we learn from the past experience, Bayesian methodology provides a natural solution for such a kind of monitoring. Moreover, a restrictive assumption about the Phase-I data set to set up monitoring structure, can easily be tackled within Bayesian framework. In this chapter, we propose Bayesian control charts for TBE of the Poisson process (cf. Theorem-1.1.3). A predictive approach is adopted for the development of control charts. In addition to the Shewhart chart, a comparison of the CUSUM and the EWMA charts is also given in this study. Since the control limits are sequentially updated, to detect a possible drift in the control limits, a practical test is also introduced in this chapter. The performance of the proposed control charts is studied in-detail, and some interesting comparisons are shown.

7.1 Motivation

There are many situations in which data arise sequentially, e.g., time between a system failure, and engineers or quality practitioners are interested in the sequentially predictive control limits for the future data points. In many engineering fields, classical sequential methods are commonly used for online filtering, and Kalman's filter is a prime example for this purpose. However, the classical process monitoring techniques require a very large phase-I data set to set up initial process monitoring limits and to overcome estimation error (cf. Albers and Kallenberg [2004b], Kumar and Chakraborti [2014b] and, Chapters

3 and 6). In some processes, this assumption of the large phase-I data make sense, i.e., data collection may be cheap. However, there are some processes, e.g. high-quality processes, where we have the problem of a short production run, limited phase-I data, or expansive sampling. Therefore, the assumption of a large phase-I data is no more valid there. Thus, it is a necessity of time and modern quality application to look some other alternatives instead of classical process monitoring techniques. A promising and a comprehensive methodology to deal with sequential and adaptive process monitoring, is Bayesian methodology. In Bayesian, the Bayes theorem plays a central role while the notion of exchangeability helps us in prediction.

In the existing literature, Zhang et al. [2006] introduced exponential chart based on the classical sequential sampling procedure while Yang et al. [2015a] evaluated the performance of the exponential chart using average time to signal (ATS). They also studied the unbiased property of the ATS within a sequential sampling procedure. On the Bayesian side, Sturm et al. [1990] suggested empirical Bayesian approach based on the sufficient statistic for the normal process. They used the posterior distribution for the detection of change in the mean of a normal process. To detect abrupt changes in the mean of a normal process, Sturm et al. [1991] introduced a weighted empirical Bayes estimator, i.e., similar to the EWMA statistic, $\hat{\mu} = \sum_{j=1}^{i} \lambda^{i-j} X_j / \sum_{j=1}^{i} \lambda^{i-j}$, where λ is weight and X_i denotes the most-recent observation. To alert the engineer about a shift in the process the idea of a coverage probability of the posterior intervals is also discussed in Sturm et al. [1991]. In addition to these, to test a shift in the process mean a likelihood ratio test for the posterior distribution was also introduced.

Recently, Wu et al. [2015] also used the Bayesian approach to multi-batch process monitoring where the chi-square, the ANOVA and Bartlett's test are used in the decision making for the homogeneity of a normal process.

Bayesian estimation has also been used as a method of parameter estimation instead of pure sequential approach in quality control by various authors. For example, Zhang et al. [2013] compared the maximum likelihood estimate of the geometric distribution with the Bayes estimate. Zhang et al. [2013] noticed that Bayesian method can even be used when the number of nonconformities is zero. Lee et al. [2013] also compared Bayesian and maximum likelihood estimates for the Bernoulli CUSUM chart.

Raubenheimer and van der Merwe [2014] used a predictive approach for the designing of a c chart based on the Poisson distribution. However, they did not try their approach in pure sequential setting, and that's why they could show chart performance. Bayarri and García-Donato [2005] motivated by the fact that in the usual implementation of control charts, a large sample size is required to set up control limits and overcome estimation error. However, the restriction of phase-I/base period sample is very restrictive and in many applications, e.g. short-run production, etc., such large sample is not available to set up control chart limits. Due to a sequential and adaptive nature of Bayes theorem, this

problem can easily be addressed. Bayarri and García-Donato [2005] proposed a sequential u chart and compared it with the classical chart. A chart based on empirical Bayes estimates is also developed and compared with sequential chart. They used objective priors and suggested to consider only few observations such that the posterior becomes proper, e.g. three observations in their case. Although their approach is purely sequential, they did not explore the chart performance for various shifts. Since the control limits are sequentially updated, we would expect that control limits also deteriorate/drift with time. Thus, in such a situation, an observation which is actually out-of-control might be considered wrongly in-control. Later, to address the problem of control limit's deterioration and study the chart performance, Toubia-Stucky et al. [2012] proposed a predictive control chart based on geometric distribution. The authors proposed two decision rules (Section 3.3 (page 208) of Toubia-Stucky et al. [2012]) to stop the lower control limit deterioration. A comprehensive overview of the Bayesian methodology in sequential and non-sequential setting for the process monitoring has been given in Section-2.8 of Chapter-2.

The main focus of this chapter is to relax the restrictive assumption of a large phase-I data set as such knowledge is seldom available in real applications. Therefore, we will introduce a new predictive limits control chart for the exponential distribution, i.e., $N(t) \sim$ Poisson process. A test to check deterioration or improvement of the control limits is also proposed in this study. We will investigate the predictive limits chart performance in-detail for different size of shifts, which were ignored in the previous studies. Moreover, the CUSUM and the EWMA charts in a predictive setup will be discussed here. The rest of the study is categorized as follows: Some brief discussions about the Bayesian predictive hypothesis testing and credible interval are given in Section 7.2. A brief discussion about exponential family is given in Section 7.3. The process monitoring settings using Bayesian predictive distribution, are defined in Section 7.4. The Shewhart, EWMA and CUSUM charts are also discussed in the same Section 7.4. A numerical study to assess the performance of different control charts, is given in Section 7.5. The idea of random and sustained shifts is also discussed in the same Section 7.5. Section 7.6 deals with two illustrative examples. Some thoughts about the revision of a prior information and the false alarm probability by the decision theory approach are also discussed in Section 7.6. Three case studies are discussed in Section 7.7. We epitomize the chapter in the last Section 7.8.

7.2 Bayesian Predictive Hypotheses Testing and Credible Interval

In this section, we discuss some approaches of the predictive hypothesis testing. In the classical statistics and Bayesian posterior setups, we know that there are well-defined hy-

pothesis procedures for a parameter testing. However, in the case of Bayesian predictive distribution, the procedure of hypothesis testing is ambiguous. This ambiguity arises as the posterior predictive distribution is free of a parameter. Poirier [1997] motivated by "how to specify a loss function for parametric hypothesis testing, which may be facilitated by considering a related predictive hypothesis, and requiring that the decision which minimizes expected posterior loss (MEPL) over the parametric hypotheses is in accordance with the indisputable choice among predictive hypotheses" and defined a decision procedure to accomplish the task. To define Poirier [1997] procedure, let's suppose that $\mathbf{x}$ denotes a vector of observations from the specified sampling distribution which depends on the parameter vector $\lambda \in \Lambda$ and $L(\mathbf{x};\lambda) \propto f(\mathbf{x}|\lambda)$ be the observed likelihood function. Similarly, let $p(\lambda)$ be the prior distribution and $p(\lambda|\mathbf{x})$ is the corresponding posterior distribution. Furthermore, suppose that $f(y|\lambda)$ is a sampling density of an out-of-sample observation $y = x_{n+1}$ whereas $f(y|\mathbf{x}) = E_{\lambda|\mathbf{x}}\big(f(y|\lambda)\big) = \int_\Lambda f(y|\mathbf{x},\lambda)f(\lambda|\mathbf{x})d\lambda$ the corresponding predictive density. If λ is known, then by exchangeability property, we have $f(y|\mathbf{x},\lambda) = f(y|\lambda)$. In the predictive setup, a basic problem is how to define hypothesis and more relevantly, what should be a loss function?

Since we know by the iterated expectation that $E(y|\mathbf{X}) = E_{\lambda|\mathbf{x}}[E(y|\mathbf{x},\lambda)] = E(\lambda|\mathbf{x})$, the above question can be addressed by defining a predictive hypothesis as $H_0 : E(\lambda|\mathbf{x}) \leq s$ and $H_1 : E(\lambda|\mathbf{x}) > s$, for some constant s. To get a minimum expected posterior loss (MEPL), Poirier [1997] considered a general quadratic loss structure defined as: $L(d = i,\lambda|H_j) = a_i + b_i(\lambda - s) + c_i(\lambda - s)^2$ and $L(d = i,\lambda|H_i) = 0(i = 0,1; i \neq j)$, where $d = i$ denotes the decision corresponding to $H_i(i = 0,1)$, $a_i \geq 0, c_i \geq 0, b_1 \geq 0$ and $b_2 < 0$ are the decision constants. The MEPL yields $d = 0$ (i.e., H_0) iff

$$\begin{aligned} E[L(d=0,\lambda)|\mathbf{x}] - E[L(d=1,\lambda)|\mathbf{x}] &= p_1\{a_0 + b_0E[(\lambda-s)|\mathbf{x},H_1] + c_0E[(\lambda-s)^2|\mathbf{x},H_1]\} \\ &\quad - p_0\{a_1 + b_1E[(\lambda-s)|\mathbf{x},H_0] + c_1E[(\lambda-s)^2|\mathbf{x},H_0]\} \\ &= \big\{[(p_1a_0 - p_0a_1) - (p_1b_0 - p_0b_1)s] + b_0E(\lambda|\mathbf{x}) + \\ &\quad c_0E[(\lambda-s)^2|\mathbf{x}] - (b_0 + b_1p_0E(\lambda|\mathbf{x},H_0) - (c_0+c_1)\times \\ &\quad p_0E[(\lambda-s)^2|\mathbf{x},H_0]\big\} \leq 0 \end{aligned} \tag{7.1}$$

where $p_i = Prob(H_i|\mathbf{x})(i = 0,1)$ denotes the posterior probability of the each hypothesis. Poirier [1997] further showed that if $b_i = c_i = 0$ then posterior odds characterize MEPL, i.e., $d = 0$ iff $p_0/(1-p_0) \geq d_1/d_0$. In order to grantee Equation-7.1, a necessary and sufficient condition is $a_i = c_i = 0, d_0 = 1$ and $d_1 = -1$. Thus, the loss function becomes $L(d = i,\lambda|H_j) = |\lambda - s|(j \neq i)$. The absolute loss is not the only loss function that provides the desired result but used due to its simplicity. He further wrote that "choosing a relevant predictive hypothesis forces the researcher to consider how the parameters are linked to observations and replacing the parameter by its posterior mean, seems natural."

In Bayesian testing of a sharp or precise null hypothesis, one can conclude a totally opposite result than the classical testing. This fact is well-known and called Jeffreys-Lindley' paradox. Girón et al. [1999] inspired by the notion of exchangeability and argued that with this assumption, one can test homogeneity of two samples using the predictive credible interval.

Definition 7.2.1 *Girón et al. [1999]: Two samples* $\mathbf{x_1} = (x_{11}, x_{12}, \cdots, x_{1n_1})$ *and* $\mathbf{x_2} = (x_{21}, x_{22}, \cdots, x_{2n_2})$ *are said to be* homogenous, *and will be denoted by* $\mathbf{x_1} \overset{h}{=} \mathbf{x_2}$, *if the resulting joint sample* $(\mathbf{x_1}, \mathbf{x_2})$ *is exchangeable.*

Therefore, by Definition-7.2.1, it is equivalent to assume that the two populations share the same parameters only if the definition holds true for all sample sizes n_1 and n_2. The proposed homogeneity test of Girón et al. [1999] can be described as: let R_1 and R_2 be the highest predictive regions of $\mathbf{x}_1|\mathbf{x}_2$ and $\mathbf{x}_2|\mathbf{x}_1$ with a probabilistic content $1-\alpha$. Accept the null hypothesis of homogeneity of the two samples, $H_0 : \mathbf{x_1} \overset{\text{h}}{=} \mathbf{x_2}$, at level $1-\alpha$ if $\mathbf{x_1} \in R_1$ and $\mathbf{x_2} \in R_2$. Similarly, reject the homogeneity hypothesis if $\mathbf{x_1} \notin R_1$ and $\mathbf{x_2} \notin R_2$, otherwise, the test is neither accepted nor rejected, i.e., inconclusive, that might be in a sequential setup. A fixed dimension statistic $T(\mathbf{x})$ can be tested in a similar way. Another possible way to conduct a homogeneity test is to use the Kullback-Leibler divergence between the two predictive distributions, i.e., $T(\mathbf{x}_1)|\mathbf{x}_2$ and $T(\mathbf{x}_2)|\mathbf{x}_1$, $KL(p(T(\mathbf{x}_1)|\mathbf{x}_2 \ , \ T(\mathbf{x}_2)|\mathbf{x}_1))$. A decision criterion in this case would be: Accept H_0 if $KL(.) \leq c$, otherwise reject H_0; where c is a some suitable positive constant.

Since the credible sets avoid unnecessary complication of imposing explicit probabilities on the hypotheses, Lindley's paradox could be avoided. It is worth mentioning that central/credible intervals are computationally simpler than the highest posterior density (HPD) intervals and therefore, commonly used (cf. Thulin [2014]). Moreover, credible intervals also have a close agreement with the classical intervals. Note that a HPD interval can be defined as the interval having the shortest length among $1-\alpha$ credible sets.

Our Approach for Predictive Hypothesis Testing: It is worth mentioning that Girón et al. [1999] approach is good if one compares two samples of sizes n_1 and n_2, respectively. However, in the case of sequential setting where one observes one by one items/failure points, e.g. TBE settings, the approach suggested by Girón et al. [1999] is a somewhat complex, i.e., comparison of a sample of size $n_1 > 1$ with $n_2 = 1$. Therefore, an alternative is the predictive cumulative distribution check (PCDC) which is also commonly known as a predictive p-value in the Bayesian literature. Let us suppose that we have to take one of the following two decisions at each observation, $d = 0$: the process is in-control and continued inspection, and $d = 1$: the process is out-of-control, stop and

rectify it. Suppose a loss to take one of the above decisions is

$$L(Y_{n+1}, d) = \begin{cases} K_0 \mathbf{I}_{\{Y_{n+1} > y_{n+1}\}}, & \text{if } d = 0 \\ K_1 \mathbf{I}_{\{Y_{n+1} \leq y_{n+1}\}}, & \text{if } d = 1. \end{cases}$$

The first row gives the loss earned by taking a decision $d = 0$, and the second row is the loss which we collect by taking decision $d = 1$. The expected value of this loss with respect to a predictive distribution is:

$$E_{y|\mathbf{x}}[L(F, d)] = \begin{cases} K_0 Pr\{Y_{n+1} > y_{n+1}|\mathbf{x}\}, & \text{if } d = 0 \\ K_1 Pr\{Y_{n+1} \leq y_{n+1}|\mathbf{x}\}, & \text{if } d = 1. \end{cases}$$

Thus, we take a decision $d = 0$ if $K_0 Pr\{Y_{n+1} > y_{n+1}|\mathbf{x}\} \leq K_1 Pr\{Y_{n+1} \leq y_{n+1}|\mathbf{x}\}$, which is further simplified as $F(y_{n+1}|\mathbf{x}) \geq \frac{K_0}{K_0+K_1}$, otherwise $d = 1$. With this inequality, one can take a decision about the process with a specified probability, e.g. $\frac{K_0}{K_0+K_1} = 1 - \gamma$, and $1 - \gamma = 0.95$ or 0.9973, etc. We have depicted power curves of the proposed test in Figure-7.1 by considering different base periods.

How to select/set stopping criterion? Let $s = \frac{K_0}{K_0+K_1}$ be a stopping criterion, and we have the following explanation to select it properly. When the process is in-control, the probability that a new observation falls below the mean in the case of exponential distribution, i.e., $\frac{1}{\lambda}$, can be computed as $F_x(1/\lambda) = 1 - \exp(-1) \approx 0.6321206$. Thus, a rule can be established based on 5 observations and considering 10% as a threshold, i.e., the probability that five consecutive observations fall below the mean is $(0.6321206)^5 = 0.1009252$. Moreover, a cumulative distribution function (CDF) has the property of non-decreasing and right-continuous, i.e., $\lim_{x\to-\infty} F(x) = 0$ and $\lim_{x\to\infty} F(x) = 1$. Therefore, whenever a process deteriorates, it shortens the TBE and $F(y|\mathbf{x})$ would be closed to zero. Similarly, $F(y|\mathbf{x})$ will be close to one for the process improvement, i.e., TBE is lengthened, and around 0.5 for the in-control process. Hence, the proposed stopping criterion is quite realistic.

7.3 Exponential Family

In this section, we discuss exponential family and some of its properties form a Bayesian point of view.

An important question in Bayesian statistics is how to select a suitable prior which may facilitate numerical computations without the Markov Chain Monte Carlo (MCMC)? Therefore, if a sampling density belongs to exponential family, then one could answer this question very easily. Exponential families are classes of probability's measure constructed

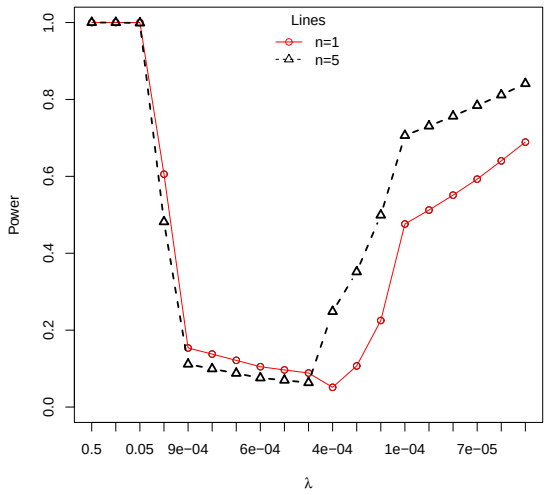

Figure 7.1: Comparison of the power for the base period one and five

from a dominating measure and a statistic. To define a general form of the exponential family, let $\Lambda(\lambda)$ be a vector of parameters, $T(x)$ a vector of sufficient statistics, and $A(\lambda)$ be a cumulant generating function. Then

$$f(x) = h(x)\exp(\Lambda(\lambda)T(x) - A(\lambda)) \tag{7.2}$$

is called a mathematical form of the exponential family. It is interesting to note that x and λ mix in $\exp[\Lambda(\lambda)T(x)]$ not elsewhere. Note that $A(\lambda)$ is also known as a logarithm of the Laplace transform of $h(x)$, and it is convex. Products of exponential family are again exponential family but may not have a nice parametric form anymore. Finding the mean, the covariance and the maximum likelihood estimate of exponential family are very easy, i.e., $A'(\lambda) = E_{f_\Lambda}\{T(x)\}$, $A''(\lambda) = E_{f_\Lambda}\{T^2(x)\} - E^2_{f_\Lambda}\{T(x)\} = Cov_{f_\Lambda}\{T(x)\}$ (positive definite) and MLE $= A'(\hat{\lambda}) = n^{-1}\sum_{i=1}^{n} T(x_i)$, respectively.

Moreover, one can get an elegant closed form of a conjugate prior to the exponential family. To derive a conjugate prior, let $T : x \to \Re$, $A, \Lambda : \lambda \to \Re$ and define $K_{a,b} := \int_\lambda \exp(\Lambda(\lambda)a - bA(\lambda))d\lambda < \infty; a \in \Re^q, b \in \Re$. A conjugate prior can be constructed by replacing data with hyperparameters in the exponential family (cf. Diaconis and Ylvisaker [1979]), i.e., $p(\lambda|a,b) = K^{-1}_{a,b}\exp(\Lambda(\lambda)a - bA(\lambda))$, which yields a posterior distribution

$$p(\lambda|\mathbf{x}) \propto \exp\{\Lambda(\lambda)(a + T_n(x)) - A(\lambda)(b+n)\} = p(\lambda|\beta = a + T_n(x), \phi = b + n) \tag{7.3}$$

Many well-known distributions (cf. Section-7.8) belong to exponential family, and we refer to Casella and Berger [2002] for further details.

The posterior predictive distribution in exponential family can be derived as follows:

$$f(x_{n+1}|\mathbf{x}) = h(x_{n+1})h(a+T_n(x), b+n)\int_\lambda \exp(\Lambda(\lambda)(a+T_n(x)+T(x_{n+1}))- A(\lambda)(b+n+1))d\lambda$$
$$= \frac{h(x_{n+1})h(a+T_n(x), b+n)}{h(a+T_n(x)+T(x_{n+1}), b+n+1)} = f(x_n+1|\mathbf{x}; a+T_n(x), b+n) \quad (7.4)$$

It is worth mentioning that when a conjugate prior is used, the posterior predictive distribution belongs to the same family as the prior predictive, i.e., marginal, distribution. This can be determined simply by plugging the updated hyperparameters for the posterior distribution into the prior predictive distribution. Note that the posterior predictive distribution of an exponential-family random variable with a conjugate prior can always be written in closed form (provided that the normalizing factor of the exponential-family distribution can itself be written in closed form).

7.4 Predictive Control Charts

In this section, we define a process monitoring strategy using the Bayesian predictive approach (cf. Equation-7.4). Let us assume that the defects are being produced by the Poisson process where the distribution of time is exponential with the rate parameter λ. We want to develop a control chart that should be either free from the assumption of phase-I data set or use a minimum number of observations to monitor the future TBE. To accomplish this task, a natural solution is to construct a chart based on the posterior predictive distribution (cf. Equation-7.4). Note that this approach is self-adaptive and suitable for online process monitoring, i.e., sequential nature of Bayes theorem plays an important role.

In this chapter, the word "revise" is used when the parameters of the initial prior distribution are recomputed while the word "update" is used when the posterior and predictive distributions of the parameter and of the data y, respectively, are calculated after incorporating the in-control observations to date.

Assuming the exponential distribution for the TBE, we have the posterior distribution $p(\lambda|\mathbf{x}) = \frac{\beta^\phi}{\Gamma(\phi)}\lambda^{\phi-1}\exp(-\beta\lambda)$ (cf. Equation-7.3), i.e., assuming gamma distribution $[p(\lambda) = b^a/\Gamma(a)\lambda^{a-1}\exp(-b\lambda)]$ as the prior, where $\phi = a+n$ and $\beta = b+\sum_{i=1}^n x_i = b+n\bar{x}$. Note that here we used the likelihood for n observations to generalize the concept to a situation where one could have a few phase-I data observations. However, if the phase-I data set is not available, then one can set up control limits by using an informative prior. Similarly, for the noninformative or the objective priors, we suggest to collect as many observations as the posterior becomes a proper distribution. This idea, i.e., the use of

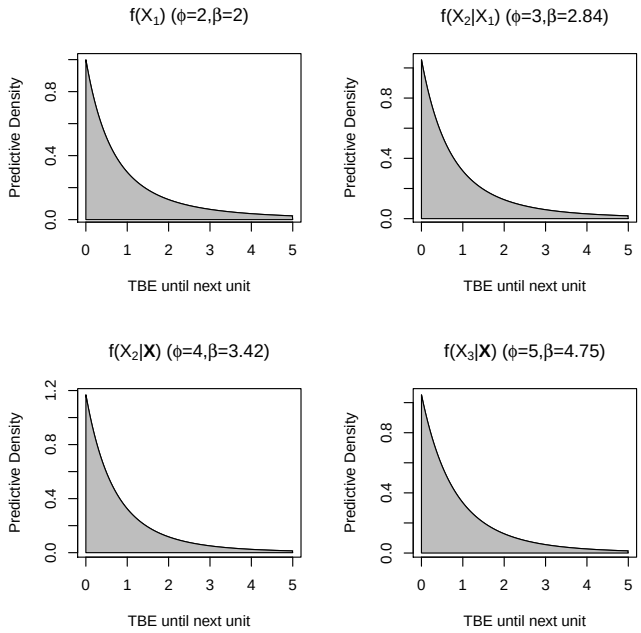

Figure 7.2: Sequential Predictive Distribution using hyperparameters $a = 2$ and $b = 1$

a minimum number of data points such that the posterior becomes proper, is similar to Bayarri and García-Donato [2005] where they suggested the use of $3 - 5$ data points to get a proper posterior distribution. Later, Toubia-Stucky et al. [2012] also suggested the use of three data points in the case of empirical Bayes. The posterior predictive for the future observation $y = x_{n+1}$ is given by (cf. Equation-7.4)

$$f(y|\mathbf{x}) = \frac{\phi}{\beta\big(1 + \frac{y}{\beta}\big)^{\phi+1}}, \qquad y > 0 \tag{7.5}$$

which is the Pareto type-II and commonly known as the Lomax distribution. It is interesting to note that the predictive distribution is a monotone decreasing in $y > 0$ (cf. Figure-7.2).

A general form of the cumulative distribution function of Equation-7.5 is

$$F(y|\mathbf{x}) = 1 - \big(1 + \frac{y}{\beta}\big)^{-\phi}, \qquad y > 0 \tag{7.6}$$

To construct a two-sided control chart, one needs to find $LCL = F^{-1}(\alpha/2|\mathbf{x})$ and $UCL = F^{-1}(1 - \alpha/2|\mathbf{x})$, where α is a prespecified probability of the false alarm. Since $F(y|\mathbf{x})$ is available in explicit form (cf. Equation-7.6), the control limits in sequential settings can be written as: $LCL_{i+1} = \beta_i\big[\big(\frac{1}{1-\alpha/2}\big)^{1/\phi_i} - 1\big]$ and $UCL_{i+1} = \beta_i\big[\big(\frac{1}{\alpha/2}\big)^{1/\phi_i} - 1\big]$, where j is the TBE observation index and $i \geq 0$. To obtain the one-sided control charts, find

$LCL = F^{-1}(\alpha|\mathbf{x})$ and $UCL = F^{-1}(1-\alpha|\mathbf{x})$, respectively. The simplified control limits for the one-sided sequential monitoring are: $LCL_{i+1(\text{one-sided})} = \beta_i\big[\big(\frac{1}{1-\alpha}\big)^{1/\phi_i} - 1\big]$ and $UCL_{i+1(\text{one-sided})} = \beta_i\big[\big(\frac{1}{\alpha}\big)^{1/\phi_i} - 1\big]$, respectively.

A predictive control chart with Shewhart structure is obtained by plotting the observed value of TBE X_{i+1} against the LCL_{i+1} and UCL_{i+1}. If the point is plotted below the LCL_{i+1}, i.e., $X_{i+1} < LCL_{i+1}$ then it is a signal that the process may have deteriorated while if a point is plotted above the UCL_{i+1}, i.e., $X_{i+1} > UCL_{i+1}$, it is a sign of that process may have improved. Moreover, if the new observation falls within the control limits, then it will be used to update the posterior distribution of parameter λ and the predictive distribution of data Y, respectively. Therefore, continue in this fashion, the predictive distribution of each step would be used to establish the next control limits, i.e., the control limits for the time $i+2$ are determined right after we compare X_{i+1} with (LCL_{i+1}, UCL_{i+1}) and update $F_{i+1}(y|\mathbf{x})$. To make a control chart adaptive, if an observation falls outside the control limits, the most-recent observation is discarded, and all the previous in-control observations to date, could be used to revise prior parameter (if one wishes) and start process monitoring once again. Thus, with this approach the aim is to detect any change in the process as quickly as possible. Moreover, it also alleviates the requirement of a large phase-I data set to set up control limits.

7.4.1 EWMA and CUSUM

In the previous section, we have defined the Shewhart process monitoring design of the Bayesian charts. It is a well known fact that Shewhart control charts are used to detect a large shift. Alternatively, the EWMA and the CUSUM control charts are widely used for the detection of small shifts, and they come under the banner of a memory type control charts. Gan [1998] introduced the exponential EWMA chart where the upper-sided EWMA chart was used for the detection of an increase in the mean of the exponential distribution (or decrease in the rate parameter). The one-sided EWMA chart can be formed by plotting

$$Q_i = \max\{A, (1-\theta_Q)Q_{i-1} + \theta_Q X_i\} \tag{7.7}$$

against i, for $i = 1, 2, \cdots$; where θ_Q is a smoothing constant such that $0 < \theta_Q < 1$ and mostly it is $0.10 < \theta_Q < 0.25$ as suggested by Montgomery [2009] for the optimal properties of the EWMA chart. A is a boundary which is nonnegative and $Q_0 = u, A \leq u < UCL_i$, i.e., for the predictive setting. A signal will issue at the time i for which $Q_i \geq UCL_i$. Similarly, a lower-sided EWMA chart is designed to detect an increase in the rate parameter, which is

$$q_i = \min\{B, (1-\theta_q)q_{i-1} + \theta_q X_i\} \tag{7.8}$$

against i, for $i = 1, 2, \cdots$; where θ_q is a smoothing constant such that $0 < \theta_q < 1$ and mostly it is $0.10 < \theta_q < 0.25$ as suggested by Montgomery [2009] for the optimal properties of the EWMA chart. B is a boundary which is nonnegative and $q_0 = v, LCL_i < v \leq B$, i.e., LCL_i for the predictive setting. A signal will issue at the time i for which $q_i \leq LCL$. The use of the boundary as suggested by Gan [1998] is appealing because it ensures that the EWMA chart is at most at a certain distance ($UCL_i - A$ for the upper-sided chart and $B - LCL_i$ for the lower-sided chart) from the chart limit, irrespective of a situation. The EWMA charts with a worst-case scenario can be designed by selecting $q_0 = B$ and $Q_0 = A$.

There are two methods in the literature to design a two-sided EWMA chart. The first method to obtain a two-sided EWMA chart is by plotting

$$Z_i = (1 - \theta_Z)Z_{i-1} + \theta_Z X_i \tag{7.9}$$

against i, for $i = 1, 2, \cdots$; where θ_Z is a smoothing constant such that $0 < \theta_Z < 1$ and mostly it is $0.10 < \theta_Z < 0.25$ while $Z_0 = w$ and $LCL_i < w < UCL_i$. A signal will be issued at the time i if $Z_i \leq LCL_i$ or $Z_i \geq UCL_i$. The second method to establish a two-sided EWMA chart is the simultaneous use of both, the lower and the upper sided charts. This approach is sometimes known as combined EWMA scheme.

The upper-sided CUSUM chart is used to detect a decrease in the rate parameter and obtained by plotting

$$S_i = \max\{0, S_{i-1} + X_i - K\} \tag{7.10}$$

against i, for $i = 1, 2, \cdots$; where $K = \frac{\ln(\lambda_0) - \ln(\lambda_1)}{\lambda_0 - \lambda_1}$ is a positive constant and $S_0 = u, 0 \leq u < UCL_i$. A signal will be issued at the time i if $S_i \geq UCL_i$. Similarly, the lower-sided CUSUM is defined by

$$s_i = \min\{0, s_{i-1} + X_i - K\} \tag{7.11}$$

For the worst-case scenarios, $S_0 = s_0 = 0$, however, the starting values may be set to some nonzero values such as the out-of-control signal can be detected earlier when the process starts from out-of-control state. A two-sided CUSUM can be designed by simultaneously using S_i and s_i. Liu et al. [2006b] compared the performance of the EWMA and the CUSUM charts for the exponential distribution by considering the fixed control limits of the both charts.

In the traditional EWMA setup, there are two proposals to find control limits of the chart. The first method is where one assumes that the process has reached stationarity and therefore, control limits are held constant. The second approach is where control limits vary with the order of time but not with the actual value of the data. However, in both approaches, the monitoring statistic is updated with the actual data points. Contrary to these approaches, we shall study the EWMA and the CUSUM charts not only by

updating the monitoring statistic but also the control limits. The unique feature of the proposed control charts is the control limits are data dependent, i.e., the control limits are updated with each in-control data point. Note that, recently, time and sample size varying EWMA charts (cf. Shen et al. [2013], Shu et al. [2014], and Shen et al. [2015]), risk adjusted CUSUM (cf. Tian et al. [2015]), and adaptive CUSUM (cf. Wu et al. [2009c]) have been proposed in the literature. However, there is a fundamental difference between the existing and our approach. We use a predictive distribution to find the control limits and the monitoring statistic whereas the existing did not have it. Moreover, our proposed EWMA and CUSUM charts also have a self-starting feature. Similarly, our proposed control charts could even be developed without any phase-I data point. Therefore, one can consider this work as a generalization of the existing approaches. To find the predictive control limits of the CUSUM and the EWMA charts, we will use the following procedure:

1. If there is no out-of control signal at time $i(i \geq 1)$, $Y^*_{i,k}(k = 1, 2, \cdots, M)$ are generated from $F_i(y|\mathbf{x})$.

2. Sort the M values in ascending order and find the specified empirical quantile of these M values. This approximated value is used for approximating the control limits of the time $i + 1$.

3. Compare the value of EMWA or CUSUM statistic, which is calculated based on the observed Y_i, with control limits to decide whether to raise an out-of-control alarm or to wait for the next TBE.

In this chapter, we used $M = 10^4$. Next, suppose that we are interested in the upper-sided CUSUM S_i chart. The above steps ensured us that $Pr(S_i > UCL_i) = \alpha$ as $M \to \infty$. However, the conditional probability defined by $Pr(S_i > UCL_i|S_j < UCL_j) = \alpha$ where $1 \leq j < i$, i.e., the probability that the charting statistic exceeds the control limits given no prior signals, may be more suitable to increase the sensitivity of the chart (cf. Shen et al. [2013]). Therefore, to determine the control limit UCL_{i+1}, one should ensure that the values of pseudo test statistic $S^*_{i,k}$ is less than or equal to UCL_i. Thus, one needs the ranked values of $S^*_{i,M^*} = \{S^*_{i,(1)}, \cdots, S^*_{i,(M^*)}\}$, where $M^* = \lfloor M(1-\alpha) \rfloor$, and $\lfloor V \rfloor$ denotes the largest integer less or equal to V. At step $i + 1$, the starting value to calculate the pseudo test statistic and finding the control limits, i.e., $S^*_{1,k}$ of the CUSUM statistic, should be selected uniformly from S^*_{i,M^*}. Therefore, to increase the sensitivity of the CUSUM and EWMA charts, we modify the steps given in Shen et al. [2013] for our settings as follows:

1. If there is no out-of control signal at time $i(i \geq 1)$, $Y^*_{i,k}(k = 1, 2, \cdots, M)$ are generated from $F_i(y|\mathbf{x})$. Compute the pseudo test statistic of the EWMA or the CUSUM by using the values $Y^*_{i,k}$, say $S^*_{i,k}$ (or $q^*_{i,k}$, $Q^*_{i,k}$, $s^*_{i,k}$, $Z^*_{i,k}$).

2. Sort the M values of step-1 in ascending order. Find the specified empirical quantile of step-1' M values to obtain the control limits.

3. Compare the value of EWMA or CUSUM statistic, which is calculated based on the observed Y_i, with control limits computed in step-2 to decide whether to raise an out-of-control alarm or to wait for the next TBE.

4. If it is decided to go on, set $M^* = \lfloor M(1-\alpha) \rfloor$ and discard the values that are greater than and equal to the control limit. Go back to step 1.

Similarly, the above steps can be generalized to compute the control limits of lower, upper, and two-sided EWMA/CUSUM charts.

To monitor a process improvement with the UCL_i, we shall use zero as a starting value for the CUSUM, i.e., considering a worst-case scenario, while a positive value is used for the EWMA to represent a worst-case scenario. Similarly, to design a lower-sided EWMA and CUSUM charts, we shall assume the fast initial response approach. A fast initial response chart is designed to get a quick signal by assuming a positive starting value of the CUSUM or EWMA, which is opposite to a simple EWMA or CUSUM chart where one has zero as a starting value (cf. Montgomery [2009]).

7.5 Discussion of ARL Study

In Table-7.1, we have computed the average run length (ARL) and the coefficient of variation (CV) of the run-length distribution for the lower, upper and two-sided charts. These measures were computed by assuming different size of shifts in the parameter. The standard deviation of the run-length (SDRL) distribution can easily be recovered using the ARL and CV values. The values of the hyperparameters have been selected such that the mean of the prior distribution was greater than 1700 with a small variance. For this reason, the shape parameter of gamma distribution was selected very small as compared to the rate parameter, i.e., informative prior. A misspecified prior distribution has also been considered where we selected the hyperparameters such that the mean was greater than 1500 but with a large value of the variance, i.e., noninformative prior. From Table-7.1, one can observe that a larger shift is detected quickly as compared to small shifts. The control charts are completely ineffective for the detection of small to moderate shifts. More specifically, to detect the process deterioration for small shifts, the performance of lower-sided and two-sided charts are approximately the same. However, for large shifts, the lower-sided chart outperforms than the two-sided chart. The CV of the one-sided chart is highly variable as compared to the two-sided chart. For the detection of a process improvement, the one-sided chart is quite effective than the two-sided chart. However, the detection is not quick as we observed in the case of a process deterioration.

Again, it is worth mentioning that we use the predictive control limits to design the EWMA and the CUSUM. The steps to obtain these limits have been mentioned in the previous section.

A comparison study of the EWMA and the CUSUM charts has been given in Tables 7.1-7.2. We observed that the one-sided EWMA chart was an effective in detection of a small to moderate shifts than the CUSUM. However, in the case of two-sided chart, the EWMA chart performance is appreciated over the CUSUM only for the large shifts. The CUSUM chart outperforms for small shifts than the EWMA chart. For the upper-sided chart, the CUSUM gives a quicker detection than the two-sided chart and for large shifts, the EWMA chart is preferred over the CUSUM. In the case of two-sided chart, the CUSUM outperforms uniformly, which is against the believed perception, i.e., EWMA chart performs better than a CUSUM for large shifts, and we argue this verifies the importance of the base period. Therefore, to see the effect of a base period, we have Table-7.2. From Table-7.2, one can notice that the predictive control chart performance can be improved by using a large base period (cf. Tables 7.1-7.2). We notice that the CUSUM chart is very effective for the detection of small shifts, and EWMA chart is good for large shifts (cf. Table-7.2). Therefore, we have an advantage of a large base period, i.e., it improves the detection ability of a control chart. This statement should not be taken as the predictive chart can only be developed/used if a base period is available. The main contribution of this study is to introduce a sophisticated process monitoring technique that could be applicable without a base period requirement.

7.5.1 Improved Predictive Control Charts

In the previous section, we noticed that the performance of predictive charts was not the same as expected. Thus, a natural question would be, why do all the charts have a poor detection/performance? To address this question, we have the following explanation: Since each observation contributes to uncertainty of the control limits, this causes deterioration or improvement in the control limits. Therefore, this uncertainty will either move up or down the control limit than its in-control position. To understand it in a better way, let's take a closer look of these control limits by depicting them. In Figure-7.3, we have plotted control limits using the base period equals to one and five, respectively, for the process deterioration and improvement monitoring. From Figure-7.3, clearly, the control limits with a small base period are more variable than the case of large phase-I data set, i.e., compare the control limits for base period one and five. As the process deteriorates or improves, these control limits also drift down or up. Thus, in such a situation, a system which is actually an out-of-control may be thought in-control (cf. Figure-7.3). We also notice that the same problem is present in the case of a misspecified prior (cf. Figure-7.4).

Suppose that we have an observation $y = x_{i+1}$ and by comparing this observation with

the control limits, which were established at step i, i.e., (LCL_{i+1}, UCL_{i+1}), we found that the observation y is in-control. Now, we have to decide whether to update the control limits using this observation or not. Since the observation has been declared in a safe region, i.e., in-control, it must be used to get the updated control limits for the monitoring of TBE at time point $i+2$. We have shown in Figure-7.3, however, the control limits also drift when we update them, i.e., inclusion of an observed time causes them to drift. Therefore, one has to wait a long time to detect an out-of-control alarm, and it leads to control chart insensitivity. Note that this behavior is not acceptable in many situations, e.g. short-run production processes. Similarly, one might have knowledge about the occurrence of a shift at a particular time point, but insensitivity of the control limits delay the search operation.

The emphasis of a production management is to keep the process on target rather than allowing it to drift upward or downward. Therefore, one needs to introduce a measure or a check that may inspect the control limits and gives an alarm when a minimum allowable drift has been attained. With such a precautionary check, the out-of-control signal could be an indication that an action must be exercised to stop the process form further drift/deterioration.

To prevent such kinds of drifts in the lower-sided geometric chart, Toubia-Stucky et al. [2012] proposed two decision rules (Section 3.3 of Toubia-Stucky et al. [2012], page 208), which are:

1. The first set of decision rules has a higher power for deterioration detection but also has a higher false alarm rate. The authors recommended its use when the risk of a potential deterioration is very serious. The rules requires that in four consecutive observations, any of the conditions apply:

    - the sum of the deteriorations shows at least 20% deterioration in LCLs;
    - one deterioration shows at least 15% deterioration in LCL; and
    - there is at least 5% deterioration in each of three consecutive LCLs.

2. The second set of rules is more stringent and has less power but smaller false alarm rate. In these rule, a necessary but not sufficient condition for deterioration detection is to observe three deteriorations out of the four recent observations. A sufficient condition is to have any of the following:

    - the sum of the deterioration shows at least 25% deterioration in LCLs;
    - one observation shows at least 20% deterioration in LCL; and
    - there is at least 5% deterioration in each of three consecutive LCLs.

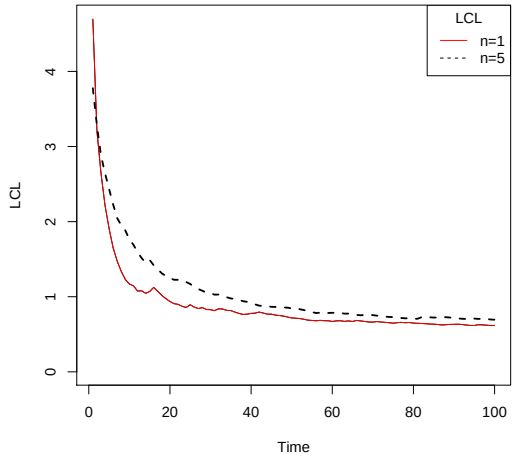

(a) LCL for $\lambda = 0.005$

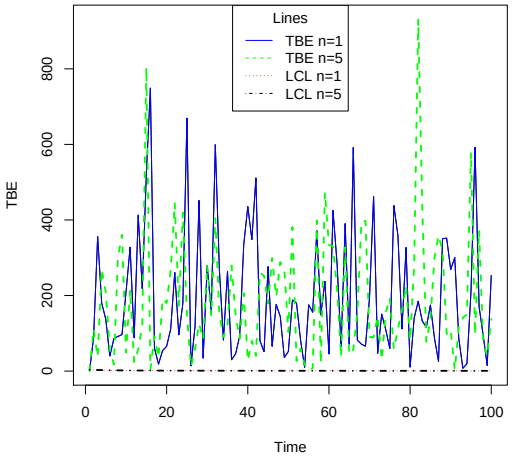

(b) Deterioration Detection for $\lambda = 0.005$

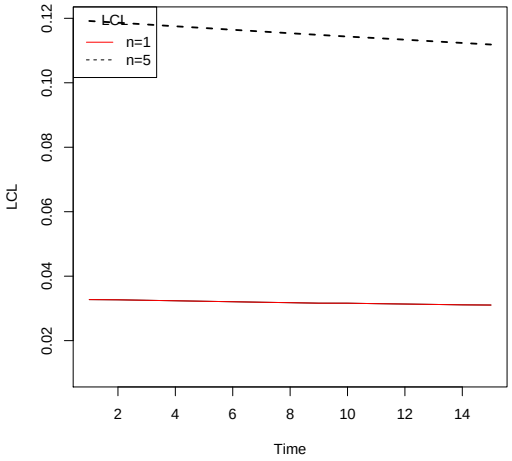

(c) Deterioration Detection for $\lambda = 0.5$

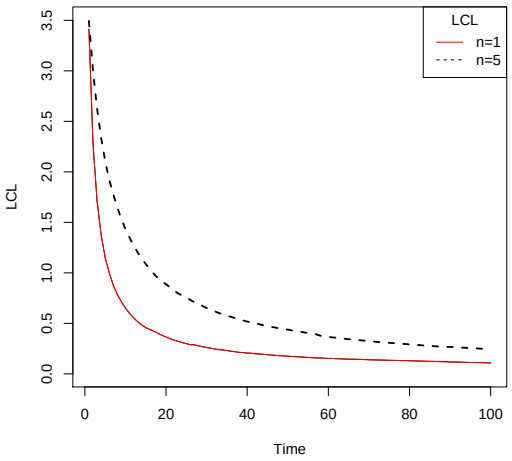

(d) Deterioration Detection for $\lambda = 0.05$

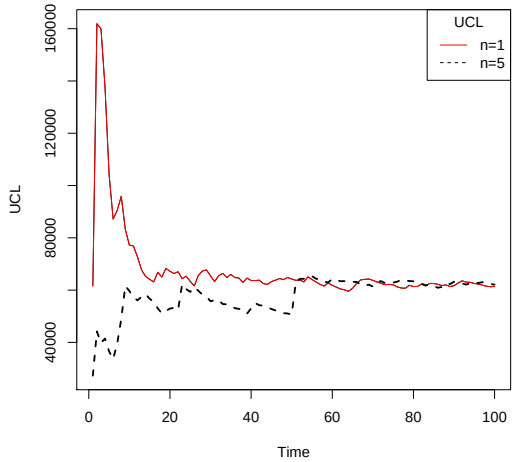

(e) UCL for $\lambda = 0.0001$

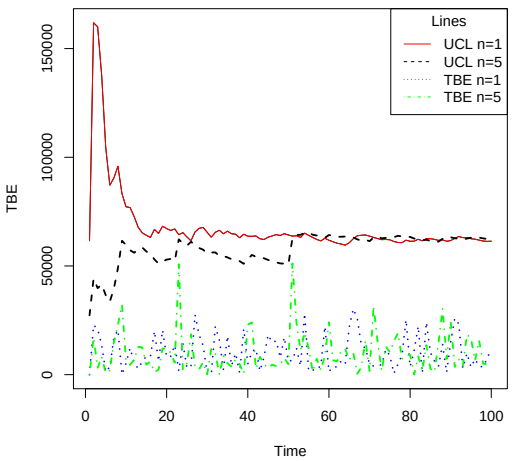

(f) Improvement Detection for $\lambda = 0.0001$

Figure 7.3: Sequential Control Limits Comparison for the base period $n = 1$ and $n = 5$

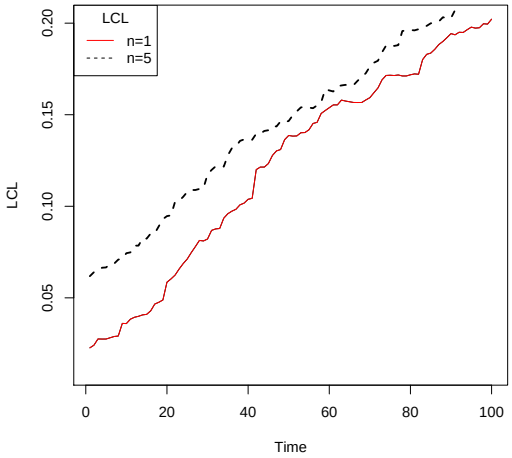

(a) LCL for $\lambda = 0.005$

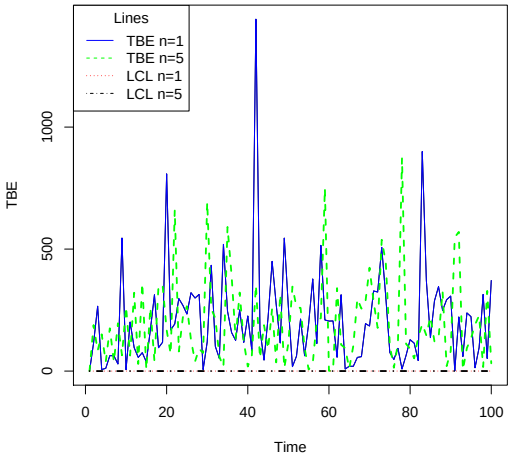

(b) Deterioration Detection for $\lambda = 0.005$

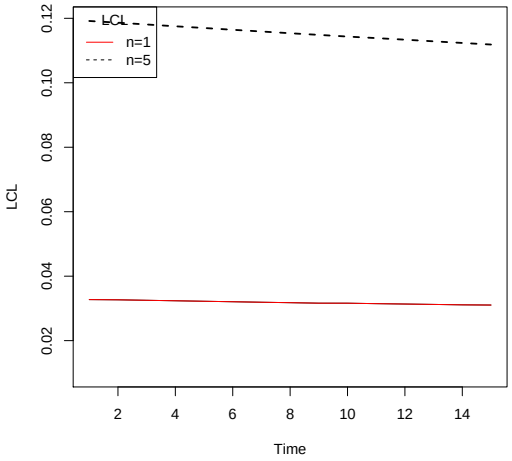

(c) Deterioration Detection for $\lambda = 0.5$

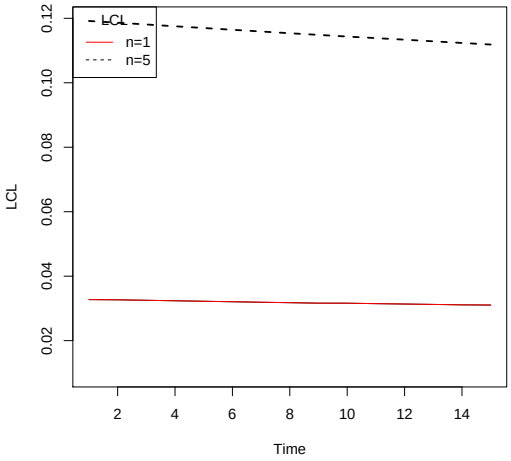

(d) Deterioration Detection for $\lambda = 0.05$

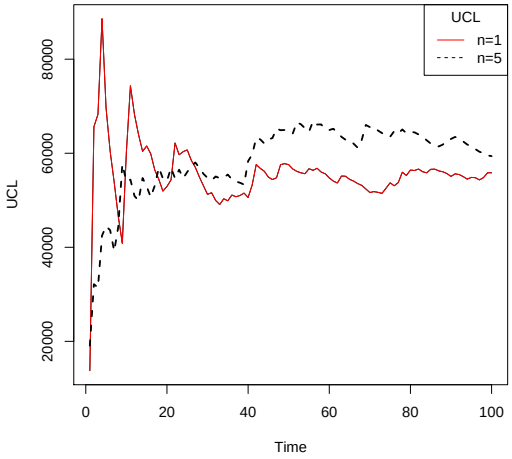

(e) UCL for $\lambda = 0.0001$

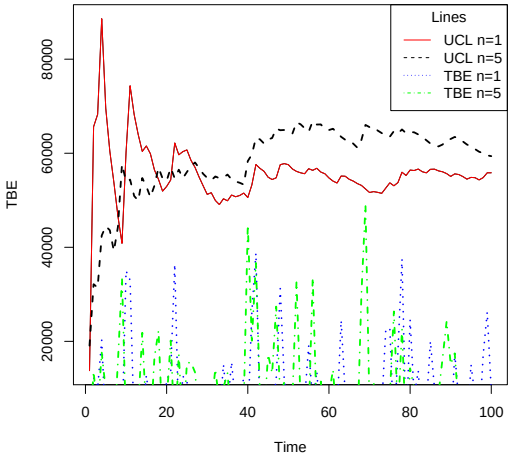

(f) Improvement Detection for $\lambda = 0.0001$

Figure 7.4: Sequential Control Limits Comparison for the base period $n = 1$ and $n = 5$: the case of a misspecified prior

To make the control chart adaptive, Toubia-Stucky et al. [2012] proposed that if 6 points are below the LCL, then revise the prior distribution to adopt a possible trend. With a simulation study, they showed that the proposed chart works efficiently in different scenarios. However, from the rules proposed by Toubia-Stucky et al. [2012], it is not easy to define a precise criterion for the evaluation of a deterioration in the LCL. Thus, motivated by this fact, we have proposed a mathematical formulation in Section-7.2 to evaluate the control limits' deterioration. Moreover, our proposed criterion is suitable for all types of shifts, i.e., small, large and time varying shifts (will be discussed in Section-7.5.2). With the traditional predictive control limits, this cogent identity would assist to decide whether one should stop or not for the possible inspection of a process.

Note that this marriage of the predictive control limits with the PCDC could be thought as a use of a synthetic chart, i.e., combining the predictive chart with the cumulative probability control chart. The basic notion behind this criterion is to minimize the impact of a drift and increase the sensitivity of the predictive chart. We define the following steps to monitor a process with the PCDC and the predictive chart.

1. Fix c, and find the predictive control limits at time i, i.e., (LCL_{i+1}, UCL_{i+1}), and wait for the next TBE appearance X_{i+1}. Note that i denotes the time index associated with a system failure.

2. If $X_{i+1} \in (LCL_{i+1}, UCL_{i+1})$, go to the next step.

3. Check whether X_{i+1} satisfies the PCDC at the specified value of c. If the condition is satisfied, go to step 1. Otherwise, go to the next step.

4. Inspect the process for a possible deterioration or improvement.

We used $c = 0.10$ and $c = 0.90$ as the stopping criteria in PCDC and results have been given in Tables 7.3-7.4. From Tables 7.3-7.4, it is clear that using the PCDC, the control charts' sensitivity has been greatly improved. By comparing the lower-sided chart with the two-sided chart, i.e., Table-7.3, one can notice that two-sided chart outperforms than the one-sided chart. If we fix $c = 0.95$, however, the one-sided chart becomes superior than the two-sided chart. The CV gradually decreases with the size of a shift in both charts. This observation is also true for the process improvement case with one addition, i.e., the upper-sided chart is superior than its counterpart, two-sided chart, especially for large shifts. We observed that having a base period is advantageous and the numerical study tabulated in Table-7.4 supports this conclusion. By comparing Tables 7.1-7.2 and Table 7.3-7.4, one can distinguish that the control charts detection ability has greatly been improved by the PCDC. We also observed that $s = 0.0015$ led to the nominal ARL, i.e. 370, but the performance of the predictive control chart was compromised, i.e., the results were approximately the same as reported in Tables 7.1-7.2.

The EWMA and the CUSUM charts have also been designed with the PCDC, and we noticed an improved performance of these charts over the simple EWMA and CUSUM charts (cf. Tables 7.3-7.4 versus Table 7.1-7.2). However, the CV behavior is opposite as we observed in the case of Shewhart charts, i.e., the CV increased with the size of a shift. The lower-sided EWMA outperforms than the two-sided EWMA chart for a process deterioration detection. For the process improvement case, however, a reverse behavior has been observed. The small size shifts were detected efficiently by the CUSUM while large shifts by the EWMA chart. The two-sided CUSUM detects the shifts quickly as compared to the one-sided. Moreover, we have observed that the one-sided charts become more efficient than the two-sided charts with the usage of a large base period. Therefore, it is an indication that a base period has a positive effect on the control chart performance (cf. Table-7.1 versus Table-7.4), if available.

Misspecification of prior: In addition to informative prior, we have also studied the effect of a misspecified prior information on the control chart performance for $n = 1$ and $n = 5$, respectively. In this case, the hyperparameters were selected to reflect a high level of the prior uncertainty, i.e., the mean of the prior distribution was selected close to 1700 with a large value of the prior variance. The ARL has been computed in this case again, and results are summarized in Figures 7.5-7.6 for the lower, upper and the two-sided Shewhart, EWMA and CUSUM control charts, respectively. We notice that the misspecification of a prior has a significant effect on the chart performance, and again our proposed criterion of the PCDC works efficiently. One must be very careful about the choice or selection of the hyperparameters to design a control chart.

Table 7.1: ARL comparison based on $\alpha = 0.0027, n = 1, \lambda_0 = 0.0005$ for the predictive charts.

λ	PM	Lower-Sided			Upper-Sided			Two-Sided		
		Shewhart	EWMA	CUSUM	Shewhart	EWMA	CUSUM	Shewhart	EWMA	CUSUM
0.5	ARL	1.11751	5	8.156271	.	.	.	1.696	7.5241	28.00227
	CV	0.389586	0.00602	0.927325	.	.	.	1.014861	0.102671	0.001699
0.1	ARL	13.49612	5	10.351771	.	.	.	169.3478	7.556171	30.36865
	CV	3.911209	0.001604	0.942970	.	.	.	1.553131	0.123516	0.018997
0.05	ARL	16.60209	5.00108	27.37181	.	.	.	189.5884	7.718161	32.12037
	CV	3.758719	0.006568	0.956196	.	.	.	1.459648	0.145161	0.029227
0.005	ARL	288.8547	5.36503	34.16258	.	.	.	305.0023	8.168	35.65317
	CV	1.201923	0.089752	0.896834	.	.	.	1.334888	0.223671	0.268752
0.0009	ARL	351.7705	9.20493	229.7637	.	.	.	353.16241	14.16271	227.653284
	CV	1.031917	0.310811	0.791761	.	.	.	1.30145	0.252618	0.345624
0.0008	ARL	363.2888	39.80445	170.296	.	.	.	362.127818	45.462819	180.66533
	CV	0.995812	1.277075	0.799027	.	.	.	1.229172	0.672514	0.436754
0.0007	ARL	365.9619	59.453713	134.8705	.	.	.	366.724517	165.161721	150.785325
	CV	1.006588	1.283627	0.753391	.	.	.	1.168261	0.987161	0.512387
0.0006	ARL	370.8377	65.35271	100.2968	.	.	.	371.368119	187.17156	130.25372
	CV	0.996533	1.313462	0.714211	.	.	.	1.118256	0.998161	0.643527
0.00055	ARL	371.8719	76.342561	81.90896	.	.	.	372.17261	190.16711	100.654238
	CV	0.993126	1.338161	0.702672	.	.	.	1.062781	1.027167	0.765321
0.0004	ARL	.	.	.	370.3136	34.62671	39.16613	372.3303	45.67528	44.69146
	CV	.	.	.	0.994412	1.216535	0.632355	0.988483	1.20431	0.631582
0.0003	ARL	.	.	.	369.0865	32.16382	26.50686	360.2013	42.36271	29.02461
	CV	.	.	.	0.993886	1.286001	0.498395	1.013227	1.156721	0.494659
0.0002	ARL	.	.	.	319.0701	29.14086	16.67229	353.768	40.16171	19.86776
	CV	.	.	.	1.111468	1.378603	0.423853	1.024611	1.136372	0.341530
0.0001	ARL	.	.	.	310.7443	27.15721	10.86007	346.3985	38.161783	12.48067
	CV	.	.	.	1.140515	1.523123	0.324427	1.053064	1.113836	0.281696
0.00009	ARL	.	.	.	292.3253	22.16271	11.59877	333.0463	35.62718	11.91697
	CV	.	.	.	1.200851	1.632476	0.230802	1.090416	1.082625	0.281389
0.00008	ARL	.	.	.	271.5607	14.55617	10.08818	320.5763	30.252715	11.84683
	CV	.	.	.	1.275436	1.797293	0.295902	1.112811	1.056721	0.230973
0.00007	ARL	.	.	.	247.5009	9.9664	9.41871	290.16271	26.748191	10.99361
	CV	.	.	.	1.221054	1.856962	0.317764	1.125271	1.036271	0.260795
0.00006	ARL	.	.	.	220.9925	8.21189	9.27332	263.11721	21.362717	10.427
	CV	.	.	.	1.236559	1.566832	0.276679	1.136271	1.00877	0.267303
0.00005	ARL	.	.	.	175.1687	7.89594	8.34888	231.37831	12.637381	9.45426

	CV	.	.	.	1.253776	1.556245	0.341021	1.145613	0.965318	0.333349

Table 7.2: ARL comparison based on $\alpha = 0.0027, n = 5, \lambda_0 = 0.0005$ for the predictive charts.

λ	PM	Lower-Sided			Upper-Sided			Two-Sided		
		Shewhart	EWMA	CUSUM	Shewhart	EWMA	CUSUM	Shewhart	EWMA	CUSUM
0.5	ARL	1.11444	2	5.45271	.	.	.	1.40675	2	14.87433
	CV	0.335701	0.00005	0.710237	.	.	.	0.616504	0.051617	0.105414
0.1	ARL	3.89043	2	10.36271	.	.	.	42.26126	2	16.712826
	CV	1.600053	0.000388	0.744262	.	.	.	3.175982	0.124511	0.129446
0.05	ARL	4.750639	2	14.62819	.	.	.	119.1324	2	16.73628
	CV	2.491653	0.000432	0.764527	.	.	.	2.475554	0.156171	0.226738
0.005	ARL	191.1802	2.00002	25.17168	.	.	.	159.2654	2.168	27.746347
	CV	1.486304	0.002236	0.785267	.	.	.	1.672571	0.173420	0.326177
0.0009	ARL	264.4589	2.25866	220.9948	.	.	.	288.0223	20.464712	189.727281
	CV	1.004845	0.224456	0.8073968				1.506721	0.556237	0.489261
0.0008	ARL	330.778	2.1107	160.3423	.	.	.	334.162721	25.637188	176.63721
	CV	1.085457	0.152705	0.833019	.	.	.	1.372625	0.764728	0.572628
0.0007	ARL	352.753	3.08346	122.9291	.	.	.	355.715138	29.647271	150.454621
	CV	1.03256	0.519544	0.799609	.	.	.	1.202635	0.807353	0.698362
0.0006	ARL	362.2115	63.51835	87.17527	.	.	.	364.37271	89.637214	130.487201
	CV	0.990646	0.325849	0.760985	.	.	.	1.147251	0.998462	0.765881
0.00055	ARL	371.208	62.56802	73.58579	.	.	.	371.98621	98.736231	64.32288
	CV	0.990160	0.345567	0.737288	.	.	.	1.085241	0.996518	0.852617
0.0004	ARL	.	.	.	348.7692	34.57281	37.07558	366.3807	78.563726	26.20959
	CV	.	.	.	1.04572	0.820405	0.667424	0.999474	1.043537	0.587541
0.0003	ARL	.	.	.	282.5849	31.67821	25.22783	358.1821	65.352371	23.79701
	CV	.	.	.	1.205145	0.856742	0.538253	1.022826	1.102726	0.627307
0.0002	ARL	.	.	.	183.9078	28.75241	16.59847	291.262711	54.252718	17.0224
	CV	.	.	.	1.609179	0.885891	0.406721	0.992263	1.127483	0.530307
0.0001	ARL	.	.	.	170.8358	25.16281	8.81098	192.9316	47.362184	9.12609
	CV	.	.	.	1.695015	0.919880	0.438932	1.014186	1.156382	0.467324
0.00009	ARL	.	.	.	116.798	8.67218	6.11287	170.36172	30.563472	9.30243
	CV	.	.	.	2.123062	0.953371	0.632753	1.101172	1.156372	0.406031
0.00008	ARL	.	.	.	82.68207	7.62771	7.42497	103.95871	20.74382	8.06135
	CV	.	.	.	2.552883	0.953438	0.463356	1.091711	1.172627	0.662849
0.00007	ARL	.	.	.	67.73738	4.15267	4.94047	92.11671	10.26261	5.216373
	CV	.	.	.	2.881811	0.983391	0.670445	1.116271	1.20273	0.857978

0.00006	ARL	.	.	.	34.17376	3.15172	4.08792	78.52612	5.736214	5.84638
	CV	.	.	.	2.45103	0.830638	0.722518	1.121728	1.21022	0.821579
0.00005	ARL	.	.	.	17.0419	1.68262	2.93325	32.25171	3.36371	4.30126
	CV	.	.	.	2.358239	1.060026	0.804909	1.128161	1.183737	0.713636

Table 7.3: ARL comparison based on $\alpha = 0.0027, n = 1, \lambda_0 = 0.0005$ for the predictive charts.

λ	PM	Lower-Sided			Upper-Sided			Two-Sided		
		Shewhart	EWMA	CUSUM	Shewhart	EWMA	CUSUM	Shewhart	EWMA	CUSUM
0.5	ARL	1	1	1	.	.	.	1	1	1
	CV	0	0	0	.	.	.	0	0	0
0.1	ARL	1	1	1	.	.	.	1	1	1
	CV	0	0	0	.	.	.	0	0	0
0.05	ARL	1.00235	1.0004	1	.	.	.	1.00112	1.0054	1.01167
	CV	0.048512	0.019988	0	.	.	.	0.033410	0.073703	0.107711
0.005	ARL	3.0678	1.61343	3.30622	.	.	.	2.57826	1.91637	2.99375
	CV	1.1704	0.310714	1.175427	.	.	.	0.935662	1.005225	1.136073
0.0009	ARL	9.01241	6.46371	10.22498	.	.	.	6.00417	6.08092	4.68603
	CV	0.958089	0.846123	0.909021	.	.	.	0.852171	0.801911	1.033385
0.0008	ARL	10.115262	5.14936	7.76323	.	.	.	6.14032	5.90768	6.12198
	CV	1.029564	0.778976	0.827372	.	.	.	0.818365	0.784510	0.824486
0.0007	ARL	9.93009	6.08596	5.32905	.	.	.	5.13183	5.87116	5.9691
	CV	0.938149	0.829496	0.945883	.	.	.	0.799075	0.785703	0.788439
0.0006	ARL	10.22693	9.40633	7.21498	.	.	.	5.96384	6.03002	5.73424
	CV	0.922607	0.861411	0.988039	.	.	.	0.879704	0.790148	0.912815
0.00055	ARL	11.14897	11.03286	7.50859	.	.	.	5.69067	5.81907	5.589981
	CV	0.886427	0.889951	0.970954	.	.	.	0.782307	0.888212	0.878461
0.0004	ARL	.	.	.	5.92805	7.14327	6.64098	4.74622	5.78219	4.74277
	CV	.	.	.	0.855337	0.839678	0.844475	0.810708	0.903497	0.840233
0.0003	ARL	.	.	.	11.78675	5.65179	5.40085	3.67629	3.13395	4.41233
	CV	.	.	.	0.738681	0.93497	0.822638	0.855609	0.864077	0.817386
0.0002	ARL	.	.	.	9.72262	3.49029	3.430159	3.94705	2.28317	3.15708
	CV	.	.	.	0.913541	0.955745	0.802672	0.842989	0.815462	0.855181
0.0001	ARL	.	.	.	1.89232	3.7898	3.404924	2.01395	1.51277	1.94267
	CV	.	.	.	0.701019	0.965233	0.815777	0.723537	0.590802	0.755780
0.00009	ARL	.	.	.	2.56441	2.98798	3.23473	1.7004	2.03464	1.59957
	CV	.	.	.	0.886370	0.932754	0.817668	0.696659	0.781058	0.658168
0.00008	ARL	.	.	.	1.90361	2.19687	2.397	1.94542	1.44283	1.40254

	CV	.	.	.	0.768883	0.839666	0.560271	0.756792	0.585316	0.541558
0.00007	ARL	.	.	.	1.81976	1.65955	1.732584	2.85956	1.59965	1.86058
	CV	.	.	.	0.738816	0.641613	0.51767	0.853433	0.656054	0.740773
0.00006	ARL	.	.	.	1.36575	1.99177	1.742883	2.39124	2.24957	1.58007
	CV	.	.	.	0.523131	0.718285	0.577869	0.829172	0.812893	0.612041
0.00005	ARL	.	.	.	1.256557	1.4179	1.43823	2.28024	1.29664	1.24738
	CV	.	.	.	0.506371	0.657432	0.529321	0.820450	0.498254	0.457833

Table 7.4: ARL comparison based on $\alpha = 0.0027, n = 5, \lambda_0 = 0.0005$ for the predictive charts.

λ	PM	Lower-Sided			Upper-Sided			Two-Sided		
		Shewhart	EWMA	CUSUM	Shewhart	EWMA	CUSUM	Shewhart	EWMA	CUSUM
0.5	ARL	1	1	1	.	.	.	1	1	1
	CV	0	0	0	.	.	.	0	0	0
0.1	ARL	1	1.00001	1	.	.	.	1	1	1
	CV	0	0.003162	0	.	.	.	0	0	0
0.05	ARL	1	1.00093	1.00004	.	.	.	1.00001	1.0002	1.00001
	CV	0	0.030454	0.006324	.	.	.	0.003162	0.014138	0.003162
0.005	ARL	1.26945	1.42115	1.56541				1.94153	1.53944	1.81658
	CV	0.494581	0.581021	0.676015	.	.	.	0.989247	0.662959	0.772218
0.0009	ARL	7.31874	1.99756	6.37002	.	.	.	5.97862	5.79034	4.1883
	CV	1.061354	0.302759	1.036145	.	.	.	0.866860	0.909040	0.844237
0.0008	ARL	7.46359	2.21873	4.76323	.	.	.	5.90957	5.29253	5.75702
	CV	1.056876	0.340651	1.026943	.	.	.	0.852643	0.835734	0.913075
0.0007	ARL	9.68561	2.18198	3.67418	.	.	.	5.3181	5.99912	5.88322
	CV	0.949954	0.334894	0.920492	.	.	.	0.959019	0.860602	0.845419
0.0006	ARL	7.18507	3.1268	3.186535	.	.	.	5.96384	5.55811	4.7053
	CV	1.014462	0.596939	0.895704	.	.	.	0.879704	0.841591	0.812969
0.00055	ARL	7.9086	3.01801	2.835419	.	.	.	5.99925	4.70786	4.28281
	CV	0.991162	0.568909	0.865289	.	.	.	0.876082	0.843877	0.842425
0.0004	ARL	.	.	.	4.98567	4.78579	3.48571	4.51681	3.49605	3.95951
	CV	.	.	.	0.946240	0.955364	0.775390	0.841255	0.836428	0.840783
0.0003	ARL	.	.	.	4.9108	3.56326	2.10462	3.01291	2.00297	3.39377
	CV	.	.	.	0.872261	0.849437	0.738532	0.815658	0.722723	0.836099
0.0002	ARL	.	.	.	4.90644	3.97847	3.73384	1.96546	2.01677	2.91835
	CV	.	.	.	0.869382	0.865419	0.851230	0.711452	0.724078	0.815429
0.0001	ARL	.	.	.	1.52581	1.93089	1.97334	1.80145	1.4699	1.79409
	CV	.	.	.	0.622242	0.708649	0.778042	0.724876	0.598479	0.680551

0.00009	ARL	.	.	.	1.4956	1.31919	2.20984	1.68455	1.49181	1.56918
	CV	.	.	.	0.582700	0.497769	0.752065	0.650537	0.582467	0.608598
0.00008	ARL	.	.	.	1.27087	1.45595	1.58278	1.33747	1.37271	1.4016
	CV	.	.	.	0.466924	0.564305	0.61525	0.510216	0.528553	0.561172
0.00007	ARL	.	.	.	1.30191	1.38012	1.428629	1.36753	1.29646	1.4635
	CV	.	.	.	0.485429	0.555638	0.476109	0.524195	0.483518	0.570497
0.00006	ARL	.	.	.	1.28766	1.33123	1.420783	1.34278	1.32993	1.35127
	CV	.	.	.	0.491090	0.519558	0.414445	0.511581	0.502190	0.533943
0.00005	ARL	.	.	.	1.180772	1.14998	1.28166	1.33558	1.28241	1.38072
	CV	.	.	.	0.478352	0.364340	0.473349	0.504902	0.476292	0.395243

7.5.2 Some Other Experiments

In previous discussions, we mainly focused at shifts that were sustained in the process. Since the control limits are updated with time, it is natural to assume random and time varying shifts in a process to study the control chart performance. The importance of random shifts has recently been highlighted by Woodall and Driscoll [2015]. To enhance the ambit of the sequential charts, we also studied them for random and time varying shifts in this section. A summary of the run-length distribution has been depicted in Figures 7.7-7.8 by assuming different base periods. The red line in Figures 7.7-7.8 indicates the mean of the run-length distribution, i.e., ARL, while the blue line for the SDRL. In Figure-7.7, panel A and B, the histogram of the run-length distribution has been produced for the Shewhart control charts, i.e., without using the PCDC. We observe that even in the case of a random shift, the control charts are quite slow to give the out-of-control signal. However, by using the PCDC, one can see that the detection power of the control charts has been improved (cf. Figure-7.7, panel C and D). Note that to study the behavior of predictive charts, we generated the random shifts using a uniform distribution. The parameters of the uniform distribution have been selected to represent either the process improvement or deterioration, depending on a situation. However, the choice of uniform distribution has been done purely illustrative purpose, and one can consider some more realistic distributions for a random shift generation.

In Figure-7.8, we have presented histograms of the random but time varying shift, i.e., with the passage of time shift either increase or decrease. Again in this figure, the red line has been used to indicate the ARL while blue for the SDRL. It is worth mentioning that the simple control chart, i.e., without PCDC, performs very well for the time-varying shifts. Note that here we used the two-sided control chart, and we have the following explanation of its usage: since we have a random shift which varies with time, we do not know whether the process will either improve or deteriorate. Thus, instead of using a one-sided chart, it makes sense to use a two-sided chart. From our study, i.e., Figure-7.7 and Figure-7.8, we noticed that the predictive limits' control chart performs well for random but time varying shifts. However, in the case of just random shifts, one needs to use the PCDC to get an appreciable performance.

Penalizing the lower control limit for the process deterioration monitoring: For a process deterioration detection, a lower-sided control chart is commonly used. From Tables 7.1-7.2, we observed that the detection power of the lower-sided control chart is slow. Thus, a naive way to improve the detection power of the lower-sided chart, is to penalize it with a suitable factor. For this purpose, we designed a chart by penalizing the lower control limit, i.e., $LCL_{i+1} = i^p \times \beta_i\big[\big(\frac{1}{1-\alpha/2}\big)^{1/\phi_i} - 1\big]$, where i is a time index, and p denotes a penalizing factor. To choose an appropriate p and to compare it with the proposed improved control chart, i.e., with PCDC, we have Figure-7.9 for different values

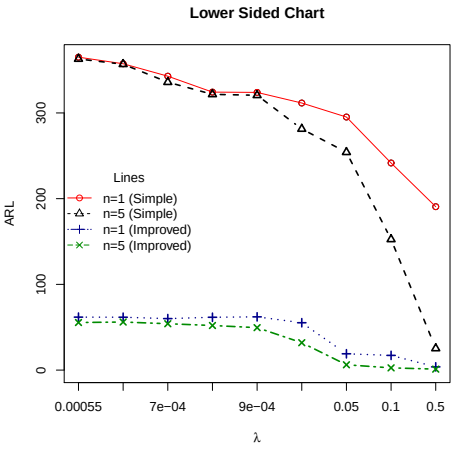

(a) Lower-sided Shewhart control chart

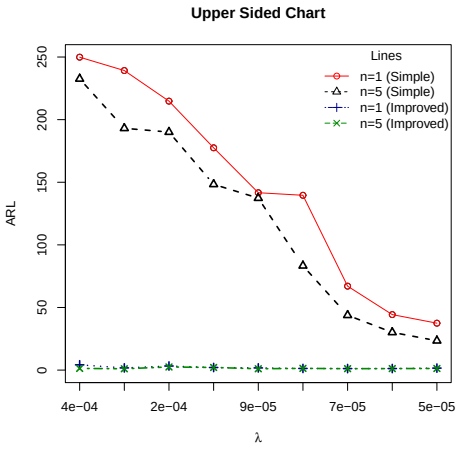

(b) Upper-sided Shewhart control chart

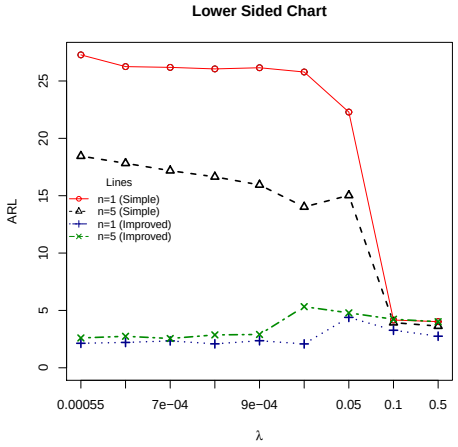

(c) Lower-sided EWMA control chart

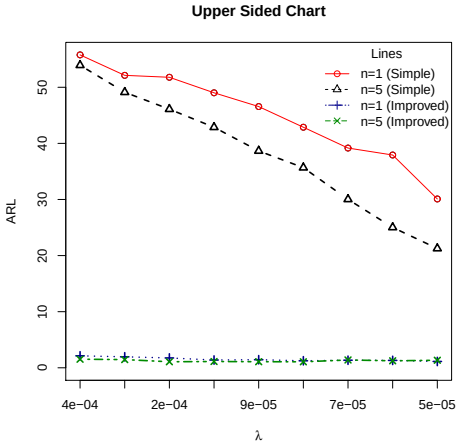

(d) Upper-sided EWMA control chart

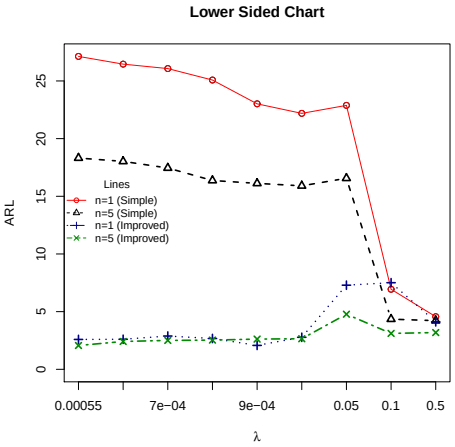

(e) Lower-sided CUSUM control chart

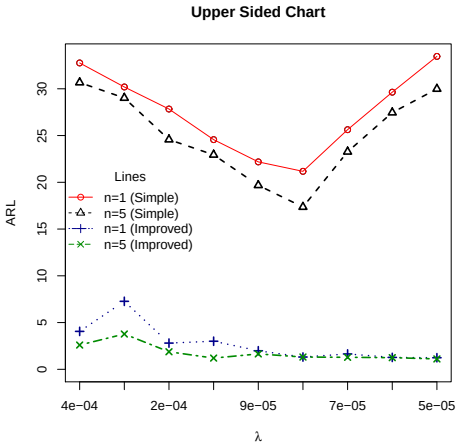

(f) Upper-sided CUSUM control chart

Figure 7.5: Comparison of the one-sided Shewhart, EWMA and CUSUM control charts for $n = 1$ and $n = 5$ using $\alpha = 0.0027$ under misspecified prior

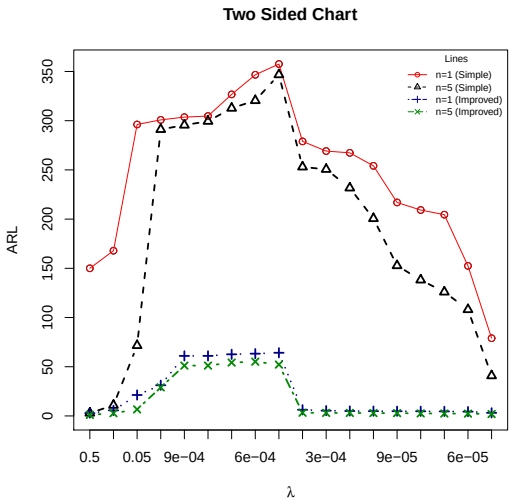

(a) Two-sided Shewhart control chart

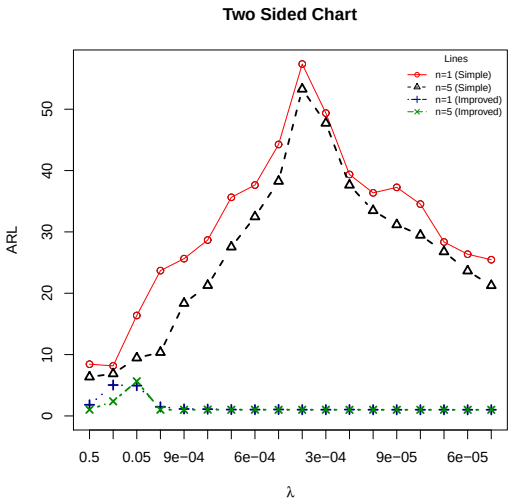

(b) Two-sided EWMA control chart

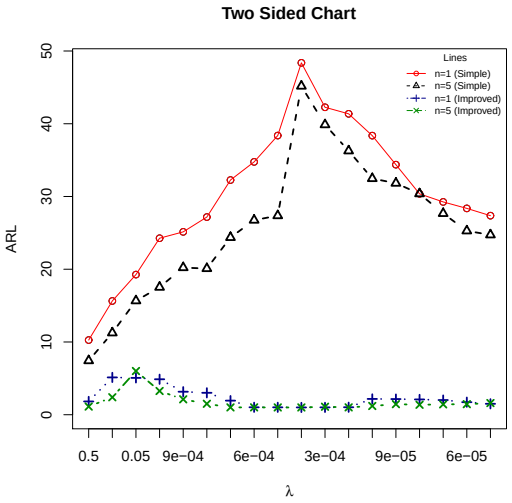

(c) Two-sided CUSUM control chart

Figure 7.6: Comparison of the two-sided Shewhart, EWMA and CUSUM control charts for $n = 1$ and $n = 5$ using $\alpha = 0.0027$ under misspecified prior

of p. We noticed that $p > 1.5$ would lead to approximately the same performance as it has been observed in a chart with the PCDC. Moreover, we also noticed that the selection of a penalized factor is not unique for all shifts, i.e., small and large shifts. One must be very careful to select an appropriate "p" for different size of shifts as it may lead to a different conclusion for different "p." However, our PCDC gives a consistent and uniform performance as compared to this penalization approach. The usefulness of a penalized control limit may be appreciated if someone is interested to study an estimated predictive value for tracking a target value, e.g. $\hat{y} = \frac{\sum_{i=1}^{j} y_i}{j}$ or $\hat{y} = \frac{\sum_{i=1}^{j} \psi^{j-i} y_i}{\sum_{i=1}^{j} \psi^{j-i}}$, where $0 < \psi < 1$ denotes the relative weight or importance factor for the current and the past values of y, which should be fixed in-advance.

7.6 Illustrative Examples

In this section, we discuss two illustrative examples to show the implementation of the proposed control charts in a real situation. The first example is about the deterioration detection while the second for the process improvement detection. To monitor the process deterioration, the first 8 observations in Table-7.5 have been considered in-control and generated by using $\lambda = 0.0005$ while the next 7 by using $\lambda = 0.005$, and the last 5 by using $\lambda = 0.05$. Hence, we have 8 observations from the in-control process while 12 from the out-of-control process. Note that to design a predictive charts, we will use $\alpha = 0.0027$ as a false alarm probability.

From Table-7.5, one can observe that using the Shewhart charts, either the one-sided or the two-sided chart, we do not get an out-of-control alarm, and thus the process could be considered in-control. However, by using $F < 0.10$ as the PCDC, we noticed that the chart raised a signal at the observation number 11. Therefore, predictive charts' sensitivity can be improved by our deterioration check. We put an asterisk "$\star$" in Table-7.5 to represent the process deterioration detection with the PCDC.

Similarly, to check the process improvement with the proposed predictive control charts, we have generated the first 8 in-control observations using $\lambda = 0.0005$ in Table-7.6. The next 7 observations have been generated using $\lambda = 0.0003$ while the last 5 from $\lambda = 0.00009$ to represent the out-of-control situation. In Table-7.6, an asterisk "$\star$" has been used to mark the improvement detection either by the upper-sided chart or by the proposed check. The double asterisk "$\star\star$" has been used to show the process improvement jointly by the PCDC and the Shewhart chart. Note that to detect a process improvement with the PCDC, we used $F > 0.90$ as the stopping criterion. From Table-7.6, both charts, i.e., the upper and the two sided, indicate that the process shows an improvement signal at the observation 12. The same conclusion is also supported by the PCDC. We also

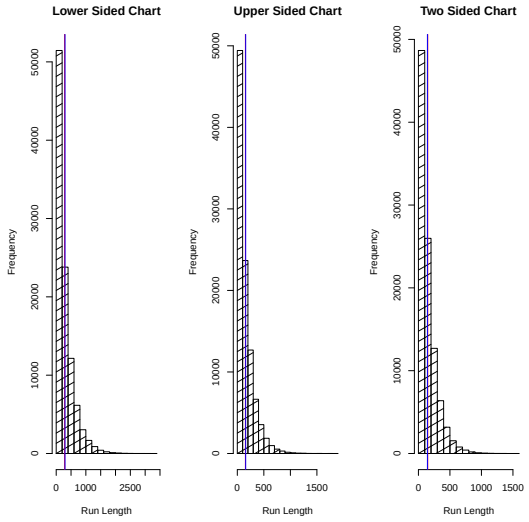

(a) Simple Shewhart Chart for $n = 1$

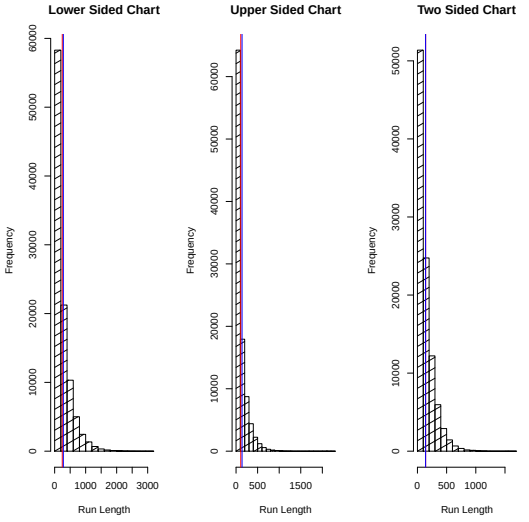

(b) Simple Shewhart Chart for $n = 5$

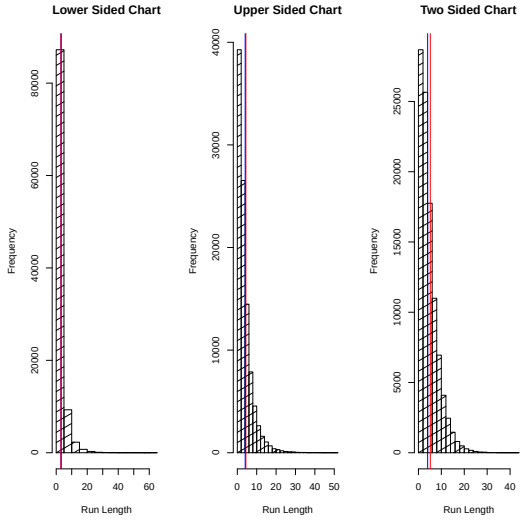

(c) Improved Shewhart Chart for $n = 1$

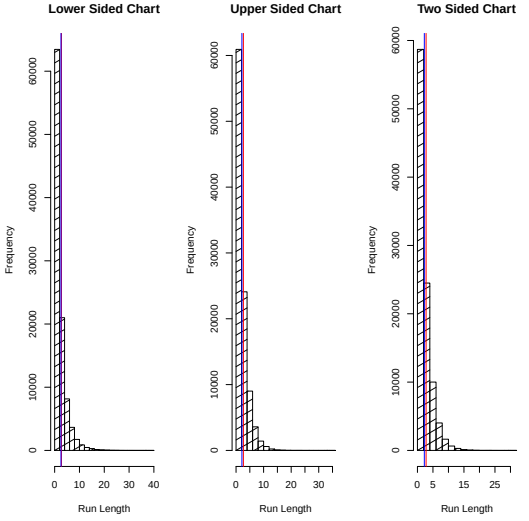

(d) Improved Shewhart Chart for $n = 5$

Figure 7.7: Comparison of the simple and improved Shewhart control charts for random shift in the process, red line represents the ARL while blue line SDRL

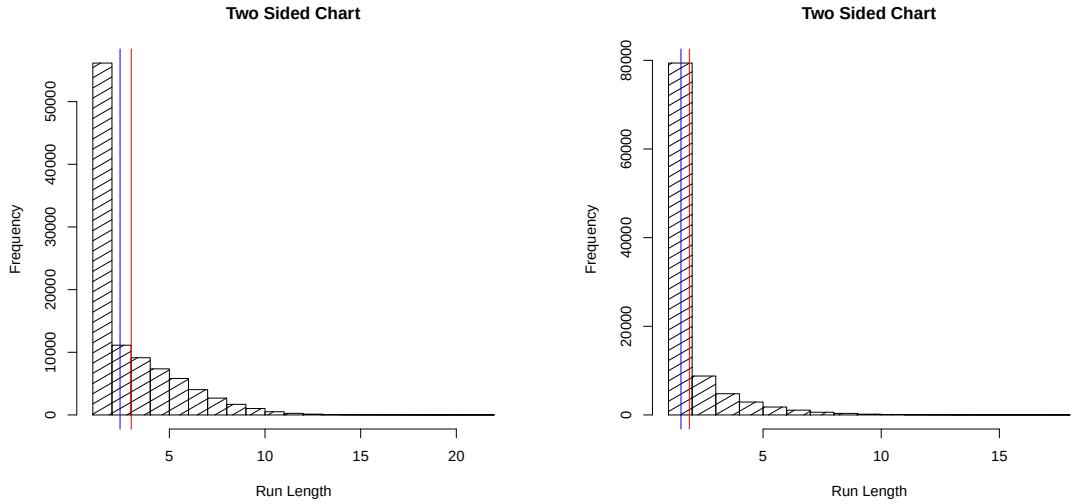

(a) Shewhart Chart for $n = 1$ (b) Shewhart Chart for $n = 5$

Figure 7.8: Comparison of the Two-sided Shewhart control chart for time varying random shift in the process, red line indicates the ARL while blue line SDRL

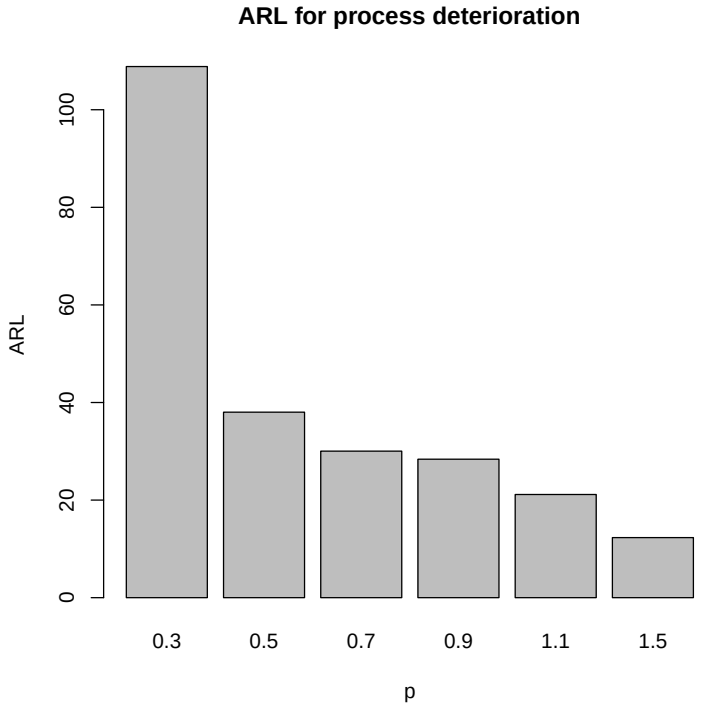

Figure 7.9: Average run length for the process deterioration by considering different penalization factors at $\lambda = 0.0008$

Table 7.5: Illustration of predictive charts for the process deterioration with base period equals to one.

Sr. No.	Y	LCL (one-sided)	UCL (one-sided)	LCL (two-sided)	UCL (two-sided)	F	Posterior Mean
1	2226.3477	.	.	.	.	.	0.000503
2	3837.6864	5.378964	72548.499	2.686755	104246.129	0.741049	0.000384
3	1077.786	7.045316	24579.590	3.519483	62887.805	0.321337	0.000449
4	2786.6162	6.012127	13467.545	3.003524	37496.348	0.663935	0.000428
5	1530.5017	6.316592	9001.767	3.155734	32105.816	0.459763	0.000454
6	733.7275	5.953402	6679.559	2.974354	26523.536	0.277009	0.000502
7	1431.1919	5.386199	5279.845	2.691019	21891.569	0.495408	0.000520
8	597.9523	5.196572	4352.097	2.596310	19741.018	0.263064	0.000563
9	816.53806	4.798744	3695.295	2.397570	17309.923	0.361567	0.000596
10	299.53444	4.539598	3207.349	2.268111	15718.479	0.162090	0.000644
11	119.32692	4.200487	2831.295	2.098695	14069.932	0.073691*	0.000697
12	65.35899	3.877295	2532.999	1.937228	12636.259	0.044475*	0.000753
13	32.44043	3.592605	2290.826	1.794995	11441.880	0.024098*	0.000809
14	211.89106	3.342231	2090.434	1.669905	10437.644	0.156657	0.000856
15	11.96006	3.157591	1921.951	1.577657	9695.593	0.010186*	0.000913
16	12.904326	2.962246	1778.371	1.480059	8962.717	0.011705*	0.000969
17	6.624713	2.790035	1654.588	1.394019	8333.045	0.006398*	0.001026
18	9.862966	2.636016	1546.796	1.317068	7783.242	0.010063*	0.001082
19	21.914817	2.498672	1452.101	1.248447	7302.619	0.023421*	0.001138
20	26.135665	2.376693	1368.264	1.187503	6882.641	0.029274*	0.001193
21	.	2.266875	1293.528	1.132635	6510.456	.	.

notice that after the observation 12, one-sided Shewhart chart gives a persistent signal of the process improvement. However, one should be very careful to believe this singling because of the control limits deterioration or drift. Therefore, the PCDC helps to decide whether the process improvement is real or not.

7.6.1 Revision of Prior

In this section, we discuss some methods to revise a prior information. Although we are not in favor of changing or revising a prior information, the effect of a prior information would automatically be minimized as one gathered more and more data. Since our predictive approach can be implemented practically with one data point, many researchers may be comfortable by revising their prior information. We suggest that one should adopt this approach only after confirming the out-of-control signal (cf. Toubia-Stucky et al. [2012]), i.e., whether it is true out-of-control or just a false alarm. Therefore, we suggest empirical Bayes approach, particularly the method of moments and the maximum likelihood method, for the revision of a prior information.

Empirical Bayes procedures utilize the past data as a means of bypassing the necessity of identifying a completely unknown and unspecified prior distribution, and have a frequency interpretation. We refer interested readers to Petrone et al. [2014b], and Petrone

Table 7.6: Illustration of predictive charts for process improvement with base period equals to one.

Sr. No.	Y	LCL (one-sided)	UCL (one-sided)	LCL (two-sided)	UCL (two-sided)	F	Posterior Mean
1	2226.3477	.	.	.	.	0.000503	
2	3837.6864	5.378964	72548.499	2.686755	104246.13	0.741049	0.0003839
3	1077.786	7.045316	24579.590	3.519483	62887.81	0.3213374	0.000449
4	2786.6162	6.012127	13467.545	3.003524	37496.35	0.6639345	0.000428
5	1530.5017	6.316592	9001.767	3.155734	32105.82	0.4597634	0.000454
6	733.7275	5.953402	6679.559	2.974354	26523.54	0.2770096	0.000502
7	1431.1919	5.386199	5279.845	2.691019	21891.57	0.4954076	0.000520
8	597.9523	5.196572	4352.097	2.596310	19741.02	0.2630640	0.000563
9	1665.0554	4.798744	3695.295	2.397570	17309.92	0.5903673	0.000567
10	1029.5954	4.769038	3207.349	2.382746	16512.92	0.4329855	0.000589
11	612.0787	4.588528	2831.295	2.292572	15369.71	0.2987605	0.000622
12	16076.8912**	4.344027	2532.999	2.170423	14157.36	0.9993091*	0.000368
13	3061.0868*	7.353747	2290.826	3.674197	23420.52	0.6602216	0.000364
14	2913.5639*	7.419636	2090.434	3.707131	23171.21	0.6406445	0.000363
15	7475.5625*	7.450147	1921.951	3.722388	22876.17	0.9174070*	0.000328
16	10085.387*	8.247788	1778.371	4.120932	24954.91	0.9504853*	0.000289
17	16249.293*	9.366676	1654.588	4.679986	27975.61	0.9841148*	0.000239
18	11563.262*	11.287140	1546.796	5.639543	33327.01	0.9239590*	0.000219
19	2091.274*	12.338577	1452.101	6.164899	36060.72	0.3641782	0.000225
20	5214.645*	12.004329	1368.264	5.997905	34763.22	0.6806101	0.000223
21	.	12.104062	1293.528	6.047746	34762.82	.	.

et al. [2014a], for theoretical justifications of empirical Bayes. In empirical Bayes setup, one assumes the availability of $x_1, x_2, \cdots, x_n$ of 'n' independent observations from an experiment and ith observation, i.e., x_i, is assumed to be generated by the pdf $f(x_i|\theta_i)$. Note that each θ_i itself is considered as a random variable and x_i are exchangeable with specific θ_i. Therefore, one assumes a prior distribution to entertain the uncertainty of θ.

To implement empirical Bayes procedure, the first task is to find a marginal (prior predictive) distribution, i.e., $m(x) = \int_\Theta f(x|\theta)g(\theta)d\theta$, which is a function of the observed data and the hyperparameters. For finding hyperparameters by the method of moments, find moments of a marginal distribution and solve them by equating to observed data moments. Similarly, one can use a marginal distribution to find the maximum likelihood estimates of the hyperparameters. In our case, we have the Lomax distribution as the marginal distribution, i.e., $f(x) = \frac{a}{b}\big(1 + \frac{x}{b}\big)^{-(a+1)}$, with the mean (cf. 7.8)

$$E(x) = \frac{b}{a-1}, a > 1 \tag{7.12}$$

and the variance

$$V(x) = \frac{ab^2}{(a-1)^2(a-2)} \tag{7.13}$$

To have a finite variance a should be grater or equal to 2. Note that there exist an inverse relationship between the prior mean (a/b) and the marginal distribution's mean, whereas the posterior predictive mean can be written as

$$E(y|\mathbf{x}) = \frac{\beta}{\phi - 1} = \frac{b + n\bar{x}}{a + n - 1} = \big[E(\lambda)\big]^{-1}(1-w)\frac{a}{a-1} + w\bar{x} \tag{7.14}$$

where $w = \frac{n}{a+n-1}$. Equating the sample mean and the variance with Equation 7.12-7.13 and solving for hyperparameters (a and b), one can get

$$b = \frac{m(v + m^2)}{v - m^2} \tag{7.15}$$

and

$$a = \frac{2v}{v - m^2} \tag{7.16}$$

where m and v denote the sample mean and the variance, respectively.

The method of moments is easy to implement, but sometimes it suffers from undesirable properties, e.g. asymptotic properties, etc. Thus, an alternative method is the maximum likelihood method. The log-likelihood of the marginal density can be written as:

$$l(\mathbf{x}; a, b) = n\log(a) - n\log(b) - (a+1)\sum_{i=1}^{n}\log\big(1 + \frac{x_i}{b}\big) \tag{7.17}$$

Therefore, the normal equations for a and b can be derived as:

$$\frac{\partial l(.)}{\partial a} = \frac{n}{a} - \sum_{i=1}^{n} \log\big(1 + \frac{x_i}{b}\big) \tag{7.18}$$
$$\frac{\partial l(.)}{\partial a} = 0 \Rightarrow \hat{a} = \frac{n}{\sum_{i=1}^{n} \log\big(1 + \frac{x_i}{b}\big)}$$

and by using the profile likelihood, one can get

$$\frac{\partial l(.)}{\partial b} = \frac{-n}{b} + \frac{1}{b}\sum_{i=1}^{n} \frac{x_i}{b + x_i}\left(1 + \frac{n}{\sum_{i=1}^{n} \log\big(1 + \frac{x_i}{b}\big)}\right) = h(b) \tag{7.19}$$

To find $\hat{b}$, one needs to use an iterative procedure for Equation-7.19. Thus, we propose a simple iterative scheme to solve it for b. Start with an initial guess of $b^{(0)}$, obtain $b^{(1)} = h(b^{(0)})$ and proceeding in this fashion, obtain $b^{(n+1)} = h(b^{(n)})$. Stop the iterative procedure, when $|b^{(n+1)} - b^{(n)}| < \epsilon$, where ϵ is pre-assigned tolerance constant. An alternative way to solve it, is by using the Newton Raphson method. For this method, we need

$$\frac{\partial l(.)}{\partial b} = \frac{-n}{b} + \frac{a+1}{b}\sum_{i=1}^{n} \frac{x_i}{b + x_i}$$
$$\frac{\partial^2 l(.)}{\partial a^2} = \frac{-n}{a^2}$$
$$\frac{\partial^2 l(.)}{\partial b^2} = \frac{n}{b^2} - \frac{a+1}{b^2}\sum_{i=1}^{n} \frac{x_i}{b + x_i} - \frac{a+1}{b}\sum_{i=1}^{n} \frac{x_i}{(b + x_i)^2}$$
$$\frac{\partial^2 l(.)}{\partial b \partial a} = \frac{1}{b}\sum_{i=1}^{n} \frac{x_i}{b + x_i}$$

Furthermore, to find the variance of the maximum likelihood estimates, i.e., by inverting the Fisher information matrix, we need the following proposition:

Proposition 7.6.1.1 *If X has a Lomax distribution with parameters a and b then $E\big[x(x+b)^{-r}\big] = \frac{ab^{1-r}}{(a+r)(a+r-1)}$ for $r = 1, 2, \cdots$ and $a + r > 1$.*

Proof :

$$E\big[x(x+b)^{-r}\big] = \int_0^{\infty} x(x+b)^{-r}\frac{a}{b}\big(1 + \frac{x}{b}\big)^{-(a+1)}dx = ab^a\int_0^{\infty} x(x+b)^{-(a+r+1)}dx$$

Then, by letting $y = b + x$ we have

$$ab^a\int_b^{\infty} (y-b)y^{-(a+r+1)}dy = \frac{ab^{1-r}}{(a+r)(a+r-1)}$$

for $r = 1, 2, \cdots$ and $a + r > 1$.

Therefore, $E\left[\frac{\partial^2 l(.)}{\partial a^2}\right] = \frac{-n}{a^2}$, $E\left[\frac{\partial^2 l(.)}{\partial b^2}\right] = \frac{-na}{b^2(a+2)}$ and $E\left[\frac{\partial^2 l(.)}{\partial b \partial a}\right] = \frac{n}{b(a+2)}$, respectively.

7.6.2 Revise the False Alarm Probability

An alternative way instead of revising a prior information, is to revise the false alarm probability and choose an optimal coverage of a prediction interval (cf. Landon and Singpurwalla [2008]) for future monitoring. Landon and Singpurwalla [2008] motivated by the statement of Granger [1996], who wrote, "academic writers concentrate almost exclusively on 95% intervals, whereas practical forecasting seems to prefer 50% intervals. The larger the coverage probability, we have a wider the prediction interval, and the vice versa. But wide prediction intervals tend to be of little value." Granger [1996] noticed that wider intervals tend to be the embarrassment for a practitioner. Similarly, a narrow interval is also risky, especially in quality control, because it gives too many false alarms when the actual process is in-control. Therefore, to avoid the possible consequences of the wide and narrow intervals, Landon and Singpurwalla [2008] suggested that the coverage probability for a prediction interval should be chosen by considering a decision theoretic approach.

In decision theory, utility measures the worth of a consequence while disutility is a penalty or loss as a consequence. A decision maker always tries to choose an action which gives minimum expected loss. Thus, using a specific disutility, the job of a decision maker is to look for a type-I error "α" for which the total expected disutility would be minimum. To elaborate this idea further, let d_α denotes the width of a prediction interval which is $d_\alpha = UCL_{i+1} - LCL_{i+1} = \beta_i\left[\left(\frac{2}{\alpha}\right)^{1/\phi_i} - \left(\frac{2}{2-\alpha}\right)^{1/\phi_i}\right]$, here the coverage probability is $1-\alpha$. Using the notations as defined in Landon and Singpurwalla [2008], let $c(d_\alpha)$ be the disutility associated with the use of d_α or more specifically with α. Clearly, $c(d_\alpha)$ should be zero when $d_\alpha = 0$ (alternatively when α is large), and $c(d_\alpha)$ must increase with d_α (or when α is small). A suitable choice for $c(d_\alpha)$ could be $c(d_\alpha) = d_\alpha^k$, for $k > 0$. Note that Young and Mills [2014] defined $c(d_\alpha) = \min\{d_\alpha^k, \gamma\}$ where $\gamma > 0$, which allows analysts to truncate the cost/inspection at a threshold γ, i.e., any interval beyond this value will serve a little purpose. Moreover, when $k \leq 1, c(d_\alpha)$ is concave increasing function of d_α, and when $k > 1$, $c(d_\alpha)$ is convex and increasing in d_α. More specifically (for our case), $c(d_\alpha)$ is a convex for $k > 1$ and $\forall \alpha \in [0, 1]$, while $c(d_\alpha)$ is convex for $\alpha \leq 0.5$ and concave for $\alpha > 0.5$. Note that the choice of k is dependent on the particular application.

Let $U_\alpha = UCL_{i+1}$ and $L_\alpha = LCL_{i+1}$. Moreover, let $L(d_\alpha, y)$ denotes the loss by using a prediction interval of width d_α. When Y reveals itself as y, $L(d_\alpha, y)$ could be of the

form

$$L(d_\alpha, y) = \begin{cases} \frac{1}{S_1} f_1(y - U_\alpha), & \text{if } y > U_\alpha; \\ 0, & \text{if } L_\alpha < y < U_\alpha; \\ \frac{1}{S_2} f_2(L_\alpha - y), & \text{if } y < L_\alpha. \end{cases}$$

where S_1 and $S_2 > 0$ are scaled constant (cf. Young and Mills [2014]) and their choice depends on the application; f_1 and f_2 are increasing functions of their arguments which summaries the loss of a point falling below or above the control limits, respectively. To obtain α, we know that the value of y is unknown and thus, $L(d_\alpha, y)$ needs to be averaged out. Because of the availability of predictive distribution, this task is easy to accomplish. Therefore, one can compute the risk function as follows $R(d_\alpha) = E_Y[L(d_\alpha, Y)]$. Note that $c(d_\alpha)$ is free from any unknown quantity, therefore, by combining it with $R(d_\alpha)$ one could get a total expected disutility function, $D(d_\alpha) = c(d_\alpha) + R(d_\alpha)$. According to Landon and Singpurwalla [2008], the additive structure of $D(d_\alpha)$ is not necessary and one could use any suitable structure. Therefore, one needs to choose α such that it minimizes the $D(d_\alpha)$.

We suggest to choose the specific form of $f_1(y - U_\alpha) = (y - U_\alpha)^2 / U_\alpha^c$ and $f_2(L_\alpha - y) = (L_\alpha - y)^2 / L_\alpha^c$, where $c = 0$ would result into the squared error loss function, $c = 1$ the precautionary loss function, and $c = 2$ the Degroot loss function, respectively (cf. Table-3.10). The risk function for our problem can be written as

$$R(d_\alpha) = \int_{U_\alpha}^{\infty} \frac{\left(y - \beta\left[\left(2/\alpha\right)^{1/\phi} - 1\right]\right)^2}{\beta^c\left[\left(2/\alpha\right)^{1/\phi} - 1\right]^c} f(y|\mathbf{x})dy + \int_0^{L_\alpha} \frac{\left(\beta\left[\left(2/(2-\alpha)\right)^{1/\phi} - 1\right] - y\right)^2}{\beta^c\left[\left(2/(2-\alpha)\right)^{1/\phi} - 1\right]^c} f(y|\mathbf{x})dy \tag{7.20}$$

Since our predictive distribution is the Lomax distribution, Equation-7.20 has the following simplified form (see detail in Appendix 7.8):

$$\begin{aligned} R(d_\alpha) = & \frac{1}{\beta^c\left[\left(2/\alpha\right)^{1/\phi} - 1\right]^c} \Bigg\{ \frac{\alpha}{2(\phi-1)(\phi-2)} \Big[2\beta^2 + 2\beta^2\phi\left[\left(2/\alpha\right)^{1/\phi} - 1\right] + \phi(\phi-1)\beta^2 \\ & \left[\left(2/\alpha\right)^{1/\phi} - 1\right]^2\Big] + \frac{\alpha\beta^2}{2}\left[\left(2/\alpha\right)^{1/\phi} - 1\right]^2 - \frac{\alpha\beta^2}{\phi-1}\left[\left(2/\alpha\right)^{1/\phi} - 1\right]\Big[1 + \phi \\ & \left\{\left(2/\alpha\right)^{1/\phi} - 1\right\}\Big]\Bigg\} + \frac{1}{\beta^c\left[\left(2/(2-\alpha)\right)^{1/\phi} - 1\right]^c} \Bigg\{ \frac{\alpha\beta^2}{2}\left[\left(2/(2-\alpha)\right)^{1/\phi} - 1\right]^2 \\ & + \frac{2-\alpha}{2(\phi-1)(\phi-2))}\Bigg[\frac{2\alpha\beta^2}{2-\alpha} - 2\beta^2\phi\left[\left(2/(2-\alpha)\right)^{1/\phi} - 1\right] + \beta^2\left[\left(2/(2-\alpha)\right)^{1/\phi} - 1\right]^2 \\ & \phi(\phi-1)\Bigg] - \frac{\beta(2-\alpha)}{\phi-1}\left[\left(2/(2-\alpha)\right)^{1/\phi} - 1\right]\left[\frac{\beta\alpha}{2-\alpha} - \beta\phi\left[\left(2/(2-\alpha)\right)^{1/\phi} - 1\right]\right]\Bigg\} \end{aligned}$$

To compute the revised false alarm probability, we used the data set given in Tables 7.5-

Table 7.7: Revision of the false alarm probability after getting out-of-control signal for various choices of k.

k	c	0	1	2
0.1	α_r	0.015332	0.015332	0.293867
	Coverage Probability	0.984668	0.984668	0.706143
0.5	α_r	0.015332	0.015332	0.477172
	Coverage Probability	0.984668	0.984668	0.522828
1.0	α_r	0.015332	0.369806	0.477172
	Coverage Probability	0.984668	0.630194	0.522828
1.5	α_r	0.104751	0.477172	0.477172
	Coverage Probability	0.895249	0.522828	0.522828
2.0	α_r	0.477172	0.477172	0.477172
	Coverage Probability	0.522828	0.522828	0.522828

7.6, and results have been reported in Table-7.7. In Table-7.7 α_r denotes the revised values of the false alarm, i.e., after receiving the first out-of-control signal form the data sets given in Tables 7.5-7.6. Note that to minimize Equation-7.20, we used the mathematical software Mathematica, Wolfram Research [2014]. It is interesting to note that for $k < 1$, the revised false alarm probabilities under the squared error and the precautionary loss functions, are approximately the same. However, for the Degroot loss function, the revised false alarm probability is quite high. Thus, for small k, the coverage probability of the Degroot loss function is less than the squared error and precautionary loss functions. Moreover, for a large value of k, all loss functions have the same coverage probability (see the very last row $k = 2$ given in Table-7.7).

7.7 Real Data Examples

In this section, we discuss real-life data sets and show the implementation of the predictive control chart. We use an asterisk "$\star$" to mark the deterioration or the improvement detected by the PCDC while an asterisk within a circle "$\circledast$" to denote the detection of a signal by a simple chart, i.e., without PCDC.

Example-1: Dunsmore [1974] (page 459, table 1) provides a data set of the times to first breakdown of 20 machines in hours. We use this data set for the construction of one and two sided control charts to see whether breakdowns were statistically out-of-control or not. For this data set, the exponential distribution is well fitted with $\hat{\lambda} = 0.012571$. To develop the Bayesian charts, we used $a = 1$ and $b = 80$ as hyperparameters' values of the gamma prior distribution. The data set and the control limits have been given in Table-7.8. Note that we used $\alpha = 0.0027$ to construct control limits. The observations at the following points, 4, 16$-$18 and 20, have been tagged as improved by the simple upper-sided predictive control chart. Moreover, we confirm the same conclusion by using the PCDC,

Table 7.8: Real Data of Example 1

Sr. No.	Y	LCL (one-sided)	UCL (one-sided)	LCL (two-sided)	UCL (two-sided)	F	Posterior Mean
1	18	.	.	.	.	.	0.020408
2	23	0.132569	1788.01088	0.066217	2569.2222	0.344033	0.024793
3	29	0.109096	605.7820	0.054499	973.8151	0.475093	0.026667
4	409$^{\circledast}$	0.101421	331.91751	0.050668	632.5423	0.994815*	0.008945
5	24	0.302350	221.85513	0.151052	1536.7769	0.189569	0.010292
6	74	0.262764	164.62261	0.131278	1170.6635	0.511776	0.010654
7	13	0.253806	130.12564	0.126805	1031.5646	0.128166	0.011940
8	62	0.226469	107.26061	0.113148	860.3229	0.507383	0.012295
9	46	0.219930	91.07326	0.109882	793.3267	0.422192	0.012853
10	4	0.210373	79.04746	0.105108	728.4205	0.049989*	0.014066
11	57	0.192229	69.77933	0.096043	643.8883	0.538796	0.014303
12	19	0.189052	62.42760	0.094457	616.1267	0.235643	0.015152
13	47	0.178459	56.45909	0.089165	568.3656	0.500077	0.015469
14	13	0.174789	51.52028	0.087331	545.8574	0.181003	0.016339
15	19	0.165478	47.36789	0.082679	508.1124	0.264562	0.017076
16	208$^{\circledast}$	0.158346	43.82926	0.079116	479.0994	0.959547*	0.014847
17	119$^{\circledast}$	0.182113	40.77854	0.090992	543.9212	0.813794	0.014241
18	209$^{\circledast}$	0.189871	38.12193	0.094868	560.6223	0.936350*	0.012899
19	10	0.209619	35.78809	0.104735	612.6326	0.120633	0.013486
20	188$^{\circledast}$	0.200489	33.72187	0.100174	580.5950	0.908105*	0.012567
21	.	0.215147	31.87994	0.107497	617.9021	.	.

i.e., 0.10 for the lower-sided while 0.90 for the upper-sided chart, except observation number 17, which should not be marked as improved according to the PCDC. However, we have not noticed any alarm of either the process improvement or deterioration by the two-sided control chart.

Example-2: Dunsmore [1974] (page 460, table 3) has given a data set of the failure times (in mins) up to the 10th component failure of a machine. We assume the Poisson process for this data and fit exponential distribution. Therefore, the estimated value of the rate parameter is $\hat{\lambda} = 0.003307$. To develop the Bayesian predictive chart, we used $a = 1$ and $b = 303$ as hyperparameters values of a gamma prior. Control limits of the one and the two-sided control charts have been constructed using $\alpha = 0.0027$ and given in Table-7.9. In this case study, we have not detected any signal of either the process improvement or deterioration by the predictive charts. Therefore, we conclude that the failure process is statistically in-control.

Example-3 An electronic device has two kinds of major failures, i.e., modes-solder/Cu pad interface fracture (commonly known as a catastrophic failure) and light intensity degradation (a degradation failure). According to Huang and Askin [2003], and Cha and Pulcini [2015], the failure modes are independent of each other. Huang and Askin [2003] conducted a life test on electronic packaging related items for the solder/Cu pad' interface fatigue lifetime in days (page 245, Table 2 of Huang and Askin [2003]). We

Table 7.9: Real Data of Example 2

Sr. No.	Y	LCL (one-sided)	UCL (one-sided)	LCL (two-sided)	UCL (two-sided)	F	Posterior Mean
1	276	.	.	.	.	.	0.003454
2	279	0.783236	10563.8602	0.391221	15179.384	0.544611	0.003497
3	289	0.773593	3579.0590	0.386448	6905.234	0.581427	0.003487
4	294	0.775534	1961.0228	0.387439	4836.840	0.598581	0.003469
5	295	0.779403	1310.7563	0.389386	3961.530	0.605932	0.003456
6	298	0.782433	972.6173	0.390908	3485.886	0.613462	0.003441
7	304	0.785756	768.8036	0.392574	3193.611	0.622823	0.003422
8	326	0.790276	633.7132	0.394837	3002.142	0.648049	0.003378
9	327	0.800401	538.0757	0.399900	2887.189	0.647256	0.003343
10	336	0.808772	467.0253	0.404085	2800.393	0.655145	0.003306
11	.	0.817832	412.2677	0.408615	2739.407	.	.

Table 7.10: Real Data Example 3

Sr. No.	Y	LCL (one-sided)	UCL (one-sided)	LCL (two-sided)	UCL (two-sided)	F	Posterior Mean
1	171	.	.	.	.	.	0.007968
2	49	0.339538	4579.4973	0.169597	6580.3547	0.299989	0.0100
3	69	0.270487	1551.5437	0.135122	2414.4176	0.462616	0.01084
4	135	0.249496	850.1153	0.124643	1556.0540	0.712668	0.009921
5	21	0.272602	568.2208	0.136190	1385.5735	0.184627	0.011429
6	49	0.236623	421.6355	0.118218	1054.1995	0.414557	0.012195
7	93	0.221742	333.2810	0.110786	901.2452	0.650456	0.011994
8	57	0.225455	274.7185	0.112642	856.4707	0.481083	0.012431
9	49	0.217526	233.2591	0.108682	784.6565	0.559254	0.012611
10	.	0.214429	202.4583	0.107135	742.4646	.	.

fitted exponential distribution on the TBE of Solder/Cu pad interface fatigue' data, and found that it is a good candidate for the collected TBE data with $\lambda = 0.012622$. To design the Bayesian one and two sided control charts, we have used $a = 1$ and $b = 80$ as hyperparameters values of the gamma distribution. Control limits for the one and the two-sided control charts have been constructed using $\alpha = 0.0027$ (cf. Table-7.10). In this case study, we noticed that the recorded TBE of the electronic device were in statistical control. Moreover, we have not detected any signal of either the process improvement or deterioration by the proposed charts.

Example-4 (Historical Data set) This data set is taken from Jarrett [1979] and have recently been used by Yang et al. [2015a,c] to develop the unbiased design of the exponential and gamma charts. The data set is about the time intervals in days between the explosions in coal mines from 15 March 1851 to 22 March 1962. We are not reproducing data set here for the sake of space and refer to either Jarrett [1979] or Yang et al. [2015a,c]. Yang et al. [2015a,c] used the classical approach while the rate parameter of the exponential distribution was estimated by a sequential sampling scheme. There are

Table 7.11: Detection of a Signal for the Coal-Mining Data using different Charts

Chart	LCL	UCL
A B	80	14,134,153,156,182,187,188
C D	80	134,153,156,182,187,188,189
E F G	80	134,153,182,188
H	80	134,153,156,182,188
I	3,5,6,16,48,51,66,79 ,80,86,88,103,165,169 ,178,185,186	8,13-14,25,41,52,73,81,100,106 ,109,119-120,125,127-130,134-137 ,140-141,148-149,151-153 ,156,158,173,182,187-190
J	Same as the Informative Prior case except observation number 5	Same as the Informative Prior except one addition , i.e., observation number 35
K L	- -	129-190
M N	- -	14,130-190
O P	- -	130-190
Q R	- -	130-132,134-190
S	-	131-132,134-190

total 190 observations and Yang et al. [2015a] considered the first 30 observations as a phase-I to sequentially estimate the rate parameter of the exponential chart. We compare our proposed predictive chart with the ARL and ATS-unbiased charts studied by Yang et al. [2015a]. Moreover, we shall also study these charts where the parameter has been estimated by the classical sequential approach, i.e., without considering the first 30 observations as the phase-I data. In this approach, we used both the biased and the unbiased estimates. Note that the rate parameter was estimated by the maximum likelihood method in the frequentist approach. A CUSUM chart has also been constructed with the predictive UCL. Moreover, the Bayesian chart has not only been developed for the informative prior but also using Jeffreys' prior. The results for the coal-mining monitoring have been summarized in Figure-7.10. In Table-7.11 we used the following capital alphabets to denote different charts:

A: Bayesian Predictive (Informative+Jeffreys), B: ARL-Unbiased by Yang et al. [2015a], C: ATS-Unbiased by Yang et al. [2015a], D: Simple Sequential (with biased and unbiased estimate of λ, E: Simple Sequential with unbiased ARL design and biased estimate of λ, F: Simple Sequential with unbiased ARL design and unbiased estimate of λ, G: Simple Sequential with unbiased ATS design and unbiased estimate of λ, H: Simple Sequential with unbiased ATS design and biased estimate of λ, I: PCDC with Informative Prior,

J: PCDC with Jeffreys prior, K: CUSUM Predictive, L: CUSUM with Sequential and Biased estimate, M: CUSUM with Sequential and Unbiased estimate, N: CUSUM with ARL-unbiased of Yang et al. [2015a], O: CUSUM with ATS-unbiased of Yang et al. [2015a], P: CUSUM with ATS-unbiased and biased estimate of λ, Q: CUSUM with ARL-unbiased and biased estimate of λ, R: CUSUM with ATS-unbiased and unbiased estimate of λ, S: CUSUM with ARL-unbiased and unbiased estimate of λ.

We noticed that all the charts listed in Table-7.11 raised a signal of process deterioration at the 80th sample point. Seven sample points are above the UCL of the predictive chart whereas using PCDC, we have 17 sample points below the LCL while 37 sample points fall above the UCL. The details on these points for different charts, have been summarized in Table-7.11. Therefore, we believe that the safety of coal-mining began to improve between $1900-1920$ using the Bayesian predictive chart. However, with the PCDC we believe that the safety began to improve after 1930.

Example-5 (Another Historical Data Set) Lucas [1985] gave a data set which is about the time intervals in days between accidents in a manufacturing plant. This data set has been used by Zhang et al. [2007b] for the gamma chart and more recently Yang et al. [2015a] for the ATS-unbiased exponential chart. For the sake of space, we are not reproducing data set here and refer to Lucas [1985], or Yang et al. [2015a]. This data set consists of 177 observations and Yang et al. [2015a] used the first 110 as a phase-I to design the ATS-unbiased exponential chart. We design the Bayesian predictive chart for this data set, and further it would be compared with the sequential sampling ARL and ATS unbiased charts. Moreover, a CUSUM chart has also been designed in this study. The resulting study has been depicted in Figure-7.11. We observed that using the Bayesian predictive chart, the sample point 129th fell above the UCL, which indicates the occurrence rate of accidents was begun to decrease from the 129th observation, similar to what was obtained by the Poisson CUSUM chart in Lucas [1985], gamma chart in Zhang et al. [2007b] and the ATS-unbiased exponential chart by Yang et al. [2015a]. However, with our designed CUSUM, we noticed that the first improvement shift was occurred around $50-53$ observations and the second at 129th sample point. A similar behavior has also been observed in the case of ATS-unbiased design chart with the biased and the unbiased sequential estimates of the rate parameter. For the biased sequential estimate of the rate parameter, we noticed that the observations, $49-55$ and $129-177$, signalled out-of-control situation by the CUSUM chart. Similarly, the following observations have been indicated out-of-control $49-53$, 55, and $129-177$, by the CUSUM with the unbiased estimate of λ (cf. Figure-7.11[E]). For the CUSUM chart with the ARL-unbiased design chart using the biased and the unbiased sequential estimates of the rate parameter, we have 50-th and $129-177$ observations fall above the UCL. From Figure-7.11[A-D], nine observations, i.e., 14, 17, 21, 25, 42, 56, 116, 141, 149, are below LCL while with the PCDC we have, 14, 17, 19, 21, 25, 34, 42, 51, 56, 73, 94, 116, 126, $141-142$, 149,

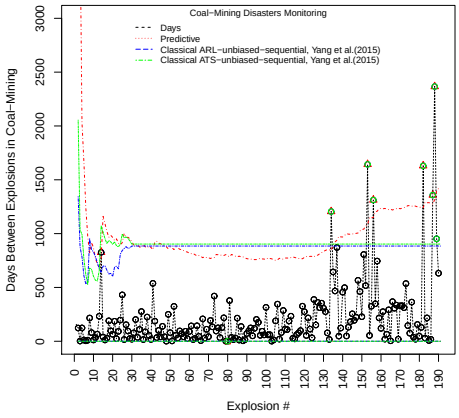

(a) Predictive Chart comparison with Yang et al. [2015a] ARL and ATS unbiased charts for the Coal-mining Data

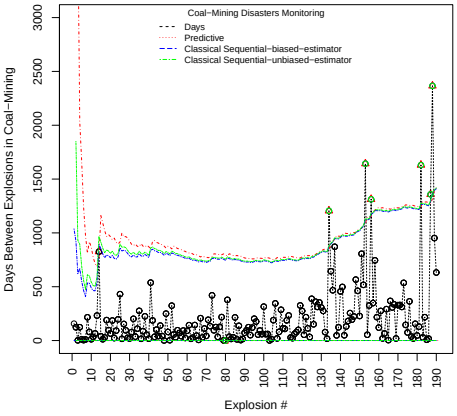

(b) Predictive Chart comparison with biased and unbiased Sequential estimate of λ for the Coal-mining Data

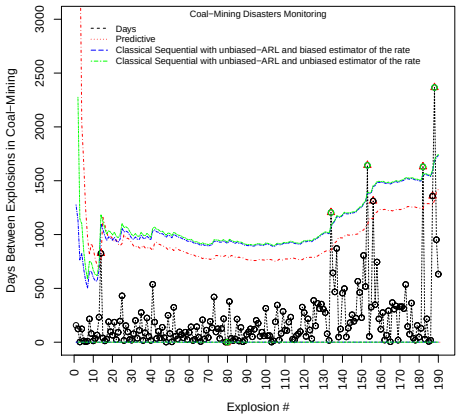

(c) Predictive Chart comparison with unbiased design of ARL proposed by Yang et al. [2015a] and using biased and unbiased Sequential estimate of λ for the Coal-mining Data

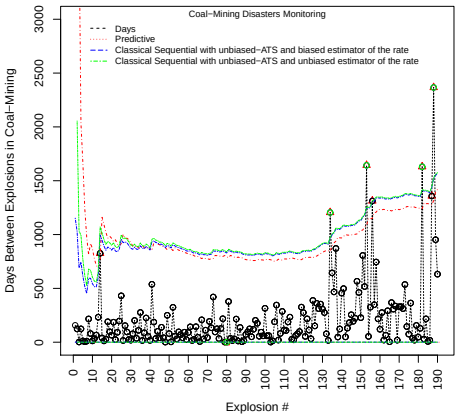

(d) Predictive Chart comparison with unbiased design of ATS proposed by Yang et al. [2015a] and using biased and unbiased Sequential estimate of λ for the Coal-mining Data

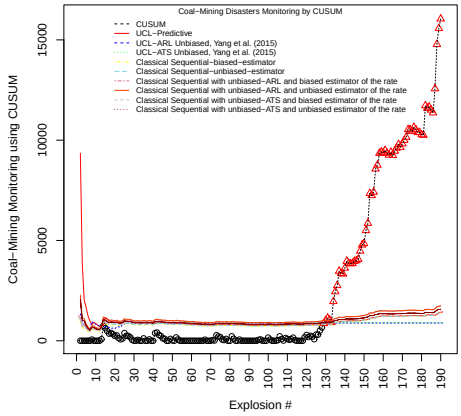

(e) CUSUM chart for the Coal-mining Data with Sequential UCL

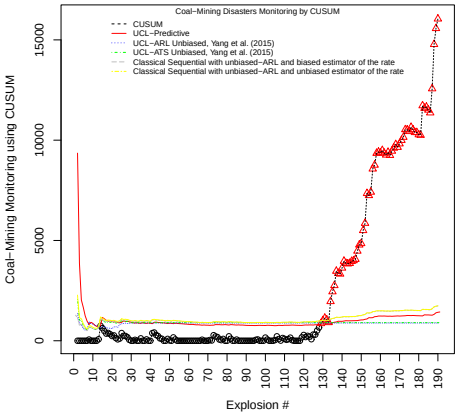

(f) CUSUM chart for the Coal-mining Data with Sequential UCL

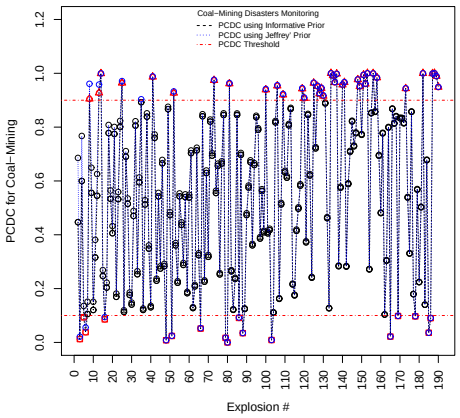

(g) Control Chart with PCDC for the Coal-mining Data

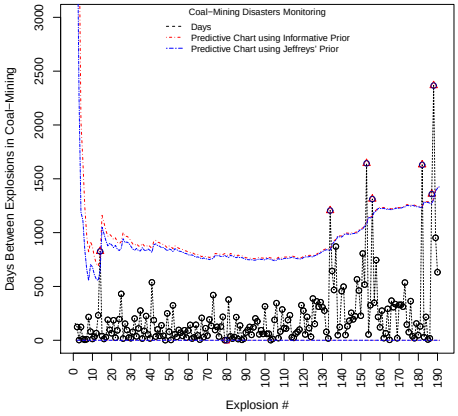

(h) Comparison of the Informative and Jeffreys' priors for the Bayesian Chart using Coal-mining Data

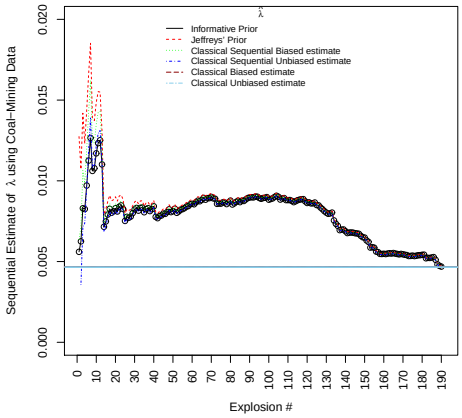

(i) Comparison of Classical and Bayesian estimates of λ

Figure 7.10: Predictive Control Chart and some Comparison for the Coal-mining Disaster Data using $\alpha = 0.002703$

$165-166$. Similarly using the PCDC, 28, 32, 41, 44, $48-50$, 72, 83, 104, 107, 127, $129-130$, 133, $136-137$, $151-152$, $156-157$, 159, 161, 167, and 174, falls above the UCL.

7.8 Conclusion

In this chapter, we have proposed a Bayesian predictive control chart for the exponential TBE setting. The performance of the proposed chart has been studied in-detail with by simulations and by real data examples. It has been pointed out in many studies, that to set ordinary control chart's limits, a large number of base period observations are required. This requirement of a base period is difficult to fulfill in many applications. The unique feature of the proposed control chart is its implementation without a large base period. Since the Bayesian approach is a natural way to include the additional information about the process, we proposed control charts using the Bayesian predictive distribution. Moreover, the suggested approach has a self-starting feature. However, we also noticed that the use of a base period could significantly influence the charts' sensitivity. If the base period is not available, then we suggest the use of precise informative prior distribution. A flowchart to epitomize the Bayesian predictive chart has been given in Figure-7.12.

It has been shown that the predictive control chart was ineffective for small to moderate size of shifts due to the presence of a drift or deterioration in the control limits. Therefore, to detect a possible drift or deterioration in the control limits, a criterion using the observed predictive cumulative distribution function (commonly known as a Bayesian p-value), has also been proposed and implemented in this chapter. By using the PCDC as a stopping criterion for the control limits deterioration, we observed that the performance of a predictive chart was improved significantly. Moreover, we noticed that the detection power of the control chart was improved not only for large shifts but also for small to moderate shifts.

To detect small shifts, the CUSUM and the EWMA charts have also been designed and studied with the predictive control limits. Using the CUSUM and the EWMA charts, we noticed that to detect a relatively small size of shifts, the CUSUM outperforms than the EWMA chart. We also noticed that the performance of the one-sided chart with a small base period is undermined than the two-sided chart. However, it is worth mentioning here that the performance of a predictive control chart can be improved by increasing a base period. We observed that with a small base period, the two-sided chart was more efficient in the detection of a shift than the one-sided chart, and vice versa.

An interesting experiment that studies the properties of the predictive control chart with random and time varying shifts, has also been introduced in this chapter. Since

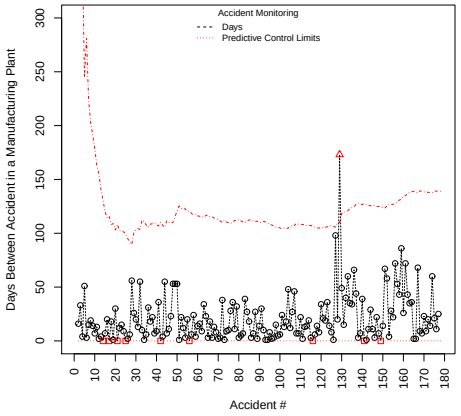

(a) Predictive Chart for the Manufacturing Plant Data

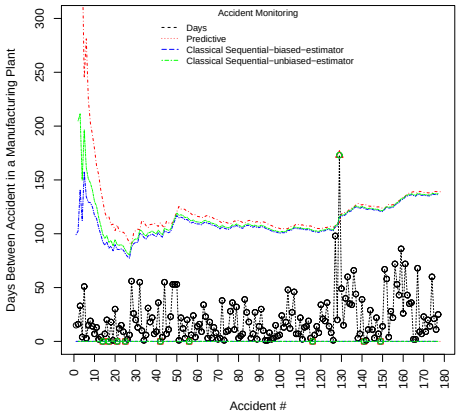

(b) Predictive Chart comparison the Classical Sequential Chart using biased and unbiased estimates of λ for the Manufacturing Plant Data

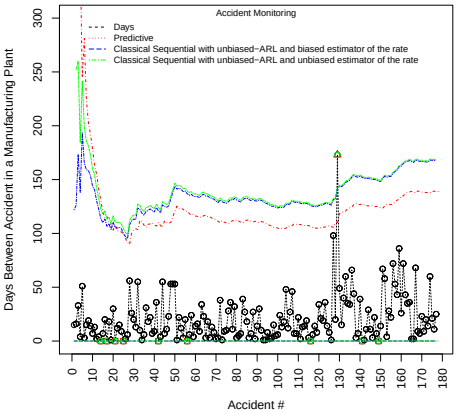

(c) Predictive Chart comparison with unbiased design of ARL proposed by Yang et al. [2015a] and using biased and unbiased Sequential estimate of λ for the Manufacturing Plant Data

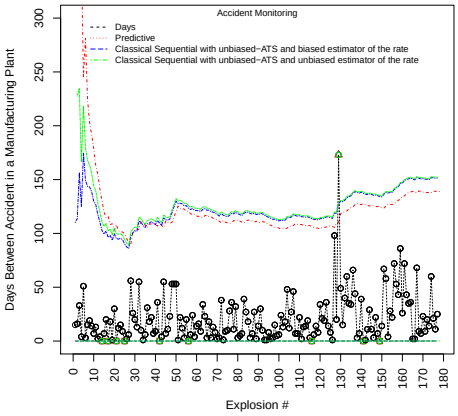

(d) Predictive Chart comparison with unbiased design of ATS proposed by Yang et al. [2015a] and using biased and unbiased Sequential estimate of λ for the Manufacturing Plant Data

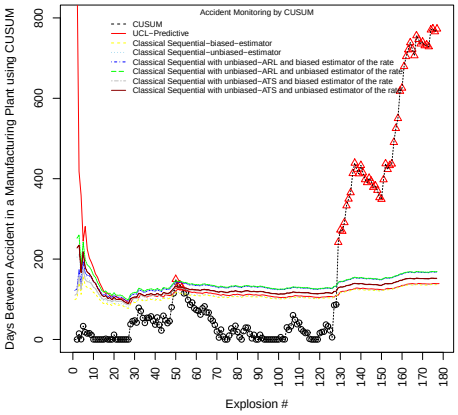

(e) CUSUM chart for the Manufacturing Plant Data with Sequential UCL

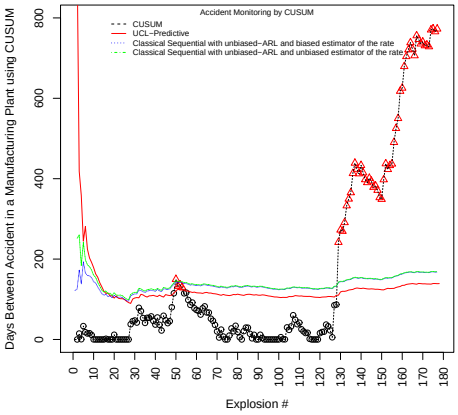

(f) CUSUM chart for the Manufacturing Plant Data with Sequential UCL

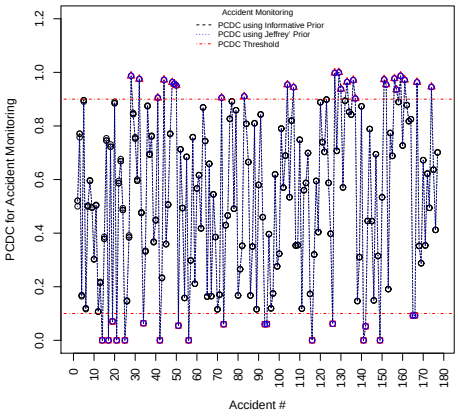

(g) Control Chart with PCDC for the Manufacturing Plant Data

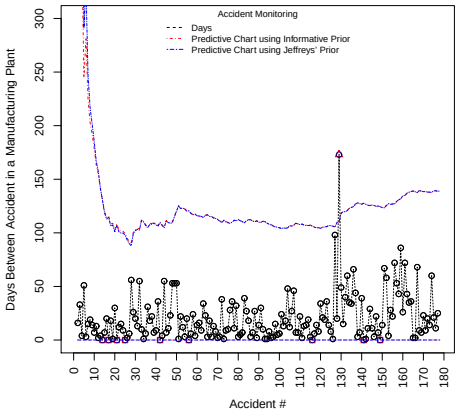

(h) Comparison of the Informative and Jeffreys' priors for the Bayesian Chart using the Manufacturing Plant Data

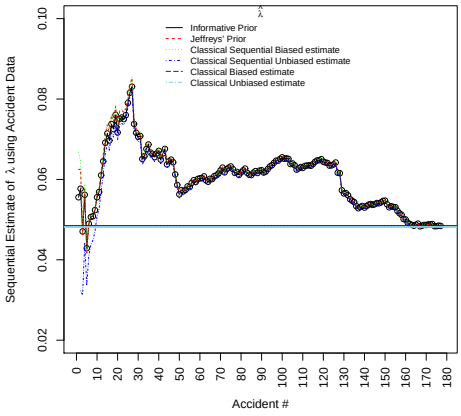

(i) Comparison of Classical and Bayesian estimates of λ

Figure 7.11: Predictive Control Chart and some Comparison for the Manufacturing Plant Data using $\alpha = 0.002703$

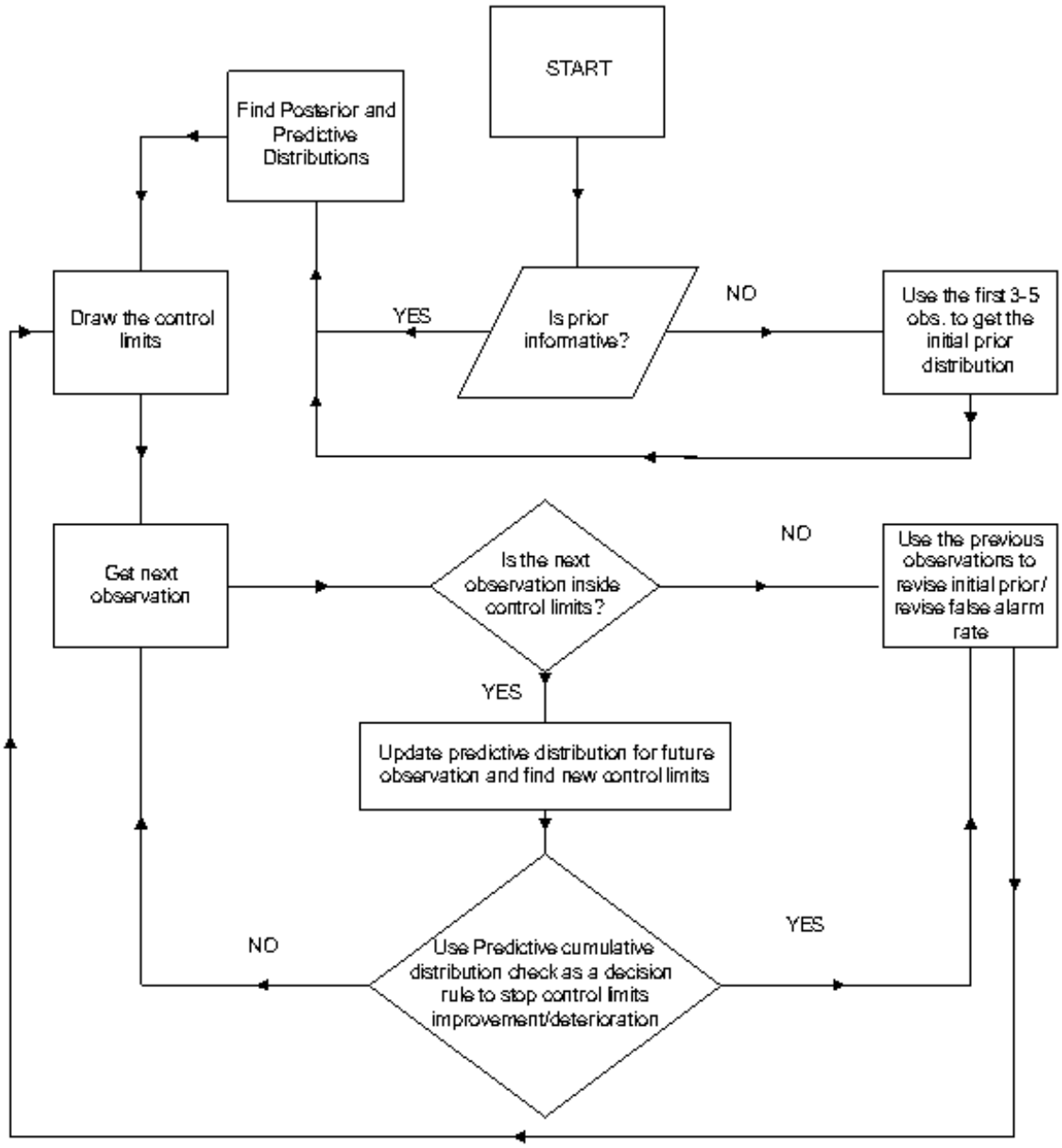

Figure 7.12: Flowchart to set-up Bayesian Predictive Control Chart

the control limits of a predictive chart vary with observed failure time, and it is difficult to achieve their stability, it makes sense to study the control charts properties under random and time varying shifts. We noticed that the control charts were ineffective for the detection of random shifts. Moreover, if we have random and time varying shifts, then the predictive control chart outperforms without using the deterioration check. Note that for random and time varying shifts, we used the two-sided chart as the knowledge about the direction of a shift was not available. Moreover, we also think that the use of the one-sided chart might have some possible consequences, i.e., poor detection or opposite direction shift in a process, etc.

Another interesting idea that has been discussed in this chapter is the revision of the false alarm probability using decision theory. One can use this approach either before setting up control limits, i.e., by using phase-I data set, or after receiving an out-of-control alarm by the predictive chart. A numerical optimization procedure, however, is required to implement this idea. By an illustrative example, we showed that this idea is quite effective instead of revising the prior distribution. Note that we are not against the idea of revising a prior information because it is an interesting and an impressive idea in many situations to set up control limits. We are only skeptical just to avoid the double usage of data. Therefore, we have discussed mathematical formulation of empirical Bayes. Similarly, the idea of a noninformative priors is quite useful, especially when it is difficult to obtain a precise prior information about the process which may be due to the rapid technological developments.

Appendix

Appendix A: Exponential Family and Related Distributions

The following distributions belong to exponential family (cf. Section-7.3): Bernoulli, Beta, exponential, gamma, inverted gamma, chi-squared, scaled chi-squared, geometric, inverse normal, normal, normal gamma, log normal, Poisson, Dirichlet, von-Mises, von-Mises-Fisher, Wishart, multivariate normal and inverse Wishart distributions. Some distributions are exponential if some of their parameters held constant, e.g. Pareto (fix minimum bound), binomial and multinomial (fix number of trials), negative binomial (fix number of failure), Weibull (fix shape parameter) and Laplace (fix location parameter).

Appendix B: Properties of the Lomax Distribution

The rth moment (cf. Section-7.6.1) with the scale parameter b and a as the shape parameter, can be written as $E(x^r) = \frac{ab^r\Gamma(r+1)\Gamma(a-r)}{\Gamma(a+1)}, a > r \quad \text{and} \quad r = 1, 2, \cdots$. The median of the Lomax distribution is $b(2^{(1/a)} - 1)$ while mode is zero. The skewness and the excess kurtosis are $\frac{2(1+a)}{a-3}\sqrt{\frac{a-2}{a}}, a > 3$ and $\frac{6(a^3+a^2-6a-2)}{a(a-3)(a-4)}, a > 4$, respectively. The Lomax distribution also satisfies the following differential equations:

$$(b + x)f^{'}(x) + (a + 1)f(x) = 0 \tag{B.1}$$

and

$$f(0) = \frac{a}{b} \tag{B.2}$$

Moreover, the Lomax distribution is a special case of the generalized Pareto distribution, specifically: $\mu = 0, \psi = \frac{1}{a}, \sigma = \frac{b}{a}$.

Appendix C: Derivation Detail

To derive the risk function mentioned in Section-7.6.2, we need the following facts.

$\int_0^{L_\alpha} f(y|\mathbf{x})dy = F(L_\alpha|\mathbf{x}) = 1 - \left(1 + L_\alpha/\beta\right)^{-\phi}$,

$\int_{U_\alpha}^{\infty} f(y|\mathbf{x})dy = \left(\frac{\beta}{\beta+U_\alpha}\right)^{-\phi}$

$\int_0^{L_\alpha} y^2 f(y|\mathbf{x})dy = \frac{\left(1+L_\alpha/\beta\right)^{-\phi}\left[2\{-1+(1+L_\alpha/\beta)^{\phi}\}\beta^2-2L_\alpha\beta\phi-L_\alpha^2\phi(\phi-1)\right]}{(\phi-1)(\phi-2)}$,

$\int_0^{L_\alpha} y f(y|\mathbf{x})dy = \frac{\left(1+L_\alpha/\beta\right)^{-\phi}\left[\beta\{-1+(1+L_\alpha/\beta)^{\phi}\}-L_\alpha\phi\right]}{(\phi-1)}$,

$\int_{U_\alpha}^{\infty} y^2 f(y|\mathbf{x})dy = \left(\frac{\beta}{\beta+U_\alpha}\right)^{\phi}\frac{2\beta^2+2U_\alpha\beta\phi+U_\alpha^2\phi(\phi-1)}{(\phi-1)(\phi-2)}$,

$\int_{U_\alpha}^{\infty} y f(y|\mathbf{x})dy = \left(\frac{\beta}{\beta+U_\alpha}\right)^{\phi}\frac{U_\alpha\phi+\beta}{(\phi-1)}$.

This page is left blank intentionally.

Chapter 8

Practical Advice

In Chapter 3, we proposed control charts based on the renewal process. However, before constructing control charts, it is important to decide whether recurrent data satisfies renewal process assumptions or not. Another important question is: how one can decide about constant, increasing, decreasing or bathtub shaped hazard rate? In this chapter, I will summarize some methodologies with examples to address these concerns. The rest of the chapter is organized as follows: Statistical tests for testing a renewal process assumptions are summarized in Section 8.1. Testing exponentiality is an important problem and related tests are discussed in Section 8.2 while some properties of the hazard rate function are given in Section 8.3. In Section 8.4, some graphical and mathematical approaches to test the hazard rate properties are discussed. Note that tests for HPP versus NHPP have been discussed in Section 6.6.

8.1 Tests for Renewal Process

Meeker and Escobar [1998] stated that before using a renewal process model, it is important to check for departures from the model such as trend and non-independence of TBE. There are different definitions of trend in the literature (cf. Lawless et al. [2012]). The commonly accepted definition is: a tendency for the rate of event occurrence to change over time in some systematic way. The well-known Laplace test has a good basis for testing of the trend. If the underlying process is HPP, over a period of time $(0, T]$, the test statistic of the Laplace test is $Z_{LP} = \frac{\sum_{i=1}^{n} T_i/T_n - n/2}{\sqrt{n/12}}$, which has approximately, a $N(0, 1)$ distribution. However, Meeker and Escobar [1998] noticed that Laplace test can give misleading conclusion for the situation where there is no trend but the underlying process is a renewal process other than HPP. Therefore, the Lewis-Robinson test for trend uses $Z_{LR} = Z_{LP} \times \bar{X}/Sd(X) = Z_{LP} \times CV^{-1}$, where $\bar{X}$ and $Sd(X)$ the sample mean and standard deviation of the TBE. In large samples, Z_{LR} follows approximately a $N(0, 1)$ distribution if the underlying process is a renewal process (renewal processes, in general,

have no trend). The statistic Z_{LR} was derived from heuristic arguments to allow for non-exponential TBE by adjusting for a different coefficient of variation, i.e., the exponential distribution has a coefficient of variation equal to 1. Meeker and Escobar [1998] remarked that Z_{LR} is preferable to Z_{LP} as a general test of trend in point-process data.

When assessing the adequacy of a renewal process model, it is also necessary to check if the model assumption of independent TBE is consistent with the data. To do this we consider the serial correlation in the sequence of TBE. Plotting TBE versus lagged TBE (X_i, versus X_{i+j}) provides a graphical representation of serial correlation (the correlation between adjacent TBE). The serial correlation coefficient of lag-j is $\rho_j = Cov(X_i, X_{i+j})/Var(X_i)$. It is worthy to mention here that first order serial correlation ($j = 1$) is the most important to check. For observed sample of size n, i.e., $X_1, X_2, \cdots, X_n$ the sample serial correlation coefficient is

$$\hat{\rho}_j = \frac{\sum_{i=1}^{n-j}(X_i - \bar{X})(X_{i+j} - \bar{X})}{\sqrt{\sum_{i=1}^{n}(X_i - \bar{X})^2}} \tag{8.1}$$

where $\bar{X} = \sum_{i=1}^{n} X_i/n$. When $\hat{\rho}_j = 0$ and n is large, $\sqrt{n-j}\hat{\rho}_j \approx N(0,1)$. Thus, this approximation help us to assess if $\hat{\rho}_j$ is different from zero or not (see examples in Meeker and Escobar [1998], page 411-416). I refer to Lawless et al. [2012] for some generalizations of the Laplace and Lewis-Robinson tests based on the score test.

Lawless et al. [2012] (page 157) did not discuss tests for non-monotonic trends, and suggested model fitting and associated diagnostic checks, rather than usual application of a hypothesis test for trend. Lawless et al. [2012] wrote, "Naive application of the tests considered here, however, may produce misleading results. Generally speaking, when the factors affecting event occurrence and duration of the processes are more complex, modelling of the processes is valuable, and often essential." Therefore, in the coming sections, I focus on the TBE distribution testing approach.

8.2 Testing exponentiality

To test the hypothesis H_0 : Data are from a renewal process, versus H_1 : Data are not from a renewal process, Karr [1991] (page 102) noted that "it is harder to test the hypothesis that a stationary point process is a renewal process than to test the hypothesis that it is Poisson, because the former is broader." Therefore, one must either narrow the structural assumptions or consider restricted hypothesis other than renewal. To reformulate the above hypothesis, one could consider H_0 : Data are from a Poisson process, versus H_1 : Data are not from a Poisson (i.e., renewal) process. Since we are concerned with the distribution of TBE and know that the TBE follows exponential distribution in a Poisson process (cf. Theorem-1.1.3). We know from Chapter-3 that $T_n \leq t \iff N(t) \geq n$,

therefore, we can define the above hypothesis as: H_0 : TBE data follow the exponential distribution, versus H_1 : TBE data do not follow the exponential distribution. A wide range of tests are available in statistical literature to test the exponentiality and some of them will be discussed here. For a comprehensive review of these tests, see Henze and Meintanis [2005] and references cited therein.

Before proceeding further, suppose $Exp(\lambda)$ denotes the exponential distribution with density $\lambda \exp(-\lambda x)$, $x > 0$. Given a non-negative random variable X with density f, distribution function F and mean $E(X)$, we want to test the null hypothesis H_0 : the law of X is $Exp(\lambda)$ for some $\lambda > 0$, against general alternatives, based on independent copies $X_1, \cdots, X_n$ of X. A scale invariant exponential distribution can be obtained by considering $Z_i = X_i \times \lambda_n$ for $1 \leq i \leq n$.

8.2.1 Tests based on the Empirical Distribution Function (EDF)

These tests are based on direct measure of discrepancy between the EDF $F_n(z) = n^{-1} \sum_{i=1}^{n} \mathbf{1}\{Z_i \leq z\}$ of the scaled data $Z_1, \cdots, Z_n$ and the standard exponential distribution. The most widely used EDF tests for exponentiality are the Kolomgorov-Smirnov (numerically discussed in Section-3.6) and the Cramér-von Mises test. The hypothesis H_0 is rejected for the large values of

$$\begin{aligned} KS &= \sup_{z \geq 0} |F_n(z) - (1 - \exp(-z))| \\ &= \max\Big\{ \max_{1 \leq i \leq n} (i/n - Z_{(j)}), \max_{1 \leq i \leq n} (Z_{(j)} - (i-1)/n) \Big\} \end{aligned} \tag{8.2}$$

and

$$\begin{aligned} CM^2 &= \int_0^{\infty} \big\{ F_n(z) - (1 - \exp(-z)) \big\} \exp(-z) dz \\ &= \frac{1}{12n} + \sum_{i=1}^{n} \big(Z_{(i)} - (2i-1)/2n \big)^2 \end{aligned} \tag{8.3}$$

respectively. The critical values of these tests can be seen in Bagdonaviéus et al. [2010], and Hollander et al. [2014].

8.2.2 Tests based on spacings and the Gini index

D'Agostino and Stephens [1986] (page 447) proposed the following statistic based on the normalized spacings $D_i = (n + 1 - i)(X_{(i)} - X_{(i-1)})$, $X_{(0)} = 0$: Calculate $W_j = \sum_{k=1}^{j} D_k / \sum_{j=1}^{n} X_j$, $1 < k \leq n - 1$, which under H_0 is a sample of size $n - 1$ from a uniform distribution $(0, 1)$. A two-sided test is based on $S_n = \sum_{j=1}^{n-1} W_j = 2n - 2\sum_{j=1}^{n} jZ_{(j)}/n$. Since $(n-1)^{-1} S_n = 1 - G_n$, where $G_n = \sum_{i,j=1}^{n} |Y_i - Y_j| / 2n(n-1)$

denotes the Gini index, then a test based on S_n is equivalent to a two-sided test for exponentiality based on G_n. Such a test was proposed and thoroughly studied by Gail and Gastwirth [1978], who also stated the exact null distribution of G_n. The limiting null distribution of $\sqrt{12(n-1)}\{G_n - 0.5\}$ is standard normal. Earlier, Hoeffding [1949] shows that, under the condition of $E(X^2) < \infty$, $\{G_n - E(G_n)\}/\sqrt{G_n}$ has a limiting standard normal distribution. Notice that

$$\frac{S_n}{n-1} = 1 - G_n \to 1 - \frac{E|X_1 - X_2|}{2E(X)} \tag{8.4}$$

as $n \to \infty$ almost surely provided that $0 < E(X) < \infty$. The limit in Equation-8.4 is equal to 0.5 if X has an exponential distribution.

8.2.3 Tests based on the entropy characterization

It is a well known fact that among all distributions with density f concentrated on $[0, \infty)$ and fixed mean μ, the entropy $H = -\int_0^\infty f(x) \log f(x) dx$ is maximized by the exponential distribution. Ebrahimi et al. [1992] and Grzegorzewski and Wieczorkowski [1999] used this result to construct goodness-of-fit tests of exponentiality based on the entropy estimator

$$H_{m,n} = \frac{1}{n} \sum_{i=1}^{n} \log\Big\{ \frac{n}{2m} [X_{(i+m)} - X_{(i-m)}] \Big\} \tag{8.5}$$

Here, m is an integer satisfying $1 \le m < n/2$ and $X_{(i-m)} = X_{(1)}$, $X_{(i+m)} = X_{(n)}$, if $i - m \le 0$ or $i + m \ge n$, respectively. Rejection of H_0 is for small values of $H_{m,n}$. Ebrahimi et al. [1992] showed that, if $m, n \to \infty$ and $m/n \to 0$, the test is consistent against distributions with finite mean, while Grzegorzewski and Wieczorkowski [1999] removed the condition on moments.

8.2.4 The statistic of Cox and Oakes

Ascher [1990] summarized the simulation results of 15 test statistics for exponentiality and concluded that if nothing a priori is known about the alternative distribution, the test of Cox and Oakes [1984], which rejects the null hypothesis for both small and large values of

$$CO_n = n + \sum_{i=1}^{n} (1 - Z_i) \log Z_i \tag{8.6}$$

is the 'best'. The asymptotic null distribution of CO_n can be derived by assuming $E(X) = 1$ and notice that

$$\frac{1}{\sqrt{n}} CO_n = \frac{1}{\sqrt{n}} \sum_{i=1}^{n} [1 + (1 - Z_i) \log Z_i] \tag{8.7}$$

Now letting $h(\lambda) = (1 - \lambda X)\log(X)$, a Taylor expansion of $h(\hat{\lambda}_n)$ around $\lambda = 1$ yields

$$\frac{1}{\sqrt{n}} CO_n \approx \frac{1}{\sqrt{n}} \sum_{i=1}^{n} Y_i \tag{8.8}$$

where $Y_i = 1+(1-X_i)\log X_i+(1-\gamma)(X_i-1)$ and $\gamma = 0.5772\cdots$ denotes Euler's constant. Moreover, $E(W_1) = 0$ and $E(W_1^2) = \pi^2/6$, the central limit theorem and Equation-8.8 imply that the limiting null distribution of $\sqrt{6/n}(CO_n/\pi)$ is standard normal. It was also noted by Cox and Oakes [1984] that the test is consistent against finite-mean distributions with $E[X \log X - \log X] \neq 1$, provided that the expectation exists.

8.3 Hazard Rate

The reliability (survival) function is used to measure the chance that breakdowns of a system occurs beyond a given time point. To monitor the lifetime of a system across the support of its lifetime distribution, the hazard rate $h(x) = \lim_{dx\to 0} \frac{Pr(x\leq X<x+dx)}{dx.S(x)} = \frac{f(x)}{S(x)}$, where $S(x) = 1 - F(x)$, is used. For this reason, consideration of the hazard rate may be the dominant method for summarizing survival data (cf. Cox and Oakes [1984]). It has different names depending on the field of application (cf. Rinne [2014], page 9-10). Since most materials, structures and devices wear out with time, the class of failure distributions for which the hazard rate is increasing is one of special interest. The phenomenon of work hardening of certain materials and the debugging of complex systems make the class of failure distributions with decreasing hazard rate also of interest. There are, of course, examples such as dynamic loading of structures or structures undergoing adjustment and modification, where a monotonic or non-monotonic hazard function would be appropriate. Therefore, in case of departure of the TBE distribution from exponential, one can identify the direction of the departure in terms of hazard function shape, without specifying a precise alternative from the start. Note that each shape corresponds to a class of distributions and is not restricted to single family models. In the next section, I will focus more on the testing of hazard function shape.

8.3.1 Increasing (Decreasing) Hazard Rate

Theorem : *Increasing hazard rate (IHR) or decreasing hazard rate (DHR)*

- *A lifetime distribution $F(.)$ is said to be IHR (DHR) if its hazard rate has a non-negative (non-positive) first derivative, i.e.,*

$$\frac{dh(x)}{dx} = \frac{d.f(x)}{dx.S(x)} = \frac{S(x)f'(x) - [f(x)]^2}{[S(x)]^2} \geq (\leq) 0 \tag{8.9}$$

- *$F(.)$ is IHR (DHR) if and only if its logarithmic survival function $\ln S(x)$ is concave (convex), i.e., its second derivative has to be non-positive (non-negative),*

$$\frac{d^2[\ln S(x)]}{dx^2} = -\frac{S(x)f^{'}(x) - [f(x)]^2}{[S(x)]^2} \leq (\geq)0 \tag{8.10}$$

Rinne [2014] (page 72) noted that for an IHR (DHR) distribution with $\mu = E(X)$, the $\mu_r = E(X^r) \leq (\geq) r!\mu^2$, $r = 1, 2, \cdots$ holds. Therefore, consequently we have an inequality on the coefficient of variation (CV), i.e., $\frac{SD(X)}{\mu} \leq (\geq)1$, for IHR (DHR) distributions. This CV check is particularly useful to check exponentiality or constant hazard rate assumption, i.e., $CV = 1$. *If $CV \not\approx 1$, then renewal process could be good alternative to the Poisson process.*

8.3.2 Non-monotone Hazard Rate: Mathematical Test

The IHR property is characteristic for systems that consistently deteriorate with time, whereas the DHR for systems that improve with time. However, there are many systems or processes which exhibits hazard rate that are not monotone. Currently, reliability engineers are more interested in hazard rate which first decrease and afterwards increase and look like a bathtub, e.g. human mortality, or which first increase and then decrease and look like an upside-down (inverted) bathtub, e.g. accelerated life testing, in which the systems tested are subject to abnormal high stress levels. We will abbreviate the bathtub property by DIHR (decreasing-increasing hazard rate) and the upside-down bathtub property by IDHR (increasing-decreasing hazard rate).

Rinne [2014] noted that the decision regarding DIHR or IDHR can be done by investigating its first derivative in the case of a continuous variate or its first difference in the case of a discrete variable. A general definition which extend the idea of DIHR and IDHR to situations where the hazard rate itself does not exist is

Definition : *A lifetime distribution $F(x)$ with $x \in [0, \infty)$ is said to be DIHR (IDHR) if there exists a $x_0 > 0$ such that $-\ln[1 - F(x)]$ is concave (convex) on $[0, x_0)$ and convex (concave) on $[x_0, \infty)$.*

Glaser [1980] has given sufficient conditions to characterize a given lifetime distribution as being IHR, DHR, IDHR, and DIHR, assuming that its $f(x)$ is continuous and second derivative exists on $[0, \infty)$. Before quoting Glaser [1980]'s theorem, the following information is necessary: $g(x) = \frac{S(x)}{f(x)}$ with first derivative $g^{'}(x) = g(x)\psi(x) - 1$, where $\psi(x) = -\frac{f^{'}(x)}{f(x)}$ and $\psi^{'}(x) = [\psi(x)]^2 - \frac{f^{''}(x)}{f(x)}$.

Theorem : *A lifetime distribution $F(x)$ is said to be IHR, DHR, IDHR, or DIHR, if it satisfies the following conditions:*

1. *If* $\psi^{'}(x) > 0 \ \forall \ x \geq 0$, *then IHR.*

2. *If* $\psi^{'}(x) < 0 \ \forall \ x \geq 0$, *then DHR.*

3. *Suppose there exists* $x_0 > 0$ *such that*

$$\psi^{'}(x) < 0 \forall x \in [0, \infty), \quad \psi^{'}(x_0) = 0 \quad \textit{and} \quad \psi^{'}(x) > 0 \forall x > x_0 \tag{8.11}$$

   - *If there exists* $y_0 > 0$ *such that* $g^{'}(y_0) = 0$, *then DIHR.*
   - *If there does not exists* $y_0 > 0$ *such that* $g^{'}(y_0) = 0$, *then IHR.*

4. *Suppose there exists* $x_0 > 0$ *such that*

$$\psi^{'}(x) > 0 \forall x \in [0, \infty), \quad \psi^{'}(x_0) = 0 \quad \textit{and} \quad \psi^{'}(x) < 0 \forall x > x_0 \tag{8.12}$$

   - *If there exists* $y_0 > 0$ *such that* $g^{'}(y_0) = 0$, *then IDHR.*
   - *If there does not exists* $y_0 > 0$ *such that* $g^{'}(y_0) = 0$, *then DHR.*

Glaser [1980] provided the following lemma that helps to avoid finding a root y_0 of $g^{'}(.)$ in above theorem.

Lemma : *Suppose that Equation-8.11 or 8.12 holds in above theorem.*

1. *Suppose* $\epsilon = \lim_{x \to 0^+} f(x)$ *exists, possibly equals to* 0 *or* ∞.

   - *If* $\epsilon = \infty$ *and Equation-8.11 holds, then DIHR.*
   - *If* $\epsilon = 0$ *and Equation-8.11 holds, then IHR.*
   - *If* $\epsilon = \infty$ *and Equation-8.12 holds, then DHR.*
   - *If* $\epsilon = 0$ *and Equation-8.12 holds, then IDHR.*

2. *Suppose* $\delta = \lim_{x \to 0^+} g(x)\psi(x)$ *exists, possibly equals to* 0 *or* $-\infty$.

   - *If* $\delta > 1$ *and Equation-8.11 holds, then DIHR.*
   - *If* $\delta < 1$ *and Equation-8.11 holds, then IHR.*
   - *If* $\delta > 1$ *and Equation-8.12 holds, then DHR.*
   - *If* $\delta < 1$ *and Equation-8.12 holds, then IDHR.*

8.3.3 Graphical Methods for Hazard

The estimation of hazard rate can be done by different methods (cf. Cox and Oakes [1984], Lawless [2011], and Rinne [2014]), e.g., parametric, nonparametric and smoothing methods. However, a graphical approach like hazard plot or nonparametric test, i.e.,

total-time-on-test (TTT) (cf. Epstein and Sobel [1953]), is the most commonly used because one picture is worth a thousand words. However, Rinne [2014] noticed (page 212) that hazard plotting can be successfully applied to location-scale distributions and to those distributions that after suitable transformation can be converted into a location-scale type. Hazards plots and probability plots are very similar, the main difference is the scaling of the y-axis where to lay down the cumulative hazard rate instead of the $F(.)$ and the choice of the plotting position, i.e., the ordinate-value to be plotted against the $X_{(i)}$ on the x-axis. Next, I present the procedure of the TTT statistic.

Let the difference S_i of two adjacent order statistics $X_{(i-1)}$, $X_{(i)}$ be called spacing, i.e., $S_i = X_{(i)} - X_{(i-1)}$, $i = 2, 3, \cdots, n$. The total time T_n spent on the test by the n sample until the failure of the longest living unit, can be expressed in two different ways: as the sum of all observed times, i.e., $T_n = \sum_{i=1}^{n} X_{(i)}$, or by the sum of all normalized spacings, i.e., $T_n = \sum_{i=1}^{n}(n-i+1)(X_{(i)} - X_{(i-1)}) = \sum_{i=1}^{n} D_i$. T_n is known as TTT-statistic. The consecutive TTT-statistics can be obtained either by $T_i = \sum_{k=1}^{i} X_{(k)} + (n-i)X_{(i)}$ or $T_i = \sum_{k=1}^{i}(n-k+1)(X_{(k)} - X_{(k-1)}) = \sum_{k=1}^{i} D_k$. The scaled TTT-statistics, i.e., on $[0, 1]$, are defined as: $T_i^* = T_i/T_n$.

By plotting scaled TTT-statistics on the y-axis against the empirical distribution function, $F_n(x_{(i)}) = i/n$ on the x-axis and by joining these points in a straight line we get a curve within the unit square of the (x, y)-plan, known as TTT-plot. The interpretation of the TTT-plot is very easy, i.e., the shortest living $100(i/n)\%$ of the sample data contribute $100(T_i^*)\%$ of the total time lived by all sample.

For a parametric distribution F, let $H(t)$ be the cumulative hazard (CH) $\int_0^t h(x)dx$ and $H_F^{-1}(P)$ be the P-th percentile of the CH. In fact $H_F^{-1}(P) = \int_0^{F^{-1}(P)} S(x)dx$, $0 \leq P \leq 1$ is the counterpart of T_i and called the TTT-transform of $F(.)$. Note that $F^{-1}(P)$ denotes the percentile x_P of order P. Moreover, $H_F^{-1}(1) = \mu = E(X)$ for $P = 1$. Similarly, the counterpart of T_i^* is

$$\phi_F(P) = \frac{H_F^{-1}(P)}{H_F^{-1}(1)} = \frac{H_F^{-1}(P)}{\mu} \tag{8.13}$$

the scaled TTT-transform of $F(.)$. It is interesting to note that the TTT-plot of a sample from a population with $F(.)$ will approach the graph of the scaled TTT-transform $\phi_F(P)$ of $F(.)$ as the sample size, n, increases. This is guaranteed by the Glivenko-Cantelli theorem and the strong law of large numbers with probability one:

$$T_i = \sum_{k=1}^{i}(n-k+1)(X_{(k)} - X_{(k-1)}) = \int_0^{F_n^{-1}(i/n)} S_n(x)dx \to \int_0^{F^{-1}(P)} S(x)dx \tag{8.14}$$

uniformly in $[0, 1]$ when $n \to \infty$ and $i/n \to F(.)$. Rinne [2014] stated the following properties of the TTT-transform $H_F^{-1}(P)$:

- There is one-to-one correspondence between life distribution and their TTT-transforms.

- If $F(.)$ is strictly increasing or, equivalently, if $F^{-1}(.)$ is continuous, then $H_F^{-1}(P)$ is continuous.

- If $F(.)$ is absolutely continuous and strictly increasing, then the derivative of $H_F^{-1}(P)$ is $\frac{dH_F^{-1}(P)}{dP} = \frac{1}{h(x)}$ for almost all $P \in [0,1]$. This property plays an important role in finding test statistics for hypotheses on the hazard rate.

8.4 Testing Hazard Rate Properties

We want to test the behavior of the hazard rate whether it is constant, IHR, DHR, DIHR or IDHR.

8.4.1 Constancy of the Hazard Rate

The exponential distribution is the only continuous distribution with constant hazard rate. Thus, testing $H_0 : h(x)$ is constant, against $H_1 : h(x)$ is not constant, we can proceed as: For an exponential distribution with $F(x) = 1 - \exp(-\lambda x)$, $F^{-1}(P) = -\ln(1-P)/\lambda$ and $\mu = 1/\lambda$, we have $H_F^{-1}(P) = P/\lambda$ and $\phi_F(P) = P$. Therefore, the TTT-plot will be a 45^o-line running from $(0,0)$ to $(1,1)$, see Figure-8.1.

8.4.2 Monotonicity of the Hazard Rate

To test whether a distribution is IHR (DHR) or not, i.e., $H_0 : F(x) = 1-\exp(-\lambda x)$ where λ is unknown, against $H_1 : F(x)$ is IHR and not exponential, or $H_1^* : F(x)$ is DHR and not exponential, we know that $\frac{d\phi_F(P)}{dP} = \frac{d}{dP}(H_F^{-1}(P)/\mu) = \frac{1}{\mu.h(x)}$. Therefore, the graph of the scaled TTT-transform $\phi_F(P)$ will be

- a straight line for an exponential distribution,

- concave for an IHR distribution, and

- convex for a DHR distribution.

Since the graph of $\phi_F(P)$ runs from $(0,0)$ to $(1,1)$, an IHR distribution will have a decreasing slope and lie above the 45^o-line. Similarly, an increasing slope which lies below the 45^o-line indicates a DHR distribution. Figure-8.1 shows $\phi_F(P)$ for three Weibull distributions having $h(x) = \beta\lambda^\beta x^{\beta-1}$: $\beta = 0.5$ gives DHR, $\beta = 1$ gives the exponential distribution and $\beta = 1.5$ gives IHR. Therefore, the hypothesis regarding the validity of concave (convex) hazard can easily be tested.

A numerical testing procedure associated with the TTT-transform goes back to Klefsjö [1982] and applicable only to uncensored data. Suppose that the $\phi_F(P)$ graph is concave

(convex). Since the graph of the scaled TTT-statistic T_i^* converge to $\phi_F(P)$, it is reasonable to expect the TTT-plot based on a sample from an IHR (DHR) distribution to behave concavely (convexly), too, i.e., $2T_i^* - T_{i-1}^* - T_{i+1}^* > (<)0$ for $i = 1, 2, \cdots, n-1$ and $T_0^* = 0, T_n^* = 1$. Therefore, a possible test statistic against the IHR (DHR) alter-

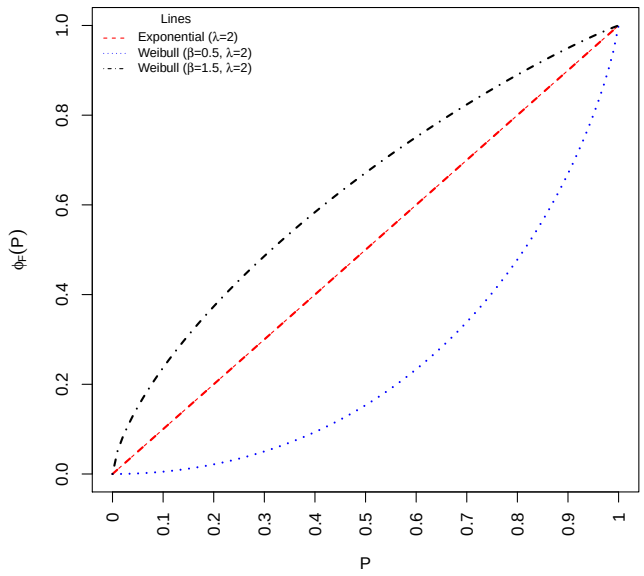

Figure 8.1: Scaled TTT-transform of Weibull distribution

native could be $B_{H_1} = \sum_{i=1}^{n-1}(2T_i^* - T_{i-1}^* - T_{i+1}^*)$ and we expect a positive (negative) value of B_{H_1} if $F(.)$ is IHR (DHR), but not exponential. For a normalized spacings D_i, $B_{H_1} = (D_1 - D_n)/T_n$. Klefsjö [1982] gives the asymptotic distribution of B_{H_1} under H_0 as a Laplace distribution and remarked that since the enumerator $(D_1 - D_n)$ of B_{H_1} is independent of $D_2, \cdots, D_{n-1}$, a test based on B_{H_1} is not consistent against the whole IHR (DHR) class. Therefore, he suggested another test to tackle this problem. The new test is based on the idea that, when $\phi_F(P)$ is concave (convex) we expect $T_i^* + (T_{i+j}^* - T_i^*)k/(j/n)n > (<)T_{j+k}^*$ for $i = 1, \cdots, n-1$, $j = 2, 3, \cdots, n-i$ and $k = 1, 2, \cdots j-1$. An alternative representation is $(T_{i+j}^* - T_i^*)k > (<)j(T_{j+k}^* - T_j^*)$. Therefore, we have the test statistic

$$B_{H_1}^* = \sum_{i=0}^{n-2}\sum_{j=2}^{n-i}\sum_{k=1}^{j-1}[(T_{i+j}^* - T_i^*)k - j(T_{j+k}^* - T_j^*)] \tag{8.15}$$

For $F(.)$ to be IHR (DHR), but not exponential, we expect $B_{H_1}^*$ to be positive (negative). Another representation of $B_{H_1}^*$ is $\sum_{i=1}^{n}\psi_i D_i/T_n$ where $\psi_i = [(n+1)^3 i - 3(n+1)^2 i^2 + 2(n+1)i^3]/6$. Klefsjö [1982] then considers the slightly modified test statistic $B_H = B_{H_1}^*\sqrt{7560/n^7}$ which is asymptotically $N(0,1)$. H_0 is rejected in favor of $H_A(H_A^*)$ at level

of α when B_H is greater (smaller) than the critical value. Exact critical values have also been given in Klefsjö [1982].

Many test of H_0 versus H_1 or H_1^* are based on the normalized spacings $D_i = (n-i+1)(X_{(i)}-X_{(i-1)})$ while other tests only use the ranks of the normalized spacings. One of the oldest test normalized spacings is the cttot-test (cumulative total-time-on-test) of Barlow [1968], and Epstein [1960]. This test is applicable for censored as well as uncensored data. Since under H_0 the $T_i = \sum_{k=1}^{i} D_k$ are uniformly distributed over $[0, T_r]$ where $1 \leq r \leq n$ is the number of failures in a sample of size n. The test statistic is

$$Y_r = \frac{\sum_{i=1}^{r-1}\sum_{k=1}^{i} D_k}{\sum_{k=1}^{r} D_k} = \frac{\sum_{i=1}^{r-1}(r-i)D_i}{\sum_{k=1}^{r} D_k} \tag{8.16}$$

Epstein [1960] has given the exact critical values for this test. H_0 is rejected in favor of $H_A(H_A^*)$ at level α if $Y_r \geq y_{r,1-\alpha}(Y_r \leq y_{r,\alpha})$. Moreover, for small r we can use a normal approximation of Y_r under H_0, i.e., $y_{r,\gamma} \approx (r-1)/2 + \tau_\gamma\sqrt{(r-1)/12}$ where τ_γ denotes the γ percentile of $N(0,1)$.

Bickel and Doksum [1969] extensively studied tests of One of H_0 versus $H_1(H_1^*)$ based on the ranks of the normalized spacings. In fact their statistics were motivated by the test of Proschan and Pyke [1967] and requires uncensored samples, which is as follows. Let $W_{ij} = 1$ if $D_i \geq D_j$ for $i, j = 1, 2, \cdots, n$ and $W_{ij} = 0$, otherwise. The test statistic is

$$W_n = \sum_{\substack{i,j=1 \\ i<j}} W_{ij} \tag{8.17}$$

H_0 would be rejected in favor of $H_1(H_1^*)$ at α level if $W_n \geq w_{n,1-\alpha}(W_n \leq w_{n,\alpha})$, whereas $w_{n,\gamma} = Pr(W_n < w_{n,\gamma}|H_0) = \gamma$. The exact value of $w_{n,\gamma}$ is calculated from (cf. Rinne [2014]) $Pr(W_n = m|H_0) = P_n(m)/n!$ and $P_n(m)$ denotes the number of orderings of $D_1, D_2, \cdots, D_n$ with exactly m inversions of indices, i.e., an inversion of indices $i < j$ occurs when $D_i > D_j$. Moreover, W_n is asymptotically normal with $E(W_n) = 0.25n(n-1)$ and $Var(W_n) = n(2n+5)(n-1)/72$ and therefore, $w_{n,\gamma} \approx 0.25n(n-1) + \tau_\gamma\sqrt{\frac{n(2n+5)(n-1)}{72}}$. The justification of this is as follows: Under H_0 the normalized spacings are *iid*, each with $F(x) = 1 - \exp(-\lambda x)$. Therefore, $Pr(W_{ij} = 1) = 0.5$ with $i \neq j$. However, under H_1, we have $Pr(W_{ij} = 1) > 0.5$ for $i < j$. Thus, each W_{ij} and W_n tend to be larger under H_1, which leads to the rejection of H_0 in favor of H_1 for large values of W_n. It is interesting to mention here that the asymptotic relative efficiency of the cttot-test is higher than the test proposed by Proschan and Pyke [1967].

Using ranks of the spacings, i.e., R_i is rank of D_i, Bickel and Doksum [1969] suggested many test statistics and some of them are: $V_0 = \sum_{i=1}^{n} iR_i/(n+1)^2$, $V_1 = \sum_{i=1}^{n} \frac{-i}{n+1}\ln\big(1 - R_i/(n+1)\big)$, $V_2 = \sum_{i=1}^{n} \ln\big(1 - i/(n+1)\big)\ln\big(1 - R_i/(n+1)\big)$, and $V_3 = \sum_{i=1}^{n} \ln\big[-\ln\big(1 - i/(n+1)\big)\big]\ln\big(1 - R_i/(n+1)\big)$. Large (small) values of these test statistics are significant

for $H_1(H_1^*)$.

Example-1 Rinne [2014] consider a data set of $r = n = 15$ generated from the Weibull distribution with $\lambda = 0.1$ and $\beta = 0.7$ is: 00309, 0.3641, 0.5317, 0.9545, 1.0119, 1.9145, 3.5331, 3.9321, 4.1219, 10.9776, 13.5405, 14.9801, 15.2600, 15.8278, 31.4019. Thus, data are from a DHR distribution. The cott-test gives $Y_r = 5.58$, thus H_0 is rejected in favor of H_1^* (DHR) at $\alpha = 0.10$. A test given by Klefsjö [1982] results into $B_H = -1.766$, and again H_0 is rejected in favor of H_1^*. Similarly, Proschan and Pyke [1967] test gives $W_n = 41$, and H_0 is rejected in favor of H_1^* approximately at $\alpha = 0.12$.

Example-2 Another data set of $n = 20$ from the IHR Weibull distribution with $\beta = 2$ and $\lambda = 0.05$ is: 2.5349, 2.6149, 4.4532, 4.8567, 5.7627, 11.0273, 15.5141, 16.8996, 18.3318, 18.5556, 18.6857, 19.8772, 20.7875, 22.1906, 22.9138, 25.4471, 26.2949, 29.9485, 34.3137, 40.8301. The cttot-test $Y_r = 12.57$, thus H_0 is rejected in favor of H_1 (IHR) at $\alpha < 0.01$. Klefsjö [1982] test results into $B_H = 3.26$, which reject H_0 with $\alpha \ll 0.01$. Proschan and Pyke [1967] test gives $W_n = 122$, and H_0 is rejected at $\alpha \approx 0.04$.

8.4.3 Bathtub Shape of the Hazard Rate

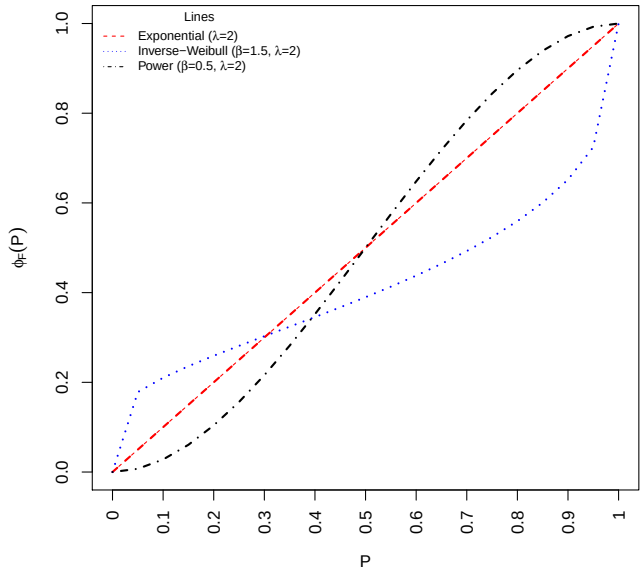

Figure 8.2: Scaled TTT-transform of Inverse-Weibull and power function distributions

There are two types of non-monotonic hazard rates which are interested: the bathtub shape DIHR where the hazard rate initially decrease (infant mortality) then constant (useful life) and finally increase (wear-out); and the inverted bathtub shape, IDHR where the situation is reversed as mentioned in case of the DIHR. From the scaled TTT-transform $\phi_F(P)$ of $F(.)$ for the DIHR, we expect that $\phi_F(P)$ is convex and lies below the 45^o-line

for P being small and $\phi_F(P)$ is concave lies above the line. Similarly, for the IDHR the said order is reversed. Figure-8.2 shows the scaled TTT-transforms of the inverse Weibull $F(x) = \exp(-\lambda x)^{-\beta}, x > 0$, which is IDHR distribution, and of the power function $F(x) = (x\lambda)^{\beta}, x < \lambda$ distribution, which is DIHR.

Bergman [1979] suggested the following procedure of testing $H_0 : F(.)$ is the exponential distribution versus $H_1 : F(.)$ is DIHR, for the uncensored data: Define

$$W_n^* = \begin{cases} \min\{i \geq 1 : T_i^* \geq i/n\} \\ n, \quad \text{if} \quad T_i^* < i/n \quad \text{for} \quad i = 1, 2, \cdots, n-1. \end{cases} \tag{8.18}$$

$$Y_n^* = \begin{cases} \max\{i \leq n-1 : T_i^* \leq i/n\} \\ 0, \quad \text{if} \quad T_i^* > i/n \quad \text{for} \quad i = 1, 2, \cdots, n-1. \end{cases} \tag{8.19}$$

and $D_n^* = W_n^* + n - Y_n^*$. Reject H_0 when D_n^* is large. The idea behind the test is when the distribution is IDHR, we may expect W_n^* as well as $n - Y_n^*$ to be large and therefore, D_n^* takes integer values in $[2, n+1]$. Since the graph of $\phi_F(P)$ for an IDHR is the reflection of the $\phi_F(P)$ for a DIHR, thus, we can modify Equations 8.22 and 8.19 to develop test for IDHR as:

$$W_n^{**} = \begin{cases} \min\{i \geq 1 : T_i^* \leq i/n\} \\ n, \quad \text{if} \quad T_i^* > i/n \quad \text{for} \quad i = 1, 2, \cdots, n-1. \end{cases} \tag{8.20}$$

$$Y_n^{**} = \begin{cases} \max\{i \leq n-1 : T_i^* \geq i/n\} \\ 0, \quad \text{if} \quad T_i^* < i/n \quad \text{for} \quad i = 1, 2, \cdots, n-1. \end{cases} \tag{8.21}$$

and $D_n^{**} = W_n^{**} + n - Y_n^{**}$. H_0 is rejected when D_n^{**} is large.

Aarset [1985] derived the following null distribution, i.e., assuming exponentiality, of D_n^*:

$$Pr(D_n^* = j) = \begin{cases} \sum_{i=1}^{j-1} \frac{(n-1)!}{(j-1)!(n-j+1)!(j-i-1)!} \left(\frac{i}{n}\right)^{i-1} \times \\ \left(\frac{n-j}{n}\right)^{n-j+1} \left(\frac{j-i}{n}\right)^{j-i-1} \frac{1}{i(j-i)} \quad \text{for} \quad j = 2, \cdots, n-1 \\ 0, \quad \text{for} \quad i = n \\ \frac{2}{n}\left(\frac{n+1}{n}\right)^{n-2} \quad \text{for} \quad i = n+1. \end{cases} \tag{8.22}$$

see page 59 of Aarset [1985] for the critical values. Moreover, Aarset [1985] also derived an asymptotic result: $\lim_{n\to\infty} Pr(D_n^* = n - l) = 2l^{l+1}\exp(-l)/(l+1)!$. Later, Aarset [1987] suggested modification of Cramér-Von-Mises goodness-of-fit test for uncensored

data. Aarset [1987] defines $R_n = \int_0^1 \Delta_n^2(v)dv$, where

$$\Delta_n(v) = \begin{cases} \sqrt{n}[T_i^* - \phi_F(v)] & \text{for} \quad \dfrac{i-1}{n} < v \leq \dfrac{i}{n}, 1 \leq i \leq n \\ 0, & \text{for} \quad v = 0. \end{cases} \tag{8.23}$$

Under H_0, i.e., $F(.)$ is the exponential distribution, R_n can be written as: $R_n = \sum_{i=1}^n T_i^* \times[T_i^* - (2i-1)/n] + n/3$ and has the same asymptotic distribution (due to invariance principle) as the Cramér-Von-Mises test.

Example 3 We are interested to know whether the data set given in Rinne [2014] (page 247): 0.2, 0.4, 2, 2, 2, 2, 2, 4, 6, 12, 14, 22, 24, 36, 36, 36, 36, 36, 43, 64, 72, 80, 90, 92, 94, 100, 110, 120, 126, 126, 134, 134, 134, 134, 144, 150, 158, 164, 164, 166, 168, 168, 168, 170, 170, 170, 170, 170, 172, and 172, of 50 observations comes from a DIHR distribution or not. The Bergman [1979] test is $D_{50}^* = 45$ and $Pr(D_{50}^* \geq 45) \approx 0.14$ which favor the hypothesis of DIHR. Similarly, Aarset [1987] test gives $R_{50} = 1.2922$ and again we favor DIHR at $\alpha \ll 0.001$. The graphical presentation is given in Figure-8.3a.

Similarly, using the data set given in Example 2, we have $D_{20}^* = 21$, which favors both the DIHR and the IDHR, and $R_{20} = 0.88$ also favors H_1. However, Figure-8.3b indicates neither DIHR nor IDHR but IHR.

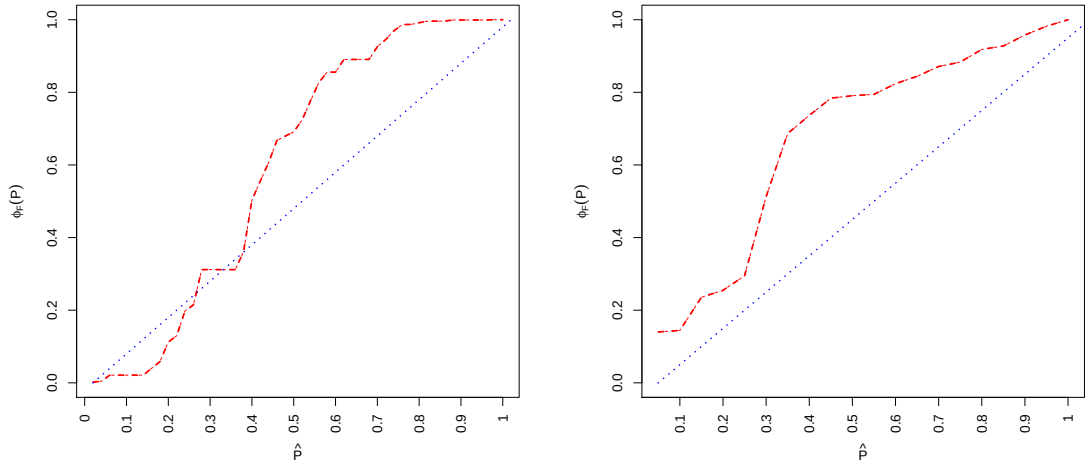

(a) TTT-plot for a data set from DIHR distribution

(b) TTT-plot for a data set from an IHR distribution

Figure 8.3: TTT-plot for checking DIHR and IHR distributions

Çiğşar [2010] also suggested some tests for testing trend and carryover effect (i.e., event intensity may be temporarily increased or decreased) for recurrent event processes. Moreover, I refer to see Dykstra and Laud [1981], Singpurwalla [1995], and Hjort [1990] for estimation and testing of the random hazard function using nonparametric Bayesian approach.

Chapter 9

Conclusion and Recommendations

The results and contributions of the research works included in this dissertation are summarized in this chapter. The limitations of current works are discussed, and some future works are also suggested.

9.1 Conclusion

The success and progress of human society depend on the reliable physical infrastructures, i.e., roads, bridges, hospitals, fire stations, dams, sewage, gas pipelines, nuclear power plant, transmission lines, etc., for distributing resources and essential services to the public. A common problem associated with the infrastructure is that, as the service time progresses, the infrastructure ages, its performance deteriorates and its reliability declines. The deteriorating infrastructure can have an adverse impact on a utility's profit and sometimes even on a whole nation's economy. Statistical quality control is a collection of statistical methods, which are used to monitor and improve the quality of a process. Currently, statistical quality control is not limited to manufacturing industry, but also used in environmental science, biology, genetics, epidemiology, medicine, finance, law enforcement and athletics.

TBE charts were shown to be highly effective in both industry system improvement and human management. The example areas of applications of the TBE charts include the manufacturing systems, reliability and maintenance monitoring problems, human health surveillance, etc. Despite its effectiveness and generality of applications, the current TBE chart techniques are facing more and more challenges as the implementing circumstance becomes more complex. To monitor complex TBE data, therefore, the need of generalized processes is emerging. In addition, there is a strong need to develop control charts for reliability data to ensure the product/process maintains the expected reliability standards as recently highlighted by Vining et al. [2015].

This thesis expanded the application area of the TBE charts by developing them using

the renewal, renewal reward and nonhomogeneous Poisson processes. The renewal process was used to generalize the existing TBE charts which are based on the Poisson process while the renewal reward process for the joint monitoring of the time and magnitude. Similarly, the nonhomogeneous Poisson process with power law intensity is used to generalize the existing work to a situation where failure risk varies over time, and the quality engineer requires adaptive monitoring. A Bayesian chart using the predictive distribution, to overcome the restrictive assumption of a large phase-I data, was also introduced in this thesis. We have demonstrated that proposed control charts' performance in monitoring different types of complex data set is quite effective. The proposed control charts are assessed using different commonly used performance measures, including average run length, coefficient of variation of the run-length distribution and the length of inspection distribution. The guidelines for various situations in which the proposed charts would work are given in each respective chapter. Results from each chapter showed that the control charts proposed in this thesis did improve the effectiveness of the TBE charting technique and made it more practical for complex TBE data monitoring. However, this thesis also has its limitations which, along with future research direction are discussed in the next section.

In Chapter 2, we have reviewed 114 articles related to the TBE or high-quality concept and 63% of the reviewed articles deal with discrete or attribute data while 31% deal with continuous data and the remaining 6% with both. Thus, the trend of research is highly influenced by the discrete distributions. Of our reviewed articles, only 23 deal with the parameter estimation problem while in the remaining ones, i.e., 91 articles, the parameter is assumed known. The maximum likelihood method is used 4 times in the continuous case while 6 times in the discrete case. The use of Bayesian methods is not very popular in the continuous case as compared to the discrete case. Geometric and negative binomial models are commonly used in discrete cases while the exponential model is used for continuous data. It is observed that CUSUM, EWMA and synthetic or joint charts are used for both types of data. We also noticed from Chapter 2 that the existing TBE control charts are either based on approximations or simple processes. Parameter estimation is also often overlooked, and most of the previous research has been done by assuming known parameter values.

In Chapter 3, we proposed a control chart based on the renewal process where a class of continuous distribution was assumed for the TBE. The use of a renewal process was motivated by TBE with a non-constant hazard rate. The control chart performance was studied in terms of different commonly used measures like ARL, CV of the run-length distribution, and CV of the length of inspection (or time to signal) distribution. In previous studies, mostly it is assumed that the parameters of the TBE distribution are known. When the parameters are unknown or unspecified, these should be estimated from reference data or Phase-I data. However, in practice, parameter's estimation is subject

to estimation and approximation error. Therefore, we examined the performance of the renewal process chart in terms of different sample sizes by assuming that both parameters unknown of the Weibull distribution. We found that a very large sample size is required to overcome estimation and approximation error. A method for the detection of a shift, i.e., to decide whether a shift is in the shape or the rate parameter, based on the coefficient of variation was also proposed in Chapter 3. Furthermore, some historical data sets were also analyzed to show the implementation and effectiveness of the proposed chart.

In Chapter 4, we proposed a control chart for the joint monitoring of time and magnitude by assuming a fixed threshold/critical value. Since obtaining an explicit form of the first-passage distribution is extremely difficult in general cases, we proposed an algorithm to compute the control limits for any lifetime distribution of the time and the magnitude, respectively. Moreover, an algorithm to compute the effectiveness of the control chart was also proposed in the same chapter. We noticed that the performance of the renewal reward process's control chart is mainly dependent on the magnitude distribution. Therefore, we suggest the use of the one-sided chart only if one has an idea about the direction of a shift and in general cases, the two-sided chart is recommended. Similarly, we proposed a control chart with the random threshold to monitor jointly the time and magnitude in Chapter 5. It was shown by the ARL study that the proposed chart is quite effective in different situations where the threshold varies over time.

Chapters 6 and 7 deal with the control charts which are suitable for sequential and adaptive monitoring. In Chapter 6, we have proposed a TBE chart based on the nonhomogeneous Poisson process for the adaptive process monitoring. In particular, we considered the power law intensity for the nonhomogeneous process. We found that the proposed chart was also useful to monitor a time-varying failure risk (cf. Chapter 6). With simulation studies and real data examples, it has been shown that the proposed chart is quite effective to handle different situations. However, it is shown in Chapter 6 that one needs a large phase-I/base period data to estimate the unknown parameters of the power law process. Therefore, to overcome this restrictive assumption, we proposed a Bayesian predictive chart based on the Poisson process in Chapter 7. Since the sequential use of Bayes theorem helps us to calculate the posterior distribution of parameter and the predictive distribution of data, the proposed methodology is also suitable for the online sequential and adaptive monitoring. We have shown successfully in this chapter that the restrictive assumption about the availability of a large base period could be avoided by using a predictive approach. Moreover, the EWMA and the CUSUM charts for the predictive setup have been proposed and studied in this Chapter 7. The charts in chapters 6 and 7 are tested under different scenarios, i.e., fixed/sustained versus random and time varying shifts. In the case of nonhomogeneous Poisson, we noticed that performance of the sequential limits' chart was good for random and time varying shifts while predictive chart was efficient for random shifts. Furthermore, since both the chapters deal with the control

limits which are sequential updated, we showed that the control limits deteriorate with the inclusion of each new observation. The price of these sequentially updated control limits is that the designed charts are insensitive to moderate size shifts and useful only for a very large shift. Therefore, we proposed a check to improve the detection power of the charts in chapters 6 and 7.

Some people may feel comfortable with the idea of revising a prior information in the light of observed data. This approach is not commonly welcomed in the classical Bayesian analysis, however, many researchers favor it. Therefore, we proposed empirical Bayesian approach in Chapter 7 for this purpose. We suggest that the Bayesian approach should be used with extreme care, especially in control chart setting. A method to select the false alarm probability by using a decision theory approach has also been discussed in Chapter 7. However, a numerical optimization procedure is required to implement this approach.

To help practitioners and to verify the assumptions of the renewal process, some statistical tests have been discussed in Chapter 8. Moreover, testing of exponentiality is an important problem in statistics, and related tests have been mentioned in the same Chapter 8. It is also important to verify whether the incoming data have the constant, decreasing or increasing hazard rate, to develop a suitable control chart. Therefore, parametric and nonparametric tests for testing hazard shape have been given in Chapter 8, with some examples.

9.2 Future Work

The importance of TBE control charts continues to grow, and we suggest the quality engineers, practitioners, statisticians to do further research in this area. Moreover, it is a necessity of the modern industry to look for some other general processes, which are more appropriate for the (new) complex data sets, e.g., spatiotemporal data. After the book of Xie et al. [2002a], a comprehensive literature review has been given in Chapter 2, where we have attempted to classify a large number of papers, can help locating groups of articles by subject and by methodology, providing a starting point for study.

In this thesis, we presented some new type of TBE control charts for improving and monitoring complex system's reliability. However, several concerns of the proposed charts using the generalized (stochastic) processes still require further exploration. Firstly, we have not introduced EWMA and CUSUM charts based on the nonhomogeneous Poisson process. In future, it would be interesting to study the properties of nonhomogeneous Poisson CUSUM and EWMA charts. Moreover, the effect of aggregation of data under these different designed charts is an open issue and there is a room for improvement.

Due to the impact of estimation error on the detection power of control charts, special attention is required for the selection of a sample size in the SPC setup. Some new process

monitoring strategies are needed to account for estimation error efficiently. In processes where collecting large amount of phase-I data is infeasible, it has been recommended by several researchers that monitoring should start using the available data and parameter estimate should be updated as more data become available. Therefore, we suggest the use of a Bayesian approach in such a situation. Moreover, the impact of updating control limits, for sequential monitoring, to account for the extra variability introduced by parameter estimation at each step, needs special attention.

In Chapter 3, we observed that when a large shift was appeared in the shape parameter than the nominal value, the control chart performance was biased. Therefore, in the future, an interesting work could be to consider unbiased design of the Weibull chart by assuming both parameters unknown.

Another widely studied method for designing control charts is the economic approach which has not discussed throughout this thesis. In future, one could introduce and study the proposed charts' properties within the economic design framework.

A related but significantly different area to process monitoring is a process control (see Chapter 11 of Montgomery [2009]). Many practitioners do not distinguish between these two related areas, but there is an important difference. Process control deals with maintaining the output of a specific process within a desired range. For instance, the temperature of a chemical reactor may be controlled to maintain a consistent product output. Process monitoring deals with the decision, whether the finished good is up to customer requirement or not. We have not studied the chart performance in the control theory setup, and it would be an interesting study to move from process monitoring to control theory, i.e., integration of process monitoring and process control techniques, in the future.

Moreover, there are lots of multivariate attributes or variable TBE models with important applications in literature. In the existing TBE literature, multivariate TBE charts for monitoring several TBE quantities at the same time have been rarely studied. Although some authors have developed various non-parametric control charts for bivariate data, the performances of such charts are usually poor compared to distribution-based control charts. To improve the effectiveness of the control charts and to overcome the weakness of the univariate TBE charts for correlated quantities, it would be beneficial to extend the univariate TBE charts, especially for the time and magnitude monitoring.

Future work is also needed on developing strategies to deal with the monitoring of multiple data streams, such as studies on the effect of TBE data aggregation (cf. Schuh et al. [2014]), accompanied by appropriate methods for visualizing large data sets.

Finally, the overwhelming majority of research on monitoring high quality processes restricts attention to process response data. Among the reviewed studies (cf. Chapter 2), only Steiner and MacKay [2004] take covariates into account. This research pattern does not reflect industrial reality. Modern high quality manufacturing technology

accounts for factors influencing the process response, in particular, machine conditions and material characteristics. Usually the factor-response relationships are well-studied and documented, and the relevant levels of factors are continuously measured over time. Instead of assuming an artificial setting of restricted information, monitoring research should rather exploit the wealth of information and measurements available under modern manufacturing technology, particularly in data-rich environments as addressed by the Industry 4.0 concept, by appropriately designed covariate-response models. This will enable more successful monitoring schemes, and will significantly increase the disposition of the engineering community to use statistical monitoring.

Bibliography

M. V. Aarset. The null distribution for a test of constant versus bathtub-failure rate. *Scandinavian Journal of Statistics*, 12:55–62, 1985.

M. V. Aarset. How to identify a bathtub hazard rate? *IEEE Transaction on Reliability*, 36:106–108, 1987.

M. Abramowitz and I. A. Stegun. *Handbook of Mathematical Functions, With Formulas, Graphs, and Mathematical Tables*. Dover Publications, Incorporated, 1974.

C. A. Acosta-Mejia. Two sided charts for monitoring nonconforming parts per million. *Quality Engineering*, 25:34–45, 2013.

S. B. Adnaik, M. P. Gadre, and R. N. Rattihalli. Single attribute control charts for a markovian dependent process. *Communications in Statistics - Theory and Methods*, iFirst:DOI:10.1080/03610926.2013.810263, 2013.

S. Aebtarm and N. Bouguila. An optimal bivariate Poisson field chart for controlling high-quality manufacturing processes. *Expert Systems with Applications*, 37:5498–5506, 2010.

M. V. Ahmadi, M. Doostparast, and J. Ahmadi. Statistical inference for the lifetime performance index based on generalized order statistics from exponential distribution. *International Journal of Systems Science*, 46:1094–1107, 2015.

W. Albers. The optimal choice of negative binomial charts for monitoring high quality processes. *Journal of Statistical Planning and Inference*, 140:214–225, 2010.

W. Albers. Improved binomial charts for high quality processes. *Produc$\tilde{a}$o*, 21:209–216, 2011a.

W. Albers. Empirical nonparametric control charts for high quality processes. *Journal of Statistical Planning and Inference*, 141:3151–3159, 2011b.

W. Albers. Control charts for health care monitoring under overdispersion. *Metrika*, 74: 67–83, 2011c.

W. Albers. Control charts for high quality processes: MAX or CUMAX? *Journal of Statistical Planning and Inference*, 142:1924–1932, 2012a.

W. Albers. Nonparametric control charts for bivariate high quality processes. *International Journal of Pure and Applied Mathematics*, 79:139–154, 2012b.

W. Albers and W. C. M. Kallenberg. Estimation in Shewhart control charts: effects and corrections. *Metrika*, 59:207–234, 2004a.

W. Albers and W. C. M. Kallenberg. Are estimated control charts in control? *Statistics: A Journal of Theocratical and Applied Statistics*, 38:67–79, 2004b.

L. Alemi and D. Neuhauser. Time-between control charts for monitoring asthma attacks. *Joint Commission Journal on Quality and Safety*, 30:95–102, 2004.

M. S. Aminzadeh. Bayesian estimation of the expected time of first arrival past a truncated time T: the case of NHPP with power law intensity. *Computational Statistics*, 28:2465–2477, 2013.

A. Amiri and R. Khosravi. Estimating the change point of the cumulative count of a conforming control chart under a drift. *Scientia Iranica Transactions E: Industrial Engineering*, 19:856–861, 2012.

A. S. T. Andersen. *Lévy processes in finance: Lévy Heath-Jarrow-Morton Models*. Master Thesis, Department of Finance, Copenhagen Business School, 2008.

D. W. Apley. Posterior distribution charts: A Bayesian approach for graphically exploring a process mean. *Technometrics*, 54:293–307, 2012.

S. Ascher. A survey of tests for exponentiality. *Communications in Statistics-Theory and Methods*, 19:1811–1825, 1990.

M. Aslam, N. Khan, M. Azam, and Chi-Hyuck. Jun. Designing of a new monitoring t-chart using repetitive sampling. *Information Sciences*, 269:210–216, 2014.

M. Aslam, M. Azam, N. Khan, and Chi-Hyuck. Jun. A control chart for an exponential distribution using multiple dependent state sampling. *Quality and Quantity*, 49:455–462, 2015.

V. Bagdonaviéus, J. Kruopis, and M. Nikulin. *Nonparametric tests for complete data*. John Wiley & Sons, New York, 2010.

L. J. Bain and M. Engelhardt. *Statistical Analysis of Reliability and Life testing Models*. Marcel Dekker, 2nd Edition New York, 1991.

S. K. Bar-Lev, I. Lavi, and B. Reiser. Bayesian inference for the power law process. *Annal of Institute of Statistical Mathematics*, 44:623–639, 1992.

R. E. Barlow. Likelihood ratio tests for restricted families of distributions. *Annals of Mathematical Statistics*, 39:547–566, 1968.

R. E. Barlow and L. C. Hunter. Optimum preventive maintenance policies. *Operations Research*, 8:90–100, 1960.

R. E. Barlow and F. Proschan. *Mathematical Theory of Reliability*. Jhon Wiley and Sons. Reprinted (1996) SIAM, Philadelphia, PA., 1965.

M. J. Bayarri and G. García-Donato. A Bayesian sequential look at u control charts. *Technometrics*, 47:142–151, 2005.

J. C. Benneyan. Statistical quality control methods in infection control and hospital epidemiology, part I: Introduction and basic theory. *Infection Control and Hospital Epidemiology*, 19:194–214, 1998a.

J. C. Benneyan. Statistical quality control methods in infection control and hospital epidemiology, part II: Chart use, statistical properties and research issues. *Infection Control and Hospital Epidemiology*, 19:265–283, 1998b.

B. Bergman. On age replacement and the total time on test concept. *Scandinavian Journal of Statistics*, 6:161–168, 1979.

S. Bersimis, M. V. Koutras, and P. E. Maravelakis. A compound control chart for monitoring and controlling high quality processes. *European Journal of Operational Research*, 233:595–603, 2014.

P. J. Bickel and K. A. Doksum. Tests for monotone failure rate based on normalized spacings. *Annals of Mathematical Statistics*, 40:1261–1235, 1969.

D. P. Bischak and E. A. Silver. Estimating the out-of-control rate from control chart data in the presence of multiple causes and process improvement. *International Journal of Production Research*, 42:5217–5233, 2004.

C. M. Borror and D. C. Keats, J. B. Montgomery. Robustness of the time between events CUSUM. *International Journal of Production Research*, 41:3435–3444, 2003.

P.D. Bourke. Sample size and the binomial CUSUM control chart: the case of 100% inspection. *Metrika*, 53:51–70, 2001.

G. E. P. Box and T. Kramer. Statistical process monitoring and feedback adjustment. A discussion. *Technometrics*, 34:251–285, 1992.

F.W. Breyfogle. *Implementing Six Sigma: Smarter Solutions Using Statistical Methods*. Jhon Wiley and Sons., Hoboken, New Jersey, 2003.

P. D. Brouke. Detecting a shift in the fraction of nonconforming items using run length control charts with 100% inspection. *Journal of Quality Technology*, 23:225–238, 1984.

R. Calabria, M. Guida, and G. Pulcini. Some modified maximum likelihood estimators for the Weibull process. *Reliability Engineering and System Safety*, 23:51–58, 1987.

R. Calabria, M. Guida, and G. Pulcini. A Bayes procedure for estimation of current system reliability. *IEEE Transition on Reliability*, 41:69–92, 1992.

T. W. Calvin. Quality control techniques for zero defects. *IEEE Transaction on Components Hybrids Manufacturing Technology*, 6:323–328, 1983.

G. Casella and R. L. Berger. *Statistical Inference*. Duxbury Thomson Learning, California, 2002.

C. Çiğşar. *Some and tests for carryover effects and trends in recurrent event processes*. Ph.d thesis, Department of Statistics, University of Waterloo, University of Waterloo, 2010. https://uwspace.uwaterloo.ca/handle/10012/5554?show=full, Accessed on 05-10-2015.

J. H. Cha and G. Pulcini. A dependent competing risks model for technological units subject to degradation phnomena and catastrophic failures. *Quality and Reliability Enginerring International*, iFirst:DOI: 10.1002/qre.1767, 2015.

S. Chakraborti, S. W. Human, and M. A. Graham. Phase I statistical process control charts: An overview and some results. *Quality Engineering*, 21:52–62, 2008.

L. Y. Chan, M. Xie, and T. N. Goh. Two stage control charts for high yield processes. *International Journal of Reliability, Quality and Safety Engineering*, 4:149–165, 1997a.

L. Y. Chan, M. Xie, and T. N. Goh. Two-stage control charts for high yield processes. *International Journal of Reliability, Quality and Safe Engineering*, 4:149165, 1997b.

L. Y. Chan, M. Xie, and T. N. Goh. Cumulative quantity control charts for monitoring production processes. *International Journal of Production Research*, 38:397–408, 2000.

L. Y. Chan, K. J. Lin Dennis, M. Xie, and T. N. Goh. Cumulative probability control charts for geometric and exponential process characteristics. *International Journal of Production Research*, 40:133–150, 2002.

L. Y. Chan, C. D. Lai, M. Xie, and T. N. Goh. A two-stage decision procedure for monitoring processes with low fraction nonconforming. *European Journal of Operational Research*, 150:420–436, 2003.

T. C. Chang and F. F. Gan. Cumulative Sum charts for high yield processes. *Statistica Sinica*, 11:791–805, 2001.

T. C. Chang and F. F. Gan. Modified Shewhart chart for high yield processes. *Journal of Applied Statistics*, 34:857–877, 2007.

M. A. Chaudhry and S. M. Zubair. Generalized incomplete gamma functions with applications. *Journal of Computational and Applied Mathematics*, 55:99–124, 1994.

Ching-Wen. Chen. Using geometric Poisson exponentially weighted moving average control schemes in a compound Poisson production environment. *Computer and Industrial Engineering*, 63:374–381, 2012.

Jung-Tai. Chen. A new approach to setting control limits of cumulative count of conforming charts for high-yield processes. *Quality and Reliability Engineering International*, 25:973–986, 2009.

Jung-Tai. Chen. Design of cumulative count of conforming charts for high-yield processes based on average number of items inspected. *International Journal of Quality and Reliability Management*, 30:942–957, 2013a.

Jung-Tai. Chen. A Shewhart-type control scheme to monitor Weibull data without subgrouping. *Quality and Reliability Engineering International*, 30:1197–1214, 2014.

N. Chen, S. Zhou, Tzyy-Shuh. Chang, and H. Huang. Attribute control charts using generalized zero-inflated Poisson distribution. *Quality and Reliability Engineering International*, 24:793–806, 2008.

Pei-Wen. Chen and Chuen-Sheng. Cheng. An ARL unbiased approach to setting control limits of ccc-r chart for high yield processes. *Journal of Quality*, 17:435–451, 2010.

Pei-Wen. Chen and Chuen-Sheng. Cheng. On statistical design of the cumulative quantity control chart for monitoring high yield processes. *Communications in Statistics-Theory and Methods*, 40:1911–1928, 2011.

Y. K. Chen and C. Y. Chen. Cumulative conformance count charts with variable sample sizes. *International Journal of Trade, Economics and Finance*, 3:187–193, 2012.

Yan-Kwang. Chen. Cumulative conformance count charts with variable sampling intervals for correlated samples. *Computer and Industrial Engineering*, 64:302–308, 2013b.

Chuen-Sheng. Cheng and Pei-Wen. Chen. An ARL-unbiased design of time-between-events control charts with runs rules. *Journal of Statistical Computation and Simulation*, 81:857–871, 2011.

Jing-Er. Chiu and Chih-Hsin. Tsai. Properties and performance of one sided cumulative count of conforming chart with parameter estimation in high-quality processes. *Journal of Applied Statistics*, 40:2341–2353, 2013.

R. Cont and P. Tankov. *Financial Modelling with Jump Processes*. Chapman and Hall/CRC Financial Mathematics Series, 2004.

D. R. Cox and D. Oakes. *Analysis of survival data*. Chapman and Hall, New York, 1984.

R. D'Agostino and M. Stephens. *Goodness-of-fit techniques*. Marcel Dekker, Inc., New York, 1986.

M. D. de Oliveira, E. A. Colosimo, and G. L. Gilardoni. Bayesian inference for Power law processes with applications in repairable systems. *Journal of Statistical Planning and Inference*, 142:1151–1160, 2012.

A. De Vries and J. K. Reneau. Application of statistical process control charts to monitor changes in animal production systems. *Journal of Animal Science*, 88:E11–E24, 2010.

W.E. Deming. *Out of the Crisis*. Massachusetts Institute of Technology, Center for Advanced Engineering Study, 2000.

H. Demirhan and C. Hamurkaroglu. Bayesian $\bar{X}$ control limits for exponentially distributed measurements. *Journal of Statistical Computation and Simulation*, 84:628–643, 2014.

L. Devroye. A simple algorithm for generating random variates with log-concave density. *Computing*, 33:247–257, 1984.

A. Di Bucchianico, G. D. Mooiweer, and E. J. G. Moonen. Monitoring infrequent failures of high-volume production processes. *Quality and Reliability Engineering International*, 21:521–528, 2005.

P. Diaconis and D. Ylvisaker. Conjugate priors for exponential families. *The Annals of Statistics*, 7:269–281, 1979.

E. Dogu. Monitoring time between medical errors to improve health-care quality. *International Journal for Quality Research*, 6:151–157, 2012.

E. Dogu. Change point estimation based statistical monitoring with variable time between events (TBE) control charts. *Quality Technology and Quantative Management*, 1:383–400, 2014.

I. R. Dunsmore. The Bayesian predictive distribution in life testing models. *Thechnometrics*, 16:455–460, 1974.

R. I. Duran and S. L. Albin. Monitoring a fraction with easy and reliable settings of the false alarm rate. *Quality and Reliability Engineering International*, 25:10291043, 2009.

R. l. Dykstra and P. Laud. A Bayesian nonparametric approach to reliability. *The Annals of Statistics*, 9:356–367, 1981.

N. Ebrahimi, M. Habibullah, and E. S. Soofi. Testing exponentiality based on Kullback-Leibler information. *Journal of the Royal Statistical Society B*, 54:739–748, 1992.

T. Emura and Yi-Shuan. Lin. A comparison of normal approximation rules for attribute control charts. *Quality and Reliability Engineering International*, 31:411–418, 2015.

B. Epstein. Testing for the validity of the assumption that the underlying distribution of life is exponential. *Technometrics*, 2:167–183, 1960.

B. Epstein and M. Sobel. Life testing. *Journal of the American Statistical Association*, 48:486–502, 1953.

J. D. Esary, A. W. Marshall, and F. Proschan. Shock models and wear processes. *The Annals of Probability*, 1:627–649, 1973.

P. Eto and G. Pallotta. A new control chart for Weibull technological processes. *Quality Technology and Quantitative Management*, 4:553–567, 2007.

J. Eva. Comparison of two Bayesian approaches to SPC. *Aplimat-Journal of Applied Mathematics*, 5:259–268, 2012.

Y. Y. Fang, M. B. C. Khoo, and M. H. Lee. Synthetic-Type control charts for time between events monitoring. *PLoS ONE*, 8(6):e65440, 2013.

Y. Y. Fang, M. B. C. Khoo, S. Y. Teh, and M. Xie. Monitoring of time-between-events with a generalized group runs control chart. *Quality and Reliability Engineering International*, DOI:10.1002/qre.1789:–, 2015.

A. A. Fatahi, R. Noorossana, P. Dokouhaki, and M. Babakhani. Truncated zero inflated binomial control chart for monitoring rare health events. *International Journal of Research and Reviews in Applied Sciences (IJRRAS)*, 4:380–387, 2010.

M. C. Fu and Jian-Qiang. Hu. Efficient design and sensitivity analysis of control charts using Monte Carlo simulation. *Management Science*, 45:395–413, 1999.

M. P. Gadre and R. N. Rattihalli. Some group inspection based multi-attribute control charts to identify process deterioration. *Economic Quality Control*, 20:191–204, 2005.

M. P. Gadre and R. N. Rattihalli. Multi-attribute unit and group runs control chart to identify the process deterioration. *Journal of Statistical Computation and Simulation*, 78:999–1008, 2008.

M. H. Gail and J. L. Gastwirth. A scae-free goodness-of-fit test for exponential distribution based on the Gini statistic. *Journal of the Royal Statistical Society B*, 40:350–357, 1978.

F. F. Gan. An optimal design of CUSUM control charts for binomial counts. *Journal of Applied Statistics*, 20:445460, 1993.

F. F. Gan. Designs of one-and two-sided exponential EWMA charts. *Journal of Quality Technology*, 30:55–69, 1998.

G. L. Gilardoni and E. A. Colosimo. Optimal maintenance time for repairable systems. *Journal of Quality Technology*, 39:49–53, 2007.

F. J. Girón, M. L. Martı'nez, and E. M. Parrado. A predictive approach to some hypothesis testing problems. *Rev. R. Acad. Cienc. Exact. Fis. Nat. (Esp)*, 93:343–350, 1999.

R. E. Glaser. Bathtub and related failure rate characterizations. *Journal of the American Statistical Association*, 75:667–672, 1980.

T. N. Goh. A control chart for very high quality processes. *Quality Assurance*, 13:18–22, 1987.

U. Graf. *Applied Laplace Transforms and z-Transforms for Scientists and Engineers*. Springer Basel AG, 2004.

C. W. J. Granger. Can we improve the perceived quality of economic forecasts? *Journal of Applied Econometrics*, 11:455–473, 1996.

P. Grzegorzewski and R. Wieczorkowski. Entropy-based goodness-of-fit test for exponentiality. *Communications in Statistics-Theory and Methods*, 28:1183–1202, 1999.

M. Guida, R. Calabria, and G. Pulcini. Bayes inference for a nonhomogeneous poisson processes with power law intensity law. *IEEE Transition on Reliability*, 38:603–609, 1989.

A. Gut and J. Hüsler. *Advances in Degradation Modeling*, volume 4982 of Statistics for Industry and Technology, chapter Shock Models, pages 59–76. Birkhäuser Boston, a part of Springer Science and Business Media, 2010, 2010.

G. J. Hahn. Demings impact on industrial statistics: Some reflections. *The American Statistician*, 49:336–341, 1996.

M. Hamada. Bayesian tolerance interval control limits for attributes. *Quality and Reliability Engineering International*, 18:45–52, 2002.

S. Haridy, Z. Wu, K. Abhary, P. Castagliola, and M. Shamsuzzaman. Development of a multiattribute synthetic-np chart. *Journal of Statistical Computation and Simulation*, 84:1884–1903, 2014.

B. He, M. Xie, T. N. Goh, and K. L. Tsui. On control charts based on the generalized Poisson model. *Quality Technology and Quantitative Management*, 3:361–367, 2006.

Y. He, K. Mi, and C. Wu. A new statistical high quality process monitoring method: The counted number between Omega event control charts. *Quality and Reliability Engineering International*, 28:427–436, 2012.

N. Henze and S. G. Meintanis. Recent and classical tests for exponentiality: a partial review with comparisons. *Metrika*, 61:29–45, 2005.

N. L. Hjort. Nonparametric Bayes estimators based on beta processes in models for life history data. *The Annals of Statistics*, 18:1259–1294, 1990.

L. L. Ho and R. C. Quinino. An attribute control chart for monitoring the variability of a process. *International Journal of Production Economics*, 145:263–267, 2013.

W. Hoeffding. A class of statistics with asymptotically normal distribution. *Annals of Mathematical Statistics*, 19:293–325, 1949.

R. W. Hoerl and A. C. Palm. Discussion: Integrating SPC and APC. *Technometrics*, 34: 268–272, 1992.

D. Hoffman. Negative binomial control chart for count data with extra-Poisson variation. *Pharmaceutical Statistics*, 2:127–132, 2003.

M. Hollander, D. A. Wolfe, and E. Chicken. *Nonparametric statistical methods*. John Wiley & Sons, New York, 2014.

W. Huang and R. G. Askin. Reliability analysis of electronic devices with multiple competing failure models involving performance aging degradation. *Quality and Reliability Enginerring International*, 19:241–254, 2003.

Y. S. Huang and V. M. Bier. A natural conjugate prior for the nonhomogeneous Poisson process with power law intensity function. *Communications in Statistics- Simulation and Computations*, 27:525–551, 1998.

D. R. Insua, F. Ruggeri, and Wiper M. P. *Bayesian Analysis of Stochatic Process Models*. John Wiley & Sons, Ltd., 2012.

R. G. Jarrett. A note on the intervals between coal-mining disasters. *Biometrika*, 66: 191–193, 1979.

D. Jensen. Lecture 11: Hypothesis Tests to Control Charts. IENG 486 Statistical Quality and Process Control, 2010. South Dakota School of Mines and Technology, http://webpages.sdsmt.edu/~djensen/IENG%20486/index.htm, Accessed 26-09-2015.

A. Joarder, H. Krishna, and D. Kundu. Inference on Weibull parameters with conventional type-I censoring. *Computational Statistics and Data Analysis*, 55:1–11, 2011.

S. Joekes and E. P. Barbosa. *An improved p chart for monitoring high quality processes based on Cornish-Fisher quantile correction*. Technical Report Instituto de Matematica, Estatstica e Computacao Cientfica Universidade Estadual de Campinas, 2011. http://www.ime.unicamp.br/sites/default/files/rel_pesq/rp07-11.pdf.

J. M. Juran. Early SQC: A historical supplement. *Quality Progress*, 30:73–81, 1997.

A. Karr. *Point processes and their statistical inference*. CRC Press, New York, 1991.

N. Katemee and T. Mayureesawan. Control charts for zero-inflated Poisson models. *Applied Mathematical Sciences*, 6:2791–2803, 2012.

M. B. C. Khoo and M. Xie. A study of time between events control chart for the monitoring of regularly maintained systems. *Quality and Reliability Engineering International*, 25: 805–819, 2009.

B. Klefsjö. The HNBUE and HNWUE classes of life distributions. *Naval Research Logistics*, 29:331–344, 1982.

W. Kluge. *Time-inhomogeneous Lévy processes in interest rate and credit risk models*. Ph.D Thesis, der Albert-Ludwigs-Universität Freiburg im Breisgau, 2005.

T. Kotani, E. Kusukawa, and H. Ohta. Exponentially weighted moving average chart for high yield processes. *Industrial Engineering and Management Systems*, 4:75–81, 2005.

N. Kumar and S. Chakraborti. Phase-II Shewhart-type control charts for monitoring time between events andeffects of parameter estimation. *Quality and Reliability Engineering International*, DOI:10.1002/qre.1752:–, 2014a.

N. Kumar and S. Chakraborti. Phase II Shewhart control charts for monitoring times between events and effects of parameter estimation. *Quality and Reliability Engineering International*, DOI:10.1002/qre.1752:–, 2014b.

N. Kumar and S. Chakraborti. Improved phase-I control charts for monitoring time between events. *Quality and Reliability Engineering International*, 31:659–668, 2015.

V. Kuralmani, M. Xie, T. N. Goh, and F. F. Gan. A conditional decision procedure for high yield processes. *IIE Transactions*, 34:10211030, 2002.

C. D. Lai. The recurrent event process of a success preceded by failure and its application. *Journal of Applied Mathematics and Decision Sciences*, 1:101–117, 1997.

C. D. Lai and K. Govindaraju. Reduction of control chart signal variability for high quality processes. *Journal of Applied Statistics*, 35:671–679, 2008.

C. D. Lai, M. Xie, and K. Govindaraju. Study of a Markov model for the high-quality dependent process. *Journal of Applied Statistics*, 27:461–473, 2000.

J. Landon and N. D. Singpurwalla. Choosing a coverage probability for prediction intervals. *The American Statistician*, 62:120–124, 2008.

J. F. Lawless. *Statistical Models and Methods for Lifetime Data*. John Wiley & Sons, New York, 2011.

J. F. Lawless, C. Çiğşar, and R. J. Cook. Testing for monotone trend in recurrent event processes. *Technometrics*, 54:147–158, 2012.

J. Lee, N. Wang, L. Xu, A. Schuh, and W. H. Woodall. The effect of parameter estimation on upper-sided Bernoulli cumulative sum charts. *Quality and Reliability Engineering International*, 29:639651, 2013.

J. Y. Liu, M. Xie, T. N. Goh, and P. Ranjan. Time between events charts for online process monitoring. In *International Engineering Management Conference*, pages 1061–1065. IEEE, 2004.

J. Y. Liu, M. Xie, and T. N. Goh. CUSUM chart with transformed exponential data. *Communications in Statistics-Theory and Methods*, 35:1829–1843, 2006a.

J. Y. Liu, M. Xie, T. N. Goh, and P. R. Sharma. A comparative study of exponential time between events charts. *Quality Technology and Quantitative Management*, 3:347–359, 2006b.

J. Y. Liu, M. Xie, T. N. Goh, and L. Y. Chan. A study of EWMA chart with transformed exponential data. *International Journal of Production Research*, 45:743–763, 2007.

Y. Liu, Z. He, L. Shu, and Z. Wu. Statistical computation and analysis for attribute events. *Computational Statistics and Data Analysis*, 53:3412–3425, 2009.

Y. Liu, Z. He, M. Shamsuzzaman, and Z. Wu. A combined control scheme for monitoring the frequency and size of an attribute event. *Journal of Applied Statistics*, 37:1991–2013, 2010.

J. M. Lucas. Counted data CUSUMs. *Technometrics*, 27:129–144, 1985.

V. Makis. Multivariate Bayesian process control for a nite production run. *European Journal of Operational Research*, 194:795–806, 2009.

H. B. Mann. Nonparametric tests against trend. *Econometrica*, 13:245–259, 1945.

R. Marcellus. Bayesian statistical process control. *Quality Engineering*, 20:113–127, 2007.

E. Mavroudis and F. Nicolas. EWMA control chart for monitoring high yield processes. *Communications in Statistics-Theory and Methods*, 42:3639–3654, 2013.

E. Mavroudis and F. Nikolaos. One-sided EWMA control chart for monitoring high yield processes. In *58th World Statistical Congress, Dublin*, pages 6743–6748. Int. Statistical Inst., 2011.

B. McShane, M. Adrian, E. T. Bradlow, and P. S. Fader. Count models based on weibull inter-arrival times. *Journal of Business and Economic Statistics*, 26:369–378, 2008.

W. Q. Meeker and L. A. Escobar. *Statistical methods for reliability data*. John Wiley & Sons, New York, 1998.

Y. Mei. Is average run length to false alarm always an informative criterion? *Sequential Analysis: Design Methods and Applications*, 27:354–376, 2008.

U. Menzefricke. On the evaluation of control chart limits based on predictive distributions. *Communications in Statistics-Theory and Methods*, 31:1423–1440, 2002.

U. Menzefricke. Control charts for the generalized variance based on its predictive distribution. *Communications in Statistics-Theory and Methods*, 36:1031–1038, 2007.

U. Menzefricke. Control charts for the variance and coefficient of variation based on their predictive distribution. *Communications in Statistics-Theory and Methods*, 39: 2930–2941, 2010a.

U. Menzefricke. Multivariate exponentially weighted moving average charts for a mean based on its predictive distribution. *Communications in Statistics-Theory and Methods*, 39:2942–2960, 2010b.

U. Menzefricke. Control charts for the mean and variance based on changepoint methodology. *Communications in Statistics-Theory and Methods*, 42:988–1007, 2013a.

U. Menzefricke. Combined exponentially weighted moving average charts for the mean and variance based on the predictive distribution. *Communications in Statistics-Theory and Methods*, 42:4003–4016, 2013b.

M. A. Mohammed, P. Worthington, and W. H. Woodall. Plotting basic control charts: tutorial notes for healthcare practitioners. *Quality and Safety in Health Care (currently BMJ Quality and Safety)*, 17:137–145, 2008.

D. C. Montgomery. *Introduction to Statistical Quality Control*. John Wiley and Sons., United States of America, 2009.

K. Muralidharan, R. Shah, and D. H. Dhandhukia. Future reliability estimation based on predictive distribution in power law process. *Quality Technology and Quantitative Management*, 5:193–201, 2008.

D. N. P. Murthy, M. Xie, and R. Jiang. *Weibull Models*. John Wiley & Sons, New York, 2004.

M. K. Naeini, M. S. Owlia, and M. S. Fallahnezhad. A Bayesian approach for recognition of control char patterns. *International Journal of Industrial Engineering and Production Research*, 23:223–230, 2012.

T. Nakagawa. *Maintenance Theory of Reliability*. Springer-Verlag London, 2005.

T. Nakagawa. *Shock and damage models in Reliability Theory*. Springer-Verlag London, 2007.

L. S. Nelson. Notes on the Shewhartcontrol chart. *Journal of Quaity Technology*, 31: 124–126, 1999.

G. Nenes and G. Tagaras. The economically designed two-sided Bayesian $\bar{X}$ control chart. *European Journal of Operational Research*, 183:263–277, 2007.

S. T. A. Niaki and B. Abbasi. On the monitoring of multi-attribute high-quality production processes. *Metrika*, 66:373–388, 2007.

R. Noorossana, A. Saghaei, K. Paynabar, and Y. Samimi. On the conditional procedure for high yield processes. *Computers and Industrial Engineering*, 53:469–477, 2007.

J. R. Norris. *Markov Chains*. Cambridge University Press, 1997.

H. Ohta, E. Kusukawa, and A. Rahim. A CCC-r chart for high yield processes. *Quality and Reliability Engineering International*, 17:439–446, 2001a.

H. Ohta, E. Kusukawa, and A. Rahim. A CCC-r chart for high quality production processes. *Quality and Reliability Engineering International*, 17:439–446, 2001b.

F. W. Olver, D. W. Lozier, R. F. Boisvert, and C. W. Clark. *NIST Handbook of Mathematical Functions*. Cambridge University Press, New York, NY, USA, 2010.

Y. Ou, Z. Wu, and T. N. Goh. A new SPRT chart for monitoring process mean and variance. *International Journal of Production Economics*, 132:303–314, 2011.

Y. Ou, Z. Wu, and F. Tsung. A comparison study of effectiveness and robustness of control charts for monitoring process mean. *International Journal of Production Economics*, 135:479–490, 2012.

G. Ozsan, M. C. Testik, and Weiß. Properties of the exponential EWMA chart with parameter estimation. *Quality and Reliability Engineering International*, 26:555–569, 2010.

M. Perakis and E. Xekalaki. Assessing the proportion of conformance of a process from a Bayesian perspective. *Quality and Reliability Engineering International*, 31:381–387, 2015.

S. Petrone, S. Rizzelli, J. Rousseau, and C. Scricciolo. Empirical Bayes methods in classical and Bayesian inference. *METRON*, 72:201–215, 2014a.

S. Petrone, J. Rousseau, and C. Scricciolo. Bayes and empirical Bayes: do they merge? *Biometrika*, 101:285–302, 2014b.

D. J. Poirier. A predictive motivation for loss function specification in parameteric hypothesis testing. *Economic Letters*, 56:1–3, 1997.

Frank Proschan and Ronald Pyke. Tests for monotone failure rate. In *Proceedings of the Fifth Berkeley Symposium on Mathematical Statistics and Probability, Volume 3: Physical Sciences*, pages 293–312, Berkeley, Calif., 1967. University of California Press. URL http://projecteuclid.org/euclid.bsmsp/1200513634.

S. Psarakis, A. K. Vyniou, and P. Castagliola. Some recent developments on the effects of parameter estimation on control charts. *Quality and Reliability Engineering International*, 30:1113–1129, 2014.

G. Purdy, S. C. Richards, and W. H. Woodall. Surveillance of non-homogeneous Poisson processes. *Technometrics*, DOI: 10.1080/00401706.2014.927790:–, 2014.

H. Qiao and C. Tsokos. Best efficient estimates of the intensity function of the Power Law Process. *Journal of Applied Statistics*, 25:111–120, 1998.

L. Qu, A. Wu, and Tien-I. Liu. A control scheme integrating the T chart and TCUSUM chart. *Quality and Reliability Engineering International*, 27:529–539, 2011.

L. Qu, Z. Wu, M. B. C. Khoo, and P. Castagliola. A CUSUM scheme for event monitoring. *International Journal of Production Economics*, 145:268–280, 2013.

L. Qu, Z. Wu, M. B. C. Khoo, and A. Rahim. Time-between-event control charts for sampling inspection. *Technometrics*, 56:336–346, 2014.

R Core Team. *R: A Language and Environment for Statistical Computing*. R Foundation for Statistical Computing, Vienna, Austria, 2013. URL http://www.R-project.org/.

P. Ranjan, M. Xie, and T. N. Goh. Optimal control limits for CCC charts in the presence of inspection errors. *Quality and Reliability Engineering International*, 19:149–160, 2003.

C. R. Rao. *Statistics and Truth: Putting Chance to Work*. World Scientific, Singapore, 1997.

L. Raubenheimer and A. J. van der Merwe. Bayesian control chart for nonconformities. *Quality and Reliability Engineering International*, iFirst:DOI: 10.1002/qre.1668, 2014.

M. R. Reynolds. The Bernoulli CUSUM chart for detecting decreases in a proportion. *Quality and Reliability Engineering International*, 29:529534, 2013.

M. R. Reynolds Jr and Z. G. Stoumbos. A CUSUM chart for monitoring a proportion when inspecting continuously. *Journal of Quality Technology*, 31:87–108, 1999.

M. Riaz. Monitoring of process parameters using Bayesian methodology. *International Journal of Agricultural and Statistical Sciences*, 7:1–7, 2011.

S. E. Rigdon and A. P. Basu. *Statistical Methods for the Reliability of Repairable Systems*. John Wiley & Sons, Inc. New York USA, 2000.

H. Rinne. The Hazard Rate-Theory and Inference. Justus Liebig University, D 35394 Giessen, Germany, 2014. http://geb.uni-giessen.de/geb/volltexte/2014/10793/pdf/RinneHorst_hazardrate_2014.pdf, Accessed 26-09-2015.

A. Saghir and Z. Lin. Control charts for dispersed count data: An overview. *Quality and Reliability Engineering International*, 31:725–739, 2015.

A. M. O. Sant'Anna and C. S. ten Caten. Beta control chart for monitoring fraction data. *Expert Systems with Applications*, 39:10236–10243, 2012.

E. Santiago and S. Joel. Control charts based on the exponential distribution: Adapting run rules for the t chart. *Quality Engineering*, 25:85–96, 2013.

A. Schuh, J. A. Camelio, and W. H. Woodall. Control charts for accident frequency: a motivation for real-time occupational safety monitoring. *International Journal of Injury Control and Safety Promotion*, 21:154–162, 2014.

D. A. Serel. Economic design of the EWMA control charts based on loss functions. *Mathematical and Computer Modelling*, 49:745–759, 2009.

M. S. Shafae, R. M. Dickinson, W. H. Woodall, and J. A. Camelio. CUSUM control charts for monitoring Weibull distributed time between events. *Quality and Reliability Engineering International*, 31:839–849, 2015.

S. H. Shaha. Acuity systems and control charting. *Quality Management in Health Care*, 3:22–30, 1995.

M. Shamsuzzaman and Z. Wu. Design of EWMA control chart for minimizing the proportion of defective units. *International Journal of Quality and Reliability Management*, 29:953–969, 2012.

X. Shen, C. Zou, W. Jiang, and F. Tsung. Monitoring Poisson count data with probability control limits when sample sizes are time varying. *Navel Research Logistics*, 60:625–636, 2013.

X. Shen, Kwok-Leung. Tsui, W. H. Woodall, and C. Zou. Self-starting monitoring scheme for poisson count data with varying population sizes. *Technometrics*, -: DOI:10.1080/00401706.2015.1075423, 2015.

W. A. Shewhart. *Economic control of quality of manufactured product*. Bell Telephone Laboratories series. D. Van Nostrand, New York, NY (Republished in 1980 by American Society for Quality, Milwaukee, WI), 1931.

W.A. Shewhart and W.E. Deming. *Statistical Method from the Viewpoint of Quality Control*. Dover Books on Mathematics Series. Dover, 1939.

L. Shu, W. Jiang, and S. Wu. A one-sided EWMA control chart for monitoring process means. *Communications in Statistics-Simulation and Computation*, 36:901–920, 2007.

L. Shu, W. Su, Y. Jiang, and Kwok-Leung Tsui. A comparison of exponentially weighted moving average-based methods for monitoring increases in incidence rate with varying population size. *IIE Transactions*, 46:798–812, 2014.

E. A. Silver and D. P. Bischak. Bayesian estimation of the rate at which a process, monitored by an $\bar{x}$ chart, goes out of control. *International Journal of Production Research*, 42:1227–1242, 2004.

C. H. Sim and M. H. Lim. Attribute charts for Zero-Inflated processes. *Communications in Statistics-Simulation and Computation*, 37:1440–1452, 2008.

N. D. Singpurwalla. Survival in dynamic environments. *Statistical Science*, 10:86–103, 1995.

C. Sonesson and D. Bock. A review and discussion of prospective statistical surveillance in public health. *Journal of Royal Statistical Society (Series A)*, 166:5–21, 2003.

H. Spliid. Monitoring medical procedures by exponential smoothing. *Statistics in Medicine*, 26:124–138, 2007.

H. Spliid. An exponentially weighted moving average control chart for Bernoulli data. *Quality and Reliability Engineering International*, 26:97113, 2010.

S. H. Steiner and R. J. MacKay. *Effective monitoring of processes with part per million defective: a hard problem*. Frontier in Statistical Quality Control 7, Edited by Lenz, H. J. and Wilrich, P. T., Physica-Verlag Heidelberg, 2004.

D. Stoyan. Weibull, RRSB or extreme-value theorists? *Metrika*, 76:153–159, 2013.

G. W. Sturm, S. A. Melnyk, C. A. Feltz, and J. F. Wolter. Sufficient statistics process control: An empirical Bayes approach to process control. *International Journal of Production Research*, 28:1329–1344, 1990.

G. W. Sturm, C. A. Feltz, and M. A. Yousry. An empirical Bayes strategy for analysing manufacturing data in real time. *Quality and Reliability Enginerring International*, 7: 159–167, 1991.

J. L. Szarka and W. H. Woodall. A review and perspective on surveillance of Bernoulli processes. *Quality and Reliability Engineering International*, 27:735–752, 2011.

M. H. Y. Tan and J. Shi. A Bayesian approach for interpreting mean shifts in multivariate quality control. *Technometrics*, 54:294–307, 2012.

A. G. Tartakovsky. Discussion on "Is average run length to false alarm always an informative criterion?" by Yajun Mei. *Sequential Analysis: Design Methods and Applications*, 27:396–405, 2008.

J. Thor, J. Lundberg, J. Ask, J. Olsson, C. Carli, K. P. Härenstam, and M. Brommels. Application of statistical process control in healthcare improvement:systematic review. *Quality Safety Health Care*, 16:387–399, 2007.

M. Thulin. Decision-theoretic justifications for Bayesian hypothesis testing using credible sets. *Journal of Statistical Planning and Inference*, 146:133–138, 2014.

W. Tian, H. Sun, X. Zhang, and W. H. Woodall. The impact of varying patient populations on the in-control performance of the risk-adjusted CUSUM chart. *International Journal for Quality in Health Care*, 27:31–36, 2015.

C. Tibor. Some parameter-free tests for trend and their application to reliability analysis. *Reliability Engineering and System Safety*, 41:225–230, 1993.

E. Topalidou and S. Psarakis. Review of multinomial and multiattribute quality control charts. *Quality and Reliability Engineering International*, 25:773804, 2009.

G. Toubia-Stucky, H. Liao, and J. Twomey. A sequential Bayesian cumulative conformance count approach to deterioration detection in high yield processes. *Quality and Reliability Engineering International*, 28:203–214, 2012.

P. Tsiamyrtzis and D. M. Hawkins. A Bayesian scheme to detect changes in the mean of a short-run process. *Technometrics*, 47:446–456, 2005.

J. W Tukey. Review of Deming, W. E., Statistical adjustment of data. *Review of Scientific Instruments*, 17:152–163, 1946.

M. B. (Thijs) Vermaat and Ronald J. M. M. Does. A semi-Bayesian method for Shewhart individual control charts. *Quality Technology and Quality Management*, 3:111–125, 2006.

G. Vining, M. Kulahci, and S. Pedersen. Recent advances and future directions for quality engineering. *Quality and Reliability Engineering International*, iFirst: DOI:10.1002/qre.1797, 2015.

G. G. Vining. *Statistical Methods for Engineers*. Duxbury-Brooks/Cole, Pacific Grove, CA, 1998.

H. Wang. Comparison of p control charts for low defective rate. *Computational statistics and Data Analysis*, 53:4210–4220, 2009.

W. Wang. A simulation-based multivariate Bayesian control chart for real time condition-based maintenance of complex systems. *European Journal of Operational Research*, 218: 726–734, 2012.

W. Wang and X. Jia. A Bayesian approach in delay time maintenance model parameters estimation using both subjective a and objective data. *Quality and Reliability Engineering International*, 23:95–105, 2007.

Y. P. Wang and Z. Z. Lu. Bayesian inference and prediction analysis of the power law process based on a gamma prior distribution. *Communications in Statistics- Simulation and Computations*, 40:1383–1401, 2011.

Y. P. Wang, Z. Z. Lu, and B. Xp. Bayesian analysis for the power law process based on Markov chain Monte Carlo. *Journal of Aerospace Power*, 25:152–159, 2010.

H. R. Weischedel. Crane wire rope damage and nondestructive inspection methods. *Wire Rope News and Sling Technology*, 25:1–11, 2003.

D. J. Wheeler. *Advanced Topics in Statistical Process Control*. SPC Press, Knoxville, TN, 1995.

Inc. Wolfram Research. *Mathematica*. Wolfram Research, Inc., Champaign, Illinois, version 10.0 edition, 2014. URL http://www.wolfram.com/.

W. H. Woodall. Control charts based on attribute data: Biblography and review. *Journal of Quality Technology*, 29:172–183, 1997.

W. H. Woodall. Controversies and contradictions in statistical process control. *Journal of Quality Technology*, 32:341–350, 2000.

W. H. Woodall. The use of control charts in health-care and public-health surveillance. *Journal of Quality Technology*, 38:89104, 2006.

W. H. Woodall and A. R. Driscoll. *Frontiers in Statistical Quality Control 11*, chapter Some Recent Results on Monitoring the Rate of a Rare Event, pages 15–27. Springer International Publishing Switzerland, 2015.

W. H. Woodall and D. C. Montgomery. Some current directions in the theory and application of statistical process control. *Journal of Quality Technology*, 46:78–94, 2014.

W.H. Woodall and D.C. Montgomery. Research issues and ideas in statistical process control. *Journal of Quality Technology*, 31:376–386, 1999.

P. W. Woodward and J. C. Naylor. An application to Bayesian methods in SPC. *Journal of Royal Statistical Society. Series D (The Statistician)*, 42:461–469, 1993.

X. Wu, R. Miao, X. Zhang, Z. Jiang, and X. Chu. A conjugate Bayesian approach to control chart for multi-batch and low volume production. *International Journal of Production Research*, 53:2179–2185, 2015.

Z. Wu, X. Zhang, and S. H. Yeo. Design of the sum of conforming run length control charts. *European Journal of Operation Research*, 132:187–196, 2001.

Z. Wu, J. Jiao, and Y. Liu. A binomial CUSUM chart for detecting large shifts in fraction nonconforming. *Journal of Applied Statistics*, 35:12671276, 2008.

Z. Wu, J. Jiao, and Z. He. A single control chart for monitoring the frequency and magnitude of an event. *International Journal of Production Economics*, 119:24–33, 2009a.

Z. Wu, J. Jiao, and Z. He. A control scheme for monitoring the frequency and magnitude of an event. *International Journal of Production Research*, 47:2887–2902, 2009b.

Z. Wu, J. Jiao, M. Yang, Y. Liu, and Z. Wang. An enhanced adaptive CUSUM control chart. *IIE Transactions*, 41:642–653, 2009c.

Z. Wu, B. C. M. Khoo, L. Shu, and W. Jiang. An *np* control chart for monitoring the mean of a variable based on an attribute inspection. *International Journal of Production Economics*, 121:141–147, 2009d.

Z. Wu, Y. Liu, Z. He, and M. B. C. Khoo. A cumulative sum scheme for monitoring frequency and size of an event. *Quality and Reliability Engineering International*, 26: 541–554, 2010a.

Z. Wu, M. Yang, M. B. C. Khoo, and Fong-Jung. Yu. Optimization designs and performance comparison of two CUSUM schemes for monitoring process shifts in mean and variance. *European Journal of Operational Research*, 205:136–150, 2010b.

M. Xie and T. N. Goh. The use of probability limits for process control based on geometric distribution. *International Journal of Quality and Reliability Management*, 14:64–73, 1997.

M. Xie, T. N. Goh, and V. Kuralmani. *Statistical Models and Control Charts for High-Quality Processes*. Kluwer Academic Publishers, Boston, Mass, USA, 2002a.

M. Xie, T.N. Goh, and P. Ranjan. Some effective control chart procedures for reliability monitoring. *Reliability Engineering and System Safety*, 77:143–150, 2002b.

Y. Xie, M. Xie, and T. N. Goh. Two MEWMA charts for Gumbel's bivariate exponential distribution. *Journal of Quality Technology*, 43:50–65, 2011.

W. Yan-Ping and L. Zhen-Zhou. Bayesian inference and prediction analysis of the power law process based on a natural conjugate prior. *Journal of Statistical Computation and Simulation*, 85:881–898, 2015.

J. Yang, H. Yu, Y. Cheng, and M. Xie. Design of exponential control charts based on average time to signal using sequential sampling scheme. *International Journal of Production Research*, 53:2131–2145, 2015a.

J. Yang, H. Yu, Y. Cheng, and M. Xie. Design of exponential control charts based on average time to signal using a sequential sampling scheme. *International Journal of Production Research*, 53:2131–2145, 2015b.

J. Yang, H. Yu, Y. Cheng, and M. Xie. Design of gamma charts based on average time to signal. *Quality and Reliability Engineering International*, DOI: 10.1002/qre.1813:–, 2015c.

N. Yannaros. Weibull renewal process. *Annals of the Institute of Statistical Mathematics*, 46:641–648, 1994.

A. B. Yeh, R. N. Mcgrath, M. A. Sembower, and Q. Shen. EWMA control charts for monitoring high-quality processes based on non transformed observations. *International Journal of Production Research*, 46:5679–5699, 2008.

S. Yilmaz and N. Burnak. An economic approach to the management of high quality processes. *Quality and Reliability Engineering International*, 29:681–690, 2013.

Z. Yin and V. Makis. Economic and economic-statistical design of a multivariate Bayesian control chart for condition-based maintenance. *IMA Journal of Management Mathematics*, 22:47–63, 2011.

D. S. Young and T. M. Mills. Choosing a coverage probability for forecasting the incidence of cancer. *Statistics in Medicine*, 33:4104–4115, 2014.

S. Zacks. *Distributions of failure times associated with non-homogeneous compound Poisson damage processes*, volume Volume 45 of *Lecture Notes–Monograph Series*, pages 396–407. Institute of Mathematical Statistics, Beachwood, Ohio, USA, 2004. doi: 10.1214/lnms/1196285407. URL http://dx.doi.org/10.1214/lnms/1196285407.

C. W. Zhang, M. Xie, and T. N. Goh. Design of exponential control charts using sequential sampling scheme. *IIE Transactions*, 38:1105–1116, 2006.

C. W. Zhang, M. Xie, J. Y. Liu, and T. N. Goh. A control chart for the gamma distribution as a model of time between events. *International Journal of Production Research*, 45: 5649–5666, 2007a.

C. W. Zhang, M. Xie, J. Y. Liu, and T. N. Goh. A control chart for the gamma distribution as a model of time between events. *International Journal of Production Research*, 45: 5649–5666, 2007b.

C. W. Zhang, M. Xie, and T. N. Goh. Economic design of cumulative count of conforming charts under inspection by samples. *International Journal of Production Economics*, 111:93–104, 2008.

H. Y. Zhang, M. Shamsuzzaman, M. Xie, and T. N. Goh. Design and application of exponential chart for monitoring time-between-events data under random process shift. *The International Journal of Advanced Manufacturing Technology*, 57:849–857, 2011a.

H. Y. Zhang, M. Xie, T. N. Goh, and M. Shamsuzzaman. Economics design of time-between-events control chart system. *Computer and Industrial Engineering*, 60:485–492, 2011b.

M. Zhang, Y. Peng, A. Schuh, F. M. Megahed, and W. H. Woodall. Geometric charts with estimated control limits. *Quality and Reliability Engineering International*, 29: 209–223, 2013.

M. Zhang, F. M. Megahed, and W. H. Woodall. Exponential CUSUM charts with estimated control limits. *Quality and Reliability Engineering International*, 30:275–286, 2014a.

M. Zhang, G. Nie, and Z. He. Performance of cumulative count of conforming chart of variable sampling intervals with estimated control limits. *International Journal of Production Economics*, 150:114–124, 2014b.

C. Zhao. *Bayesian and Empirical Bayes approaches to Power law process and Microarray analysis*. Graduate school theses and dissertations, Department of Mathematics, College of Arts and Science, University of South Florida, 2004. http://scholarcommons.usf.edu/etd/992.

C. Zhao. Empirical Bayes analysis on the power law process with natural conjugate prior. *Journal of Data Science*, 8:139–149, 2010.

Y. Q. Zhou and Z. Xi. Weng. *Reliability Growth*. Science Press, Beijing China, 1992.